Faculty of Science and Engineering
Department of Electrical and Computer Engineering

Design and Control of the Energy Management System of a Smart Vehicle

Shane N Overington

This thesis is presented for the Degree of
Doctor of Philosophy
of
Curtin University

June 2014

Declaration

To the best of my knowledge and belief this thesis contains no material previously published by any other person except where due acknowledgment has been made.

This thesis contains no material which has been accepted for the award of any other degree or diploma in any university.

Signature: ……  ……

Date: ……06/06/2014……...

Abstract

This thesis demonstrates the design of both a non-predictive and predictive controller for the high efficiency control of parallel and power-split connected plug-in hybrid electric vehicles. At the beginning this research program identifies and evaluates the energy smart vehicles featured in existing technical papers in order to distinguish the inherent advantages and disadvantages. The varying performance outcomes of such vehicles are due to the selection and control of powertrain and drivetrain components. This study stipulates that the power-split plug-in hybrid electric vehicle is the best alternative to the conventional vehicle. In addition the existing control strategies of energy smart vehicles are examined with the real-time optimisation based blended controllers having superior performance over the alternative control strategies.

For the consideration of a test bench, three commercially available vehicles are modelled using the advanced vehicle simulator (ADVISOR) which is a MATLAB/Simulink add-on software package. The three vehicles include the Toyota Prius 2010, Hyundai Sonata Hybrid 2011 and Honda CR-Z 2010. Measured data of the three vehicles is analysed using known methods and techniques in understanding each individual vehicle's energy management system for modelling. This analysis realises the selection of vehicle specifications and the original controller for each of the test benches. Measured and simulated signals and performance results are compared in order to verify the representation of the three vehicles in simulation.

Contrary to the traditional approach of fuel consumption minimisation in energy management systems this thesis determines high efficiency control of the powertrain. In the first instance a non-predictive controller restricts the internal combustion engine to a predefined high efficiency region as a means to conserve fuel. This is achieved through the use of a battery bank to balance the load between the internal combustion engine and the drivetrain. The main concern for this approach is increased fuel consumption if the high efficiency controller is not calibrated correctly. Implementation of the high efficiency controller on the three test benches demonstrates fuel consumption reductions of up to 12% in comparison to the original controller. In addition the battery bank state of charge must be maintained in order to demonstrate that fuel consumption reductions are due to improved efficiency of control and not a relocation of energy from the internal combustion engine to the battery bank. Detailed analysis of the implemented non-predictive high efficiency controller reveals the potential for further improvement through the use of predictive control.

The predictive controller relies on the average vehicle velocity and absolute average acceleration of standardised drive cycles to predict the energy requirements of planned driving routes. It is expected that such an approach forms the basis for predicting the energy requirements of real-world driving, which the designed predictive controller takes advantage of. Using the predicted energy requirement in comparison to the consumed energy during driving the controller is capable of calibrating the high efficiency region of the non-predictive controller on-the-go. Testing the performance of the predictive controller on the Toyota Prius 2010 test bench, fuel consumption reductions of operation as a hybrid electric and plug-in hybrid electric vehicle are revealed. In addition error tolerance in the predicted information and the effect on the fuel savings are quantified. Implementing the predictive controller demonstrates the potential for maximising the use of stored energy while maintaining high efficiency control of the powertrain. Fuel savings for operation of the predictive controller in hybrid electric and plug-in hybrid electric vehicles are up to 4% and 22% respectively. This is in comparison to the existing controller. Fuel savings are much higher in the plug-in hybrid case since the strategy relies on charging from the grid.

Acknowledgements

First of all, I would like to express my sincere gratitude to my PhD supervisor Dr. Sumedha Rajakaruna who encouraged my interest to undertake this exciting and challenging journey. Secondly, for his continued support, useful critiques and patient guidance throughout this research program, it has been a pleasure and a privilege to work with you these past four years. Thank you to my associate supervisor Professor Syed Islam for your valuable feedback throughout the research program.

I would also like to thank the Department of Electrical and Computer Engineering at Curtin University for their technical support and provisions of research resources. In particular the people who have contributed to various aspects of the work in this thesis; Mr Mark Fowler, Mr Nick King, Mr Zibby Cielma, Mr Russel Wilkinson, Professor Sven Nordholm and Professor Peter Wolfs. I am also grateful to the staff and students within the department that have provided a professional, enjoyable and motivating atmosphere and work environment.

I would like to express my very great appreciation to Curtin University for awarding me the Australian Postgraduate Award and Curtin University Postgraduate Scholarship. The financial support provided by these awards ensured that I was able to focus all of my time and efforts on my research.

Originally from rural Western Australia I relocated to Perth for my tertiary education. Thank you to my parents for their unconditional support over the past eight years my education would not have been possible without you. Finally thank you to my friends and family who have helped me endure the demands of this research program over the past four years.

Contents

List of Figures

List of Figures

List of Figures

List of Figures

List of Figures

List of Tables

List of Tables

Glossary of Terms

Symbol/Abbreviation	Description	Unit
*	Identifies a requested signal when placed after the appropriate symbol (e.g. T_e^* is requested ICE torque however T_e is measured ICE torque)	-
.*	defines element-wise multiplication for vectors and arrays, this is used in MATLAB notation	-
./	defines element-wise division for vectors and arrays, this is used in MATLAB notation	-
//	Used to indicate the start of comments on a line in the presented algorithms	-
a	acceleration of a vehicle	m/s^2
a_1	acceleration constant for determining ICE operation when vehicle velocity exceeds a defined minimum	m/s^2
a_2	acceleration constant for determining ICE operation when vehicle velocity is below a defined minimum	m/s^2
ADVISOR	advanced vehicle simulator	-
A_f	frontal area of vehicle	m^2
Ah_{ess}	Amp-hour rating of one ESS module	Ah
$\bar{a}_j$	absolute average acceleration/deceleration	m/s^2
AT	automatic transmission	-
b	coefficient for charge or discharge of ESS, equal to 1 for discharging or -1 for charging	-
C	Carrier gear (also known as yoke)	-
C_D	coefficient of aerodynamic drag	-
CI	compression ignition	-
CO	carbon monoxide (also collective carbon emissions)	-
count_$P_{e,map}$	length of $P_{e,map}$ for which the primary for loop is required to count towards in calculating the optimal operating line (Algorithm 3.1)	-
count_$\omega_{e,map}$	length of $\omega_{e,map}$ for which the secondary for loop is required to count towards in calculating the optimal operating line (Algorithm 3.1)	-
CVT	continuously variable transmission	-
d	distance travelled during driving	km
D_e	enable signal for ICE operation, 1 for on 0 for off	-
ECE	urban segment of the NEDC	-
E_{ess}	ESS energy consumed	kJ
$E_{ess,r}$	Remaining energy stored in the ESS at time t	kJ
$E_{ess,total}$	Total energy stored in ESS at 100% SOC	kJ
E_f	fuel energy consumed	kJ
E_L	load energy consumed	kJ
E_{Ltoff}	tractive energy consumed during t_{off} period	kJ
EMS	energy management system	-

Glossary of Terms

ESS	energy storage system	-
ESV	energy smart vehicle	-
E_{total}	total tractive energy	kJ
EUDC	extra urban segment of the NEDC	-
EV	electric vehicle	-
FC	fuel consumption	L/100km
f_e	frequency of ICE on/off periods over a drive cycle	
$f_{m/g}$	frequemcy of the M/G	Hz
f_o	initial consideration for rolling resistance	-
f_r	rolling resistance coefficient	-
F_t	tractive force	N
FTP	federal test procedure	-
GPS	global positioning system	-
HC	hydrocarbon	-
HEC	High efficiency controller	-
HEC-V	high efficiency controller with varying vehicle velocity included	-
HEV	hybrid electric vehicle	-
HF	hybridization factor	-
HL07	An aggressive driving schedule determined in combination with the FTP	-
HWFET	highway fuel economy test	-
i	gear ratio for definition of drivetrain component operations	-
ICE	internal combustion engine	-
I_{chg}	maximum charging current accepted by the ESS	A
I_{ess}	terminal current of the ESS	A
i_g	transmission gear ratio	-
$i_{g,min}$	minimum transmission gear ratio	-
i_o	final drive gear ratio	-
i_{rw}	gear ratio between the ring gear and drive axle	-
i_t	total transmission and final drive gear ratio	-
J	factor representing rotational inertia of components in drivetrain	$kg.m^2$
J_e	factor for rotational inertia of components in the ICE	$kg.m^2$
$J_{m/g}$	Factor for rotational inertia of components in M/G	$kg.m^2$
J_P	generalised factor representing rotational inertia of components in the powertrain	$kg.m^2$
J_w	factor for rotational inertia of the wheels	$kg.m^2$
k	constant representing unique characteristics of individual ICE for the approximate linear relationship between fuel consumption rate and output torque	-
k_1	arbitrary gear ratio between ICE and driven wheels in a mechanical coupling	-
k_2	arbitrary gear ratio between M/G and driven wheels in a mechanical coupling	-
k_{yr}	gear ratio between the carrier gear and ring gear	-

k_{ys}	gear ratio between the yoke gear and sun gear	-
LA92	Unified driving schedule - emissions test	-
M	Vehicle mass	kg
M/G	motor/generator	-
MAPE	mean absolute percentage error	%
$\dot{m}_f$	fuel consumption rate	g/s
MT	manual transmission	-
NEDC	new European drive cycle	-
N_{ess}	Number of modules in the ESS	-
NO	nitrogen oxide	-
NOR	Logic block NOT OR	-
non-OECD	Nations outside the Organisation for Economic Corporation and Development	-
NurembergR36	Drive cycle for bus route 36 in Nuremberg, Germany	-
OECD	Organisation for Economic Corporation and Development	-
P_{av}	average tractive power requirement	W
$P_{av,act}$	average tractive power requirement using equation 3.1	W
$P_{av,est}$	average tractive power requirement using equation 5.1	W
P_{brake}	mechanical braking power	W
PBS	power balancing strategy	-
P_{chg}	charge power requested from the ICE	W
P_e	ICE power	W
$\overline{P}_e$	An array of ICE output power, indexed horizontally by $\overline{T}_e$ and vertically by ω_e having dimensions *n* by *m*	W
p_e	percentage of total input energy considered to have been supplied by the ICE	%
$P_{e,av}$	Calculated average ICE power	W
$P_{e,in}$	ICE input power or power in the fuel	W
$\overline{P}_{e,in}$	An array of ICE input power, indexed horizontally by $\overline{T}_e$ and vertically by $\overline{\omega}_e$ and is a pre-existing array in the ICE control unit for estimating fuel consumption relative to output torque and speed.	W
$\overline{P}_{e,map}$	vector containing ICE output power values with respect to $\omega_{e,map}$	W
P_{e,map_index}	for loop variable defined for evaluating the calculation of the optimal operating line as the ICE speed increases (Algorithm 3.1)	-
$\overline{P}_{e,\max}$	vector containing the maximum output power at varying ICE speeds relative to $T_{e,max\text{-}map}$	W
P_{e,max_index}	variable used to find the location of the maximum ICE power in the $P_{e,max}$ vector (Algorithm 3.1)	-
$p_{e,min}$	percentage of maximum ICE torque that ICE will operate above	%
$P_{e,min}$	vector containing minimum output power at varying ICE speeds (Algorithm 3.1)	W

Glossary of Terms

$p_{e,opt}$	percentage of maximum ICE torque for optimal ICE operation	%
$\overline{P}_{e,opt}$	vector containing the ICE output power of the optimal operating line for VSC (Algorithm 3.1)	W
PEMFC	proton exchange membrane fuel cell	-
P_{ess}	Power discharged from the ESS	W
$P_{ess,av}$	Average power discharged from the ESS	W
$P_{ess,max}$	Maximum allowable power discharged from the ESS	W
$P_{ess,min}$	Minimum allowable power discharged from the ESS	W
PGS	planetary gear set	-
PHEV	plug-in hybrid electric vehicle	-
P_L	drivetrain load power	W
$P_{L,av}$	Recorded average drivetrain load during ICE operation	kJ or W
$p_{m/g,max}$	percentage of maximum M/G torque for which M/G operation is limited to	%
$P_{m/g}$	M/G power	W
$P_{m/g,max}$	Maximum developed power from the M/G	W
$P_{m/g,min}$	Minimum developed power from the M/G	W
P_P	propulsion device power	W
P_t	tractive power	W
$P^{-}_{\eta e,low}$	minimum power for the high efficiency region relative to $\eta_{e,low}$	W
$P^{+}_{\eta e,low}$	maximum power for the high efficiency region relative to $\eta_{e,low}$	W
$P_{\eta e,max}$	power at which ICE achieves maximum efficiency	W
Q	output of the SR flip-flop	-
Q^*	conjugate of the output of the SR flip-flop	-
Q_{HV}	heating value of the fuel used	kJ/kg
R	ring gear	-
r	approximate radius of rotating components of the powertrain	m
r_d	drive wheel radius	m
R_{int}	internal resistance of ESS model	Ω
s	slip	%
S	sun gear	-
SI	spark ignition	-
SOC	state of charge	-
SOC_{final}	measured final SOC of ESS	%
SOC_{high}	high SOC limit for ESS controller	%
SOC_{ICE}	ESS SOC percentage below which the ICE is required to switch on	%
SOC_{init}	measured initial SOC of ESS	%
SOC_{low}	low SOC limit for ESS controller	%
SOC_{target}	target SOC for ESS controller	%
SR	set-reset, used in the description of an SR flip-flop	-
t	time	s

$\boldsymbol{T}$	One full period in which one charge and one discharge event occurs for the ESS	s
$\boldsymbol{t_{chg}}$	time taken for ESS to charge from SOC_{low} to SOC_{high}	s
$\boldsymbol{T_{coolant}}$	ICE coolant temperature	°C
$\boldsymbol{t_{dis}}$	time taken for ESS to discharge from SOC_{high} to SOC_{low} (s)	s
$\boldsymbol{T_e}$	ICE torque	Nm
$\overline{T}_e$	vector of length m containing the ICE torques	Nm
$\boldsymbol{T_{e,best}}$	vector used to record the optimal torque for the optimal operating line at individual points with respect to P_{e,map_index} and $\omega_{e,best\_index}$ (Algorithm 3.1)	Nm
$\boldsymbol{T_{e,max}}$	maximum ICE brake torque	Nm
$\overline{T}_{e,\max-map}$	vector that contains interpolated values of measured torque for use in calculating the optimal operating line (Algorithm 3.1)	Nm
$\overline{T}_{e,opt}$	vector containing the ICE output torque of the optimal operating line for VSC (Algorithm 3.1)	Nm
$\overline{T}_{e,Pe,map}$	vector containing ICE output torque at power and speeds relative to $P_{e,map}$ and $\omega_{e,map}$ respectively (Algorithm 3.1)	Nm
$\boldsymbol{T_{e,Pe,map\_index}}$	for loop variable defined for evaluating the calculation of the optimal operating line as the ICE speed increases (Algorithm 3.1)	-
$\boldsymbol{T_{in}}$	input torque for definition of drivetrain component operations	Nm
$\boldsymbol{T_{ICE}}$	Temperature of ICE	°C
$\boldsymbol{T_L}$	drivetrain load torque	Nm
$\boldsymbol{T_{m,max}}$	vector containing the maximum motoring torque of M/G during propulsion	Nm
$\boldsymbol{T_{m/g}}$	M/G torque	Nm
$\boldsymbol{T_{max,cont}}$	maximum continuous torque for M/G	Nm
$\boldsymbol{T_{max,peak}}$	maximum peak torque for M/G	Nm
$\boldsymbol{t_{off}}$	ICE off period	s
$\boldsymbol{t_{on}}$	ICE on period	s
$\boldsymbol{t_{on,min}}$	minimum ICE on time	s
$\boldsymbol{T_{out}}$	output torque for definition of drivetrain component operations	Nm
$\boldsymbol{T_t}$	tractive torque	Nm
$\boldsymbol{t_{trip}}$	estimated time of arrival or trip time for driving	s
$\boldsymbol{T_{tstat}}$	thermostat threshold temperature	°C
$\boldsymbol{T_{\eta e,max}}$	torque at which ICE achieves maximum efficiency	Nm
UDDS	Urban dynamo driving schedule	-
US06	US Environmental Protection Agency's supplemental FTP	-
$\boldsymbol{V}$	vehicle velocity	m/s
$\boldsymbol{V_1}$	Vehicle velocity threshold for ICE operation when SOC is greater than the target SOC in the Toyota Prius 2010 model in Section 5.7.1	m/s

Glossary of Terms

V_2	Vehicle velocity threshold for ICE operation when SOC is less than the target SOC in the Toyota Prius 2010 model in Section 5.7.1	m/s
V_3	Vehicle velocity threshold for ICE to remain on	m/s
V_{av}	average vehicle velocity	m/s
V_{bus}	bus voltage for the electrical network of the considered vehicle configuration	V
V_{ess}	terminal voltage of the ESS	V
V_{max}	maximum vehicle velocity	m/s
$V_{m/g}$	voltage of the M/G	V
V_{OC}	open circuit voltage of ESS model	V
V_{ZEV}	vehicle velocity below which a vehicle operates as a zero emissions vehicle	m/s
VSC	variable speed control	-
WVUCITY	West Virginia city driving schedule	-
X_i	calculated or predictive value for the MAPE	-
Y_i	measured value for the MAPE	-
z	quantity representing the effect of temperature on fuel, HC, NO, CO emissions	-
Z	number of teeth on a gear in between the ring gear of the PGS in the Toyota Prius and drive wheels (six gears in total)	-
Z_R	number of teeth on the ring gear	-
Z_S	number of teeth on the sun gear	-
Z_Y	number of teeth on the carrier (yoke) gear	-
α_{av}	1st variable for determining estimated average tractive power requirement of drive cycles with respect to $\bar{a}_j$	-
α_j	individual drive cycle alpha value	-
β_{av}	2nd variable for determining estimated average tractive power requirement of drive cycles with respect to $\bar{a}_j$	-
δ	mass factor	-
δ_1	constant representing the effect of rotational inertia of wheels in the mass factor	-
δ_2	constant representing the effect of rotational inertia of rotating components in the mass factor	-
ΔE	input energy threshold for consideration of ICE on/off times	kJ
ΔFC	change in fuel consumption at end of driving	L/100km
$\Delta\eta_{e,max}$	incremental value for calibrating the high efficiency region	%
$\eta_{\#,av}$	Represents average efficiency of a component, where '#' is replaced with the appropriate component label (for example $\eta_{e,av}$ is the average ICE efficiency)	%
η_c	coulomb efficiency of ESS	%
η_{chg}	ESS charge efficiency	%
η_d	final drive efficiency	%
η_{dis}	ESS discharge efficiency	%
η_{DT}	drivetrain efficiency	%

η_e	ICE efficiency	%
$\overline{\eta}_e$	array containing the ICE efficiency of operation, indexed horizontally by $\overline{T}_e$ and vertically by $\overline{\omega}_e$ having dimensions *n* by *m*	%
$\eta_{e,low}$	efficiency below which ICE operation is undesirable	%
$\eta_{e,max}$	maximum efficiency of ICE	%
$\overline{\eta}_{e,\omega e,map\_index}$	vector containing interpolated values of ICE operating efficiency with respect to $\omega_{e,map}$ and $T_{e,Pe,map}$ and indexed by ω_{e,map_index} for each iteration of the two for loops. (Algorithm 3.1)	%
$\eta_{e,\omega e,map\_index\_max}$	the maximum efficiency in the $\eta_{e,\omega e,map\ index}$ vector with respect to the current value of ω_{e,map_index} (Algorithm 3.1)	%
$\overline{\eta}_{e,\omega e,map\_index\_norm}$	vector containing the normalised values resulting from $\eta_{e,\omega e,map\_index}$ with respect to $\eta_{e,\omega e,map\_index\_max}$ (Algorithm 3.1)	%
$\eta_{m/g}$	M/G efficiency	%
η_{rw}	efficiency of energy transfer from the ring gear to the drive axle	%
η_{sr}	efficiency of energy transfer from the sun gear to the ring gear	%
η_{sys}	system efficiency	%
η_t	transmission efficiency	%
η_{tb}	combined efficiency of rear transmission and final drive	%
η_{tf}	combined efficiency of front transmission and final drive	%
η_{yr}	efficiency of energy transfer from the yoke gear to the ring gear	%
ρ	air density	kg/m^3
ρ_f	density of the fuel used	g/L
σ^2	Variance in fuel consumption	L/100km
ω_{dw}	drive wheel speed	rad/s
ω_{dwn}	fixed gear transmission input downshift speed	rad/s
ω_e	ICE speed	rad/s
$\overline{\omega}_e$	vector of length n containing the ICE speeds	rad/s
$\overline{\omega}_{e,best}$	vector used to record the optimal speed for the optimal operating line at individual points with respect to P_{e,map_index} and $\omega_{e,best\_index}$ (Algorithm 3.1)	rad/s
$\overline{\omega}_{e,map}$	vector for the ICE speed with the defined *resolution*, interpolating the measured speeds	rad/s
ω_{e,map_index}	for loop variable defined for evaluating the calculation of the optimal operating line as the ICE speed increases (Algorithm 3.1)	-
$\overline{\omega}_{e,opt}$	vector containing the ICE output speed of the optimal operating line for VSC (Algorithm 3.1)	rad/s
$\omega_{e,rated}$	ICE rated speed	rad/s
ω_{idle}	ICE idle speed	rad/s
ω_{in}	input speed for definition of drivetrain component	rad/s

	operations	
ω_L	drivetrain load speed	rad/s
$\omega_{m/g}$	M/G speed	rad/s
ω_{out}	output speed for definition of drivetrain component operations	rad/s
ω_P	propulsion device speed	rad/s
$\omega_{P\eta e,low}^{-}$	speed at which ICE achieves minimum power for the high efficiency region (Algorithm 4.1)	rad/s
$\omega_{P\eta e,low}^{+}$	speed at which ICE achieves maximum power for the high efficiency region (Algorithm 4.1)	rad/s
ω_t	tractive speed	rad/s
ω_{up}	fixed gear transmission input upshift speed	rad/s
$\omega_{\eta e,max}$	speed at which ICE achieves maximum efficiency	rad/s

CHAPTER ONE

Introduction

1.1 Background

Recent energy reports identify that the World is facing an energy crisis, due to the fossil fuel reserves nearing depletion within the next 50 years [1]. Increased energy consumption is projected for the period 2010 to 2040 due to strong economic growth and expanding populations in nations outside the Organisation for Economic Cooperation and Development (Non-OECD) [2]. OECD nations on the other hand have strict energy policies in place to help minimise energy usage and therefore projected increases to energy consumption are less. The trend of the World's increased energy requirements for the OECD and non-OECD is revealed in Figure 1.1, with non-OECD nations projected to share in more than 85% of the increase to the World's energy needs.

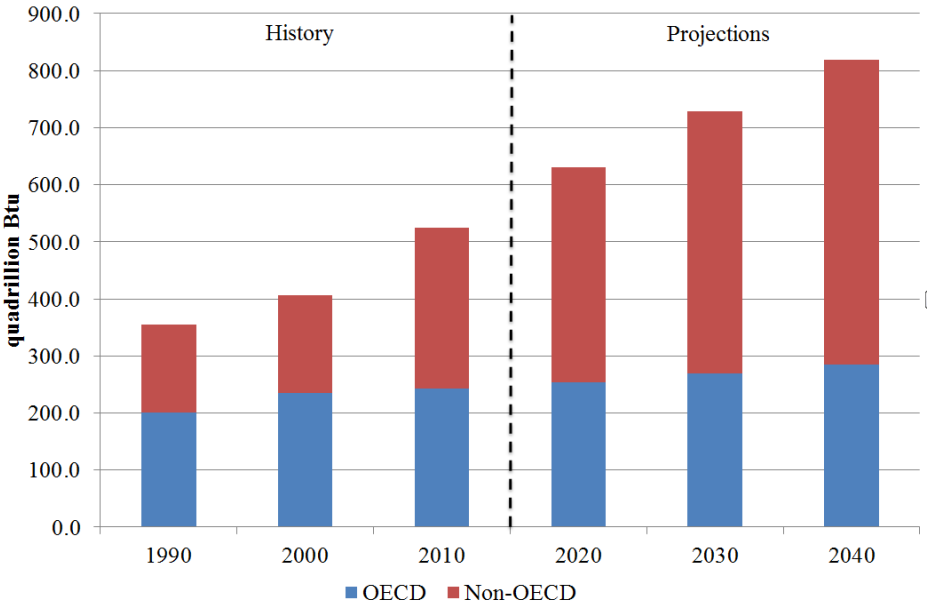

Figure 1.1 – World energy consumption, 1990 to 2040 [2].

The transportation sector accounts for up to 20% of the World's annual energy consumption, which is the second largest percentage amongst the major energy sectors [2]. Figure 1.2 from the International Energy Outlook 2013 report [2], indicates that the consumption of liquid fuels will continue to be the major contributor to the World's energy consumption. The International Energy Outlook 2013 report also identifies that the transportation sector held a share of 55 percent of the World's total liquid consumption in 2010 with a projection to

increase to 57 percent by 2040. This is relative to a 1.1 percent growth rate in the total energy consumption of the transportation sector between 2010 and 2040.

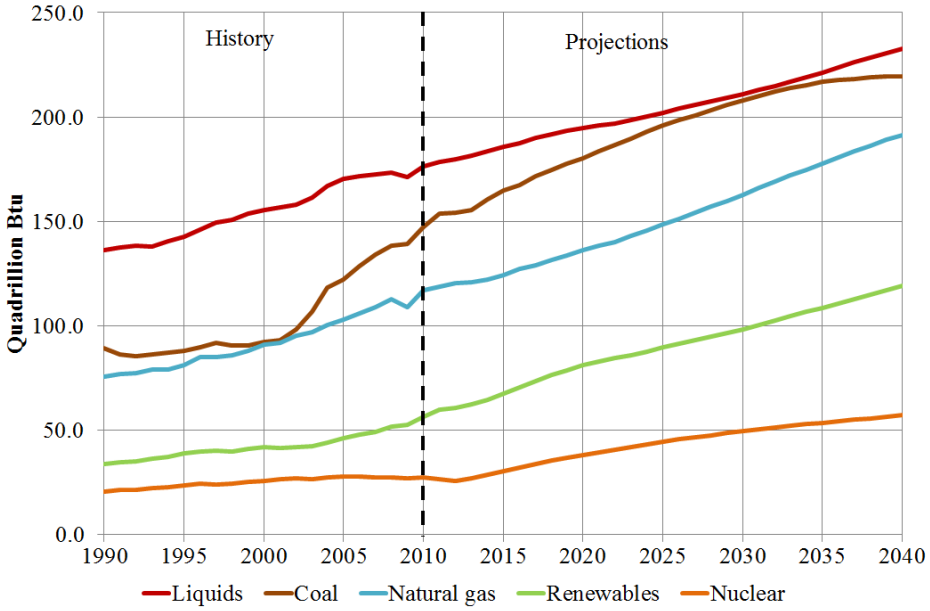

Figure 1.2 – World energy consumption by fuel type, 1990 to 2040 [2].

In Australia the transportation sector accounts for 37.1% of Australia's total energy consumption [3], the majority of this being sourced from liquid fuels. Therefore alternative energy sources are highly sort after to ensure sustainability for future generations. Here energy smart vehicles (ESVs) are investigated in the development of an energy management system (EMS) to meet the requirements of everyday driving. An energy smart vehicle as an alternative to the conventional vehicle is one that attempts to maximise energy utilisation, minimise fossil fuel consumption or reduce emissions production.

ESV applies to three categories of transportation currently considered to have the potential of competing with conventional internal combustion engine (ICE) vehicles. The three vehicle categories include electric, hybrid electric and plug-in hybrid electric. Various vehicle configurations are realised by the integration or omission of vehicle components and devices [4]. The current aim for all ESV is to achieve high performance with little to no impact on the environment [5]. The various means for achieving high performance identify a broad spectrum for the objectives featured in this research program with optimisation, energy efficiency and utilisation, and reuse and recycle.

A significant number of research papers detailing the reduction of fuel consumption in transportation offer the replacement of the conventional ICE with a form of electric propulsion [1, 4-17]. This design approach results from the high efficiency seen in energy storage systems (ESSs) and motor/generators (M/Gs) during transient loading in power systems. An initial comparison observes the average ICE efficiency being less than 30% [18]

compared with the average M/G and ESS efficiency of greater than 80% [5, 6]. The actual improvement to the energy consumption by transition to electric propulsion devices in the transportation industry is much less from a whole systems point of view [7]. Bossel compares the use of hydrogen fuel against the use of electricity in [6]. From the comparison the efficiencies of electricity generation to ESS are given as shown in Figure 1.3.

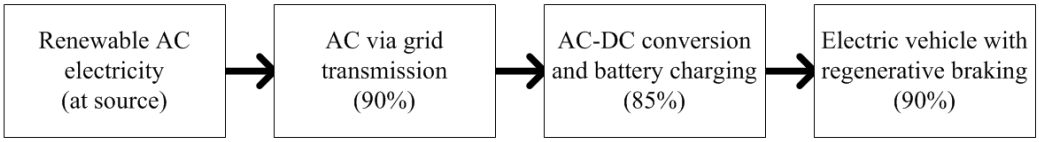

Figure 1.3 - Efficiencies of electric grid as identified in [6].

The comparison of Figure 1.3 assumes that all electrical energy comes from renewable energy sources with transmission efficiencies of up to 76.5%. This reduces the efficiency of electric vehicles (EVs) to between 61.2% and 68.85% at 80-90% efficiency during driving. Bossel has referred to the 100% renewable energy sources as a theoretical example in comparing the inefficiency of fuel cell vehicles to EVs. Note that the total average efficiency of fuel cell vehicles as determined in Bossel's example is less than 30%, this is also supported by Williamson et al in [18]. The EV and fuel cell vehicle are discussed further in Sections 2.2.2 and 2.2.3 respectively. The example referred to is considered an ultimate scenario if we transitioned towards replacing all fossil fuelled power generation with renewable power generation. This is a controversial debate of the EV with respect to greenhouse gas emissions production where EV enthusiasts declare the EV a zero emissions vehicle [19-22].

Unless governments convert all power stations to renewable energy, electric propulsion is still reliant on fossil energy [1]. Figure 1.4 identifies the projected World net electricity generation by energy source. Considering the previous example, renewable energy in 2010 made 20.6% of the World's net generated electricity with the expectation that it will make up 24.6% in 2040 [2]. This is excluding nuclear which is classified as renewable however there are concerns for the cost and sustainability of nuclear power [1]. Figure 1.4 shows that at least 60% of the World's net electrical energy is sourced from fossil fuels leading to the conclusion that EVs ultimately relocate fossil fuel consumption and emissions from the driving stage to the electricity generation stage. It is also noted that 60 to 80% of the World's net renewable energy is sourced from hydropower over the period 2010 to 2040. Hydropower requires mountainous regions and high annual rainfalls to sustain continuous power generation [23]. This limits the availability of such renewable energy sources, and highlights concerns for areas that do not have the capability for hydropower.

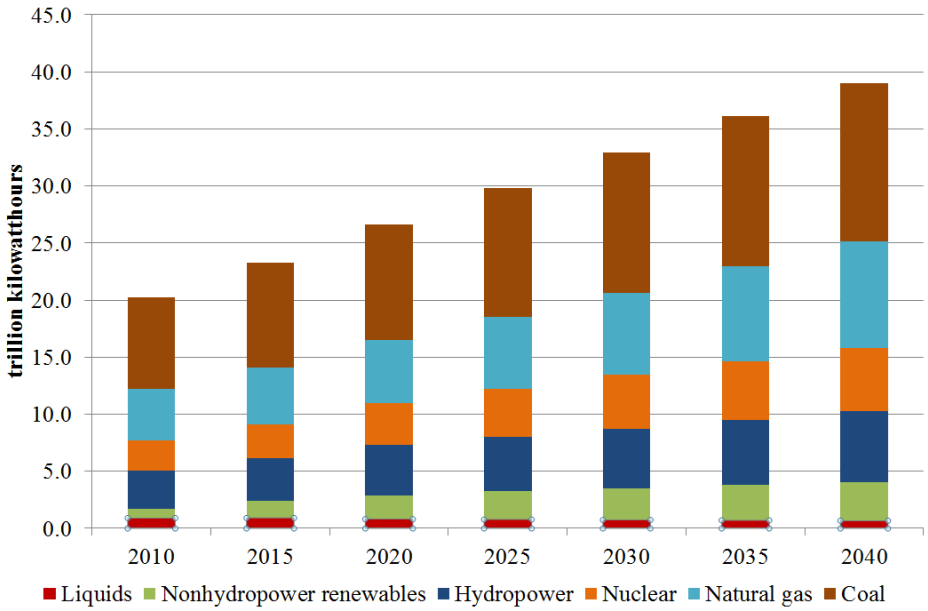

Figure 1.4 – World net electricity generation by energy source [2].

In light of the limited availability of hydropower, Australia's electricity industry energy consumption at the end of 2009-10 was sourced from three main areas. 75% was sourced from black and brown coal, 15% from gas and up to 10% from renewable energy sources [3]. The renewable energy sources contributing to the electrical energy consumption was increasing at a steady rate of 1% for the five years leading up to 2009-2010 [3]. The Australian Government through the introduction of the carbon tax in 2012 [24] and related emissions reforms [25], expect the total renewable energy generation to exceed 20% by 2020, which still leaves up to 80% electricity generation from fossil energy sources. This study suggests that the use of electricity as the main energy source in transportation will not solve the World's reliance on fossil fuels. The aim for ESVs is therefore the smart utilisation of these energy resources until the World is no longer dependent on fossil fuel resources.

1.2 Motivation

As opposed to providing a solution that requires the development, designing and marketing of a completely new product, innovation will provide a road map for easing the World into sustainable vehicles. The use of ESVs provides a pathway for the transportation industry to reduce the consumption of fossil fuels. Initially in countries like Australia, increased use of ESVs will relocate the increasing demands of fossil resources from oil reserves to coal reserves. Following the implementation of the infrastructure to support ESVs there is an expectation for increased renewable energy penetration of the electrical network, eventually sourcing all electrical energy from renewable sources [1]. This transition to renewable energy sources in combination with the preparation of ESVs provides the foundations for a sustainable future in the transportation sector.

In preparation for this transition to renewable energy sources a reduction in the fossil energy consumption of both oil and coal reserves is realised with the efficient utilisation of energy. With respect to existing literature discussing ESVs there are many powertrain and drivetrain configurations having various advantages and disadvantages (e.g. [4, 11, 15, 19, 26-34]). A comparison of the results of such literature leads to the consideration for the best performing ESV for use in this investigation. Then through adapting the novel EMS controller researched and developed in this program to new and existing ESV topologies, emissions and fuel consumption resulting from every day driving are reduced [1, 4, 20, 35].

The performance of vehicles is quantified using average fuel consumption (or fuel economy) and emissions production relative to standardised drive cycles [5, 8, 33, 36]. Standardised drive cycles represent the potential tractive load requirements of vehicles during real-world city (urban) and highway (extra urban) drive scenarios. In addition to the fuel consumption and emissions, component efficiencies, drivability and noise, vibration and harshness, are examined for a more detailed analysis [37, 38]. The main concern for ESV however is the reduction of fuel consumption and emissions [11, 38-41].

As mentioned the standardised drive cycles help in this design phase however, additional requirements outlined by bodies such as the Partnership for New Generation Vehicles and the US Environmental Protection Agency ensure that vehicle's meet minimum standards. These minimum standards include fuel consumption (fuel economy), emissions targets, acceleration requirement (0-100km/h in less than 12 seconds), drive range (greater than 610 km), noise, vibration and harshness, and minimum useful life (160,000 km) [42]. In addition, for the case of fuel consumption requirements vehicles are categorised according to tests completed by the Environmental Protection Agency [43], which aid consumers in their choice of vehicle. These strict minimum standards for the development of vehicles set the bench mark for future vehicle design and evaluation.

The designing of ESVs initially includes sizing, integration and configuration of components relative to the power and energy density requirements of driving. For best performance in vehicles high power and energy densities are desirable [20], hence the use of ICE in conventional vehicles. The obvious issue with ICE is the fact that they consume fossil fuels and produce unwanted levels of emissions. Power density ensures an energy source can meet high transient demands of the drivetrain while energy density determines the length of time the source will continuously supply an average power to the load. Energy density therefore determines the drive range of a vehicle. The problem with alternative energy sources in comparison to the fossil fuels used in ICE is that they have either limited power density or energy density. Battery banks are an example of the ESS used in ESVs, and while they have sufficient power density for drive load requirements they lack energy density [44]. Fuel cells

on the other hand have high energy density with low power density leading to the limited potential for sustaining high transient load requirements [39, 45]. The common design principle is to pair a high energy density, low power density source with a low energy density, high power density source hence the consideration for hybrid vehicles [38]. For optimal performance the design must match the control strategy employed by the EMS.

The control strategy defines the overall objective for the EMS, for example maintaining the state of charge (SOC) of a battery bank , or minimising fuel consumption [5]. There are a large number of control techniques utilised in literature to implement the control strategy. An example of some of these techniques include dynamic programming [8, 33], stochastic dynamic programming [33, 36], the equivalent consumption minimisation strategy [46], adaptive-equivalent consumption minimisation strategy [36, 47], and rule based or finite state machine [34, 41]. With the help of research such as that presented by Wirasingha et al [8], recent control strategies and techniques are categorised and compared for advantages and disadvantages in ESVs [48]. This analysis lead to a reduced scope of control strategies best suited for investigation as applied to ESVs. A general conclusion from such analysis identifies optimisation based blended controllers as having the greatest potential for reducing the consumption of fossil energy reserves.

The problem however remains as to which EMS design and control strategy to implement. ESVs through the developed EMS are required to meet the requirements of everyday driving efficiently given the identified transportation standards. This thesis identifies an EMS for ESVs that minimises fossil fuel consumption whilst acknowledging the transportation standards outlined above.

1.3 Aim and Scope

Previous literature discussing ESVs is investigated in an attempt to determine the optimal EMS design and control strategy. Optimality of the design in EMS pertains to the sizing, integration and configuration of components that provide the best performance as well as meeting the power and energy density requirements of driving. Selection of the EMS control strategy is dependent on factors such as computational complexity, flexibility in control, controller calibration and portability each having various advantages and disadvantages in the performance of the ESV. The characteristics of design and control of EMS in ESV are then quantified through a comparison of overall performance, using fuel consumption (and thereby emissions) reductions, impact on drivability and efficiency of operation to evaluate the benefits.

1.3.1 Objectives

1. Determine a robust easily implementable approach to EMS control that will improve the performance of new and existing vehicles.
2. Improve the average efficiency of operation of the ICE with respect to the constraints of the EMS inherent on hybrid electric vehicles (HEVs) and plug-in hybrid electric vehicles (PHEVs) during driving.
3. Determine a predictive controller to aid with energy management decisions in the EMS of HEV and PHEV.

1.3.2 Research Questions

Below is a list of research questions determined throughout the research program. The first 6 questions were asked in the initial stages of the research program with the final 3 questions being refined from the initial investigations. The selected format for the listed questions identifies a chronological approach in the formulation of the scope as the research progressed. The initial research questions help set the target for determining any gaps in the existing research base:

1. What is the best type of ESV to solve the World's reliance on fossil fuels in the transportation industry? Relevant to:
    a. Vehicle configuration – how components are arranged and therefore how they interact on a vehicle
    b. The powertrain – e.g. ICE, fuel cell or all electric?
    c. The drivetrain – e.g. fixed gear transmission or continuously variable transmission (CVT)?
2. What is the optimal sizing of powertrain and drivetrain components in order to meet the energy demands of everyday driving?
3. What are the recent trends in control strategies and how do they improve the performance of ESVs?
4. Where in the ESV is there the most potential for improvement?
5. Is there an EMS applicable to both new and existing vehicles?
6. Is there an acceptable test bench for developing and evaluating a novel EMS?

Following the above investigation the literature review identified three more research questions. Questions 7 to 9 outline the main research objectives identified above and provide the main focus for the research program.

7. Is there a robust, computationally low and easily implementable method for EMS control that will improve the performance of new and existing vehicles?
    a. Resulting from questions 3 and 5 and discussed in Section 2.5

8. Will maximising the efficiency of operation of the ICE lead to fuel consumption reductions?
    a. Resulting from question 4 above, with the discussion and solution featured in Chapter 4.
    b. The ICE is selected as the primary propulsion device, as a result of question 1 above, which is discussed in Section 2.2.4.
    c. The ICE has the lowest average efficiency of operation in comparison to other propulsion devices featured in ESVs.
9. Having determined an approach to real-time optimisation based blended control is there further potential for improvement using predictive control?
    a. Resulting from questions 3 to 5 and question 8 as discussed in Section 2.5 and Section 4.9.6 with the solution featured in Chapter 5.

1.3.3 Assumptions

For the analysis presented in Chapters 3, 4 and 5 the following assumptions hold:

1. Steady state operation of powertrain and drivetrain components.
2. During simulation of test vehicles, the frequency of driving data is one second. Any transients in the mechanical and electrical networks higher than 1 Hz are ignored.
3. Hot operation of the ICE and associated drivetrain components.
4. Auxiliary loads included in the measured data of test vehicles as modelled in Chapter 3 (such as heating ventilation and air conditioning, drive-by-wire and lighting loads), in simulation are integrated in the losses of components (such as the ICE or M/G efficiency).
5. Optimisation in this research program is conducted for the tank to wheels case, considering that efficient utilisation or reduction of fossil energy consumption is independent of the losses incurred by sourcing the electrical or chemical energy stores.
6. Power electronic converters are referred to as black boxes, such that steady state control of the electrical components is achieved with losses being represented in the efficiencies of the power sources they control.
7. Tractive power calculations of vehicles are considered with respect to vehicle velocity only. This analysis therefore excludes road gradients which can otherwise add additional loads to standardised drive cycles [5]. The addition of road gradients would produce an increase in the final fuel consumption proportionate to the weight of the vehicle and is therefore not influenced by the designed controller.

1.4 Contributions of Thesis

Relative to the research objectives identified in Section 1.3.1 the main contributions of this thesis include:

1. Identification of the power-split connected PHEV (including an ICE and two M/Gs coupled to the drive wheels via a planetary gear set (PGS) that acts as a CVT) as the ESV having the most potential for satisfying the World's transportation energy requirements .
2. An approach to analysing measured data of existing ESVs for increased understanding of their design and associated control strategies and for the purpose of creating accurate test benches in simulation.
3. A novel high efficiency controller in ICEs that helps in the decision process of EMSs utilising blended charge depletion or charge depletion/charge sustenance strategies in PHEVs.
4. A novel method for predictive control in the EMS based on the high efficiency controller of the ICE for increased utilisation and efficacy of the stored energy in ESSs of PHEVs.

Following the main contributions there are a number of secondary contributions including:

- A control strategy applicable to new and existing ESVs, specifically parallel and power-split connected topologies.
- An approach to achieving autonomous control of the EMS with respect to average vehicle velocity and acceleration/deceleration requirements of planned driving routes.
- A method for predicting tractive energy requirements of driving given the average vehicle velocity and average absolute acceleration/deceleration, representing the varying driver behaviour and traffic conditions.
- Comparison and improved understanding of a mathematical approach to tractive power calculation with respect to measured data
- A method for minimising the number of ICE stop/starts considering the SOC swing of the ESS. This is used as the basis for the predictive controller.
- A novel approach to analysing the performance of PHEV, such that fuel consumption reductions are calculated with respect to SOC corrections using the ICE and the grid.
- An approach to sizing the components of ESV, in particular a 2 by 2 power-split plug-in hybrid electric vehicle.

- Development of an approach to control system design regarding the limitations of the powertrain in comparison to the steady state and transient requirements of driving.
- Development of three test benches for analysing the performance of EMS control strategies in simulation.
- An overview of the factors that contribute to the improved performance of EMS control strategies relative to the latest research, for example:
    - Low computational requirement
    - Flexibility in control
    - Minimal calibration requirement
    - High portability
- An overview of the performance parameters which are important in the analysis of ESVs and thereby utilised to procure accuracy in simulation, for example:
    - Powertrain and drivetrain specifications
    - ICE on/off operation
    - ESS charge and discharge periods
    - Input and output energy, overall efficiency and average fuel consumption

1.5 Organisation of Thesis

Chapter 2 Literature review

This Chapter defines the available ESVs described in literature, the components inherent in each powertrain and drivetrain and how they have been perceived to aid with fuel consumption and emissions reduction. This discussion helps to highlight the various advantages and disadvantages of each type of ESV. For each of the ESVs there are specific modes of operation identified in literature that outline the principles for control of the EMS. The discussion relates the powertrain and drivetrain components to the vehicle configuration as a means to compare the operation and control of ESVs. Having determined the overall consideration for ESVs existing vehicles are discussed to emphasise the performance outcomes found in technical papers. Following the consideration for ESV design the control strategy highlights the means to achieve best performance. In order to relay the achievements to the improvement of control strategies in EMS, the method for categorisation in [8] is utilised with respect to recent literature. This approach provides a necessary understanding of the existing control strategies and techniques.

Finally a method for the sizing of components is discussed with respect to the development of an experimental setup. Initially the experimental setup was to be used as the test bench,

however, budget constraints restricted testing to software instead. This investigation into the sizing of components reveals important considerations in the design of the EMS.

Chapter 3 Modelling of energy smart vehicles

This Chapter identifies three methods for simulation; backward, forward and combined backward/forward facing approaches and the associated benefits of using these types of simulation packages. It then defines three existing vehicles to be modelled in the advanced vehicle simulator (ADVISOR [49]) software package which are to be utilised as the test benches for the developed control strategies in this thesis. Acknowledging the methods used for confirming tractive power requirements and drivetrain specifications, measured data of three commercially available vehicles is utilised in developing the three test benches. In addition the modes of operation of the ESV and thereby the potential control strategies utilised are revealed through a discussion of the relationships between torques and speeds of powertrain and drivetrain components. In particular focus is given to the operation of the ICE since this is the main contributor to the total energy consumption in the considered test vehicles. Finally the vehicle component models and the control strategies of each of the test vehicles are defined and verified with respect to the measured data.

Chapter 4 Design of a high efficiency controller in PHEV

Chapter 4 introduces previously used methods specific to the proposed EMS controller. In particular the discussion refers to the power balancing strategy (PBS) and variable speed control (VSC) of the ICE. The convention for requested and measured signals is established with respect to a general EMS controller in HEV and PHEV. The proposed high efficiency control is defined through the use of combined PBS and VSC while considering the operation of the ESS. Constraints for the proposed controller are described and a calibration procedure is identified. Implementing the novel controller on the three test benches developed in Chapter 3, the performance is evaluated with respect to fuel consumption reductions and the impact of the developed controller on drivability. Further analysis of the model identifies the potential for improvement by varying the calibration of the high efficiency controller for different drive cycles.

Chapter 5 Design of a predictive controller for PHEV

In this Chapter a method for predicting the energy requirements of a planned driving route is defined. Using the defined high efficiency region from Chapter 4 as the relationship between tractive power requirement and powertrain performance limitations, calibration of the high efficiency controller is achieved on-the-go. Referring to the relationship identified in Ehsani et al [5], a method for approximating the energy requirements of a drive cycle is determined as the means for calibrating the high efficiency controller. This calibration relies on the

general use of the ICE and ESS over the drive cycle such that component limitations restrict the ICE on/off times. A novel method of control is realised and employed as the basis for implementing a predictive control strategy in the Toyota Prius 2010 model developed in Chapter 3. Finally, the novel predictive controller is evaluated with respect to fuel consumption, drivability, energy utilisation and the effect of prediction errors on the performance of the vehicle.

Chapter 6 Conclusions

The outcomes of this research are summarised with respect to the research questions of Section 1.3.2. This approach was utilised in an attempt to maintain focus for the thesis presentation and to aid the reader with identifying the scope and contributions of the research. In addition future research outcomes are considered as a result of the work completed in this research program.

1.6 Publications

Journal

S. Overington and S. Rajakaruna, "High Efficiency Control of Internal Combustion Engines in Blended Charge Depletion/Charge Sustenance Strategies for Plug-in Hybrid Electric Vehicles," *Vehicular Technology, IEEE Transactions on*, 2014 (accepted).

S. Overington and S. Rajakaruna, “Optimal Predictive Control of the ICE in a Plug-in Hybrid Electric Vehicle using a Novel Energy Management Strategy,” *Vehicular Technology, IEEE Transactions on*, 2014 (submitted for review),

Conference

S. Overington, S. Rajakaruna, & S. Islam, "Design of the Experimental Setup for a Plug-in Hybrid Electric Vehicle," in *Australasian Universities Power Engineering Conference 2012*, Bali, Indonesia, 2012.

S. Overington, & S. Rajakaruna, "Review of PHEV and HEV operation and control research for future direction," in *Power Electronics for Distributed Generation (PEDG 2012)*, Aalborg, Denmark, 2012.

S. Overington, & S. Rajakaruna, "A modified method for the sizing of the plug-in hybrid electric vehicle propulsion devices," in *Australasian Universities Power Engineering Conference (AUPEC)*, 2011, pp. 1-7.

S. Overington, S. Rajakaruna, S. Islam, & T. Chandratilleke, "Investigation of feasibility of integrating alternative energy sources in a roadside assistance vehicle," in *Australasian Universities Power Engineering Conference (AUPEC)*, 2010, pp. 1-7.

CHAPTER TWO

Literature Review

2.1 Introduction

The focus for the research initially was to define the ESV as presented in technical publications. There is a significantly large research base relative to ESVs especially in the area of design and control of the EMS, as this Chapter identifies. The discussion begins with an overview of electric, hybrid electric, fuel cell and plug-in hybrid electric vehicles and the relationships between the propulsion devices and drivetrain components. Factors affecting the relationships between on-board components and the propulsion devices include vehicle configuration, technical specifications and constraints of the components included. The specific modes of operation are dependent on the components selected for an ESV, the HEV however provides an insight into the typical modes utilised. Following this definition of the ESV, the performances of existing vehicles are examined as a means for comparison of expected operation. This helps clarify the selection of the ESV that has the greatest potential for reducing the transportation industry's reliance on fossil fuels in the long term whilst providing a more efficient alternative in the short term. As a result of this discussion the power-split PHEV demands attention for use as the best alternative to the conventional vehicle.

Performance of the control strategy utilised in the EMS of the selected vehicle relies on four factors acknowledged in a number of research papers [7, 36, 46]. These four factors are the computational complexity, calibration requirement, flexibility in control and portability. Here the categorisation of control strategies discussed in Wirasingha et al [8] was referred to for distinguishing the potential benefits of controllers and strategies featured in recent literature. The four categories include hybrid, multimode, rule-based blended and optimisation-based blended controllers. In addition there are sub-categories that help to provide further insight into the performance of ESVs. This process of analysing control strategies lead to the developement of real-time optimisation based blended controllers in the selected ESV.

Note that this literature review offers a discussion toward identifying an ESV that is best suited for satisfying the World's transportation needs, however, the analysis completed in the following Chapters are applied to existing vehicles. This decision was realised during the investigation of an experimental setup for the selected ESV, which ultimately exceeded the

allocated budget for the project. Instead models for simulation are developed and utilised as the test benches such that real-world limitations are acknowledged and implemented.

2.2 Energy Smart Vehicular Technology

The term ‘energy smart’, refers to those vehicles that have reduced the overall energy consumption of travelling from one destination to another in comparison to the conventional vehicle. The category of a conventional vehicle describes a mode of transportation that uses fossil fuel as the primary energy source. The conventional vehicle as introduced in this Section, typically relies on an ICE to convert fossil fuel energy into mechanical energy [5]. Currently there are a number of different types of ESVs presented in journal articles [9, 11, 33, 50-53]. In particular the aim is to reduce the reliance transportation has on fossil resources and thereby mitigate greenhouse gas emissions production [1]. This means integrating or replacing the fossil fuel power source (i.e. ICE) with alternative power sources [6]. Alternative power sources include ESS, M/G, and renewable energy sources [7]. This Section introduces the energy smart vehicular technologies available for reducing the fossil resource reliance of the transportation sector.

2.2.1 Conventional Vehicle

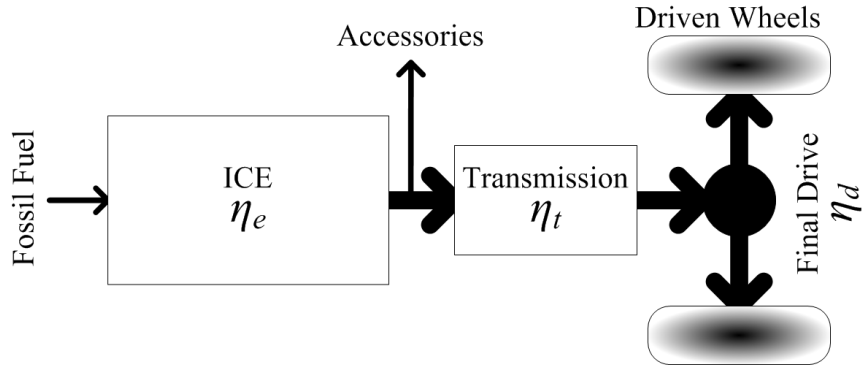

Figure 2.1 – Conventional powertrain, identifying main components from stored fuel to driven wheels. Arrows indicate energy flow between components.

Powertrain

The conventional vehicle describes the most common powertrain utilised for transportation today [5]. Referring to Figure 2.1 the ICE of a conventional vehicle provides all load power requirements during driving. The energy available on the output shaft of the ICE is consumed by the electrical and mechanical loads of the vehicle. Accessory loads (Accessories in Figure 2.1) of the vehicle fall into the category of electrical and mechanical loads that consume power in addition to the driving load requirements of the vehicle. The accessory loads include the instrumentation cluster, heating ventilation and air conditioning, power steering, water pump etc., that account for a small percentage of the vehicle load

requirements [54]. Mechanical drive loads of the conventional vehicle relates to the use of the ICE as the primary propulsion device.

Internal Combustion Engine

The mechanical loading of the vehicle is determined by the amount of energy required to overcome the aerodynamic drag, rolling resistance, grading resistance and drivetrain inertial resistance, which are proportional to the accelerator pedal position as determined by the driver [5]. The means for estimating such loads are discussed in Sections 2.6 and 3.4. There are two types of ICE utilised in conventional vehicles, the spark ignition (SI) and compression ignition (CI) ICE. Typically SI ICE are run on gasoline or natural gas fuels and CI ICE utilise diesel [54]. CI ICE are up to 10% more efficient than SI ICE however greenhouse gas emissions resulting from CI ICE are much greater [55, 56]. Fossil fuel is passed into the ICE, generating mechanical output power at efficiencies up to 40% [5]. The main component for the losses experienced in the conversion of the energy from chemical (fossil fuel) to mechanical (ICE output shaft) energy is the thermal loss [23, 54]. In addition combustion, volumetric and mechanical losses are present in the conversion process [54]. Identified losses are represented by the efficiency of the ICE using the symbol η_e in this thesis.

Average efficiencies of the ICE are especially low compared to electric machines for the propulsion of vehicles during the load requirements of normal driving. A contributing factor to the low average efficiency of the ICE is the need for the ICE power rating to achieve acceptable levels of acceleration. This requirement leads to a much higher ICE power rating than the average power requirement for normal driving. This higher power rating offsets the optimal efficiency region with respect to the average power requirement of the ICE, leading to greater fuel consumption. Typical average efficiencies for converting fossil fuel energy to mechanical energy using ICE are less than 25% [18]. This low average efficiency leads to high consumption of fossil fuels, with light weight conventional vehicles consuming greater than 6 L/100km and mid-sized conventional vehicles greater than 10 L /100km [43].

Transmission

The transmission allows for varying load torques and speeds to be delivered from the ICE to the driven wheels. The majority of conventional vehicles utilise multi-gear transmissions [5]. The need for the multi-gear transmission is to increase the torque available at the wheels at low vehicle speeds, while allowing ICE operation at high vehicle speeds [5]. The final drive increases the ratio between the transmission and driven wheels such that gear ratios of the transmission are reduced. This is to save space for the otherwise bulky transmission and to reduce the stresses on input and output shafts of the transmission [54].

More ICE power does not necessarily mean better performance in conventional vehicles. The transmission determines a number of performance characteristics during driving [5, 54]. The performance characteristics include torque available at the wheels, ease of driving, towing capability, acceleration and fuel economy. In the conventional vehicle, multi-gear (or fixed gear [34]) transmissions have an increasing number of gears for better operating capability, especially in heavy vehicles [5]. With increased number of gear ratios the user has more levels of control for the power required during operation at varying road speeds [57]. This improves fuel economy and response times of the vehicle [34]. The available multi-gear transmission types include the manual and automatic transmissions [5]. Electronic control of automatic transmissions in conventional vehicles is common in today's vehicles [58] and with today's push for smart vehicular control manual transmissions are emerging with electronic control capability [40]. In addition to the e-controlled transmissions a CVT can achieve similar if not better results.

Although rare for a conventional passenger road vehicle, CVTs offer ease of driving and improved fuel economy [43]. The CVT provides infinite gear ratios between the ICE and driven wheels allowing the ICE to operate within its most efficient torque and speed envelope [34]. Typically CVT have increased losses in comparison to multi-gear transmissions [5]. Depending on the application and desired performance requirements of a vehicle the transmission is selected accordingly. Mechanical losses in the transmission and final drive are represented by the efficiencies η_t and η_d respectively.

The mechanical load requirements of ESVs are covered in Section 2.6 with additional considerations revealed in the analysis of measured data in Chapter 3. The use of the conventional vehicle in everyday transportation is leading to significant environmental problems. Alternative means of transportation are now available to mitigate the impact of conventional vehicles on the environment, as mentioned a predominant solution is to convert all conventional vehicles to EVs.

2.2.2 Electric Vehicle

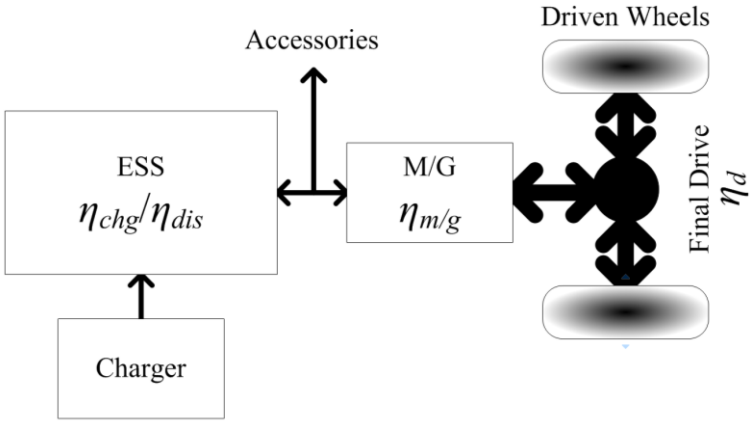

Figure 2.2 - Electric powertrain, identifying main components from energy storage to driven wheels. Arrows indicate energy flow between components.

Powertrain

By replacing the fuel tank or luggage space (in some cases) of a conventional vehicle with an ESS, and the ICE with a M/G, an EV is realised [1, 6]. The EV category includes vehicles that have been termed 'battery electric' [4], and 'all electric' vehicles [59]. During driving, energy drawn from the ESS is free of emissions, giving EVs the consideration as zero emissions vehicle [7, 8, 60, 61]. The concept of a zero emissions vehicle does not provide the full truth about EVs as discussed in Section 1.1, and while not completely false misleads consumers as to the benefits surrounding EVs [1]. As indicated by the bi-directional arrows in Figure 2.2, the main advantage for EVs over the conventional vehicle is the availability of regenerative braking. Rather than using mechanical braking to extract the momentum of the vehicle as waste heat [5], regenerative braking allows the ESS to recover up to 90% of the vehicles momentum and store it for reuse [6]. The process for regenerative braking is discussed further in Section 2.2.6.

Energy Storage System

Another concern for EVs is the limited driving range due to the low energy densities of ESS [62]. Current battery technologies used in ESS do not have the energy to weight ratios required to compete with fossil fuels [20]. This limits the maximum driving distance capable of the average EV to no more than 250 km during ideal driving conditions [19, 20], and in most cases achieving around 100 km at best [62]. Conventional vehicles are expected to have driving ranges greater than 600 km [42]. This driving limitation is referred to as the range anxiety of EVs [56], and reduces the potential applications for EVs to city driving or short distance commercial use [8, 63-65].

There are a number of available ESS mediums available each having a number of advantages and disadvantages. The available ESS include battery banks [63], ultracapacitor banks [64] (also known as supercapacitor banks [51]), flywheels [66, 67] and the hydraulic regeneration system [68]. The fundamental concern in terms of transportation is the energy and power densities of these ESSs. The energy density of fuels and storage mediums as identified in Section 1.2 determines the driving range of the vehicle [69]. The battery bank is the base ESS for EV applications since the remaining three technologies do not have the energy density to support driving for reasonable distances. On the other hand power density determines the instantaneous peak power that can be drawn from the storage device without damaging it [70].

In battery technologies this power density is relatively low and limits the performance of EVs [20], if the battery bank is to maintain a significant life cycle [64, 71]. The life cycle (or battery life) of a battery bank describes the expected number of charge and discharge cycles from a particular type of battery [72]. This life cycle determines when the battery bank will need replacing and varies with differing operating characteristics. For example if a high power is continuously charged and discharged from the battery bank this will lead to a very short battery life [73]. The remaining three energy storage mediums typically have low energy density and high power density, and have been used to extend the life cycle of the battery banks in ESVs. This identifies the reason for assuming that high power levels can be absorbed and supplied by the ESS in Section 1.2.

Motor/Generator

Electric machines operating as motors or generators in ESV are generally referred to as M/Gs [10, 74-76]. The various types of M/Gs available for ESV offer a number of performance attributes and control methods [5]. These attributes are dependent on the type of electric machine utilised as much as the technical specifications of the machine. There are three main types of electric machines, which are DC, AC synchronous and AC induction machines each having their own unique performance attributes [77]. The following provides an overview of these three types of electric machines as a means to identify their use in ESV.

Synchronous machines are named as a result of the relationship between rotor revolutions and the frequency of the sinuosoidal voltage generated at the terminals of the stator. It is advantageous in AC machines to have the low power, DC field windings on the rotor and the high power, multiphase armature on the stator. Originally synchronous machines relied on a DC current connected to the field winding via slip-rings (or similar) for excitation of the rotor, however, research in the last two decades have lead to the use of brushless options such as permenant magnets [78, 79]. While the brushed option for synchronous machines has

a reduced capital cost, such machines require more frequent maintenance [78, 79]. On the other hand a high capital cost of brushless synchronous machines such as the permanent magnet synchronous machine results from the use of rare earth metals (NdFeB) [80].

Similar to the synchronous machine, induction machines have the stator winding excited by an alternating current. The rotor winding, however, is dissimilar to the synchronous machine such that it utilises on an alternating current as well [77]. While the stator windings of the induction machine are structured the same as the synchronous machine the rotor windings must allow for an induced current [77]. The rotor windings are short circuited about the rotor providing no external connection and instead induction (i.e. transformer action) is utilised to provide excitation of the field winding; hence the name induction machine [77]. Induction machines offer a robust and often simpler design in comparison to synchronous machines, however, high starting torques and thereby large current requirements introduce alternative issues that must be accounted for in using induction machine for ESV applications.

Within the classification of DC machines there are commutated and brushless configurations. In contrast to AC machine configurations, DC machines have the armature winding located on the rotor, while the field winding is located on the stator. The need for commutation arises from the generation of a distorted AC voltage waveform that is a result of the interaction of the two magnetic fields rotation (stator and rotor interaction) [77]. The commutator is essentially acting as a rectifier, maintaining constant DC output. Alternatively to the DC powered field winding permanent magnets can be utilised, however these types of DC machines are generally considered for low power applications [77]. Brushless DC machines are more or less brushless AC machines with angular position sensors in order to accurately control the stepping of the motor using DC excitation applied at different intervals around the three or more phase connections [77].

Both AC and DC machines provide a number of options for use in ESVs. For the most part they are both highly efficient having average efficiencies greater than 90% [6], however AC machines are thought to have a slight advantage over DC machines when it comes to power density. Commutated DC machines for example are heavier, requiring larger volumes of space to house the slip-rings for the same power rating as an AC machine [78, 79]. On the other hand, AC machines used in vehicles require the additional conversion from either single or three phase AC to single phase DC for storage in the ESS and vice versa. The losses and extra weight experienced by vehicles using AC machines with power electronics may be balanced out in brushless DC machines that suffer greater switching losses as a result of the stepping operation of the machine [77]. Each individual case varies for electric machine use in ESVs, and no single electric machine can be offered as a unique solution without further investigation into the requirements of a design.

Power flow for M/Gs is directed using power electronic converters and associated EMS controllers [81]. Power electronic converters are used to deliver desired voltage and current to the M/G. Input to the power electronic converters comes from the ESS being DC power, and depending on the type of M/G utilised the power electronic converters have AC or DC output. The EMS controller determines the amount of power to draw from the ESS, by calculating the desired torque and speed on the output shaft of the M/G. This is in response to the accelerator pedal depression as instructed by the driver. In some cases a transmission is utilised to improve the performance of the M/G in EVs however due to the high torque and speed ratings of M/Gs a transmission is not necessary [5, 68].

2.2.3 Fuel Cell Vehicle

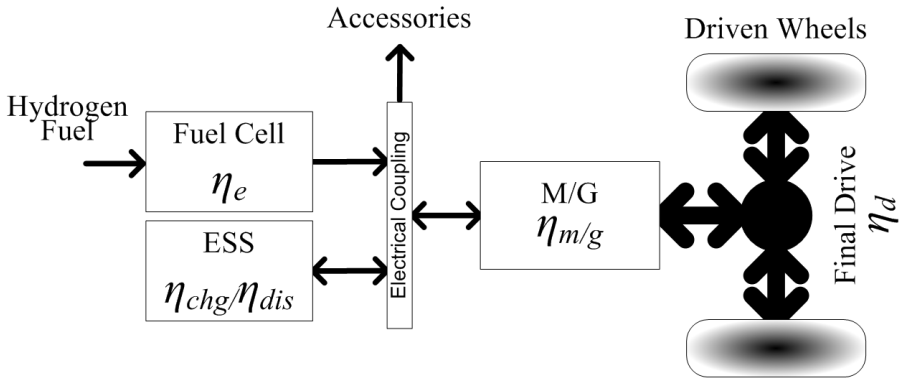

Figure 2.3 - Fuel cell vehicle, identifying main components from both stored energy forms to driven wheels. Arrows indicate mechanical and electrical energy flow.

Powertrain

Due to the energy density requirements of vehicles for long distance driving, and the poor energy densities of battery banks, fuel cell vehicle have emerged as an alternative to the conventional vehicle. The energy density of hydrogen is greater than the average ESS leading to a greater drive range than the EV [1]. Energy supplied from the fuel cell is unidirectional such that once hydrogen is consumed it cannot be recovered, without the aid of an external reforming method [45]. The fuel cell vehicle is driven by the M/G coupled to the electrical network using power electronic converters and controllers [73]. Like the EV previously identified the electrical network of the fuel cell vehicle is able to regenerate energy from the vehicle's momentum using the M/G. During driving the fuel cell vehicle has zero emissions similar to the EV [1]. This advantage of fuel cell vehicles has gained similar appeal as the EVs promotion as a zero emissions vehicle, as well as overcoming the range anxiety of EVs [45, 52, 82]. Operation as a zero emissions vehicle identifies the potential for

fuel cell vehicles to compete with conventional vehicles and steer away from fossil fuel in transportation.

Fuel Cells

The most suitable type of fuel cell for an ESV is the proton exchange membrane fuel cell (PEMFC) [19]. The conversion efficiency of the PEMFC in converting hydrogen to electrical energy is greater than 60% [83-85], identifying the fuel cell as a more efficient alternative to the ICE during driving. For the PEMFC the by-product for on-board consumption of stored hydrogen is water and as discussed above labels the fuel cell vehicle a zero emissions vehicle. And as mentioned, the fuel cell vehicle has higher energy density in hydrogen stores than battery technology at present. These advantages identify the potential for the fuel cell vehicle to replace the conventional vehicle [1, 6, 19, 20, 83-85]. There is, however, concern for the use of fuel cells in vehicles with a number of issues needing to be solved before fuel cell vehicles make it as a dominant commercial vehicle.

Concerns for Fuel Cell Vehicles

These concerns relate to the energy efficiency, production and storage of hydrogen and the overall performance of the vehicle. Firstly, to produce 1 kg of hydrogen from the electrolysis of 9 kg of water, 55 kWh of energy is needed [6]. Considering the Gibb's free energy of hydrogen gas (H_2 gas) this equates to almost 33 kWh of energy stored in 1 kg of hydrogen [23]. Meaning that electrolysis has an efficiency of nearly 60%, combining this with the average efficiency of the fuel cell (60% as identified above), the overall efficiency of the fuel cell using stored hydrogen is reduced to 36 %. Bossel in [6] argues that once you factor in the electricity transmission and distribution losses the average fuel cell vehicle efficiency would be less than 25%. This efficiency is better than the ICE used in conventional vehicles at less than 20% on average however with the combined use of ICE and ESS in HEV there is concern as to why fuel cell vehicles are needed [6, 20].

From the performance perspective of fuel cell vehicles the fuel cell needs to provide the average power for normal driving. This makes the average fuel cell power level smaller than the average ICE power size and limits the potential power at the wheels of the vehicle. In turn this means slower acceleration times for fuel cell vehicles as opposed to the conventional vehicle. According to studies completed by S.S. Williamson the fuel cell vehicle has a lower fuel economy than today's equivalent HEVs indicating that fuel cells will consume more energy [7, 55]. Finally, the infrastructure to support fuel cell vehicles is non-existent identifying a significant drawback in a plan to transition from conventional vehicles to fuel cell vehicles [19]. For example there is a much larger capital cost involved with installing hydrogen fuel stations to support fuel cell vehicles at the bowser as compared

with the existing gasoline and diesel bowsers to support HEV or PHEV [1, 6]. Alternatively fuel cell vehicles must utilise ESS to aid with transient drive loads and thus any infrastructure required to support the charging of EVs, HEVs or PHEVs will inevitably be required for fuel cell vehicles leaving fuel cell vehicles as an unrealistic option in the short term for transitioning to sustainable vehicles. The outlook for fuel cell vehicles is promising, however, that is the underlying argument of most researchers; that fuel cells are a future endeavour having many issues to solve before providing a competitive alternative to conventional vehicles [4, 5, 73, 86, 87]. In the meantime HEV and PHEV are suitable candidates.

2.2.4 Hybrid Electric Vehicle

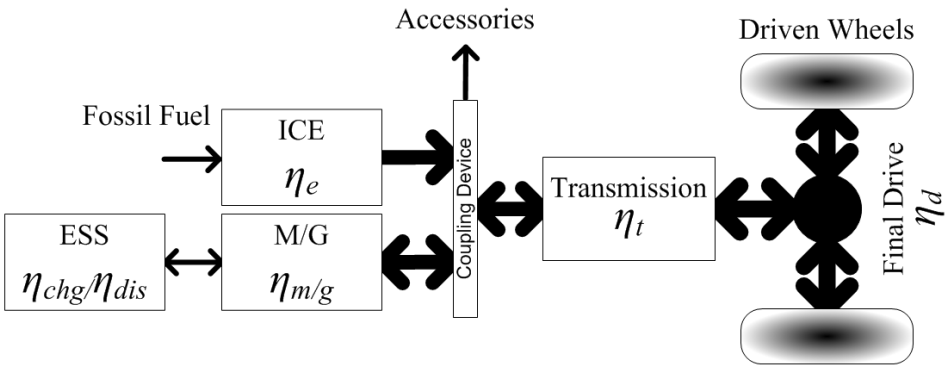

Figure 2.4 - HEV, identifying main components from both stored energy forms to driven wheels. Arrows indicate energy flow between components.

Powertrain

An HEV is determined from the combination of two power sources working to achieve the demands of a drivetrain on a given vehicle. The two power sources are typically an ICE and an ESS combined with a M/G. These two power sources have the option to operate together or separately in order to satisfy the power demands of the drivetrain [4]. There are a number of different configurations that fall into the category of HEV. The various configurations of HEV are identified in Section 2.3. Figure 2.4 serves to identify the main components inherent on a HEV and the energy flow between these components. The configuration influences the energy flow between the components however energy flow at any given time is further explained using modes of operation as in Section 2.2.6.

HEV Performance

The overall performance of HEVs varies in a number of ways to the aforementioned vehicles. In comparison to the conventional vehicle, the ICE of HEVs are smaller since the ICE is generally operated to supply average power demand at higher operating efficiencies during normal driving [33, 88]. The M/G is utilised as the transient power device, balancing

the load requirements such that the ICE operates near constant demand [61]. The presence of the M/G and ESS also allows the ICE to be switched on and off as needed during normal driving relying on stored energy from the ESS. The ESS of HEV is typically a battery bank [32, 61, 89-91].

Charge depletion of the ESS [92], occurs during low power level requests from the vehicle such that the ICE would otherwise consume excessive amounts of fuel compared to the output power [11, 32, 93]. Once the ESS has depleted to some low SOC, the ICE is switched on to maintain a minimum SOC. Alternatively the ESS is charged to a high SOC level before the ICE is again switched off [94]. Such intermittent operation of the ICE leads to improved fuel economy as opposed to operating the ICE for all driving demands [8, 11, 41]. This type of control for the HEV is known as a charge depletion/charge sustenance strategy and is discussed further in Chapter 4. Due to this constant charge and discharge of the ESS, the total energy rating of the ESS is much larger than the permissible energy requirements for driving [20]. This allows the ESS to operate within a small SOC region and increases the life expectancy of the battery bank [60]. This SOC region is normally 5 to 10% of the total SOC of the battery maximising the life cycle the battery bank will have [20]. Battery life cycles are explained further in Section 2.2.2, which discusses the use of ESS in EVs.

An advantage for the transportation industry in transitioning from conventional vehicles to HEVs is that it does not require a complete overhaul of the current manufacturing procedures. This extends from the fact that the HEV incorporates the ICE, and rather than completely redesigning and developing infrastructure to support fuel cell vehicles [19], HEVs offer the potential for continuing to utilise existing infrastructure. A potential solution is to combine two existing industries, namely electricity and transportation [1]. In addition, research has shown that conventional vehicles have the potential for conversion to HEVs such that fuel consumption is reduced on existing commercial vehicles [1, 9, 95]. The conversion of conventional vehicles to HEVs ensures utilising the otherwise redundant ICE, by integrating a M/G into the drivetrain to help balance load requirements and reduce the transient loading of ICEs [5]. Rather than developing a completely new method for transportation, research is leaning towards transitioning into an alternative form of transportation; HEVs offer a pathway to transition to sustainable transportation [70].

2.2.5 Plug-in Hybrid Electric Vehicle

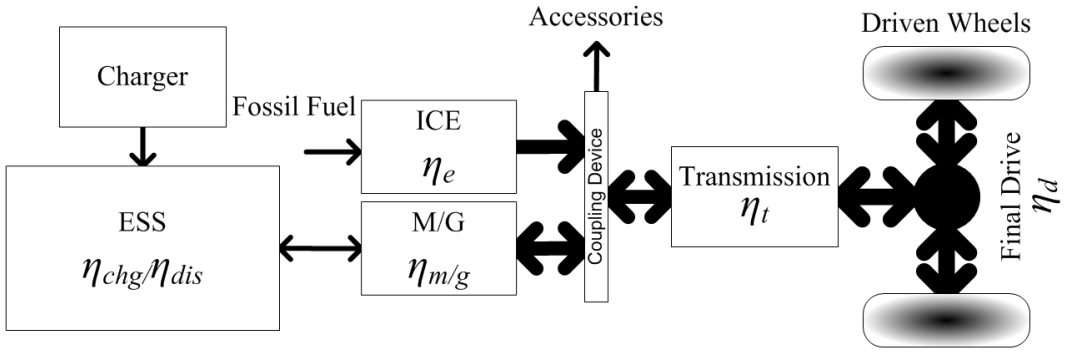

Figure 2.5 - PHEV, identifying main components from both stored energy forms to driven wheels. Arrows indicate energy flow between components.

Powertrain

Having the same components as the HEV, the PHEV includes a much larger ESS and the capability for charging the ESS from the grid. Dependent on the drive criterion for the PHEV there is the option to make use of an all-electric range. The all-electric range allows the PHEV to operate as a zero emissions vehicle similar to the EV and fuel cell vehicle for distances up to 60 km [96]. Once the excess stored energy in the larger ESS is depleted the vehicle will enter a mode of operation similar to the typical HEV [41]. The period of all-electric range is a longer duration of charge depletion since the ESS has a greater amount of energy stored [33].

Rather than discharging the battery bank continuously the ICE can switch on in order to maintain the SOC during charge depletion. This mode of operation is known as blended charge depletion [33, 89]. Blended charge depletion allows for high efficiency operation of the ICE during periods of high average power demand, while the ESS and M/G supply small transients and low average power demands [11]. The aim for blended charge depletion is to maintain the ESS SOC until the end of a given drive period. In the event that the SOC reaches some low limit the PHEV will enter charge sustenance mode of operation to maintain the SOC. The decision of when to utilise fossil energy or stored energy in such cases is one of the more challenging problems in fuel consumption reduction of PHEV.

PHEV Performance

The performance of PHEV with regards to the HEV (Section 2.2.4) is dependent on the all-electric range available to the driver. A study completed by Wirasingha et al in [7], determines that PHEV if utilised to their full potential have the ability to conserve fuel almost as much as EVs. In addition, the driver is not limited by the EVs range anxiety as mentioned in Section 2.2.2. The greater the drive distance required (relative to the size of the

ESS) from the PHEV, however, the higher the average fuel consumption becomes [7]. This is where control of PHEV and HEV is paramount. PHEV control strategies are evolving to accommodate more precise energy requirements for the everyday driver's needs. With the aid of trip based information and studies for varying driver scenarios PHEV are showing promising reductions in fuel consumption (L/100km). Until ESS energy density is capable of competing with the energy density of fossil fuels, HEV and PHEV will provide the pathway for achieving reduced reliance on fossil energy resources. In addition to the description of the available ESV, a simple investigation based on the tank to wheels [7] approach is considered in the next Section.

2.2.6 Modes of Operation

Firstly the modes of operation are identified using the HEV components identified in Figure 2.4, followed by a description of the modes of operation that exist in the five vehicle categories previously discussed. This Section serves to identify the energy paths available to the ESVs as a means for evaluating the vehicle topologies that have the most potential for improving the outlook of the transportation industry. This analysis is in addition to the comments previous made for each vehicle and also helps to introduce the typical operations expected in each ESV.

Mode 1 – ICE Only Operation

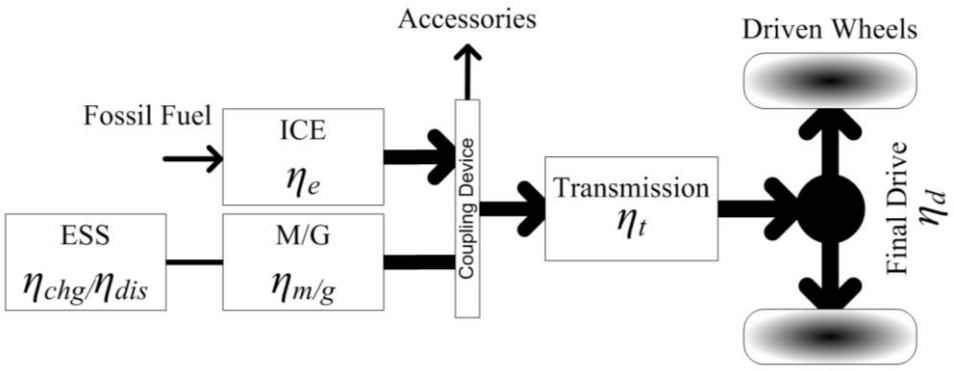

Figure 2.6 – Mode 1: ICE only.

Similar to the conventional vehicle identified above the ICE alone mode of operation observes all drivetrain and accessory load requirements being supplied by the ICE. Decoupling of the M/G from the drivetrain using a clutch will ensure fewer inertial losses for this mode of operation. In the case that there is no clutch present, simply reducing the excitation field of the M/G to zero (controlling the voltage or frequency) ensures that no power flow occurs in the M/G [97]. Power flow during this mode of operation is unidirectional such that fossil fuel is consumed in order to propel the vehicle along the road. Load power is met as follows:

$$P_L = \eta_d \eta_t \eta_e \frac{dE_f}{dt} \tag{2.1}$$

where P_L is the load power required, and dE_f is the energy in the fuel that is fed into the ICE over some time period (dt). Observing the mode of operation in the form of equation 2.1 allows for the identification of the efficiency of each component; including the ICE (η_e), transmission (η_t) and final drive (η_d). This driving mode is the least desirable since efficiencies for converting chemical energy to mechanical energy in the ICE (i.e. η_e) are low.

Mode 2 – Electric Only Operation

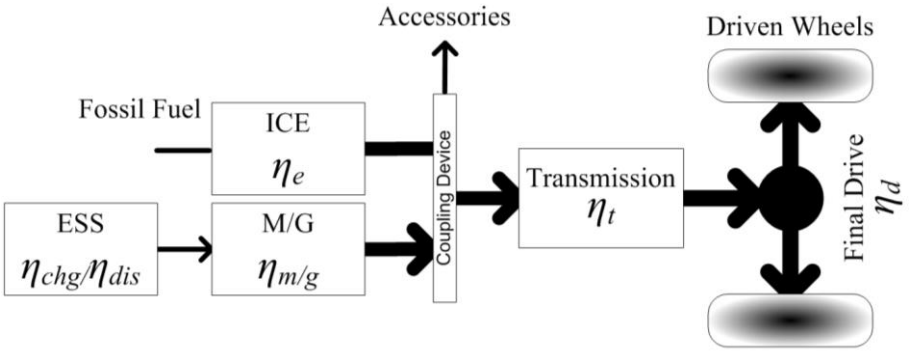

Figure 2.7 – Mode 2: Electric only.

On the other hand electric only mode of operation observes the ESS supplying energy to the M/G for satisfying the drivetrain and accessory load requirements. This is referred to as motoring only in literature since power flows from the ESS to the driven wheels [4, 5]. If there is sufficient energy remaining in the ESS this is the most desirable driving mode since the vehicle does not consume any fossil fuel and therefore operates as a zero emissions vehicle. Load is satisfied according to:

$$P_L = \eta_d \eta_t \eta_{m/g} \eta_{dis} \frac{dE_{ess}}{dt} \tag{2.2}$$

where dE_{ess} is the energy drawn from the battery over some small time period (dt). In addition to the mechanical losses of the drivetrain (η_t and η_d) observed previously there are electrical losses in the M/G ($\eta_{m/g}$) and ESS (η_{dis}). η_{dis} represents the discharge losses of the ESS. This mode of operation usually occurs during low vehicle speeds and low transient power levels [32, 74, 98].

Mode 3 – Hybrid Operation

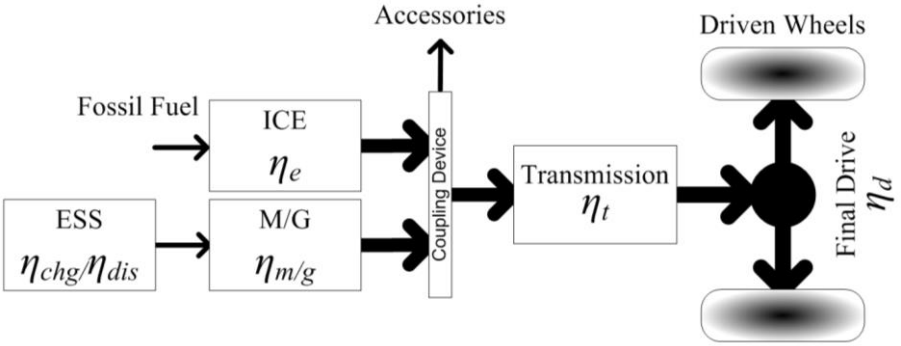

Figure 2.8 – Mode 3: Hybrid.

The hybrid mode of operation for the HEV observes partial power requirements being supplied from both the ICE and M/G to meet the load demand. The reason for entering hybrid mode is to satisfy high load demands at better efficiency levels for the ICE, thereby reducing the fuel consumption of the vehicle [8, 11, 99]. Load is satisfied according to:

$$P_L = \eta_d \eta_t \left[\eta_e \frac{dE_f}{dt} + \eta_{m/g} \eta_{dis} \frac{dE_{ess}}{dt} \right] \tag{2.3}$$

Equation 2.3 implies that load power for this mode of operation is a combination of the fuel energy and battery energy at a given moment of time. The control strategy utilised by the vehicle determines the amount of energy to be supplied from each energy source [5].

Mode 4 – Charging On-The-Go Operation

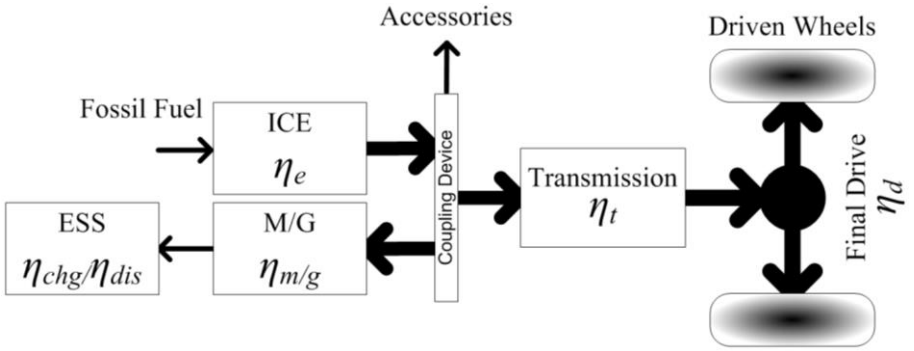

Figure 2.9 – Mode 4: Charging on-the-go.

As mentioned previously if the SOC of the ESS falls below some low limit the ICE is required to maintain this minimum SOC by generating additional power to be absorbed by the ESS. Alternatively the aim is to recharge the ESS to a defined SOC. The M/G now operates as a generator drawing power from the mechanical coupling with the requested load power being:

$$P_L = \eta_d \eta_t \left[\eta_e \frac{dE_f}{dt} - \eta_{m/g}^{-1} \eta_{chg}^{-1} \frac{dE_{ess}}{dt} \right] \tag{2.4}$$

Energy drawn from the mechanical coupling includes the energy required to charge the ESS plus the losses in transferring the energy from the mechanical coupling to the ESS. Losses in transferring energy to the ESS include the M/G generating losses ($1/\eta_{m/g}$) and the ESS charging losses ($1/\eta_{chg}$).

Mode 5 – Stationary Charging Operation

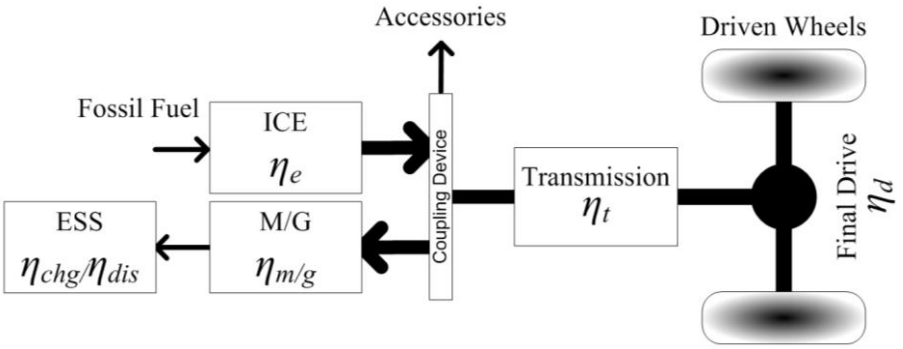

Figure 2.10 – Mode 5: Stationary charging.

HEV not having the luxury of connecting the ESS to the grid have a charging mode while the vehicle is not in drive mode. Making use of the ICE as a fossil fuel power generator in combination with the M/G the ESS is charged with no power transferred to the drivetrain. This form of charging allows the ICE to operate at its most efficient point of operation during charging since the load speed is determined by the M/G.

$$P_L = 0; \eta_e \frac{dE_f}{dt} = \eta_{m/g}^{-1} \eta_{chg}^{-1} \frac{dE_{ess}}{dt} \tag{2.5}$$

Equation 2.5 indicates that power generated from the ICE is equal to the power sent to the M/G, with the load power equal to zero.

Mode 6 – Regenerative Braking Operation

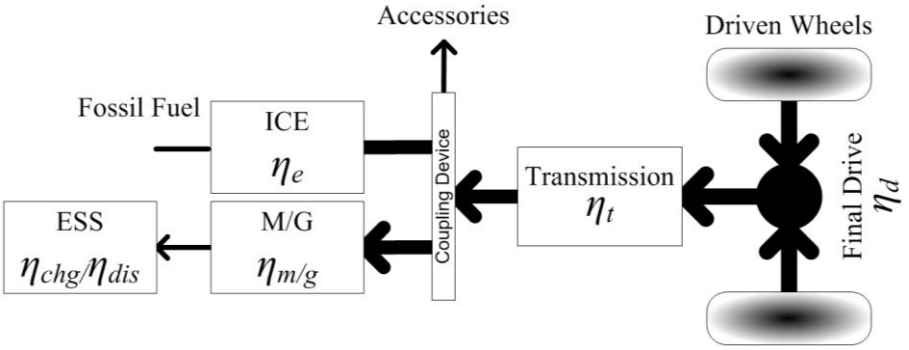

Figure 2.11 - Mode 6: Regenerative braking.

During normal braking the driver pushes the brake pedal which activates the mechanical brakes of each wheel. The momentum of the vehicle is expended as waste heat by applying the brake pads to rotor discs that are connected to the drive axle slowing the vehicle. Alternatively, disconnecting the ICE from the drivetrain and applying a negative torque to the M/G allows the energy stored in the vehicle's momentum to be absorbed by the ESS. The load power is thereby equal to:

$$P_L = \eta_d^{-1}\eta_t^{-1}\eta_{m/g}^{-1}\eta_{chg}^{-1}\frac{dE_{ess}}{dt} \tag{2.6}$$

Equation 2.6 indicates that the wheels become the source during regenerative braking and the ESS is the load absorbing energy from the wheels. The rate of deceleration required from the vehicle determines how much of the vehicle's momentum is regenerated and stored in the ESS. If the required deceleration rate is high the M/G will not be able to absorb all of the energy, since it is limited by the maximum generating torque. In the case of high rates of deceleration the mechanical brakes are activated aiding the M/G with reducing the vehicle's speed. This leads to the inclusion of a mechanical braking component added to equation 2.6:

$$P_L = \eta_d^{-1}\eta_t^{-1}\eta_{m/g}^{-1}\eta_{chg}^{-1}\frac{dE_{ess}}{dt} + P_{brake} \tag{2.7}$$

Mechanical braking is identified in equation 2.7 by P_{brake} at the wheels of the vehicle in Figure 2.11.

The modes of operation identified above define the expected interaction of powertrain and drivetrain components inherent in HEV and PHEV. In addition, these modes of operation highlight the main objectives an EMS controller aims to achieve throughout driving. The resulting performance of these modes of operation is influenced by the components included on a topology and the existing connections between them. Through examining the general vehicle configurations for HEV and PHEV further advantages and disadvantages for EMS control are revealed.

2.3 Vehicle Configurations

There are a number of variations that exist for HEV and PHEV configurations [5], this Section aims to identify the basis for distinguishing between them. A vehicle's configuration varies with component size, selection and connections. The means for distinguishing between each of the configurations is how the power sources and driven wheels of the vehicle interact [4]. There are two main types of connections that exist between the power sources and driven wheels of PHEV and HEV. These include mechanical and electrical connections [8]. Of the various configurations that exist in literature for PHEV and HEV,

there are three classes [4, 5, 7-17]. The three classes are series, parallel and power-split (also referred to as series-parallel [5, 93, 100]) configurations. For each case the inclusion of the transparent 'Charger' block in Figure 2.12, Figure 2.13 and Figure 2.14 identifies that each topology applies to both PHEV and HEV. The combination of mechanical and electrical connections determines which class a configuration falls into.

2.3.1 Series Configuration

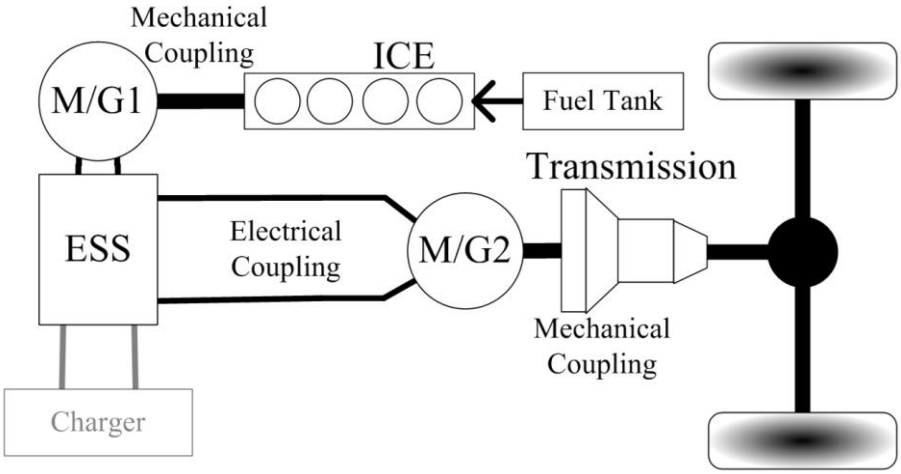

Figure 2.12 - Series PHEV and HEV configuration.

The series configuration includes two M/Gs, between the ICE and the driven wheels [101]. Referring to Figure 2.12, M/G1 operates as a generator converting the ICE mechanical energy to electrical energy for storage in the ESS or for direct supply of the driver's power request [13]. M/G2 acts as the means to meet the load, and therefore determines the performance of the vehicle [12]. The series configuration is described as an electrical coupling since the ICE is indirectly coupled to the drivetrain [102, 103]. The use of M/G2 to supply the drivetrain load reduces the need for gear ratios, since the torque and speed ranges of M/Gs are flexible and the average efficiency of the devices are high [6]. The main advantage of this topology is the indirect supply of power from the ICE to the drivetrain. This ensures that the ICE operates at peak efficiency regardless of the speed of the vehicle [14].

On the other hand the transfer of energy from mechanical (output from ICE) to electrical and then to mechanical (drivetrain) again increases the losses of the whole system [7]. The benefit seen from operating the ICE at peak efficiency is limited by the losses experienced in the energy conversion process (mechanical to electrical to mechanical) [73]. The aim for the series configuration is to minimise electrical losses while meeting the desired load. This is achieved through optimising the efficiency of operation of the M/Gs [53]. The parallel configuration in comparison to the series has complementary performance attributes.

2.3.2 Parallel Configuration

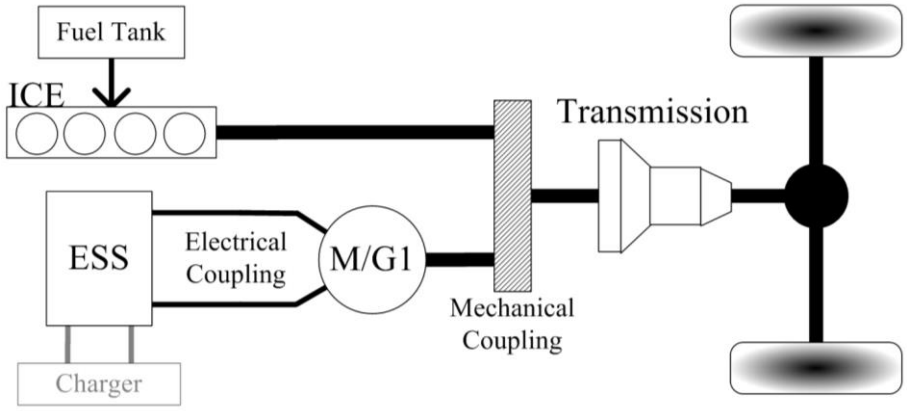

Figure 2.13 - Parallel PHEV and HEV configuration

The complementary performance qualities mentioned above identify that the parallel configuration is equal but opposite to the series configuration. Figure 2.13 identifies the main connections of a parallel configuration. The parallel configuration is described as having a mechanical coupling which is a direct connection of the ICE to the drivetrain [76, 104]. The direct connection of the ICE to the drivetrain ensures minimal losses due to energy conversion [11]. The mechanical coupling between the ICE and M/G1 allows for charging of the ESS however energy from the ICE does not have to pass through the electrical network in order to satisfy the driver's requested power [9]. There is greater flexibility in the control of the power devices; the controller has the choice of satisfying the load with the ICE or from M/G1. The energy management problem must be solved by optimising the use of stored energy and fossil fuel energy.

There is concern however, for the restricted operating conditions of the ICE [10]. The direct coupling to the drivetrain means that the ICE operating speed is proportional to the speed of the driven wheels [93]. The use of the transmission aids with improving the flexibility of the ICE operating speed however the resulting fuel consumption reduction is minimal [46]. In contrast to the series configuration the parallel configuration must minimise ICE losses through effective use of the ESS [5]. These concerns are seemingly addressed by the third vehicle configuration known as the power-split topology.

2.3.3 **Power-Split Configuration**

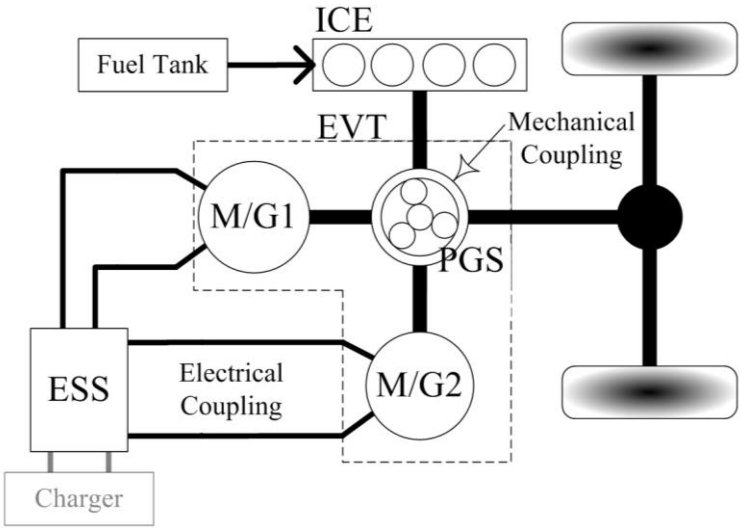

Figure 2.14 - Power-split PHEV and HEV configuration.

The power-split configuration in comparison to both the aforementioned configurations has all of the advantages and none of the disadvantages. There is however, added complexity in control and increased capital costs [15]. Referring to Figure 2.14, the power-split configuration utilises a PGS to couple the two M/Gs with the ICE [5]. By connecting all three devices to the one mechanical coupling the power-split topology has the option of operating the ICE at a particular speed or transferring energy directly to the driven wheels from the ICE [4]. This means that the ICE is not restricted by the speed of the driven wheels as in the case of the parallel configuration [16]. In addition, the losses incurred by energy conversion as seen in the series configuration are avoided [17].

The optimal control strategy employed requires the controller to select the energy path with the least losses at any given moment. The combined M/Gs in the power-split configuration are also referred to as an electric variable transmission [93]. The electric variable transmission is the same as the electrical coupling of the series configuration [34], and in some cases is combined as a single transmission for space saving in the drivetrain [100]. The electric variable transmission allows the ICE to operate at infinite speed ratios with respect to the driven wheels [100]. With this improved flexibility (using the electric variable transmission) in the ICE operating conditions, the controller is able to operate the ICE near peak efficiency [105]. The concern for the electric variable transmission is that it leads to increased losses similar to the series configuration. Use of this energy path must be compared against the efficiency for operating with the ICE coupled directly to the drivetrain.

2.3.4 Mechanical Coupling Modes of Operation

For the parallel and power-split configurations with the mechanical couplings there are additional modes of operation to those discussed in Section 2.2.6. These additional modes of operation as featured in [5], are determined by the mechanical coupling device inherent on the vehicle. Generally there are three modes of operation achieved using the mechanical coupling including torque coupling, speed coupling and torque-speed coupling. An example of such a device is the PGS identified in the previous Section. These three modes of coupling determine how the torque and speed relationships occur between the ICE and M/G to meet the load requirements.

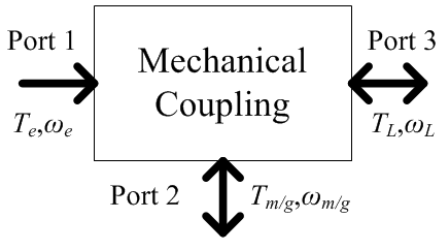

Figure 2.15 - Mechanical coupling device.

Figure 2.15 identifies the torque and speed signals experienced by the typical mechanical coupling, combining torque and speed of the ICE (T_e, ω_e) and M/G ($T_{m/g}$, $\omega_{m/g}$) to meet the demands of the drivetrain (T_L, ω_L). The common relationship for the various types of mechanical couplings is therefore the balancing of power from the ICE and M/G.

$$T_L\omega_L = T_e\omega_e + T_{m/g}\omega_{m/g} \tag{2.8}$$

Equation 2.8 must hold for the system to remain stable. This Section aims to identify the mechanical coupling modes of operation to introduce the flexibility in control for the parallel and power-split configurations; which adds to the reasons why the power-split is the preferred HEV and PHEV configuration.

Torque Coupling

A mechanical coupling typically operates in torque coupling mode for use in the parallel configuration since torque from both the M/G and ICE is combined to meet the drivetrain load torque requested [46]. The downsized ICE and the similar sized M/G need to produce torques that meet the same magnitude expected from the conventional vehicle having a large ICE. The use of the torque coupling device therefore allows the torque experienced at the wheels of the HEV or PHEV to match that of the conventional vehicle [10]. With reference to the signals of Figure 2.15 the torque coupling can be expressed as:

$$T_L = k_1T_e + k_2T_{m/g} \tag{2.9}$$

Equation 2.9 determines that the load torque (T_L) is a combination of the ICE torque (T_e) and M/G torque ($T_{m/g}$), with respect to the constant gear ratios at port 1 (k_1) and port 2 (k_2). It then follows that since the power balance of the torque coupling needs to agree with equation 2.8 that the speed relationship is determined as:

$$\omega_L = \frac{\omega_e}{k_1} = \frac{\omega_{m/g}}{k_2} \tag{2.10}$$

Speed Coupling

The alternative mechanical coupling mode is speed coupling. With reference to Figure 2.15, this type of mechanical coupling observes the summation of speeds of the ICE and M/G according to:

$$\omega_L = k_1\omega_e + k_2\omega_{m/g} \tag{2.11}$$

Again, due to the constraints of equation 2.8 the torques experienced by the system are:

$$T_L = \frac{T_e}{k_1} = \frac{T_{m/g}}{k_2} \tag{2.12}$$

An example of the speed coupling device is the PGS with the carrier gear (yoke) held to the stationary frame [5]. Equation 2.11 indicates that the load power is now dependent on the varying speeds of the powertrain components connected to ports 1 and 2 in Figure 2.15. Generally the M/G speed will vary according to the required power requested from the drivetrain in order to allow the ICE to supply the requested power at optimal efficiency. This speed coupling is described as VSC in Section 4.3.2.

Torque-Speed Coupling

A mechanical coupling device that allows both torque and speed coupling as described above ensures that the energy management controller has the option to select between the two. The PGS as mentioned above has the ability for both torque and speed coupling and while it is possible in the parallel configuration, this method for control has been designed as a result of the required operation of the power-split configuration [100]. A typical example for alternating between the two mechanical coupling modes is utilising torque coupling during high acceleration where high torques are required. This would then be followed by speed coupling during cruising at high speeds allowing the ICE to operate within its optimal speed envelope [32]. In the case of the power-split configuration M/G1 operates in speed coupling mode with the ICE, while M/G2 operates in torque coupling mode allowing for increased control flexibility. The use of the PGS in power-split configurations from the perspective of performance supports the selection of the power-split configuration when comparing ESVs.

2.4 Energy Smart Vehicle Performance

2.4.1 Measuring Performance in Vehicles

The main quantities representing the performance of ESVs as identified by a number of research papers and the underlying government bodies is the acceleration performance, fuel consumption and emissions production [8, 11, 26, 33, 38, 60, 106-108]. More recently efficiency of operation, drivability and noise, vibration and harshness have played a role in the performance analysis of vehicles in order to provide a thorough examination [38]. The main focus for the performance analysis of the ESV featured in this thesis is on the fuel consumption, efficiency of operation and drivability. Noise, vibration and harshness and emissions are excluded for reasons identified in this Section.

Firstly noise, vibration and harshness are typically independently controlled variables for ICE [109], drivetrain, suspension [110] and wheel [111] stability and can be mitigated through the use of mechanical dampeners or constraints placed on the operation of such devices. The extent to which noise, vibration and harshness are applied to the ESV featured in the studies included in this thesis is through constraints such as gear change delays, ICE speed and torque delays, rotational inertia, a minimum ICE shut off cool down time and a slip for the clutch engaging and disengaging as operational requirements vary over a drive cycle [49]. Secondly emissions considerations of PHEV and HEV in simulation packages using look-up tables such as those used in ADVISOR underestimate emissions as much as 15% when compared against emissions of real-world experiments [108]. This error in estimating the emissions is due to low torque and speed requests from the ICE at low vehicle speed. One of the main aims of the two controllers proposed in this thesis is to avoid such low torque and speed operation resulting in improved fuel consumption. Therefore, the proposed controller will potentially reduce emissions as well [108]. Alternatively a reduction in the fuel consumption corresponds to a reduction in the carbon emissions [8] and thus any fuel savings resulting from the designed controllers are expected to have a proportional reduction in emissions.

For the purpose of attracting consumers to their products, car manufacturers utilise the fuel consumption and acceleration performance of passenger vehicles. The acceleration performance is the time taken in seconds for a vehicle to accelerate from 0 to 100 km/h as defined by organisations such as the Partnership for New Generation Vehicles and Environmental Protection Agency. Alternatively, fuel consumption in litres per one-hundred kilometres (L/100km) as referred to in Australia, is known as fuel economy in miles per gallon (mpg) in countries such as the US [43]. This demonstrates the average performance consumers should expect to yield, however, studies completed by the Environmental

Protection Agency demonstrate that the majority of car manufacturers provide unrealistic fuel consumption values [43]. Finally the quantities identified for analysing the drivability of vehicles include the total number of ICE and gear shift events of a vehicle such as the study completed in [38]. This study in particular offers a comparison for varying the total number of ICE or gear shift events during driving and the impact it may have on the final fuel consumption. Fuel consumption, overall efficiency, acceleration performance and drivability are discussed in Chapter 4 with respect to the operation of the developed high efficiency controller. The following Section however refers to the fuel consumption of existing vehicles to identify a bench mark for the expected performance of HEV and PHEV.

2.4.2 Existing Vehicle Configurations

Performance wise the power-split configuration offers the best approach in comparison to the series and parallel configurations. The main issue with the power-split configuration at present is the high capital cost for consumers [8]. Alternatively parallel and series configurations are cheaper, however, fuel consumption reductions fail to meet the high expectations set by power-split configurations [1]. The parallel configuration performs better during highway driving, while the series configuration is more suitable for city driving [4]. To provide the reader with an overview on the performance of the mentioned vehicle configurations, some existing ESVs are referred to. Figure 2.16 identifies the fuel consumption reported by the US, Environmental Protection Agency [43] for the example HEVs and PHEVs.

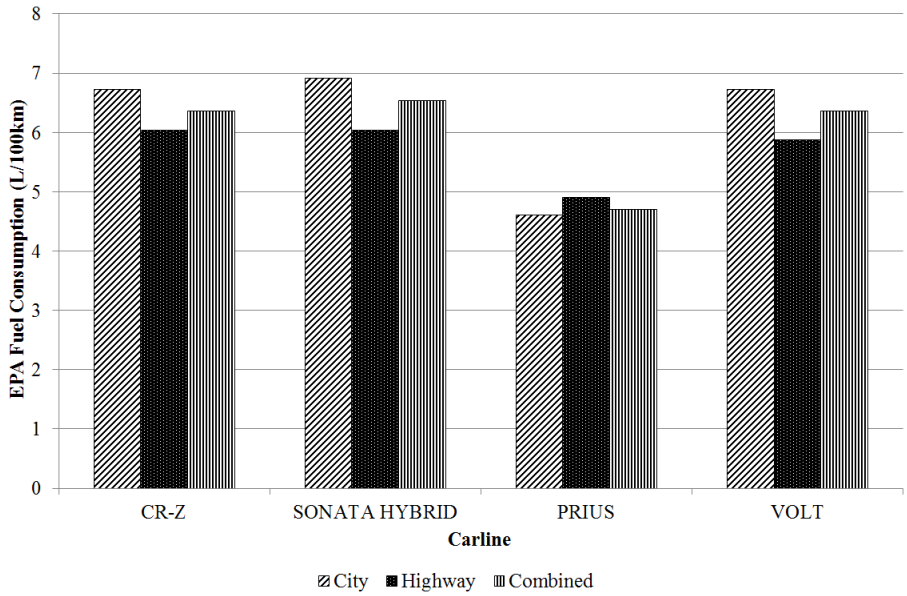

Figure 2.16 - Environmental Protection Agency reported fuel consumption for city, highway and combined driving scenarios [43].

Chevrolet Volt

The Chevrolet Volt is given the term extended range electric vehicle [112]. The Chevrolet Volt is equivalent to the Holden Volt released in Australia [113]. In light of the three vehicle classes identified above the extended range electric vehicle is a series configuration with an ESS large enough for the vehicle to be considered a PHEV [114]. The appeal of this type of vehicle for consumers is that it eliminates the range anxiety associated with the EV [115]. The extended range electric vehicle allows the vehicle to operate as an EV for a range up to 61 km (38 miles) before resorting to fossil fuel energy to maintain the ESS SOC [96]. The full driving range of the Chevrolet Volt is estimated at 611 km (380 miles) when relying on gasoline [96]. This makes the extended range electric vehicle suitable for city driving scenarios where a round trip observes the vehicle operating as an EV. With the continued use as an EV the Chevrolet Volt has the potential for significantly large fuel and emissions savings. The fuel consumption shown in Figure 2.16, is for the Chevrolet Volt operating as a HEV over longer trips where the all-electric range has been consumed.

Honda CR-Z

The first consideration for the parallel configuration here is the direct (inline) connection of the ICE and M/G found in the Honda CR-Z. This connection is referred to as integrated motor assist (IMA) and is unique to the Honda range of hybrids [116]. The Honda CR-Z includes a M/G with a power rating of 10 kW, which is low in comparison to other hybrid brands [43]. This low power rating (for the M/G) limits the potential for fuel consumption reduction [43], however the result is a cost effective alternative to the conventionally driven vehicle [117]. The limited fuel consumption reduction is evident in Figure 2.16, since the reported fuel consumption is similar to the Hyundai Sonata Hybrid which is nearly 400 kg heavier than the Honda CR-Z [118]. The Honda CR-Z is a light weight vehicle yet performs similarly to the mid-sized hybrid vehicles.

Hyundai Sonata Hybrid

Although it falls into the category of a power-split configuration the Hyundai Sonata Hybrid is more like a parallel configuration. The vehicle features an 8 kW integrated starter generator (ISG) combined with a 30 kW M/G [119]. The ISG is directly coupled to the ICE for starting and ESS charging; providing a constant charge to the ESS when the ICE is on. The coupling of the ISG to the ICE in this case does not offer the same flexibility in control as described for the power-split topology. For example the ISG is not large enough to work with the M/G as an electric variable transmission [5]. The M/G is coupled in parallel to the ICE such that the control system can alternate between each power source as required. These are the reasons the Hyundai Sonata Hybrid is considered a parallel configuration [119].

Having the larger M/G by comparison to the Honda CR-Z the fuel consumption reduction benefits are greater [43].

Toyota Prius

The Hybrid Synergy Drive (or Toyota Hybrid System) developed by Toyota for their range of hybrid vehicles refers to the power-split configuration as described in Section 2.3.3 [120]. The Prius has a smaller ESS compared with the Chevrolet Volt although it is unaffected by this restriction as shown by the reported fuel consumption of Figure 2.16. The standard Prius HEV does not offer an all-electric range like the Chevrolet Volt, however, there is another version of the Prius that does [121]. The all-electric range for the PHEV version of the Prius is up to 21 km which is not as appealing as the Chevrolet Volt, however, the reported fuel consumption is similar to that shown in Figure 2.16 [121]. Credit for the low fuel consumption of the Prius is given to the Hybrid Synergy Drive (i.e. the power-split configuration and control strategies utilised). From the available commercial vehicles it is evident that the power-split configuration has the best reported fuel consumption. This supports the consideration of power-split PHEV as studied in this thesis.

2.5 Control Strategies

The energy management problem for PHEV and HEV revolves around three main objectives; fuel consumption reduction, emissions reduction and energy conservation. This Section examines the control strategies associated with the hybrid electric and plug-in hybrid electric vehicles. With reference to the classification of control strategies identified by Wirasingha et al. [8], control strategies presented in literature are scrutinised from an analytical point of view. The four main categories include hybrid, multimode, rule-based blended and optimisation-based blended controllers. The following is a discussion of the classifications presented in [8] with reference to recent literature [5, 11, 20, 33, 34, 36, 47, 52, 89, 93, 104, 122-136]. This discussion is formed on the basis of the author's understanding of these control strategy classifications whereby [8] has been used as a guide. Due to the evolution of the control strategies from hybrid and multimode to the more recent rule-based blended and optimisation-based blended controllers examples provided also follow a chronological pattern.

2.5.1 Hybrid

The first control strategy for HEV was to operate in a hybrid mode all the time. This is similar to continuously operating in mode 3 described in Section 2.2.6. Simple control decisions are predetermined for the vehicles operation leading to a reduction in the fuel consumption. This type of control strategy does not take full advantage of the potential fuel savings of HEV and is featured in earlier versions of the hybrid vehicles [5, 125, 126].

Reference [126] discusses limiting the ICE to a speed range so that higher efficiencies of operation occur during driving, maintaining the ESS SOC while utilising the M/G as the main propulsion device.

2.5.2 Multimode

The multimode control strategy determines switching between electric only, conventional only and hybrid modes of operation. In effect it is the action of transitioning between modes 1 to 6 identified in Section 2.2.6 to achieve simple objectives. An example of the multimode is the operation of PHEV in electric only mode until the all-electric range (Sections 2.2.2 and 2.2.5) of the ESS has been consumed then switching to charging mode to maintain the SOC [20, 122]. There are three main objectives considered for this transition between modes of operation these include charge depletion, charge sustenance and a combination of charge depletion and charge sustenance [33, 127]. Depending on which of these objectives the multimode controller is aiming to achieve is the selected mode from Section 2.2.6 [5]. This type of control strategy forms the foundations for rule-base blended and optimisation-based blended control since each of these strategies can be added to multimode controllers for improved operating performance.

2.5.3 Rule-based Blended

Evolving from the multimode control strategy the rule based blended controller achieves an overlap of the 6 modes defined in Section 2.2.6. This is achieved such that the EMS controller selects the best energy path (electrical or mechanical) to satisfy current load requests as opposed to selecting the modes of operation. This type of rule-based blended controller is identified as deterministic [8]. In addition the rule-based blended control introduces multi-variable input algorithms allowing for a larger scope of inputs and therefore flexibility in control. This type of control is achieved using fuzzy logic controllers [8], due to the larger range of predetermined solutions available which can be selected based on a varying number of conditions. These conditions are received via sensors as inputs to the EMS controller for determining the best action to take and improve the energy utilisation of the vehicle.

There are a number of rule-based blended controllers available in literature, each determining the optimal operation from the predefined operating modes or conditions. Pisu et al. [36] discusses the finite state machine approach to energy management. This type of control strategy selects the optimal energy path based on event-triggered rules. The authors of [104] describe a similar controller to that featured in [36], however, the paper focuses on minimal ICE operation. The ICE is operated at maximum power while the M/G balances with the drivetrain load demand. References [93] and [128] provide a set of rules for inputs

(such as ICE torque, M/G torque etc.) to determine the best energy path for satisfying the requested load, as mentioned such controllers while having lower fuel consumption than conventional vehicles, do not take full advantage of the HEV operating potential. Zhang et al [41] and Jeongmin et al [34] develop predefined rules that are evaluated in an if-then manner to determine the optimal propulsion requirements from the ICE and M/G. Deterministic rule-based blended controllers while performing better than hybrid and multimode control strategies still lack the ability to provide an optimal solution for varying drive conditions and thus greater complexity of rule-based controllers is investigated.

Fuzzy rule-based blended controllers are developed offline and provide a range of options for interpreting and meeting driver requests. An advantage for fuzzy logic control in comparison to the determined rule based blended controller is that multiple inputs can be processed in a short period of time [129]. The fuzzy logic controllers therefore improve the performance of the vehicle with little increase to computational requirements. For this reason fuzzy logic has been utilised for local control in combination with global optimisation since a range of options are available to tweak performance with little interference to other components integrated on the vehicle [129, 130]. This capability extends from the fact that once the global optimisation has been achieved local controllers have a limited amount of time to achieve the set tasks. This means that some components will be restricted by their operating limitations which must be considered in the optimisation. Fuzzy controllers are, however, predefined over known drive cycles such that limited optimisation is achieved.

2.5.4 Optimisation-based Blended

Optimisation-based blended controllers rely on mathematical means to determine an optimal solution to the whole system. This optimal solution resulting from such control has either maximum benefit or minimum cost to the operation of the system [11, 26, 33, 38, 41, 137, 138]. Common goals for optimisation include energy conservation, fuel consumption minimisation, and greenhouse gas emissions reduction [11, 26, 32, 38]. In addition, optimisation of drivability factors such as ICE on/off and gear shifts of fixed gear transmissions are featured [32, 38, 74, 139, 140]. The more appealing optimisation-based blended controllers analyse instantaneous information to determine a unique solution to current load requirements [122, 136, 141, 142]. This type of controller has in built performance maps or cost functions that allocate particular importance to drivetrain components. Other controllers are trained according to varying conditions allowing for a number of optimal solutions that have no apparent relationship [110, 143, 144]. These types of controllers utilise artificial intelligence such as neural networks [135, 143], genetic algorithms [145] or particle swarm optimisation. The issue with these types of controllers is that they require a substantial amount of *a priori* knowledge of the drive scenario conditions

in order to make optimal energy management decisions. There are two types of optimisation-based blended controllers as identified in [8], these include global optimisation and real-time optimisation. Global is also referred to as acausal optimisation and real-time is the same as causal optimisation.

Global (acausal) optimisation is the amalgamation of multiple variables to determine the optimal operation of the combined system. The variables considered are not directly related, however, the rules or cost function developed provide the necessary connections. These rules or equations represent the whole system and are developed offline to provide the EMS with the required information to determine the global optimum; an example of this process is linear programming [8]. In addition those controllers utilising some form of artificial intelligence are also categorised as global optimisation controllers since training of these control strategies results with the best performance of the whole system.

On the other hand real-time optimisation incorporates past information to determine a cost or objective function which is updated on-the-go. By recording information during operation of the system the optimisation process is modified to improve future driving performance. Due to this recording of information and therefore the use of past information to determine optimal operation, real-time optimisation controllers are referred to as causal systems [38, 146]. Real-time optimisation identifies direct relationships among components for continuous optimal operation. The relationships developed for optimisation in this type of controller are continuous cost or objective functions relating at least two components of the vehicle to identify an optimal solution. Real-time optimisation relies on the accurate modelling or mathematical representation of components in order to achieve best results. Operations resulting from the controllers that utilise such real-time optimisation generally have better performance in comparison to the alternatives.

Optimisation-based blended controllers are therefore more complex than the aforementioned alternatives, however, the result is a far more superior performing EMS. The following identifies examples of the global optimisation and real-time optimisation controllers as found in literature. For a test bench in simulation a number of authors make use of dynamic programming [26, 33, 88, 122, 141, 147]. Dynamic programming determines the minimum energy consumed over a given drive period based on the defined operating decisions a controller is able to select from. This is an ideal scenario such that the controller is privy to future information and makes the optimal decision at any given time. Due to the unrealistic idealism of dynamic programming it is normally shown as the bench mark for comparison with a proposed controller. Dynamic programming therefore identifies the maximum benefit of a vehicle configuration with respect to any potential control strategy. Developed controllers are thereby compared against the defined optimal (i.e. dynamic programming) to

demonstrate a performance gap or as a performance target. The time taken to evaluate a dynamic programming optimisation is much greater than any permissible operating time a controller has during driving and thus dynamic programming is a theoretical approach to optimal control purely for analytical reasons.

Reference [46] determines a global optimisation control strategy with the capability for investigating the effects of varying input considerations on the fuel consumption of HEVs. A cost function is determined that relates ICE torque, transmission gear selection and battery power consumption using Lagrangian multipliers. The Lagrangian multipliers determine varying levels of sensitivity in the cost function relative to the battery SOC and ICE torque. Using methods such as simulated annealing and dynamic programming to evaluate the cost function it is possible to test the varying use of fuel energy and stored energy. This evaluation in effect calibrates the cost function for real-time implementation. In addition, the authors identify that it is possible to apply this control strategy to a number of vehicle configurations. This highlights the use for global optimisation as a theoretical study, evaluating the performance of various PHEV and HEV.

Reference [11] is an example of global optimisation as considered in the definition of acausal systems. The authors determine mathematical relationships among the ICE fuel consumption, losses in the electrical network and drive cycle power requirements as the means to minimise losses. This is then adapted to a probability density function that determines the expected power demand at any given time instant as a means to define the optimal ICE on/off power threshold for minimised system losses during blended charge depletion. Additionally, the authors of [33] define a cost function that is subject to the vehicle dynamical limitations. In forming the cost function, power supply is determined with propulsion device torques as the input variables and operating speeds as the state variables. Furthermore, the battery power is an input variable and the SOC is a state variable. The cost function in [33] is evaluated using a modified policy iteration method which is also integrated with a stochastic distribution of standardised drive cycles that help determine the optimal power supply to satisfy demand. The policy iteration method determines the cost of operating at an initial set of input conditions before re-evaluating the input conditions to determine if further minimisation of the cost function is possible. In completing the second step the controller then checks to see if the initial input conditions are within 1% of the re-evaluated input conditions before terminating the policy iteration. It is noted in [33] that in order to achieve a solution within reasonable time there is a limit to the number of iterations evaluated. The authors of [33] demonstrate that while the total number of iterations is limited the designed controller achieves desired performance during realtime operation.

The stochastic analysis associated with both [11] and [33] initially utilises past statistics or models that represent expected operations of the PHEV and HEV control strategies. In the case of being determined offline such stochastic analysis improves the operation of global optimisation. In both cases the authors have identified that if the stochastic information is updated on-the-go then this would lead to real-time optimisation. This type of controller is sometimes referred to as adaptive real-time optimisation [47, 136, 141]. There is a similar controller presented in [132], that integrates a predictive reference signal for aided real-time control. The predictive reference signal is adapted to the SOC of the ESS using global positioning system (GPS) route information that anticipates future driving requirements and the potential for regenerative braking. Real-time optimisation is a common goal for control strategies in PHEV and HEV recently [8]. The motivation leading towards real-time optimisation according to the authors of [11, 33, 46, 132] is due to the complexity and computational requirements of global optimisation control strategies and therefore the limited ability for application in real-world controllers.

The authors in [36] identify an adaptive-equivalent consumption minimisation strategy which like those mentioned previously introduces a predictive reference signal for on-the-go optimisation. An equivalence factor is utilised for determining the optimal power split between the ICE and M/G. The equivalence factor is also discussed in [132]. In order for the controller to have predictive qualities during operation the varying conditions of normal driving must be recorded and analysed on-the-go. The equivalence factor of the controller in [36] is determined by analysing past and future data values to achieve an average road load requirement over a pre-determined future time window. This estimated future loading requirement aids the controller with energy management decisions and can be periodically refreshed. The authors of [36], highlight that without the predictive capabilities of the equivalence factor the optimisation in the equivalent consumption minimisation strategy alone may degrade the vehicle operation. A simple approach to selecting the equivalence factor is to optimise it for the performance over a given drive cycle. It then results that the objectives such as charge sustenance or fuel consumption reduction may not be met during other drive cycles. The advantage of such adaptive real-time optimisation is that the fuel consumption reductions are achieved without the need for *a priori* knowledge.

Additionally, controllers that analyse trip based information are emerging for improved accuracy in energy management decisions [32, 52, 127]. Information such as trip distance, traffic conditions, vehicle speed limits, road types and elevation are considered in the analysis of the vehicles energy requirements. This is then adapted to the current load requests in order to prepare for expected load demands in the future driving conditions [107, 122, 141, 142]. The outcome for including this information is reduced fuel consumption due to

the controller having the capability for making informed decisions, e.g. when to charge or discharge the ESS. This type of controller is generally given its own category as a predictive real-time controller since the applications are not limited to optimisation of recorded vehicle information which is the main approach to energy management in optimisation-based blended controllers. Predictive controllers are discussed further in Chapter 5.

In the process of determining the best control strategy to utilise in the design of a PHEV and HEV classifying the control strategies helps discern expectations of performance. Rather than having the pre-defined modes of operation optimisation and rule-based blended controllers are leading into strategies that blend together as one mode of operation. This is more predominantly the case with optimisation based blended controllers, such that a cost function provides the basis for optimisation. These blended control strategies identify the unique solutions to the energy management problem as opposed to selecting a mode of operation that might be best suited at the time. As demonstrated above the most advantageous control strategies utilise real-time optimisation and in some cases adapting elements of predictive control.

2.6 Sizing of Components

Section 2.3 established the physical differences and general performance outcomes from utilising a particular vehicle configuration in the design of HEV and PHEV. In addition the modes of operation of Section 2.2.6 with the vehicle configurations of Section 2.3 identify the potential for improved fuel economy of the HEV and PHEV through considering the available energy paths. Here the expectations of such vehicle configurations are discussed through an example of sizing an experimental setup. This discussion aims to provide the link between the vehicle configuration and the control strategies employed and how component sizing has a large impact on the performance capabilities and therefore control requirements. Due to the constraints of the series and parallel configurations of Sections 2.3.1 and 2.3.2 this sizing demonstration is applied to a power-split topology.

Initially this investigation was for the design of a scaled experimental setup relative to the requirements for a test bench in this research program. In the consideration for a scaled version of a power-split PHEV the expectation was to minimise costs within a budget of AUD 15,000. Upon approaching a manufacturer of custom designed road vehicles the quoted build costs for the experimental setup exceeded the allocated budget. The allocated budget was enough to acquire the custom designed rolling chassis without the electric drive components and controllers. A list of components for the experimental setup outside of the rolling chassis is provided in appendix A.2. This investigation is included here as a means

for identifying important considerations in the process of designing an experimental setup and thereby the EMS.

2.6.1 Experimental Setup

Following the investigation into selecting an optimal ESV and the desired control strategy, literature surrounding the sizing of components aided with the consideration of a test bench. Selecting a power-split PHEV as the appropriate vehicle configuration the propulsion devices for an experimental setup are determined. In particular the 2 by 2 power-split PHEV is referred to as a means to simplify the mechanical connections of the drivetrain (also known as the dual drive HEV [94, 148, 149]). Figure 2.17 identifies the vehicle configuration for the experimental drivetrain. The ICE is coupled to a CVT located at the rear of the vehicle and motor/generator (M/G2) is coupled to the front wheels via a single gear transmission or differential. M/G1 acts as a generator for the majority of the time, while it has the potential to absorb negative transients from the rear axle during braking of the vehicle.

The focus for the sizing was in the selection of the propulsion devices for the defined vehicle configuration. Power electronic converters (PECs) are selected based on the rated specifications, in particular output voltage of the ESS and the input voltage range of M/G1 and M/G2, with consideration for the grid connection. The selection of these devices is not part of the scope of the study in this research program. The identification of the power electronic converters in Figure 2.17 is to demonstrate the potential number of power electronic converters required for this type of vehicle configuration and to plan for the associated costs.

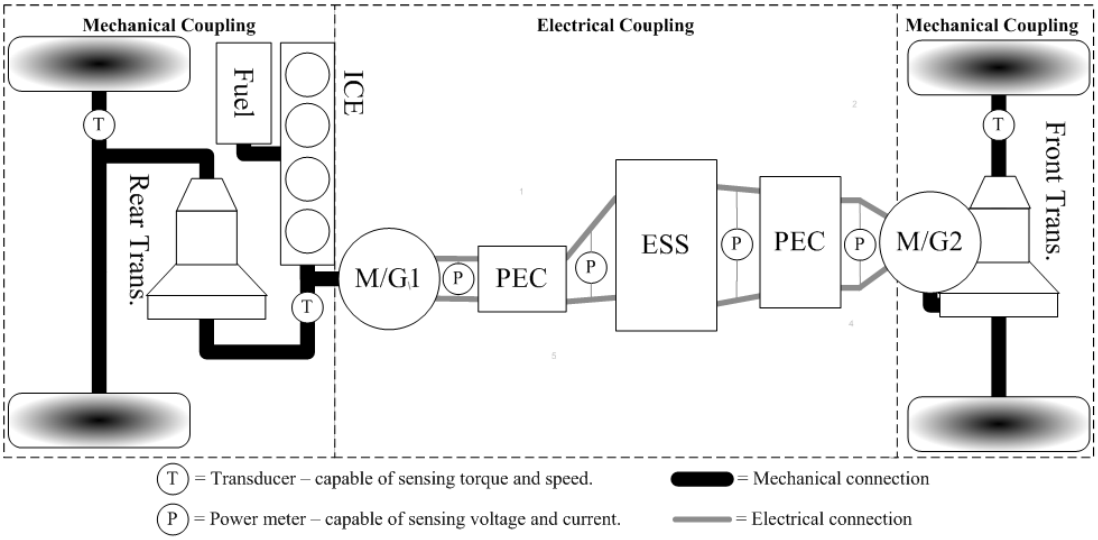

Figure 2.17 - Experimental setup considered in the initial stages of research program.

2.6.2 Powertrain Considerations

Using a scaled standardised drive cycle the average power is to be satisfied using the ICE while the transient load requirement is satisfied using the ESS and M/G2 acting as a motor. The standardised drive cycle utilised is the new European drive cycle (NEDC). In an attempt to reduce the capital costs of propulsion devices a peak velocity of 60 km/h is considered. Following selection of the propulsion device power rating a 40 km/h reduced maximum of the NEDC is selected for sizing the ESS. The original NEDC and scaled versions for power rating selection are shown in Figure 2.18.

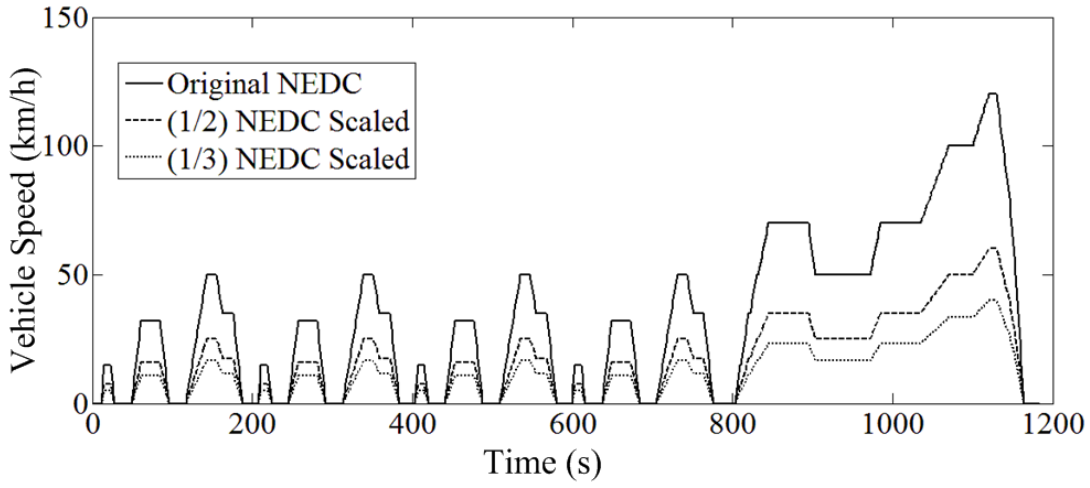

Figure 2.18 - Scaled versions of the standardised drive cycle selected for powertrain sizing.

Using the tractive power calculation of equation 3.1 featured in Section 3.4.1 and obtained from [5], the power requirement for the identified drive cycles is determined. In addition, the following equation is utilised to estimate the output power requirement of the propulsion devices at any given time:

$$P_P = \frac{P_t(1+s)}{\eta_{DT}} \tag{2.13}$$

With η_{DT} being the total efficiency of drivetrain components, P_P the power rating of the propulsion device, P_t the tractive power requirement and s the approximate percentage slip due to the traction of the wheels and rotational inertial of drivetrain components. The power rating of the propulsion devices are dependent on the continuous power requirement, the peak power requirement and the hybridization factor (HF) [4, 150].

The HF featured in the analysis of [150], identifies a means for comparison of the power rating of the ICE and M/G with respect to the fuel consumption reductions in parallel connected hybrid powertrains. The HF is equal to the left hand side of the inequality of equation 2.14. Once the M/G power rating reaches a certain percentage of the total hybrid

power rating, the fuel savings are limited. For a HF between 20% to 70% the fuel economy improvement rises from 20.2% to 28.5% indicating that the extra cost for increased M/G power rating may not be justified by the identified potential savings on fuel [150]. Using 20% HF as the minimum an inequality is determined for the sizing of the M/G with respect to the ICE or vice versa.

$$HF = \frac{P_{m/g}}{P_{m/g} + P_e} \geq 0.2 \tag{2.14}$$

Leading to:

$$P_{m/g} \geq 0.25 P_e \tag{2.15}$$

In the case of the defined inequality the M/G power rating must be at least 25% of the ICE power rating to achieve a fuel consumption reduction of more than 20.2% when compared to using the ICE alone.

2.6.3 Drivetrain Considerations

The main drivetrain consideration for this experimental setup is the ratio between the propulsion device and the driven wheels. In this case the speed of the ICE must match the speed of the rear axle and the speed of M/G2 must match the speed of the front axle. From [5], the axle speed (ω_{dw}) is determined as:

$$\omega_{dw} = \frac{V}{r_d} \tag{2.16}$$

Equation 2.16 leads to the speed of the drive axle based on the wheel radius and vehicle speed, for determining the ICE or M/G2 gear ratios as:

$$\omega_P = \omega_{dw} i_o i_g = \omega_{dw} i_t \tag{2.17}$$

where i_o and i_g represent the final drive and gearbox ratios respectively and ω_P is the speed of the propulsion device for each drive axle. For the experimental setup the wheel radius is chosen as the standard size used for an off road go-kart [151], at 0.1905 m. This choice of wheel locks in the wheel radius and allows for the consideration of the required gear ratio.

2.6.4 Specifications

In determining the specifications of the experimental setup both simulations and calculations were used as means for comparison and verification. Simulations were completed using the ADVISOR software package introduced in Section 3.2.3 and calculations were completed based on the equations for vehicle propulsion presented by Ehsani et al [5]. Signals for both simulations and calculations are identified in Figure 2.19, Figure 2.20 and Figure 2.21.

Based on the mass and vehicle shape of a quad bike featured in another powertrain sizing study completed in [152] the output power for a propulsion device on the experimental vehicle is calculated and displayed in Figure 2.19. On one hand the ICE must supply the maximum power required for driving, which is up to 8 kW (Figure 2.19). Alternatively, the ICE is required to supply the average power requirement [20, 37]. The average power required for propulsion of the vehicle is less than 2kW as shown in Figure 2.19, during propulsion device or ICE operation as in this case. Given that the optimal efficiency of an ICE is observed between 50 and 75% of the peak power rating [11, 37, 153], the ICE power rating is selected according to a compromise between the two power levels. Therefore the power rating of the ICE is selected at 6 kW.

Following selection of the ICE, M/G2 is selected according to the same output power requirement. In the case of M/G2 however, the average efficiency is much greater than the ICE and thus the optimal efficiency is not as important. M/G2 is selected with a continuous power rating of 6 kW, and a peak power rating of 12 kW. Finally, M/G1 should be selected according to the peak power rating of the ICE such that continuous operation of the ICE can be absorbed using M/G1. In this case the selection of M/G2 is more than sufficient to achieve this operation and thus M/G1 is selected at 6kW continuous and 12 kW peak as well.

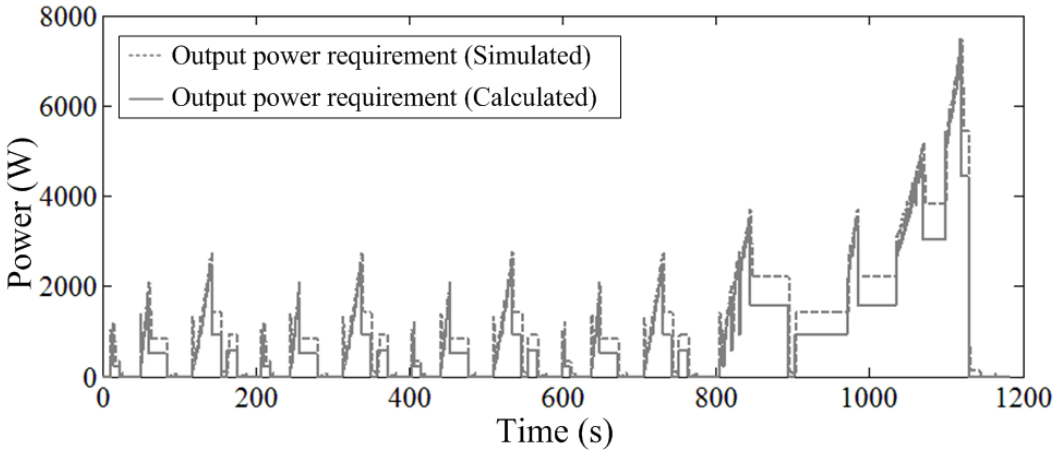

Figure 2.19 – M/G2 output power requirement for experimental setup having varying mass.

Generally the operating speeds of propulsion devices are much greater than the rotational speeds of the drive axle (i.e. rotational speed of the wheels). Therefore a step down gear ratio is required from the propulsion devices to the driven wheels. The front gear ratio between M/G2 and the front axle is dependent on the maximum speed of M/G2 and the desired maximum speed of the vehicle. In this case the maximum desired speed is 60 km/h, from the selection of M/G2 the maximum speed is 5000 rpm. Rearranging equations 2.16 and 2.17 to solve for the total front gear ratio (i_{tf}) determines a ratio of 6.1:1.

$$i_{tf} = \frac{\omega_{m/g,\max} r_d}{V_{\max}} \tag{2.18}$$

For the ICE as mentioned in Section 2.2.1 more than one fixed gear is required in order to meet the high torque required for acceleration and to improve the performance of the ICE. This is the reason for selecting a CVT in the rear for mechanical coupling of the ICE to the driven axle. In the case of the CVT there are set limits for the ratios the device can achieve from input to output. One particular consideration for the CVT ratios as featured in [154], includes 2.92:1 to 0.7:1. In this theoretical study the exact ratios the CVT can achieve is not important, as long as the method for using these ratios in the experimental setup are clearly outlined. In this case the idea for using a CVT is to ensure that the ICE speed is independent of the vehicle speed. Therefore a final drive ratio is required to ensure that the ICE can achieve efficient operation for the majority of vehicle speeds. An acceptable starting point is to determine the final drive ratio for the rear axle according to:

$$i_o = \frac{\omega_{e,rated} r_d}{V_{\max} i_{g,\min}} \tag{2.19}$$

Equation 2.19 uses the minimum ratio of the CVT ($i_{g,min}$) to ensure that the rated speed of the ICE matches the desired maximum speed of the vehicle. Then examining the constraints of the ICE the potential for control and for meeting the desired vehicle speeds is revealed.

Firstly, in this example the final drive ratio would be selected as 4.3 to ensure that the ICE can meet 60 km/h using the minimum CVT ratio at 2500 rpm. Following this initial calculation, Table 2.1 identifies the operation of the CVT relative to the constraints of the ICE and the selected final drive ratio. The selected final drive ratio is large enough to accommodate acceleration across the desired vehicle speed range while having the potential to vary the ICE operating speed. For example the ICE can maintain 2500 rpm for the vehicle speed range between 14.3 to 59.6 km/h. Theoretically speaking if 2500 rpm is the maximum efficiency for the ICE, then vehicle speeds from 0 to 14.3 km/h would occur at efficiencies below the maximum [37]. Given that M/G2 is more efficient it would be best to supply load torques occurring between 0 to 14.3 km/h using M/G2, hence the consideration for the Toyota Prius as identified in [5]. This combined ICE and M/G2 operation is discussed in more detail in Sections 4.2 and 4.3. Table 2.2 outlines the specifications for the experimental vehicle, which are based on a quad bike as featured in [152] and the analysis described above.

Table 2.1 - Comparison of operating speeds with a final drive ratio of 4.3.

Constraint	ICE Speed (ω_e)	Vehicle Speed (V)	CVT ratio (i_g) (Input: Output)
ICE Idle Speed	104.7 rad/s (1000 rpm)	5.7 km/h	2.92:1
ICE Max Speed	523.6 rad/s (5000 rpm)	60 km/h	1.39:1
ICE Rated Speed	261.8 rad/s (2500 rpm)	59.6 km/h	0.7:1
ICE Rated Speed	261.8 rad/s (2500 rpm)	14.3 km/h	2.92:1

2.6.5 Operation of Selected Components

From the performance data sheets for the selected M/G listed in Table 2.2 the torque-speed characteristic is estimated. Figure 2.20 shows the torque versus speed at constant voltage for the selected M/Gs, at 24 V, 36 V and 48 V. The torque-speed lines of Figure 2.20 are determined from the linear relationships between torque, speed and voltage as shown on the data sheet. Assuming the maximum torque to be 23 Nm at 24 V as seen in Figure 2.20, the maximum continuous torque versus speed characteristic ($T_{max,cont.}$) is estimated using a base speed of 2500 rpm, which is the speed at rated power defined by the performance data sheet. Note that the maximum continuous torque-speed characteristic agrees with the specification given in Table 2.2, with 18 Nm occuring at 3200 rpm. Next the maximum peak torque-speed characteristic ($T_{max,peak}$) with the same base speed and double the power was estimated as shown.

Table 2.2 - Specifications determined for the powertrain of the experimental vehicle.

Specification	Value
Internal combustion engine	242 cc, 5.9 kW, 16.7 Nm, @ 2500 rpm
M/G1 and M/G2	6kW continuous, 12 kW peak, 48 Vdc, 0-5000 rpm, 18 Nm @ 3200 rpm
M/G1 and M/G2 Average Efficiency	75% (worst case scenario)
Transmission/Final drive efficiency	85%
Converter efficiency	95%
ESS coulomb efficiency	80%
Vehicle Mass	350 kg
Wheel Radius	0.1905 m
Front Transmission/Final Drive Ratio (i_{tf})	6.1:1
Rear Transmission/Final Drive Ratios (i_{tr})	CVT (2.92:1 to 0.7:1), FD (4.3:1)
Vehicle Width	1112 mm
Vehicle Height	1160 mm
Aerodynamic drag coefficient	0.3
Air density	1.2 kg/m^3
Gravitational Acceleration	9.8 m/s^2

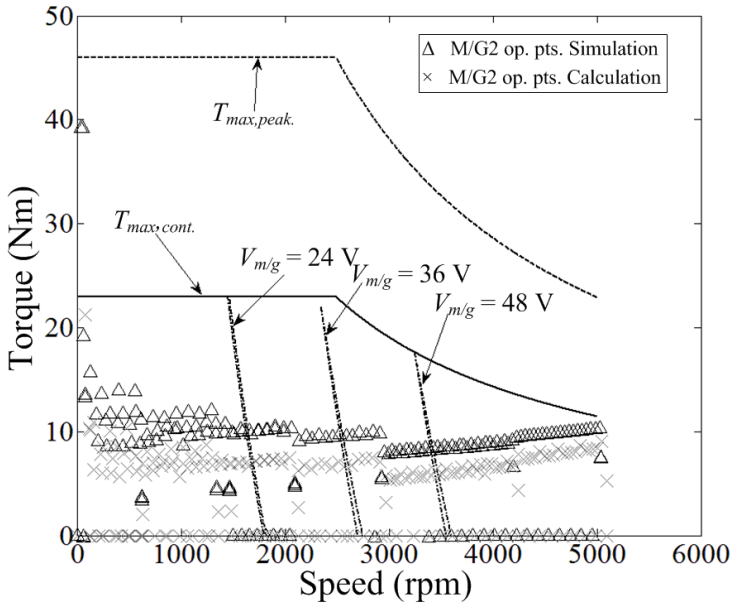

Figure 2.20 - M/G2 output torque versus speed over the (1/2) NEDC identified in Figure 2.18

Using the equations from Ehsani et al [5] and the specifications defined in Table 2.2 the operating torques and speeds are calculated for the (1/2) NEDC scaled drive profile. Adding the operating points (op. pts.) to Figure 2.20 a comparison of the torque-speed characteristic for M/G2 reveals that the selected specifications agree with the calculated and simulated operating points. Figure 2.20 also demonstrates the full speed range of the M/G for the drive profile having the maximum vehicle speed (60 km/h) occurring at the maximum M/G speed. In simulation additional losses such as inertial losses, slip and component efficiency are considered leading to an increased power requirement.

The torque and speed requested from the ICE under calculation and simulation is examined in Figure 2.21. First the maximum torque-speed characteristic of the selected ICE is estimated based on the specifications of Table 2.2. Comparing this maximum torque available from the ICE against the torque requested over the drive profile at the drive axle the potential for satisfying the load using the ICE is determined. The gear ratios utilised in Figure 2.21 occur within the range for the CVT combined with the final drive ratio (e.g. 4.3 ×2.92 = 12.56). Figure 2.21 identifies that the ICE is capable of satisfying the majority of requested loads; in particular the expectation is to satisfy loads for vehicle speeds between 14.3 to 60 km/h.

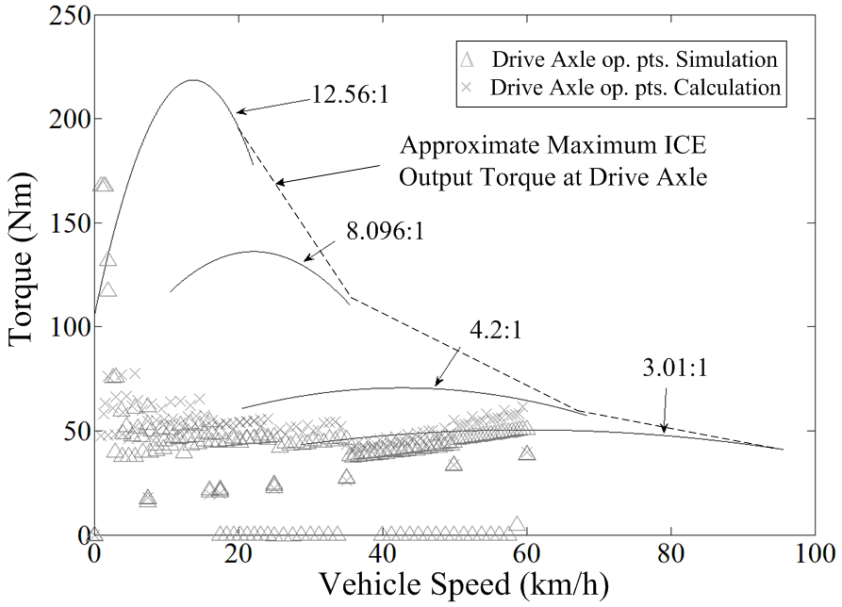

Figure 2.21 – Comparison of approximate ICE torque-speed characteristic based on specifications of Table 2.2 for four potential gear ratios at the drive axle.

For the battery energy storage requirement the PHEV all-electric range needs to be considered. Researchers have defined PHEVs according to the all-electric range, labelling each vehicle as PHEV5, PHEV10, PHEV20 etc. according to the distance travelled in miles starting with fully charged batteries for a typical day [104]. This means that a PHEV5 will have a 5 mile all-electric range, and a PHEV10 will have a 10 mile all-electric range etc. By this means of PHEV definition a PHEV20 allows for 32 km of travel during charge depletion mode of operation before it enters charge sustenance mode of operation to maintain battery SOC [7, 33]. Considering the (1/3) NEDC scaled drive profile and repeating it 9 times, leads to a total distance travelled of 32.76 km in 3 hours of driving. To design the battery energy storage capacity to propel the vehicle for this distance ensures that at least 3 hours of testing will be available for the vehicle on any given day with hybrid operating modes extending this available testing time.

Table 2.3 lists the battery energy storage requirements according to the drive profile considered. To allow for sufficient SOC remaining in the battery bank at the end of the all-electric range, the depth of discharge for the battery bank is selected at 60% [94]. Comparing the energy requirement against available lithium-ion battery banks from local suppliers, the battery energy storage requirements are selected as listed in Table 2.3 (160 Ah, 24 V). With a depth of discharge of 60% and the considered Ah energy requirement (81.24 Ah) the selection of the 160 Ah, 24 V battery bank is more than enough for the desired testing.

The analysis completed for the propulsion device power ratings and battery energy storage demonstrates that the designed vehicle is acceptable for the considered testing. Varying the

drive cycle requirements will lead to varying power ratings of components while varying propulsion device selection will lead to varying drivetrain requirements.

Table 2.3 - Specifications for battery energy storage

Specification	Value
Drive Profile	9 x scaled NEDC
Peak Velocity	40.0 km/h
Average Velocity	11.1 km/h
Time	3 hours
Distance	32.76 km
Voltage	24 V
RMS Current	29.06 A
Maximum Current	128.7 A
Energy Storage Used (Calculated)	82.46 Ah
Energy Storage Used (Calculated)	1978.7 Wh
Energy Storage Used (Simulated)	81.24 Ah
Energy Storage Used (Simulated)	1949.7 Wh
Energy Storage Requirement	160 Ah
Energy Storage Requirement	3840 Wh

2.7 Summary of Literature Review

Four main topics are covered in this Chapter. Firstly, identification of energy smart vehicles (ESVs) as referring to electric, fuel cell, hybrid electric and plug-in hybrid electric vehicles. Secondly, focus was given to the components integrated on the vehicles as a means to categorise and help understand the various ESVs. Then examining the performance of commercially available ESVs the selection of the power-split PHEV as the vehicle configuration for this research program is supported. Thirdly, having defined ESVs control strategies featured in technical papers are examined from the perspective of Wirasingha et al [8] in order to narrow the scope for designing the EMS. Finally, a method for the optimal sizing of components is demonstrated via an example for the design of an experimental setup. The following is a summary of the main points discussed in this Chapter.

Relative to the conventional vehicle compression ignition (CI) ICEs are more efficient than spark ignition (SI) ICEs however CI ICEs produce larger quantities of emissions [54]. Transmissions are generally of the fixed multi-gear type having a direct coupling between the ICE and driven wheels. This discussion on transmissions however highlights the potential for flexible control in the continuously variable transmission (CVT), even though the CVT does not feature predominantly in the conventional vehicle. The EV can be adapted from the conventional vehicle or designed from scratch. In the case of adapting a conventional vehicle to an EV the fuel tank or luggage space is utilised for housing batteries while the ICE is replaced with a M/G. Relative to ESV design there are three alternative electric machines; DC machines, AC synchronous machines and AC induction machines. The choice to use either one of these electric machines in ESVs is a result of design constraints such as control complexity, capital cost and performance attributes. Power electronic converters and controllers realise the conversion of electrical energy for controlling the M/G, consuming a small amount of energy in the process. The main concern for EVs is the limited drive range due to the poor energy density of energy storage mediums.

Following the EV configuration the addition of a fuel cell aids with the supply and maintenance of ESS SOC. The fuel cell vehicle utilises the ESS to meet the transient demands of driving while the fuel cell supplies the average power demand. Even though the fuel cell is more efficient in converting hydrogen to electrical energy than the ICE is in converting gasoline to mechanical energy there are concerns for the use of hydrogen. Hydrogen consumes energy in production and storage leading to an overall efficiency similar to the average efficiency of ICE. The hydrogen is limited by the volume to energy density for storage on vehicles, taking up luggage space that is otherwise available on the conventional vehicle. For these reasons fuel cells for use in transportation are considered to remain in the development phase.

The most common form of ESV is the HEV, realising the combination of an ICE and ESS with M/G to meet drive load requirements. The HEV uses the ICE to meet steady state loads while allowing the ESS to satisfy the transient load requirements. The HEV does not suffer range anxiety like the EV, however, it relies on the consumption of fossil fuel to meet load demands. Using HEV the transportation industry has the potential for a smooth transition from conventional vehicles to sustainable vehicles as opposed to redesigning and building the infrastructure to support a completely new approach to transportation. Alternatively the PHEV is more or less an HEV with a larger sized ESS. This allows the PHEV to operate as an EV for a short distance without the concern for range anxiety. With a larger ESS the PHEV has greater potential for fuel consumption reductions utilising cost functions to implement charge depletion/charge sustenance or blended charge depletion strategies. Ultimately charging the ESS from the grid in the case of the PHEV offers greater fuel savings than the HEV which must charge the ESS using the ICE.

The vehicle configuration identifies the arrangement of components on the PHEV or HEV and the potential for control. There are three main vehicle configurations, the series, parallel and power-split. The series configuration operates the ICE at optimal conditions however it suffers from increased drivetrain losses. The parallel configuration on the other hand has a direct mechanical coupling between the ICE and driven wheels that restricts ICE operating speed, leading to a lower average ICE operating efficiency. The parallel configuration does however have reduced drivetrain losses in comparison to the series configuration. The power-split configuration in comparison to both aforementioned configurations has all of the advantages and none of the disadvantages. There is however added complexity in control and increased capital costs associated with the power-split configuration. In addition to the vehicle configurations, the mechanical modes of operation detail the improved degree of control the power-split configuration has over the series and parallel configurations. Finally, a comparison of the commercially available vehicles relative to the identified vehicle configurations determines the power-split configuration in the Toyota Prius having the lowest fuel consumption for continuous long range driving. This discussion of the vehicle configuration and associated performance supports the selection of the power-split topology for this research program.

Control strategies are the means for achieving best performance of a selected vehicle configuration. The classification into hybrid, multimode, rule-based blended and optimisation-based blended controllers help to distinguish the advantages and disadvantages of various control strategies. In addition, this classification helps to narrow the scope for designing an EMS, identifying that real-time if not predictive optimisation yields the best results. In particular, the optimisation of energy in a power-split PHEV should be dependent

on a cost function that relates the real-time operation of powertrain components to past and/or future road load requirements.

Finally, an exercise for sizing the main powertrain and drivetrain components provides a link between the vehicle configuration and available control strategies. This is achieved through the consideration that component sizing has a large impact on the performance capabilities resulting from particular control strategies. The main criterion identified as a result of this exercise relative to desired performance includes:

- Load power is achieved for all drive profile requirements
- Traction torque developed by propulsion devices is high enough to meet the requirements for driving
- Energy storage is sufficient for desired power levels and minimum operating times
- Gear ratios ensure the propulsion devices will operate to the desired constraints
- Propulsion device efficiency is important especially in the case of the ICE
- ICE power rating must meet a minimum acceleration time, while achieving a set maximum speed and providing an outlook for efficient operation and control
- Performance improvement of the M/G and ESS to ICE operation is attributed to the HF such that a minimum HF determines the near to maximum benefit capable of a HEV

These design considerations thereby realise the means for powertrain and drivetrain component selection, in light of vehicle configuration, control limitations and performance requirements. In particular, the foundations for the development of a suitable test bench for testing the operation and control of ESVs are established. Finally, this investigation is useful in judging the expected performance or for explaining the limitations of HEVs or PHEVs.

CHAPTER THREE

Modelling of Energy Smart Vehicles

3.1 Introduction

In the previous Chapter the vehicle configurations, component sizing, relationship between components and typical methods for control were discussed as a means to select the best alternative to the conventional vehicle. The discussion in the previous Chapter leads to the selection of the power-split PHEV for investigation in this research program. As a result of the analysis for the sizing of components for an experimental setup it was realised that the cost for acquiring a scaled test bench would exceed the budget for the research program. The process, however, provided an insight into the requirements for the design of a PHEV and serves as an introduction to the investigation featured in this Chapter.

As an alternative to the experimental setup three vehicle models have been developed in the advanced vehicle simulator (ADVISOR) for use as test benches. The three vehicles are the Toyota Prius 2010, Hyundai Sonata Hybrid 2011 and Honda CR-Z 2010. The Toyota Prius 2010 is a power-split HEV, however, to demonstrate application of the designed control strategy the Hyundai and Honda are both parallel HEVs. As mentioned in Section 2.2.5, the PHEV is more or less a HEV with larger energy storage. This means that benefits of operation demonstrated on the three HEVs are expected to be seen in plug-in hybrid versions of the vehicles as well. The scope for testing on each of the simulated vehicles is outlined in Chapters 4 and 5 relative to each of the designed controllers.

Measured data from the operation of the three vehicles on standardised drive cycles is referred to for a better understanding of their performance. Operation of the ICE, M/Gs, and ESS with respect to the tractive power measured at the wheels of each vehicle is examined to reveal operating modes and the underlying control strategy. Focus is not placed on replicating the exact transient operation of components in simulation when compared to the measured signals, however, a comparison helps reveal areas requiring additional attention. Finally, input and output energy, overall efficiency and average fuel consumption on the standardised drive cycles determine the performance targets for the simulated vehicles to meet.

In particular, this investigation confirms the specifications of the components utilised on the three vehicles, including power, torque and speed ratings, efficiency of operation and definition of the rolling chassis (i.e. coefficient of aerodynamic drag, rolling resistance, etc.).

A comparison of the simulated and measured performance targets identified above reveals a maximum error of 3.87% for both the urban dynamo driving schedule (UDDS) and highway fuel economy test (HWFET) drive cycles. Through demonstrating the ability of the simulated vehicles to meet the defined performance targets three test benches for this research program are realised. Section 3.2 discusses the reasons for selecting the ADVISOR software by comparing the different approaches to simulation.

3.2 Simulation Tools

Due to the high capital costs of an experimental test bench researchers conduct simulation for the analysis of novel EMS controllers [8, 11, 26, 32, 41, 60, 89, 155, 156]. The test benches utilised in this research are developed in the ADVISOR simulation package, which is an add-on to the MATLAB/Simulink environment. This Section endeavours to identify why ADVISOR is selected for simulations in this thesis. In terms of the available software packages for vehicle analysis there are two options; dynamic vehicle simulators and lumped parameter models [11]. Dynamic vehicle simulators determine vehicle performance based on models of the dynamical systems of the vehicle [60]. On the other hand, lumped summed parameter models have simplified mathematical models for faster evaluation [11]. ADVISOR applies known vehicle specifications to models of a vehicle's components in order to determine overall performance. Small transient operations of components are ignored in favour of faster simulation for interaction between powertrain and drivetrain components [49, 157]. The ADVISOR software therefore lies somewhere in between, having lumped parameter models to overrule complex small signal responses with enough dynamical considerations to model interactions of the components inherent on the vehicles. In addition to the two types of simulation packages defined above, forward-facing or backward-facing approaches have varying advantages and disadvantages.

3.2.1 Backward-facing Approach

Backward-facing analysis determines required control signals with the assumption that outputs have already been met [158]. Applying these control signals to the vehicle model which is inclusive of the powertrain and drivetrain models shown in Figure 3.1, outputs are utilised to determine input requirements. For example input energy of the powertrain is determined from the required vehicle speed at a set time provided by the drive cycle. Primarily the input signals are the response to a backward-facing approach in simulation.

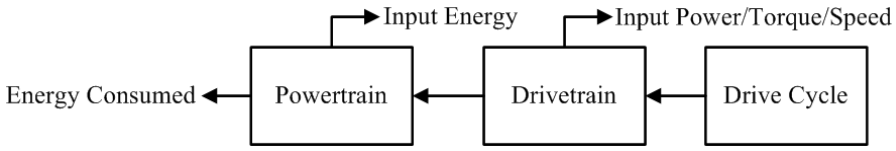

Figure 3.1 - Backward-facing approach to simulation.

The backward facing approach is beneficial in finding a fast solution since computational complexity is reduced. Rather than having to search for a solution the backward-facing approach is provided with the solution, utilising known responses of the powertrain and drivetrain to compute the input requirements. This is also the main limitation of the backward-facing approach since the idea for simulation is to test a system's response to varying inputs. Backward-facing approaches are not suitable for testing control systems relative to the constraints of vehicle components [158]. Alternatively forward-facing approaches provide more realistic test benches for control system response.

3.2.2 Forward-facing Approach

Figure 3.2 aids with the description of a forward-facing approach to simulation. With forward-facing analysis desired output (drive cycle) is converted to input signals such as the throttle position resulting from a driver model. The throttle position is then interpreted by a controller for setting the powertrain and drivetrain components as well as calculating the required input power, torque, speed, and therefore energy.

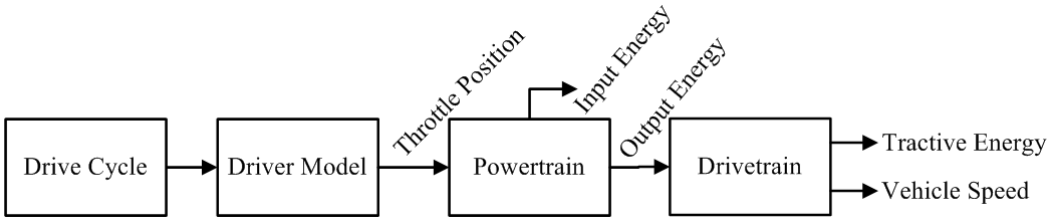

Figure 3.2 - Forward-facing approach to simulation.

The inputs are fed into the powertrain model to determine the resulting outputs, the outputs of the powertrain are fed into the drivetrain as inputs to determine the outputs of the vehicle. The forward-facing approach can therefore determine the output as a response to the input, and is a more realistic representation from a control perspective [158]. In particular, control constraints of vehicle components are considered at the input to devices which identify potential problems in simulation before hardware implementation [11]. For this reason forward-facing approaches are more desirable as a test bench for control system response [57, 159, 160]. Forward-facing approaches are more complex and require larger simulation times to optimise solutions to drive problems. The combination of forward and backward

facing approaches to simulation on the other hand determines a fast approach to simulation with the inclusion of component constraints.

3.2.3 Combined Backward/Forward-facing Approach

The combination of backward and forward facing approaches to simulation realises a test bench that achieves system responses to control decisions quickly without compromising the limitations of individual components. Referring to ADVISOR as an example the simulation setup is mostly a backward-facing approach allowing the calculation of power, torque and speed to occur via the use of look-up tables [49]. These look-up tables are discretely defined and so the dynamic response of the vehicles is limited. In order to implement the dynamic response inherent with the forward-facing approach the ADVISOR software determines the required inputs to the system relative to the defined constraints of components [49]. Figure 3.3 illustrates the application of backward and forward facing approaches in the ADVISOR software. ADVISOR simultaneously determines the available outputs due to inputs (forward) while determining the resulting inputs due to outputs (backward). This allows for an over-lap of the backward and forward-facing approaches as applied to the defined vehicle model. The backward-facing approach determines required inputs with respect to the load while the forward-facing approach dictates whether the system can meet the requested loads.

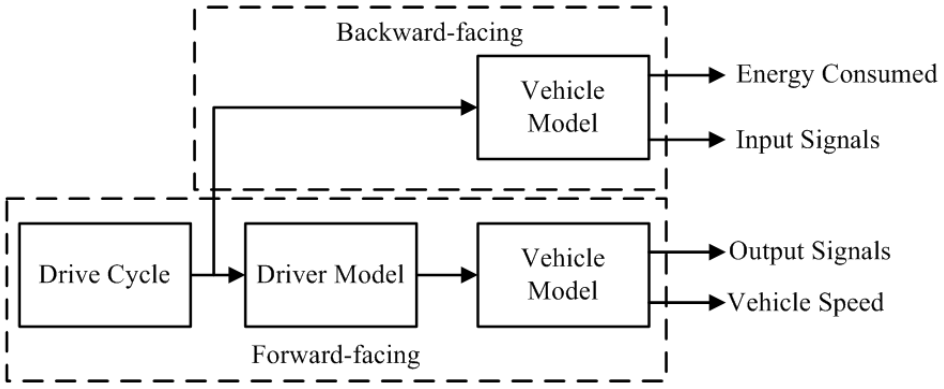

Figure 3.3 - Backward/forwards facing approach to simulation.

The ADVISOR software package has been utilised by a number of researchers [30, 50, 157, 161, 162]. Reference [50] utilises ADVISOR to model a number of vehicle configurations for a solar-assisted electric auto rickshaw, acknowledging the accuracy in predicting vehicle performance without real-world implementation. In particular, researchers identify the robust approach such software packages have in the modelling of vehicles [157]. The main point to note from such powerful software is that reasonably accurate models of individual components on a vehicle must be established in order to retrieve realistic results [161]. With these considerations in mind the ADVISOR software is chosen for the development of a test bench in simulation in this thesis.

3.3 Existing Vehicles

The data of three vehicles has been referred to in the development of three test benches for the study completed in this thesis. The three test benches include the Toyota Prius 2010, Hyundai Sonata Hybrid 2011 and Honda CR-Z 2010. Test data for these vehicles has been obtained from the Downloadable Dynamometer Database [118] which was generated at the Advanced Powertrain Research Facility at Argonne National Laboratory under the funding and guidance of the US Department of Energy. This Section details the vehicle configurations and associated specifications.

3.3.1 Toyota Prius 2010

The Toyota Prius 2010 as mentioned in Section 2.4.2 is a power-split configuration as shown in Figure 3.4. The ICE and two M/Gs are coupled to the PGS to allow torque-speed coupling between each propulsion device as discussed in Section 2.3.4. The ICE is coupled to the carrier gears (C), M/G1 to the sun gear (S), M/G2 to one side of the ring gear (R) and the driven wheels to the opposite side of the ring gear. M/G1 is primarily operated as a generator and provides the speed coupling to the ICE, while M/G2 is utilised as a motor and provides the torque coupling to the ICE. Here the Toyota Prius is an example of an existing vehicle configuration that has flexibility in control due to the PGS. For this reason the Toyota Prius is considered to be able to display the full range of operations for the control strategies featured in this thesis. Specifications for the Toyota Prius powertrain are listed in Table 3.1 with additional specifications listed in Table A.1 (in Appendix A.1).

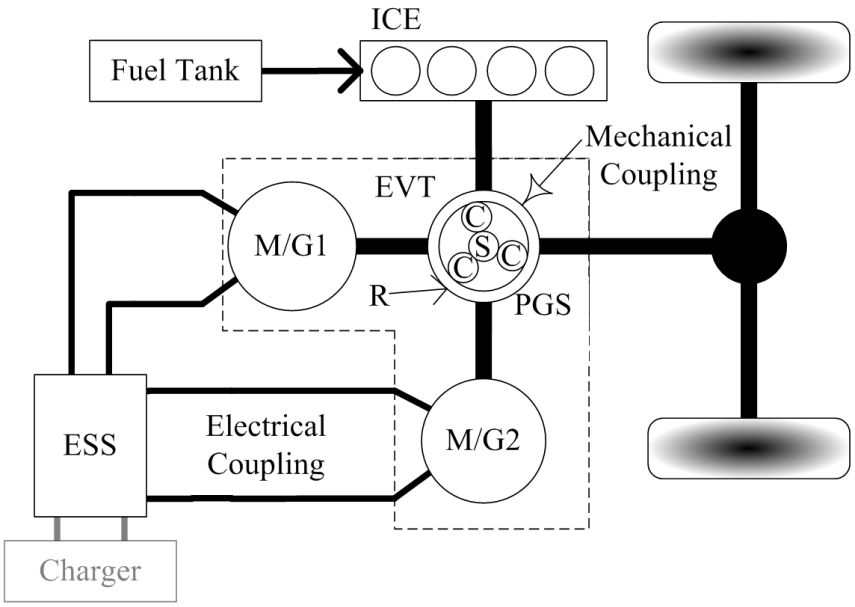

Figure 3.4 - Toyota Prius 2010 vehicle configuration.

3.3.2 Hyundai Sonata Hybrid 2011

The Hyundai Sonata Hybrid 2011 as discussed in Section 2.4.2 is a parallel connected topology with an integrated starter generator (ISG) [10]. The ISG allows for frequent start/stop of the ICE independent of the primary M/G operation ensuring that the ICE conserves fuel during low vehicle velocity or low load requirements. Due to the small size and to reduce the complexity of the model the ISG has been removed, hence the cross through the ISG in Figure 3.5. The Hyundai Sonata Hybrid utilises a mechanical coupling as opposed to the PGS of the Toyota Prius. The mechanical coupling provides torque coupling (Section 2.3.4) of the ICE and M/G1, and is coupled to a six speed automatic transmission (AT 6 spd). Refer to Table 3.1 for the Hyundai Sonata Hybrid powertrain specifications with additional specifications listed in Table A.2.

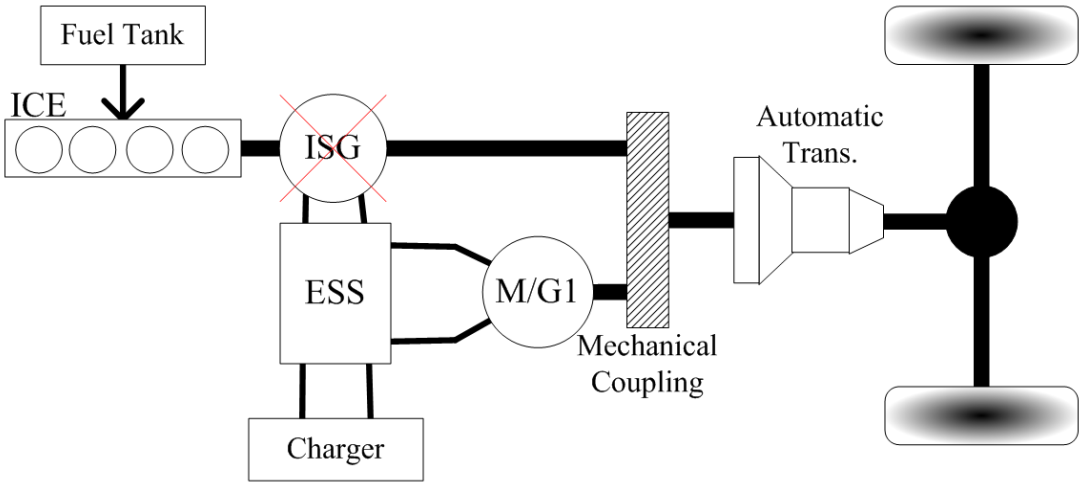

Figure 3.5 - Hyundai Sonata Hybrid 2011 vehicle configuration.

3.3.3 Honda CR-Z 2010

Based on the Honda Insight, the Honda CR-Z is also a parallel connected topology, however, the ICE is directly coupled through the M/G to the manual transmission (MT 6 spd). Further discussion of the Honda CR-Z is featured in Section 2.4.2. The ICE in the Honda CR-Z is continuously operated since the M/G is too small to accelerate the vehicle. The M/G is, however, utilised to absorb small transient operations of the drivetrain that would otherwise cause increased fuel consumption. The Honda CR-Z 2010 specifications are listed in Table 3.1 with additional specifications listed in Table A.3.

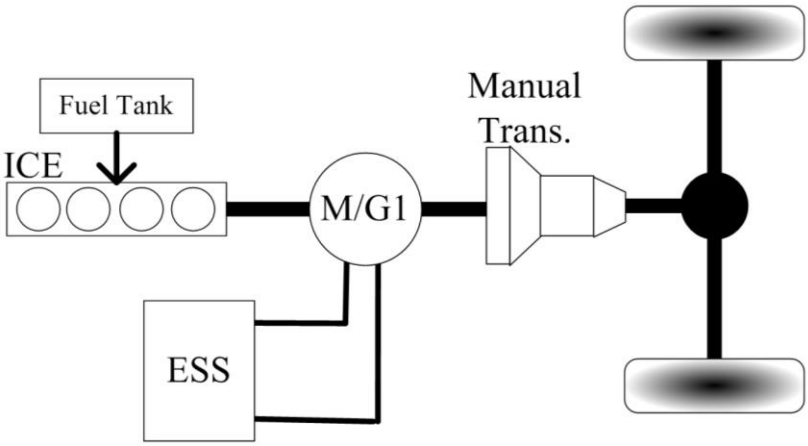

Figure 3.6 - Honda CR-Z 2010 vehicle configuration.

3.3.4 Vehicle Specifications

The vehicle specifications for the three test benches featured in this thesis are listed in Table 3.1. The asterisk (*) next to a specification in Table 3.1 indicates that the value is estimated for simulation purposes, all other listed specifications have been sort from various car manuals, advertisements and web pages detailing information about the three vehicles.

Table 3.1 - Vehicle specifications for the powertrain of the three test benches selected for simulation.

Component Parameter	Toyota Prius 2010	Hyundai Sonata Hybrid 2011	Honda CR-Z 2010
ICE peak power (kW)	73 (@5200 rpm)	131 (@6000rpm)	84 (@6000rpm)
ICE peak torque (Nm)	142 (@4000rpm)	209 (@4500rpm)	145 (@4800rpm)
ICE peak efficiency (%)	36*	36*	34*
M/G1 peak power (kW)	42	30	10
M/G1 peak torque (Nm)	84.7*	181*	79
M/G2 peak power (kW)	60	N/A	N/A
M/G2 peak torque (Nm)	207	N/A	N/A
ISG peak power (kW)	N/A	8	N/A
Transmission	CVT	AT 6spd	MT 6spd
ESS	NiMH 201.6 V and 7.2 Ah	Li-polymer 270 V and 5.3 Ah	NiMH 100.8 V and 5.3 Ah

3.4 Vehicle Tractive Energy Requirements

3.4.1 Modelling Tractive Energy

The vehicle energy requirements are determined according to forces acting on a moving mass. Using the following equation (from Ehsani et al. [5]) it is possible to determine the tractive power requirement of a vehicle travelling at a velocity determined by a driver:

$$P_t = V\left(Mgf_r + \frac{1}{2}\rho C_D A_f V^2 + M\delta \frac{dV}{dt} \right) \tag{3.1}$$

Where P_t is the tractive power required at the wheels to achieve the desired vehicle velocity V in m/s, M is the mass of the vehicle, g is the gravitational acceleration, while f_r is the rolling resistance coefficient and can be represented by:

$$f_r = f_o\left(1 + \frac{V}{160}\right) \tag{3.2}$$

Equation 3.2 provides a linear relationship between vehicle velocity (V) and rolling resistance (f_r). As shown in equation 3.2 rolling resistance can be calculated with respect to some initial value of rolling resistance f_o (equal 0.01 for asphalt/concrete road as a reasonable estimate [5]) and is valid for vehicle speeds up to 128 km/h. Referring again to equation 3.1, ρ is the air density (equal 1.2 kg/m^3), C_D is the coefficient of aerodynamic drag of the vehicle (depending on the shape), A_f is the frontal area of the vehicle and δ is the rotational inertia factor and represents the angular moments of the rotating components defined by:

$$\delta = 1 + \frac{J_w}{Mr_d^2} + \frac{i_g^2 i_o^2 J_P}{Mr^2} \tag{3.3}$$

J_w is the total angular inertial moment of the wheels and J_p is the total angular inertial moment of the power plant (i.e. propulsion device(s)) and r the approximate average radius of the rotating components associated with the power plant. Equation 3.3 can be simplified to:

$$\delta = 1 + \delta_1 + \delta_2 i_g^2 i_o^2 \tag{3.4}$$

Where δ_1 represents the second term on the right-hand side of equation 3.3, with a reasonable estimate value of 0.04, and δ_2 represents the effect of the power-plant-associated rotating parts, with a reasonable estimate value of 0.0025 [5]. Due to the unknown combination of power supplied from the hybrid powertrain it is difficult to determine the exact instantaneous value of δ, therefore δ = 1.0425 is utilised as a starting point.

3.4.2 Interpreting Measured Tractive Power

Test data of various vehicles is available from the Downloadable Dynamometer Database [118] which was generated at the Advanced Powertrain Research Facility at Argonne National Laboratory under the funding and guidance of the US Department of Energy. The available test data includes tractive force (N), vehicle speed (mph), ICE speed (rpm), fuel consumption rate (cc/s), ESS voltage (V), current (A), SOC (%) and the time step (0.1s). In terms of the available measured data of the vehicles there are some conversions required in order to compare the data with the representations described in Section 3.3.

The measured power at the wheels (tractive power) of the vehicle is a combination of the forces acting on the wheels and the known vehicle velocity:

$$P_t = T_t \omega_t \tag{3.5}$$

$$T_t = F_t r_d \tag{3.6}$$

$$\omega_t = \frac{V}{r_d} \tag{3.7}$$

$$P_t = F_t V \tag{3.8}$$

Equations 3.5 to 3.8 indicate that power is independent of the radius of the wheels and that it is calculated directly from the two measured signals (F_t and V). For the discussion of the modelling shown in this Section the measured data of the Toyota Prius is referred to. Table 3.2 lists the specifications of the Toyota Prius 2010 for use in equation 3.1. To start with the rolling resistance is considered as a constant at 0.01 instead of using equation 3.2, in addition equation 3.4 is characterised by $\delta_1 = 0.04$ and $\delta_2 = 0.0025$ with $i_o^2 i_g^2 = 1$.

Table 3.2 - Toyota Prius 2010 specifications for interpretation of the measured data.

Description	Symbol	Value	Unit
Mass	M	1530.87	kg
Rolling Resistance Coefficient	f_r	0.010	-
Air Density	ρ	1.2	kg/m^3
Coefficient of Aerodynamic Drag	C_D	0.39	-
Frontal Area of Vehicle	A_f	1.746	m^2
Gravitational Acceleration	g	9.81	m/s^2
Wheel Radius	r_d	0.287	m

For the comparison of measured and calculated tractive power using equation 3.1 the UDDS is considered. The UDDS is shown in Figure 3.7 in kilometres per hour as converted from the measured speed of the Toyota Prius 2010 [118]. Using the vehicle velocity as input to equation 3.1 the result is the calculated tractive power of Figure 3.8. Through the visual comparison of the two signals shown in Figure 3.8 it is evident that there is some discrepancy in the calculation of the tractive power as compared with the measured signal. Utilising the mean absolute percentage error (MAPE) [163] the error between the two signals is determined at 32.43%.

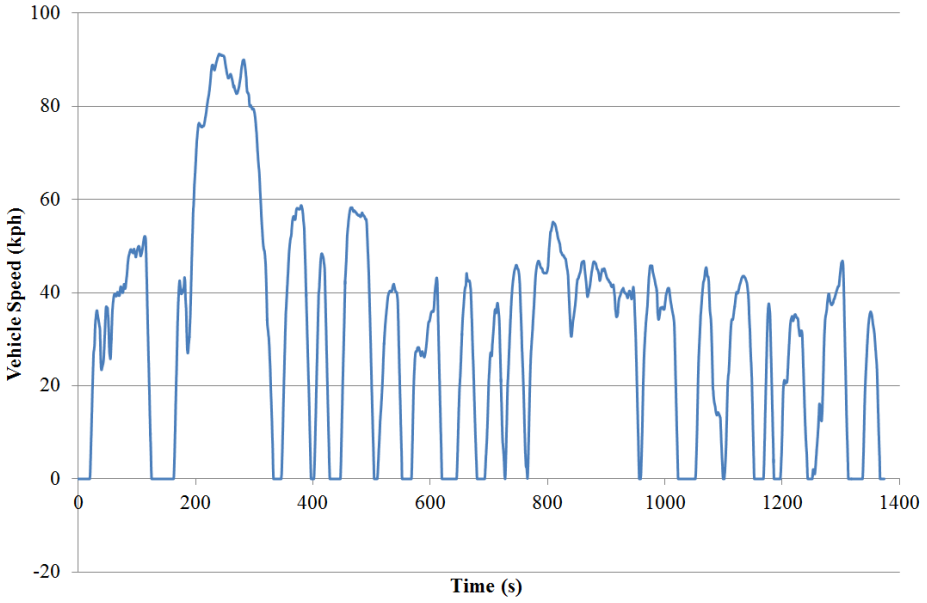

Figure 3.7 - UDDS.

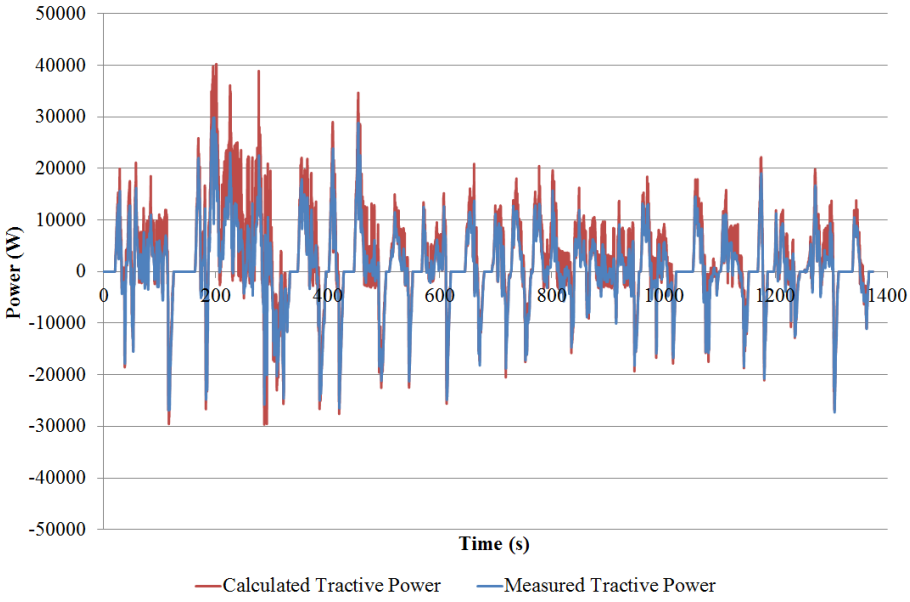

Figure 3.8 - Comparison of calculated and measured tractive power for the Toyota Prius 2010.

The MAPE as mentioned above is determined as follows:

$$MAPE = \frac{1}{n}\sum_{i=1}^{n}\left|\frac{Y_i - X_i}{Y_i}\right| \tag{3.9}$$

where Y_i is the measured value, X_i is the calculated (or predicted) value, i is the corresponding data points of the calculated and measured values and n is the total number of data points. In determining the MAPE all power magnitudes below 5 kW have been ignored due to the large inaccuracy imposed by low wheel speeds, low propulsion power requirements and small signal variations induced by the chassis dynamometer [118]. With a MAPE of 32.43% equation 3.1 is either missing characteristics of the tractive power requirement or one of the characteristics is not represented accurately in equation 3.1. Therefore an investigation of the contributions made by the components of equation 3.1 to the tractive power is undertaken to determine the best equation for representing the measured data.

Case 1: Excluding Aerodynamic Drag

Since the tests completed by the Argonne National Laboratory occurred on a chassis dynamometer it is hypothesised that the aerodynamic drag of the vehicle does not contribute to the power requirement for maintaining the vehicle velocity. Equation 3.1 contains 3 components on the right-hand side; the 1st is to account for the rolling resistance of the vehicle, the second is for the aerodynamic drag of the vehicle and the third is for the angular moments of the rotating components such as the wheels and gears throughout the drivetrain. Equation 3.1 becomes:

$$P_t = V\left(Mgf_r + M\delta\frac{dV}{dt}\right) \tag{3.10}$$

Case 2: Excluding Rolling Resistance

The chassis dynamometer measures the force on the vehicle tires and the speed of the vehicle relative to a mechanical wheel which the vehicle rests on. In this case it is hypothesised that the dynamometer is coupled to the wheels like a set of gears in order to maximise the transfer of torque and speed for measurement by the sensors connected to the chassis dynamometer mechanical wheel. Equation 3.1 is simplified to:

$$P_t = V\left(\frac{1}{2}\rho C_D A_f V^2 + M\delta\frac{dV}{dt}\right) \tag{3.11}$$

Case 3: Excluding Aerodynamic Drag and Rolling Resistance

Alternatively, consider the case where both aerodynamic drag and rolling resistance are excluded and only the inertia of rotating components is considered.

$$P_t = VM\delta\frac{dV}{dt} \tag{3.12}$$

Equation 3.12 identifies the fact that the tests are completed on a chassis dynamometer where the vehicle remains stationary and the wheels are coupled to the load. For best measurement of the force acting on the wheels of the vehicle it is assumed in this case that the wheels have as little slip as possible and therefore no rolling resistance can be present during the rotation of the wheels. Such a component would interfere with the accuracy of measurements.

Case 4: Filtering Erratic Transients in the Tractive Power Calculation

The erratic variation in the calculated signal of Figure 3.8 is another possible cause of the error. The tractive power requirement for acceleration/deceleration from one vehicle speed to the next using equation 3.1 is potentially misrepresented. Considering that the tractive power measured by the wheels is achieved through the application of power from the propulsion device the erratic behaviour is reduced due to the inertia of the vehicles rotating components. In order to reduce the erratic variation for the calculated tractive power a moving average of the acceleration component is introduced to equation 3.1 such as:

$$P_t = V\left(Mgf_r + \frac{1}{2}\rho C_D A_f V^2 + M\delta\left(\frac{dV}{dt}\right)_{AV}\right) \tag{3.13}$$

In modelling the tractive power requirement based on the requested vehicle velocity it is possible to relate the accelerator pedal position directly to expected final vehicle velocity (or resulting vehicle velocity V_n) based on the previous vehicle velocity (V_{n-1}, V_{n-2} etc.). This means that past vehicle velocity can be considered in order to predict the future tractive power requirement and reduce the erratic behaviour of the calculated tractive power. The component representing the vehicle acceleration becomes:

$$\left(\frac{dV_n}{dt_n}\right)_{AV} = \frac{1}{n-i}\left(\sum_{i=a}^{n}\frac{dV_{n-i}}{dt_{n-i}}\right) \tag{3.14}$$

Where n represents the current values in the approximation of equation 3.14, i is the variable for the moving average relative to the sample space of measurements and a is an integer value (a<1) which ensures at least one previous measurement of speed and time is considered in equation 3.13.

3.4.3 Best Representation of Tractive Power

Using each of the described methods for calculating tractive power of the Toyota Prius with the specifications listed in Table 3.2 and comparing the MAPE the most accurate method is determined. The purpose for investigating the inclusion or omission of each of the components of equation 3.1 leads to an understanding of how each characteristic contributes to the overall tractive power calculation. The results of the MAPE listed in Table 3.3 identify two of the considered methods as a better means for representing the tractive power of a vehicle running on the chassis dynamometer. Case 2 and 4 have a similar MAPE which helps to decipher the best method for representing the tractive power.

Table 3.3 - Comparison of methods for calculating tractive power.

	Equation 3.1	**Case 1**	**Case 2**	**Case 3**	**Case 4**
MAPE	32.43%	25.87%	20.94%	23.90%	20.04%

Case 2 excludes the rolling resistance component of equation 3.1, while case 4 includes this component in addition to the averaging of the vehicle acceleration/deceleration component. The results of Table 3.3 imply that the rolling resistance component should not be included in case 4. This is potentially unique to the test conditions for the vehicle such that it was completed on a chassis dynamometer, where it may be difficult to simulate the rolling resistance of the vehicle. Recalculating the tractive power using:

$$P_t = V\left(\frac{1}{2}\rho C_D A_f V^2 + M\delta\left(\frac{dV}{dt}\right)_{AV}\right) \tag{3.15}$$

The MAPE determined using equation 3.15 is 9.74% and compared to case 4 using equation 3.13 suggests that the rolling resistance should be excluded. Finally the use of δ in these equations has been considered a constant which may account for the final 9.74% error between the calculated and measured signals. To investigate the effect of δ in the case of the chassis dynamometer it is varied between 0.95 and 1.1 and compared with the original value of 1.0425. Table 3.4 lists the MAPE for equation 3.15 with varying δ values and Figure 3.9 provides a visual comparison of how well equation 3.15 represents the measured data. Figure 3.9 also identifies a method for investigating varying values of other coefficients of Table 3.2.

Table 3.4 - MAPE for tractive power calculation using equation 3.15 and varying δ values.

δ	**0.95**	**1.0**	**1.0425**	**1.1**
MAPE	10.33%	9.35%	9.74%	13.95%

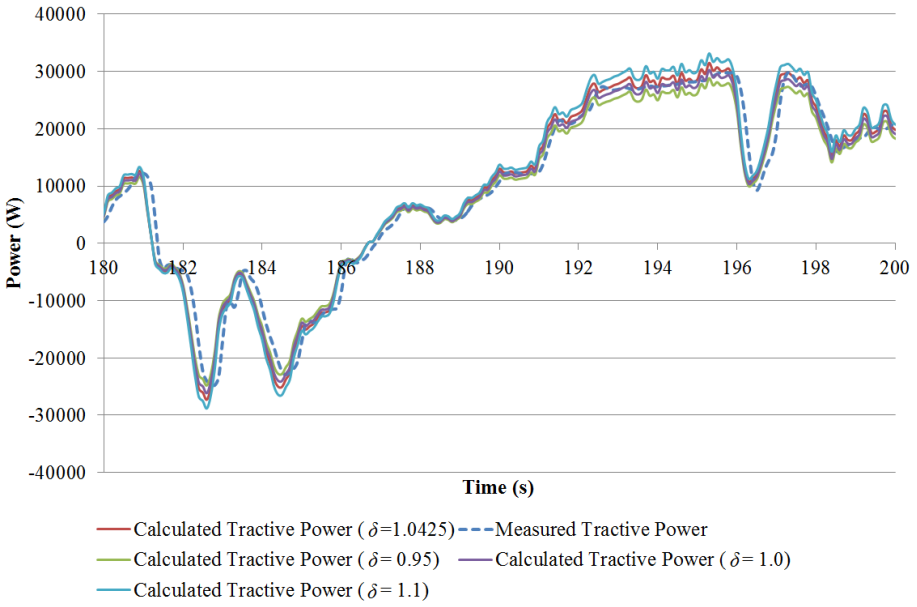

Figure 3.9 - Comparison of tractive power calculation over a 20 second interval using equation 3.15 with varying δ values.

According to the results of the MAPE for varying δ values, no inertial factor for the rotating components is required for equation 3.15. Instead the final equation for representing the tractive power of the vehicles on the dynamometer is:

$$P_t = V\left(\frac{1}{2}\rho C_D A_f V^2 + M\left(\frac{dV}{dt}\right)_{AV}\right) \tag{3.16}$$

Comparing the calculated tractive power of equation 3.1 and that determined using equation 3.16 in Figure 3.10 the error calculated in the MAPE is evident.

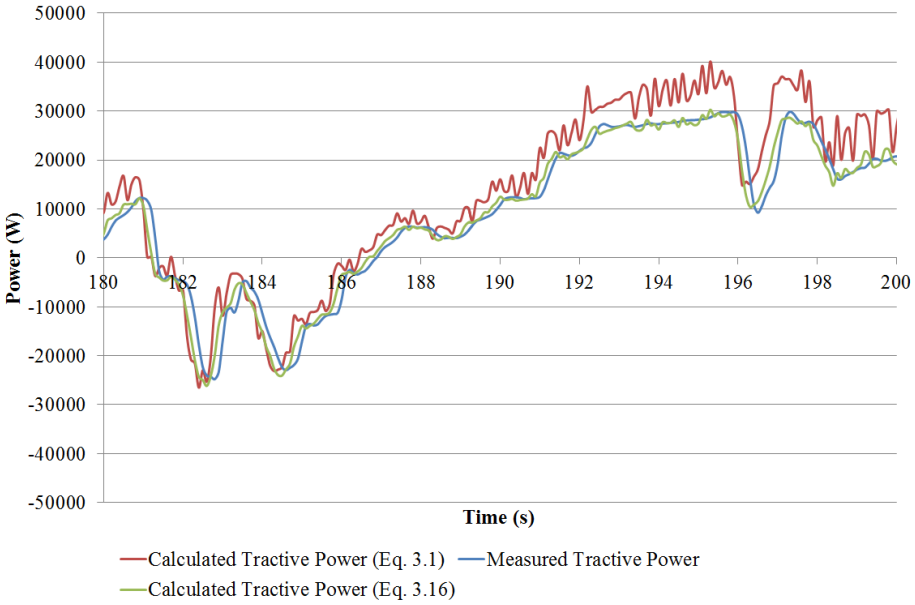

Figure 3.10 - Comparison of tractive power calculated using equation 3.1 and equation 3.16 with the measured tractive power.

Following the identification of equation 3.16 it was also tested for correlation on a second drive cycle with the measured data. This drive cycle is the HWFET as shown in Figure 3.11. A segment (380 sec to 400 sec) of the measured and calculated tractive power using the HWFET of Figure 3.11 and equations 3.1 and 3.16 are shown in Figure 3.12.

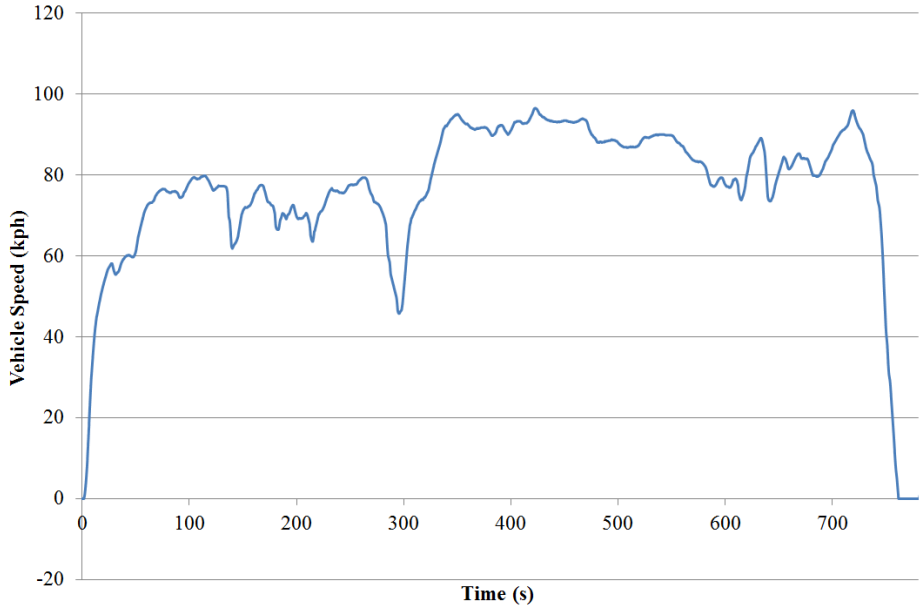

Figure 3.11 - HWFET drive cycle used to test correlation of equation 3.16.

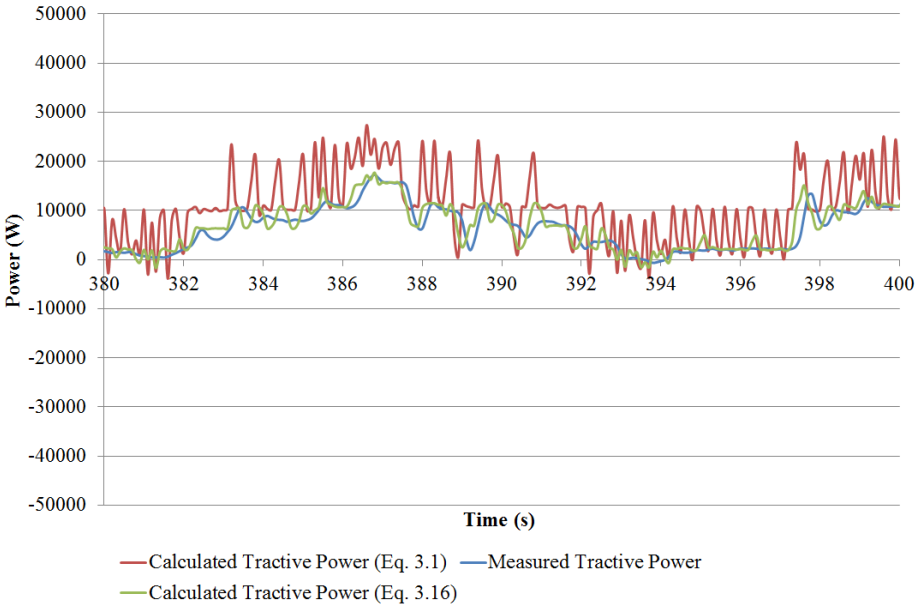

Figure 3.12 – Measured and calculated tractive power for the HWFET.

The visual comparison of Figure 3.12 supports the use of equation 3.16, in addition the MAPE using equation 3.1 and 3.16 are 55.93% and 14.50% respectively. The analysis completed is not intended to discredit the equations presented in Ehsani et al [5]. The analysis does however suggest that the forces acting on the dynamometer are different to a real-world scenario described by the equations in [5]. These differences seem to be an exclusion of the rolling resistance as well as a reduced inertia of the rotating components. Acknowledging these differences in the measured data ensures that any discrepancy in testing the vehicles will be accounted for in developing models for use as test benches. For example the fuel consumption resulting from the Toyota Prius on the UDDS is 3.1 L/100km as shown in Table 3.13 which is lower than the reported average for city driving by the Environmental Protection Agency at 4.61 L/100km [43]. The tractive power as an output of the vehicle is not changing the internal characteristics of the vehicle thus modelling based on the defined bench mark determines a reference point for both controllers proposed in Chapters 4 and 5. In addition, it is not possible to represent all characteristics of the vehicle in simulation and thus while a model must endeavour to accurately represent the vehicle there are certain limitations.

3.5 Operating Modes of Test Vehicles

Due to the uncertainty in operation of the vehicles it is not possible to determine the exact control strategy of the each tested vehicle from the measured data. The following Section identifies the methods utilised to gain knowledge about the modes of operation and thereby the control strategies of the test vehicles. For example the ESS is generally absorbing or

supplying some of the load continuously during ICE operation which makes it difficult to distinguish ICE only operations. It is, however, possible to distinguish ICE supply to the drivetrain during low power levels charged and discharged from the ESS. Such considerations lead to identifying the modes of operation. Again the Toyota Prius 2010 data is utilised as the example with similar analysis completed for the Hyundai Sonata Hybrid and Honda CR-Z as evidenced by the signal comparisons of results shown in Appendix A.1. Referring to the drivetrain combinations of Section 3.3, this provides the starting point for the relationship between tractive power and input power of the propulsion devices. For the Toyota Prius this starts with defining the gear ratios of the PGS and transaxle.

3.5.1 Initial Consideration for Transmission

The operating speed of the ICE compared with the wheel speed demonstrates the selected gear ratio for conventional vehicles (this is first identified in Section 2.2.1 and discussed further in Section 2.5.3). The Toyota Prius having the PGS makes for an increasingly difficult task in defining the transmission from the measured data. Observe the speed ratio of Figure 3.13 being continuously variable as expected between the ICE and wheels. This indicates that for the period 180 to 200 seconds on the UDDS the Prius' ICE is in speed coupling mode with M/G1, however, without having measured the speed of M/G1 it is difficult to determine the energy path chosen for the ICE developed power. The available energy paths include the mechanical or electrical couplings identified in Figure 3.4. In the case of the Hyundai Sonata Hybrid and Honda CR-Z the speed ratio between the ICE and driven wheels indicates the selected transmission gear. This also allows for the calculation of the output torque of the ICE directly from the force and speed of the wheels as measured on both these vehicles. For the Toyota Prius, however, further investigation is required for the consideration of operating modes.

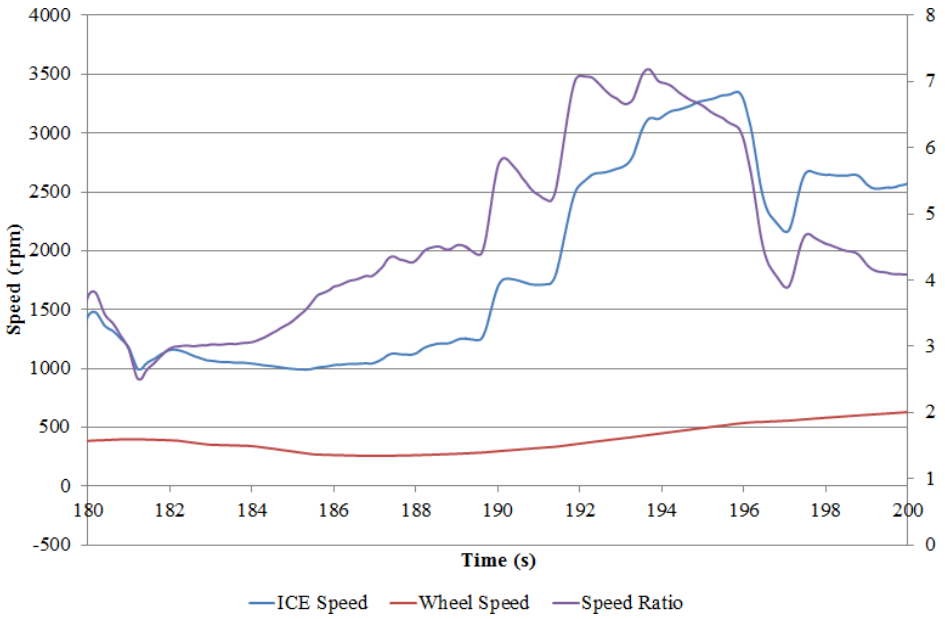

Figure 3.13 – Speed ratio for the Toyota Prius 2010; ICE speed with respect to wheel speed over the UDDS.

3.5.2 Toyota Prius PGS

In order to determine the operating modes of the Toyota Prius the mechanical relationship between the ICE and drive wheels of the vehicle need to be defined. The tractive power discussed in Section 3.4 defines the required energy to propel the vehicle along the road. The relationship between the tractive power and the measured fuel and stored energy of the ICE and ESS is unknown however. The PGS of Figure 3.4 introduces a unique relationship between torque and speed of the ICE, M/Gs and drive wheels.

Figure 3.14 defines the more detailed combination of gears for the PGS and transaxle of the Toyota Prius as featured in [5]. Table 3.5 introduces the numbers of teeth on each of the gears and allows for the definition of the relationship between the drive wheels and the ICE. There are six gears included in Figure 3.14, Z_1 to Z_6 which determine the ratio between the output of the PGS and the drive wheels. The torque and speed coupling modes of the PGS as discussed in Section 2.3.4 then determine the speed of the ICE and M/Gs. The number of teeth of the ring (Z_R), sun (Z_S) and carrier (Z_Y) gears are also listed in Table 3.5.

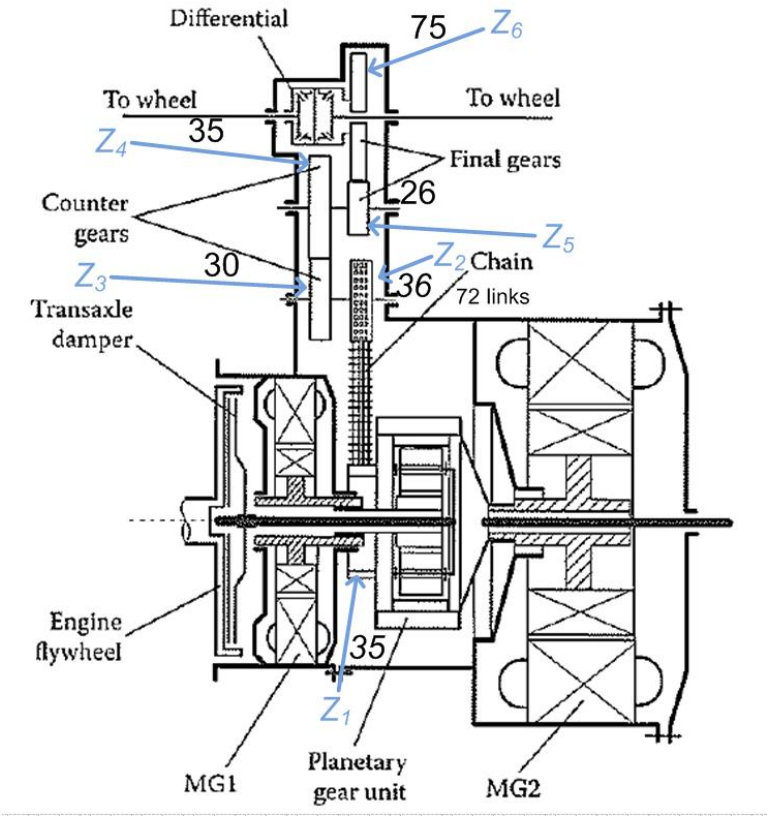

Figure 3.14 - Schematic of the Toyota Prius hybrid transaxle coupled to the PGS [5].

Table 3.5 - Toyota Prius hybrid trans axle and PGS specifications [5].

Description	Symbol	Number of Teeth
Drive Sprocket	Z_1	35
Drive Sprocket	Z_2	36
Counter Gear (Drive)	Z_3	30
Counter Gear (Driven)	Z_4	26
Final Gear (Drive)	Z_5	35
Final Gear (Driven)	Z_6	75
Ring Gear	Z_R	78
Sun Gear	Z_S	30
Yoke/Carrier Gear	Z_Y	23

From the consideration of Figure 3.14 and the connection of the ICE, M/Gs and drivetrain to the PGS as identified in Section 2.3.3 and discussed in Section 2.3.4, the following equations define the relationship of input and output speed and torque. This is for the PGS operating as a speed coupling device between the ICE and M/G1.

$$\omega_{dw} = \frac{k_{yr}}{i_{rw}}\left(\omega_e - \frac{1}{k_{ys}}\omega_{m/g1}\right) \tag{3.17}$$

ω_{dw} is the driven wheel speed, ω_e is the ICE speed, $\omega_{m/g}$ is the motor generator speed i_{rw} is the gear ratio between the output of the ring gear on the PGS to the driven wheels:

$$i_{rw} = \frac{Z_6 Z_4 Z_2}{Z_5 Z_3 Z_1} \tag{3.18}$$

And k_{yr} and k_{ys} represent the gear ratios between the yoke and ring gear, and yoke and sun gear respectively having the relationship:

$$k_{yr} = \frac{(1+i_g)}{i_g} \tag{3.19}$$

and

$$k_{ys} = (1+i_g) \tag{3.20}$$

where i_g follows as:

$$i_g = \frac{Z_R}{Z_S} \tag{3.21}$$

The torques for speed coupling mode are proportional according to,

$$T_{dw} = \frac{i_{rw}\eta_{yr}\eta_{rw}}{k_{yr}} T_e = \frac{k_{ys}\eta_{sr}^b \eta_{rw}}{k_{yr}} T_{m/g1} \tag{3.22}$$

where η_{yr} is the efficiency of energy transfer from the yoke to the ring gear, η_{rw} efficiency of energy transfer from ring gear to drive axle, η_{sr} the efficiency of energy transfer from sun gear to ring gear and b = 1 for discharging and b = -1 for charging. The number of teeth on the gears Z_1 to Z_6 are listed for the Toyota Prius 2004 in [5], which also lists a slightly different number of teeth for the gears in the 2003 model. Additionally, there is no mention if there is a ratio for the differential connecting the final gears to the drive axle. By comparison of the tractive power measured at the wheels and the equivalent maximum brake torque-speed ratings of the ICE, M/G1 and M/G2 the i_{rw} of the 2004 Toyota Prius is used as a starting point to determine i_{rw} for the 2010 model.

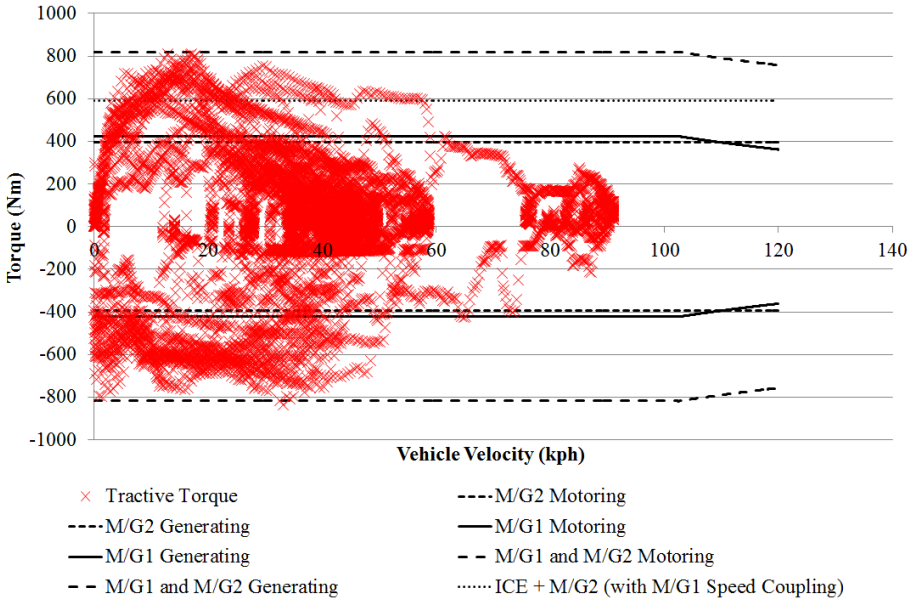

Figure 3.15 - Tractive torque and vehicle velocity data with respect to the specifications listed in Section 3.3.4 and Table 3.5.

Figure 3.15 compares the maximum brake torque produced at the wheels of the vehicle from each of the operating modes for the Toyota Prius. Due to the connection of M/G1 and M/G2 as discussed in Section 2.3.3, M/G1 combines with the ICE via speed coupling while M/G2 combines via torque coupling [5]. This means that M/G1 allows the ICE to operate at any speed independent of the drivetrain while the maximum brake torque produced at the wheels is the summation of the ICE and M/G2 at the wheels. Table 3.6 identifies the possible operating modes that were used to achieve the tractive torque identified in Figure 3.15.

From the perspective of peak output torque at some vehicle velocity, Figure 3.15 indicates that the gear ratios defined in Table 3.5 will satisfy all load requirements for the UDDS. According to the operating modes identified in [5], the Toyota Prius 2004 does not exhibit propulsion from M/G1 and M/G2 at the same time. If this is the case then the high torques at low vehicle speeds exceeds the maximum output torque capable of the vehicle. For example referring to Figure 3.15 ‘M/G1 and M/G2 Motoring’ mode is not available meaning that ‘ICE and M/G2 (with M/G1 Speed Coupling)’ produces the highest torque. Another concern is the electric only mode at low vehicle speeds (i.e. ICE start-up occurring between 24 and 32 km/h) this means that if M/G1 and M/G2 mode is not available then the maximum output torque available at the wheels comes from either M/G1 or M/G2. Using the same operation as defined in [5], it is most likely that M/G2 would be the propulsion device supplying the drivetrain load during ICE shutdown.

Table 3.6 - Operating modes of the Toyota Prius 2010 PGS.

Operating Mode	Powertrain Component	Drive Wheel Torque (T_{dw})	Drive Wheel Speed (ω_{dw})
Electric	M/G1	$\frac{i_{rw}k_{ys}T_{m/g1}}{k_{yr}}$	$\frac{k_{yr}\omega_{m/g1}}{i_{rw}k_{ys}}$
Electric	M/G2	$i_{rw}T_{m/g2}$	$\frac{\omega_{m/g2}}{i_{rw}}$
Electric	M/G1 and M/G2	$i_{rw}\left(\frac{k_{ys}T_{m/g1}}{k_{yr}}+T_{m/g2}\right)$	$\frac{k_{yr}\omega_{m/g1}}{i_{rw}k_{ys}}=\frac{\omega_{m/g2}}{i_{rw}}$
ICE Only	ICE and M/G1	$\frac{i_{rw}}{k_{yr}}T_e$	$\frac{k_{yr}}{i_{rw}}\left(\omega_e-\frac{1}{k_{ys}}\omega_{m/g1}\right)$
Hybrid Mode	ICE and M/G2	$i_{rw}\left(\frac{1}{k_{yr}}T_e+T_{m/g2}\right)$	$\frac{k_{yr}\omega_e}{i_{rw}}=\frac{\omega_{m/g2}}{i_{rw}}$
Hybrid Mode	ICE, M/G1 and M/G2	$i_{rw}\left(\frac{1}{k_{yr}}T_e+T_{m/g2}\right)$	$\frac{k_{yr}}{i_{rw}}\left(\omega_e-\frac{1}{k_{ys}}\omega_{m/g1}\right)=\frac{\omega_{m/g2}}{i_{rw}}$

Since M/G2 is nominally the tractive motor, M/G2 would be required to supply the load during low vehicle speed (below 32 km/h). According to the comparison in Figure 3.15 M/G2 operating alone will not produce the required output torque at the low vehicle velocities. For the case of negative torques applied to the vehicle, mechanical braking will absorb any negative torque requests that exceed the maximum negative torque capable of the M/Gs.

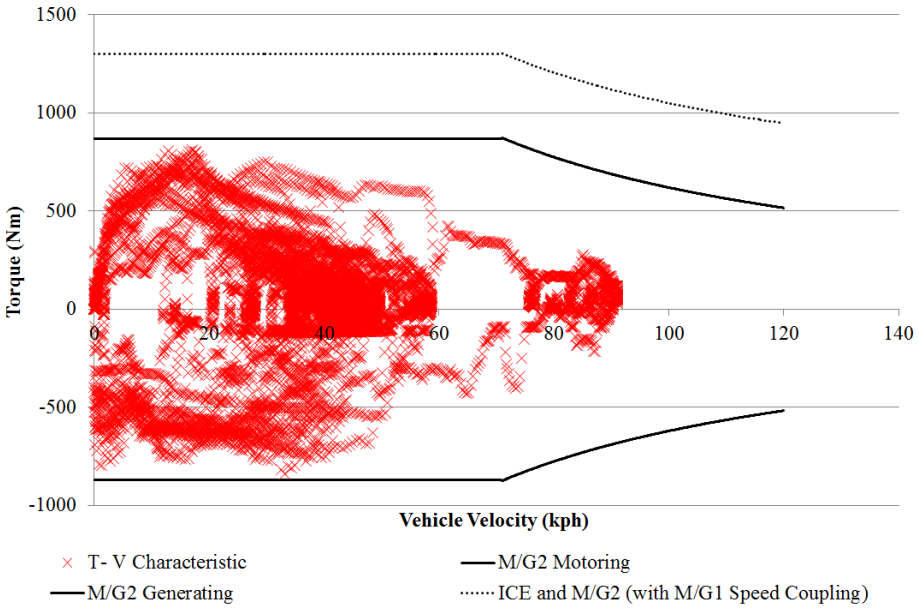

Figure 3.16 – Tractive torque and vehicle velocity data with respect to new i_{rw}: calculated such that M/G2 needs to supply torque at low vehicle velocity.

Furthermore, if M/G2 decelerates the vehicle without the aid of M/G1 a significant proportion of the negative torques requested from the vehicle will be expelled as waste heat.

Figure 3.16 displays the maximum brake torque with i_{rw} = 4.2. This gear ratio was determined according to M/G2 needing to supply a positive output torque of up to 850 Nm at the wheels. By the same consideration M/G2 is capable of absorbing all negative torques during deceleration of the vehicle as well. Having determined the drivetrain specifications for the Toyota Prius 2010 the investigation lead to determining the control strategy of the powertrain components. The following Section attempts to model the ICE operation based on the input fuel energy and output tractive energy to determine the operating points at the output shaft of the ICE.

3.5.3 Toyota Prius ICE Operation

Firstly using equation 3.7 the wheel speed of the Toyota Prius 2010 with respect to the wheel radius of Table 3.2 and the vehicle velocity of the measured data is determined in rad/s. Converting this to rpm and applying equation 3.18 (refer to Table 3.6) the ring gear speed of the PGS is determined. In the power-split topology of the Toyota Prius the ring gear is coupled to M/G2 of Figure 3.4 and is predominantly used as a motor [5]. Combining the measured ICE speed and calculated wheel speed into equation 3.15 the speed of the sun gear is determined. Figure 3.17 displays the resulting speeds calculated using equations 3.17 to 3.21. The main reason for identifying the speeds at each port of the PGS is so the relationship of load torque to ICE torque is established. The next step is to determine the relative torque at each location in the drivetrain using the calculated speeds, the measured ICE fuel consumed, measured ESS output power and measured load power.

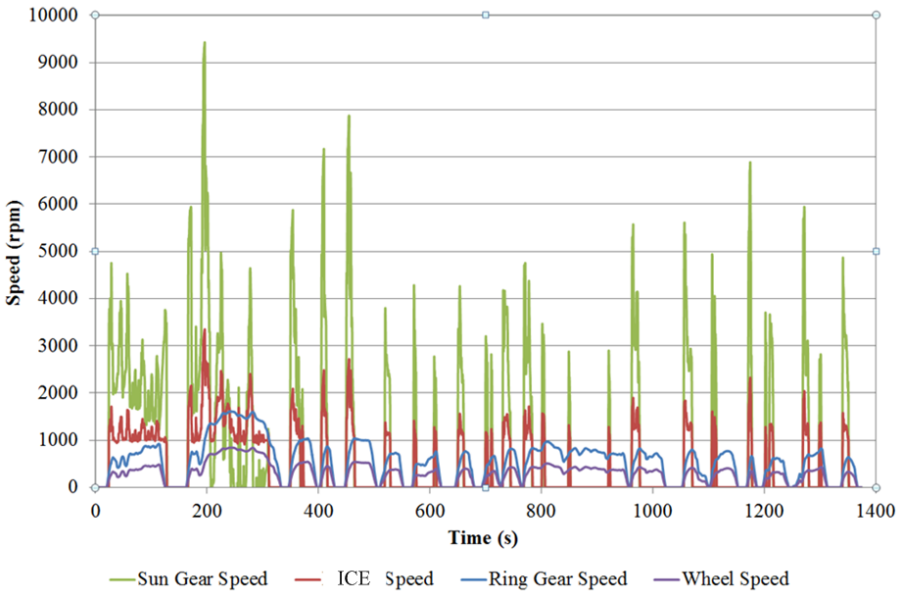

Figure 3.17 – Operating speed at each identified location on the UDDS.

Due to the coupling of the ICE to the PGS the ESS is continuously supplying or absorbing energy from the drivetrain. The summed difference between the ICE developed power and

the tractive power is dependent on the control strategy such that the ESS balances any discrepancy between the two. The issue is that the losses of the powertrain and drivetrain are unknown at each time interval and thus the input power of the ICE and ESS does not match the output power measured at the drive wheels. With the measured signals it is, however, possible to gain an idea of the control strategy based on the fuel consumption, ESS power output and tractive power since the following relationship from Section 2.2.6 holds:

$$P_L = \eta_d \eta_t \left[\eta_e \frac{dE_f}{dt} + \eta_{m/g} \eta_{dis} \frac{dE_{ess}}{dt} \right] \tag{3.23}$$

Following on from equation 3.23 the measured fuel rate is in cubic centimetres per second (cc/s) and must be converted to kilojoules per second (kJ/s) using:

$$\frac{dE_f}{dt} = \frac{\dot{m}_f (cc/s) \times Q_{HV} (J/g) \times \rho_f (g/L)}{1000(cc/L)} \tag{3.24}$$

and

$$1J.s = 1W \tag{3.25}$$

In addition, the energy of the ESS is available from the test data by using the recorded voltage and current:

$$\frac{dE_{ess}}{dt} = V_{ess} I_{ess} \tag{3.26}$$

Equation 3.23 to 3.26 establish that the measured tractive power (P_L) is proportional to the combined fuel and ESS power and that from the relationship of equation 3.23 it is possible to determined when the ICE is supplying the majority of the load. Figure 3.18 shows the input and output power of the Toyota Prius 2010 with the fuel power and ESS power compared to the measured tractive power.

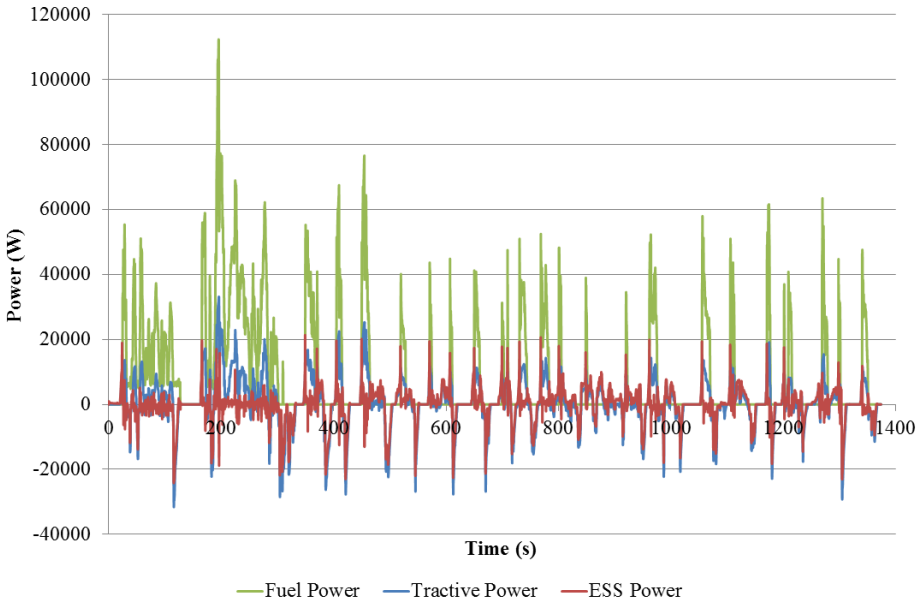

Figure 3.18 - Toyota Prius 2010 measured power consumption identifying input and output power (input = Fuel Power – ESS Power, output = Tractive Power).

Interestingly during periods when the ICE is being fed some amount of fuel the positive tractive power exhibits a similar profile: the obvious difference between fuel power and tractive power being the losses of the drivetrain. On the other hand when the ESS is absorbing power there is a larger negative tractive power indicating the losses of the electrical network during regenerative braking. Two alternative periods are identified in Figure 3.19 and Figure 3.20.

Firstly, Figure 3.19 observes periods of regenerative braking, ICE idle, hybrid, and ICE only operation which are identified by the flow of energy between the powertrain and drivetrain. Each of these operating modes is linked to the discussion presented in Section 2.2.6. Regenerative braking mode observes deceleration of the vehicle as a result of a negative torque applied to M/G2 (Figure 3.4). The tractive power measured at the wheels has a greater magnitude than the power measured at the ESS, both of which are negative for ESS charging. During this deceleration of the vehicle the ICE remains on, idling since the requested deceleration period or magntitude are not long enough or large enough to justify ICE shutdown. This then leads into a hybrid mode of operation with the ICE and M/G2 supplying the tractive power for acceleration. M/G2 operation is assumed due to the torque-speed coupling of the Toyota Prius, Figure 3.19 demonstrates the consumption of fuel energy and energy drawn from the ESS only. Then ICE only mode of operation observes acceleration of the vehicle at high vehicle velocity with no ESS energy charge/discharged. Figure 3.20 is an example of EV mode such that the ICE is off and all tractive power requirements are met using the ESS and presumably M/G2 [5].

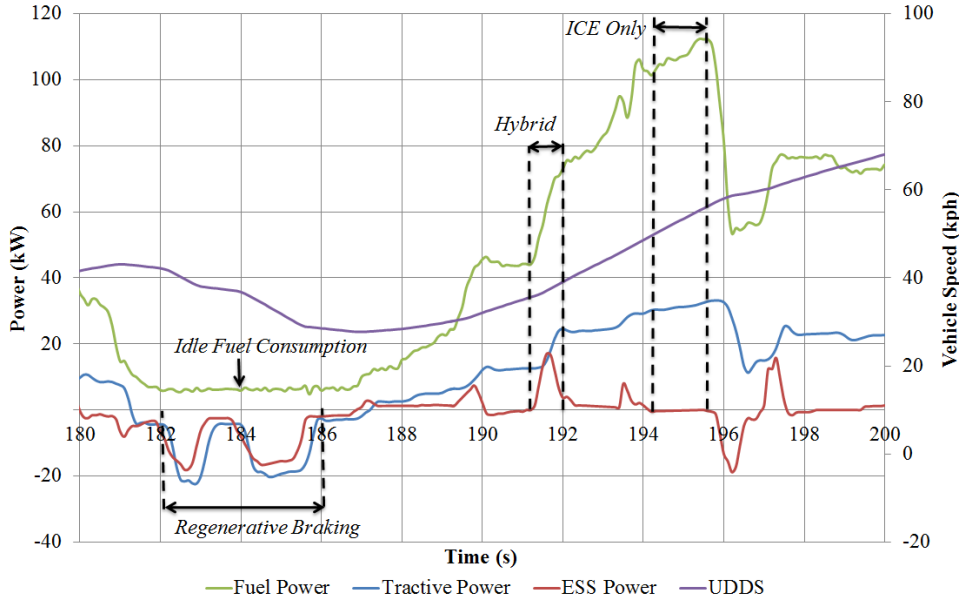

Figure 3.19 – Evidence of the operating modes of the Toyota Prius 2010.

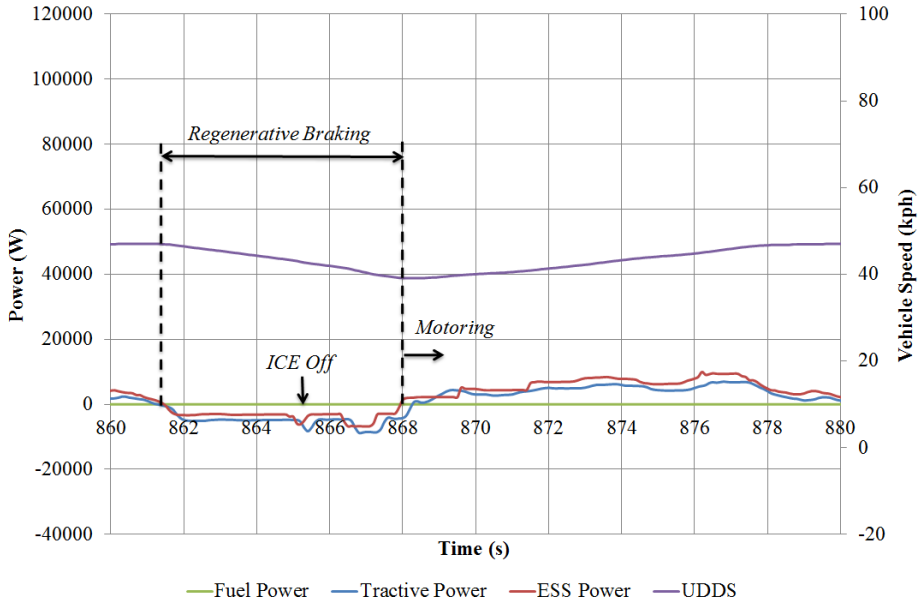

Figure 3.20 – Evidence of the electric only mode of operation in the Toyota Prius 2010.

From Figure 3.17 and Figure 3.19 the ICE on operation is identified by the ICE having a speed greater than or equal to idle or supplying a power proportional to the tractive power. This then leads to the consideration of when and how the ICE is being utilised relative to fuel consumption minimisation. As part of this analysis it is also possible to estimate the output torque of the ICE based on the measured signals and the identified operating modes. Due to the ESS continuously absorbing or supplying energy it is difficult to know when the Toyota Prius is operating in ICE only mode of operation. With the following assumptions, however, it is possible to estimate this mode of operation and therefore the output torque of the ICE.

$$\text{ICE only when: } \begin{cases} \omega_e > 0 \\ P_e > p_e(P_e + P_{ess}) \\ P_L > 0 \end{cases} \tag{3.27}$$

Equation 3.27 outlines the inequalities that determine if the ICE is supplying the tractive power. The tractive power (P_L) measured at the wheels must be greater than zero, the speed of the ICE must be on and the power developed by the ICE (P_e) must make up the majority. The variable p_e is a percentage of the total input power such that the ICE is supplying some minimum percentage of the total input power in order for it to be considered ICE only operation. Selecting p_e equal to 90% with an estimated drivetrain efficiency of 90% and using equation 3.5 the ICE torque-speed data points are shown in Figure 3.21. Figure 3.21 includes a potential torque-speed characteristic for the Toyota Prius 2010 ICE based on the technical specifications listed in Section 3.3.4. Figure 3.21 indicates that the ICE control follows some optimal operating line [91] due to the speed coupling of the PGS as discussed in Section 2.3.4 and identified by equation 3.15. The optimal operating line ensures that the requested load power from the ICE is being supplied at the most efficient operating torque and speed. This type of operation is further explained in Section 4.3.2.

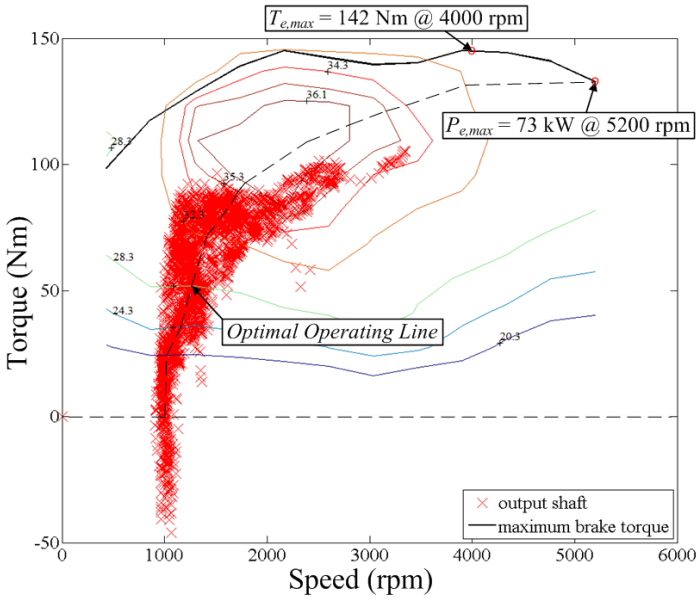

Figure 3.21 - Toyota Prius output torque-speed data points.

It was originally thought that the negative torques shown in Figure 3.21 were due to the ICE cranking during start-up. Upon closer inspection of the available measured data it was determined that the negative torques (or negative power) is actually due to braking of the vehicle. Figure 3.22 identifies the start-up period of the ICE relative to the fuel, ESS and tractive power measurements. It seems that the ICE speed sensor does not begin measuring

until most of the ICE start-up transient is finished resulting in a speed of zero until the ICE is running.

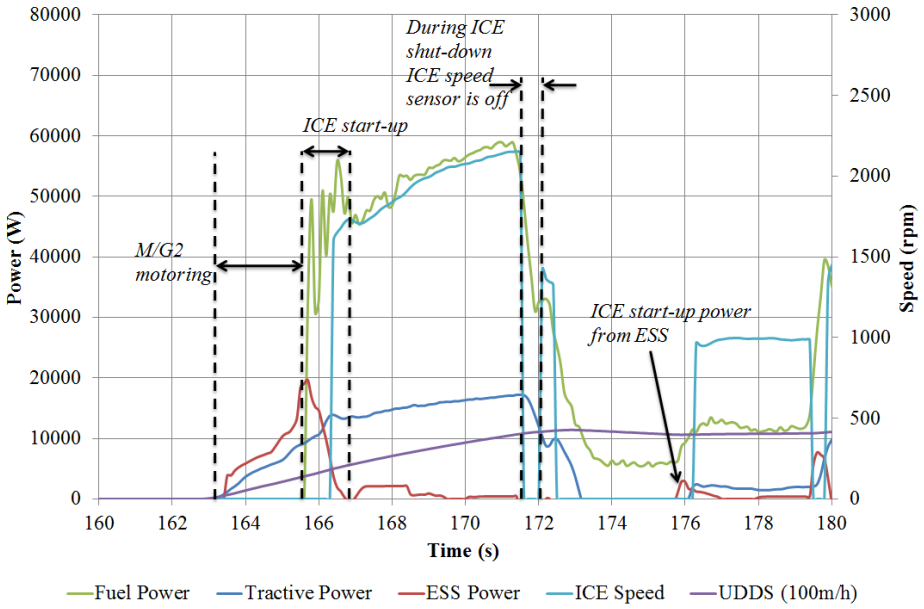

Figure 3.22 – Toyota Prius ICE start-up and shut-down operations.

Additionally, when the EMS controller requests a large negative torque (i.e. braking) the ICE switches off, instantly switching the ICE speed sensor off. This operation is shown in Figure 3.22. Another point to note from Figure 3.22 is that while the tractive power is zero there is a spike in the ESS power just before the 176th second potentially indicating the power drawn from the ESS during ICE start-up. At the same time the measured speed is zero indicating that the speed sensor is off during the beginning of the start-up transient. This means that while fuel consumption and battery energy are included in the power measurements for start-up of the ICE the individual transients are excluded. Therefore the torque-speed characteristic of Figure 3.21 relative to the inequalities of equation 3.27 indicates the operation of the ICE for positive power developed at the output shaft only and does not indicate torques acting on the ICE output shaft for ICE start-up. Alternatively to the strategic ICE operation the ESS operation balances any discrepancy between the ICE and requested load as discussed in the next Section.

3.5.4 Toyota Prius ESS Operation

From Figure 3.17 and Figure 3.18 the ICE operating speed, fuel and ESS power consumption suggest that the ICE is the primary propulsion device in the Toyota Prius. This means that the ICE provides the average tractive power while the ESS is supplying the transient tractive power in order to achieve more stable operation of the ICE and therefore reduced fuel consumption. In addition, Ehsani *et al.* [5] describes the use of the ESS to supply tractive power at low vehicle speeds in order to conserve fuel. This is evident in Figure 3.22 with the

ESS supplying the tractive power before ICE start-up where vehicle speed is low. The approximate vehicle speed in Figure 3.22 at which time the ICE has started is 16 km/h, while in Ehsani *et al.* [5] the ICE is reported to start between 24 to 32 km/h.

Finally the ESS SOC is shown in Figure 3.23 along with the ESS cell temperature. Figure 3.23 indicates that the SOC is maintained to some target SOC (SOC_{target}) such as 60%, while the operating temperature over the UDDS rises by 0.36 °C. As a result of the temperature shown in Figure 3.23 it is considered that losses due to waste heat for the Toyota Prius ESS are minimal. It is also considered that ESS charge and discharge is reliant on the ICE operation and some algorithm that notifies the ICE controller of how much power to supply to maintain SOC_{target}. This energy balance between the ICE, ESS and requested load power is discussed in further detail in Sections 4.2 and 4.3, and the algorithm for maintaining ESS SOC is described in Section 3.7.1.

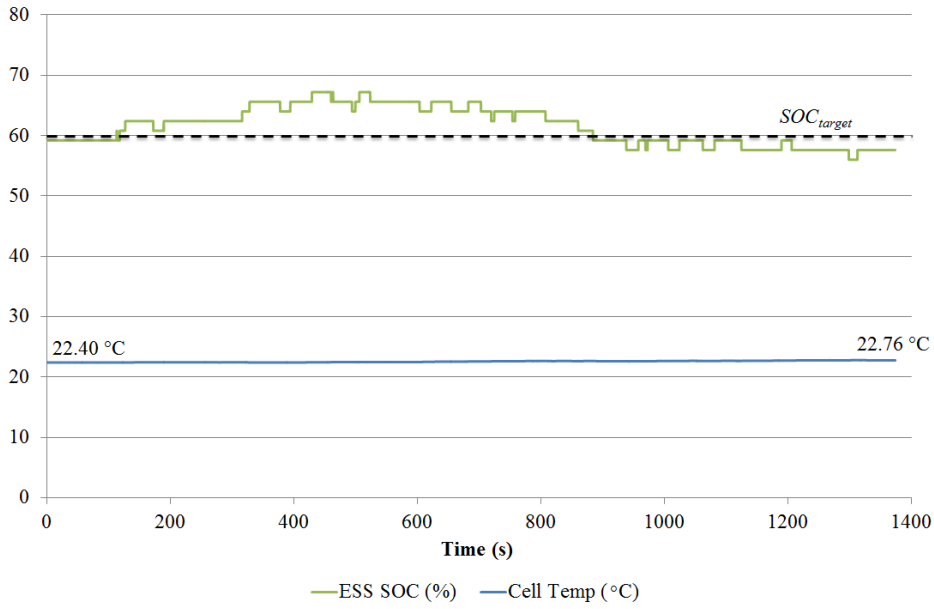

Figure 3.23 - Toyota Prius ESS SOC and operating temperature for the UDDS.

3.5.5 Toyota Prius Component Efficiencies

Having estimated the torque and speed operation of the ICE on the Toyota Prius and knowing that the ICE is utilised for average tractive power while the ESS is utilised for transient tractive power the efficiency of the drivetrain components reveals more details about the Toyota Prius EMS. The aim for this Section with respect to identifying the test vehicles' control strategy is to gain an idea of the efficiency of operation of the powertrain in order to replicate this in simulation. This then allows a comparison of input and output energies and the fuel consumed over the drive cycle for the measured and simulated quantities.

Overall Vehicle Efficiency

Primarily the total fuel energy and total battery energy determine a starting point for comparison of the test benches with the existing vehicles.

$$E_f = \sum_{i=1}^{N} \frac{\Delta E_{f,i}}{\Delta t_i} \Delta t_i \tag{3.28}$$

$$E_{ess} = \sum_{i=1}^{N} \frac{\Delta E_{ess,i}}{\Delta t_i} \Delta t_i \tag{3.29}$$

$$E_L = \sum_{i=1}^{N} P_{L,i} \Delta t_i \tag{3.30}$$

For this analysis total energy consumed is the difference between fuel and ESS energy. This convention assumes that energy entering the ESS (charging) is a load for the ICE, while energy discharged from the ESS is supplying 'free' energy to satisfy the load. Identifying the consumption of energy in this manner allows for the losses of charging the ESS to be accounted for in the final efficiency. This is due to the consideration that fuel consumption is avoided when the ESS is discharged and increased when the ESS is charged. The result is a net energy consideration of the ESS in terms of fuel energy consumed. Therefore the negative ESS energy total indicates consumed ESS energy relative to the measured data. The overall efficiency is:

$$\eta = \frac{E_L}{(E_f - E_{ess})} \tag{3.31}$$

Following the definition of equation 3.24 the fuel consumption for each of the vehicles is determined according to:

$$FC = \frac{100 E_f}{Q_{HV} \rho_f d} \tag{3.32}$$

where FC is fuel consumption in L/100km, E_f is fuel energy in J, Q_{HV} is the heating value of the fuel in J/g, ρ_f the density of the fuel in g/L and d is the drive cycle distance (km) which is obtained as a summation of measured vehicle velocity:

$$d = \sum_{i=1}^{N} V_i \Delta t_i \tag{3.33}$$

As an example the total tractive energy required to drive the Toyota Prius over the UDDS profile is 1249.850 *kJ*, with 11797.676 *kJ* of fuel energy and -262.265 *kJ* measured at the ESS terminals. The total distance travelled by the vehicle on the UDDS is 11.97 km, and the

higher heating value of gasoline fuel is 42808 *J*/*g* with a density of 741 *g*/*L*. This results with a vehicle efficiency of 10.36% according to equation 3.31 and a fuel consumption of 3.10 L/100km according to equation 3.32.

Average Efficiency of Various Modes

The individual accessory loads of the vehicle over the drive profiles are not included in the measured data. Here accessory loads are treated as losses of the vehicle such that varying the efficiency of operation of the powertrain and drivetrain components leads to a representation of any accessory loads used during the testing of the three vehicles. By ensuring that the simulation models match the input and output energy requirements of the measured data the accessory loading will be included as losses. Using the convention of equation 3.31 for the total energy consumed by the vehicle, Figure 3.24 provides the starting point for estimating the vehicle mode efficiencies on the Toyota Prius. Three specific modes of operation are identified in Figure 3.24; hybrid, electric and regenerative braking modes.

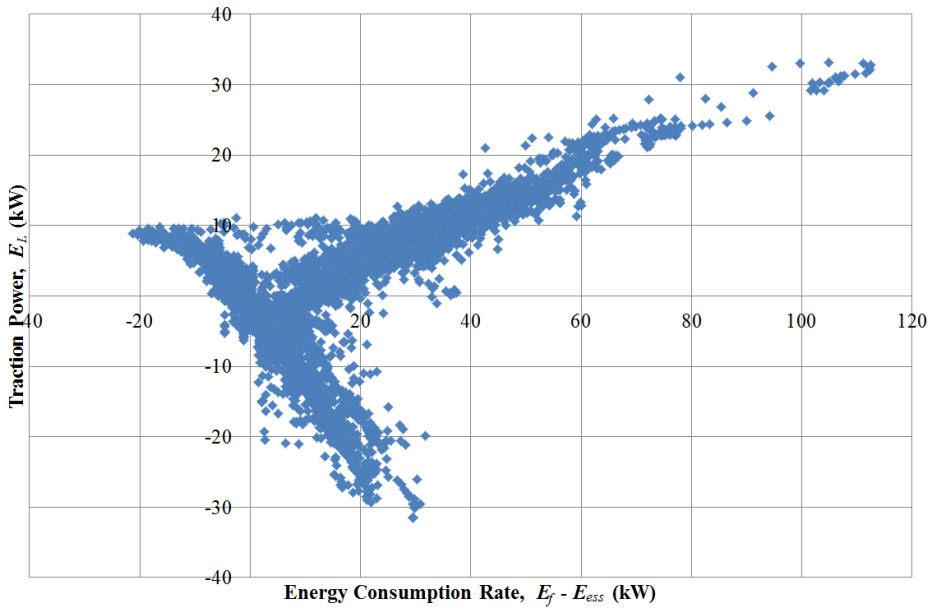

Figure 3.24 - Tractive power versus total fuel and ESS energy.

These modes are outlined in Table 3.7. Energy consumed from the ESS being negative and energy supplied to the ESS being positive with respect to fuel energy. The mode description indicates the input and output power of equation 3.31, with the remaining two columns identifying the data of interest for the respective quadrant in classifying the unknown data of Figure 3.24. The resulting operating modes are displayed in Figure 3.25 where it is noted that a large proportion of data is ignored due to the considerations of Table 3.7.

Table 3.7 - Component efficiencies identified using total input and output energy.

Mode	Mode Description	Total Power	Tractive Power
Hybrid Accelerating	ICE is primary power source. Therefore total power is greater than tractive power.	$\left(\frac{\Delta E_{f,i}}{\Delta t_i} - \frac{\Delta E_{ess,i}}{\Delta t_i}\right) > 0$	$P_L > 0$
EV Accelerating	ESS is primary power source. Therefore discharged power is greater than tractive power.	$\left(\frac{\Delta E_{f,i}}{\Delta t_i} - \frac{\Delta E_{ess,i}}{\Delta t_i}\right) \leq 0$ $\frac{\Delta E_{f,i}}{\Delta t_i} = 0$	$P_L > 0$
Regenerative Braking	Deceleration of vehicle is primary power source. Therefore tractive power is greater than charged power.	$\left(\frac{\Delta E_{f,i}}{\Delta t_i} - \frac{\Delta E_{ess,i}}{\Delta t_i}\right) > 0$ $\frac{\Delta E_{f,i}}{\Delta t_i} = 0$	$P_L \leq 0$

This analysis therefore excludes expenditure of energy during the transition from one mode to another as well as at zero tractive power leading to a much greater efficiency. As a result, the calculated average efficiency may reflect that of the propulsion devices during the identified modes of operation. For each quadrant identified by Figure 3.25 the total numbers of data points in each quadrant that have been included are listed in Table 3.8. The reasons not all data points are included are due to the inequalities of Table 3.7.

There are two possible causes for mismatch. Firstly, the measured data may be recorded during transient operations of the vehicle and therefore mismatched due to the delay between each vehicle component. For example when a propulsion device begins to drive the vehicle it will take a noticeable delay (up to 0.5 seconds) for the response to be received at the wheels of the vehicle. This delay inhibits the accuracy of equation 3.31 in using the data due to the transient nature of the drive cycle. Secondly, ICE power developed does not match the tractive power developed due to the charge/discharge of the ESS, associated losses or accessory loading. In addition, the drive cycle contains frequent transients and therefore increased potential for mismatch of measured data at the input and output.

Table 3.8 - Total number of data points considered in analysis of Figure 3.25.

Mode	Total Data Considered	Actual Data	Percentage of Total
Hybrid Accelerating	3672	3560	25.72%
EV Accelerating	3201	2974	21.49%
Regenerative Braking	3094	2300	16.62%
Total Data	13841	8834	63.82%

Figure 3.25 displays the gradients of each of the three modes of operation. These gradients are relative to equation 3.31 such that the efficiency of operation between tractive power and total power are demonstrated. Due to the exclusion of some of the data not all energy expended by the vehicle is included and thus overall efficiency is not proportional to the efficiencies identified by the gradients. Figure 3.25 does, however, provide an insight into the average efficiency of each mode. Hybrid mode with ICE and ESS energy consumed leads to an average efficiency of 28.78%, while electric only mode of operation is 61.87% efficient. Inverting the gradient of regenerative braking mode the efficiency is 79.45% for those data points considered. The low efficiency of operation for the EV mode at 61.87% is reflective of the primary use of the stored energy in the ESS. The zero emissions mode of operation occurs at low vehicle speed (V < 32km/h), accelerating the vehicle to a speed where the ICE is allowed to start. M/G2 output speed is proportional to the vehicle speed such that low vehicle speeds may lead to low efficiency of operation for M/G2.

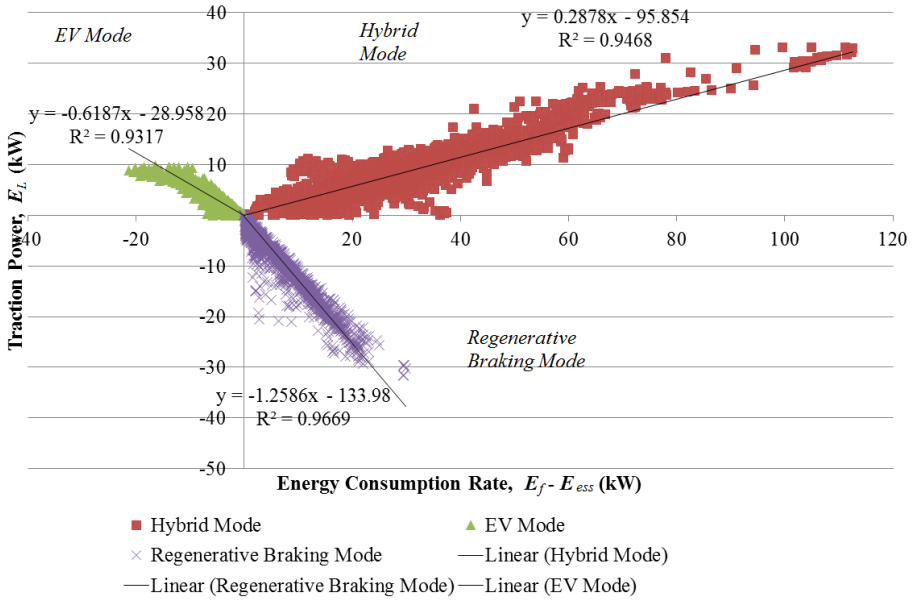

Figure 3.25 - Tractive power versus total fuel and ESS energy; separated into three modes of operation.

The efficiencies of these modes of operation as identified in Figure 3.25 are similar to those expected in literature [55]. With respect to the total data points of Table 3.8, 64% are included in the efficiencies of Figure 3.25, indicating that for 64% of the UDDS drive cycle the vehicle is operating at efficiencies around those identified. The additional losses in the remaining 36% of the UDDS drive cycle (as outlined in Table 3.8) leads to the final average efficiency of 10.36%. This highlights the potential for investigation into the additional losses experienced by EMS, however, without further information from the existing vehicles this investigation must focus on EMS optimisation of the defined operations (i.e. 64% Table 3.8).

ICE Operation – Fuel Flow Rate

Following the total power versus tractive power additional ICE operation is supported by the fuel flow rate versus tractive power. Figure 3.26 identifies that for tractive power above 10 kW the ICE is continuously operating. Figure 3.26 also suggests that the ICE idling during negative tractive power is a result of deceleration from higher vehicle speeds. Once the vehicle speed falls below a certain threshold such as that identified by Ehsani *et al* [5] the ICE shuts down again. This may also be the case for large negative torques requested from the EMS controller as identified in the discussion of Figure 3.19. The negative tractive power for which the ICE is already shutdown can be attributed to the ICE not starting up in the first place or the ICE shutting down once the SOC of the ESS is high (i.e. greater than the SOC_{target}).

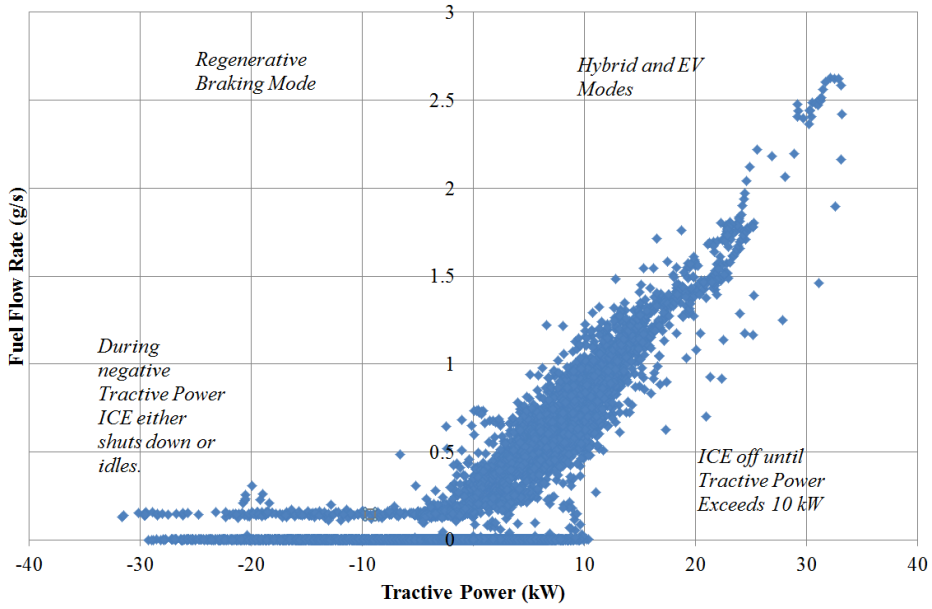

Figure 3.26 - Fuel flow rate with respect to tractive power.

ICE Efficiency Characteristic

Combining the torque-speed data of Figure 3.21 with the corresponding input fuel data of Figure 3.26 the efficiency of operation for the ICE at different torque and speeds is approximated. This relies on the assumption that the drivetrain is 90% efficient between the output of the ICE and the driven wheels as outlined in Section 3.5.3. Figure 3.27 compares the efficiency of converting fuel energy to mechanical energy using the Toyota Prius ICE at varying torque and speed for the hybrid mode of operation identified in Table 3.8. Note that 3307 data points of the total 3560 data points are used to generate Figure 3.27. The exact values of efficiency at each torque and speed according to the analysis of Section 3.5.5 may result in unrealistic efficiencies, however, the shape of the data with respect to the torque and speed confirms a pattern for the operational efficiency of the ICE.

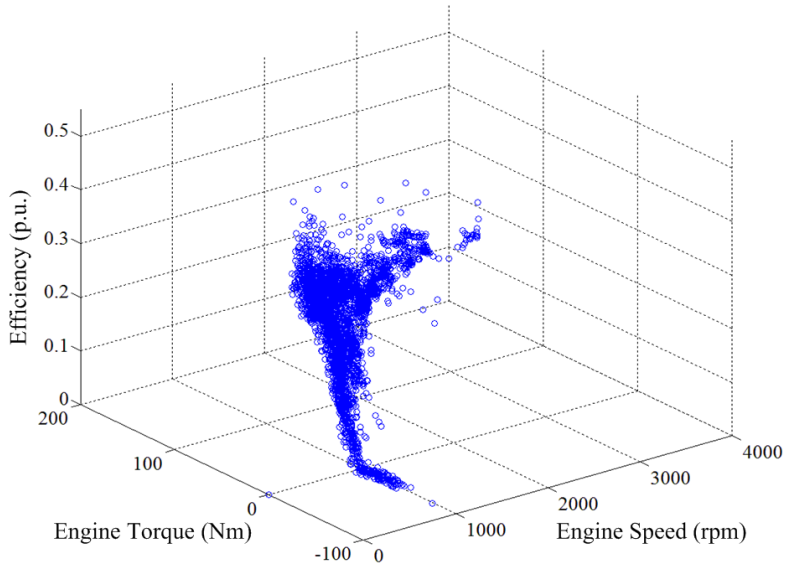

Figure 3.27 – Toyota Prius 2010 ICE efficiency of operation at varying torque and speed on the UDDS.

Firstly, the efficiency versus speed of Figure 3.28 identifies that at speeds around idle the output power compared with input power is generally low. The higher efficiency points (circled data in Figure 3.28) are possibly due to the mismatched data (Section 3.5.5), e.g. ESS supplying a larger percentage of the tractive power than the power that was recorded at the time or due to the unknown efficiency of the drivetrain. On the other hand output efficiency at higher ICE speed is around 25% which supports the performance map of Figure 3.21 where efficiency of operation increases at higher ICE speed. At the midsection of the ICE operation between 1500 to 2000 rpm the ICE seems to have greater average efficiency than at either speed extreme (idle or max speed).

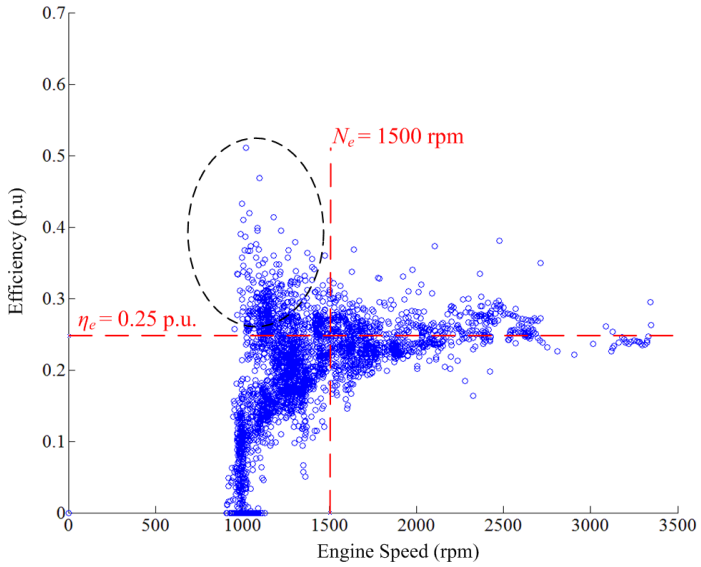

Figure 3.28 – Toyota Prius 2010 ICE efficiency of operation with respect to output speed on the UDDS.

Following the comparison of ICE speed, the ICE torque also supports the performance map of Figure 3.21. Increasing fuel consumption leads to increasing efficiency and therefore a greater percentage of the fuel energy is converted to output torque.

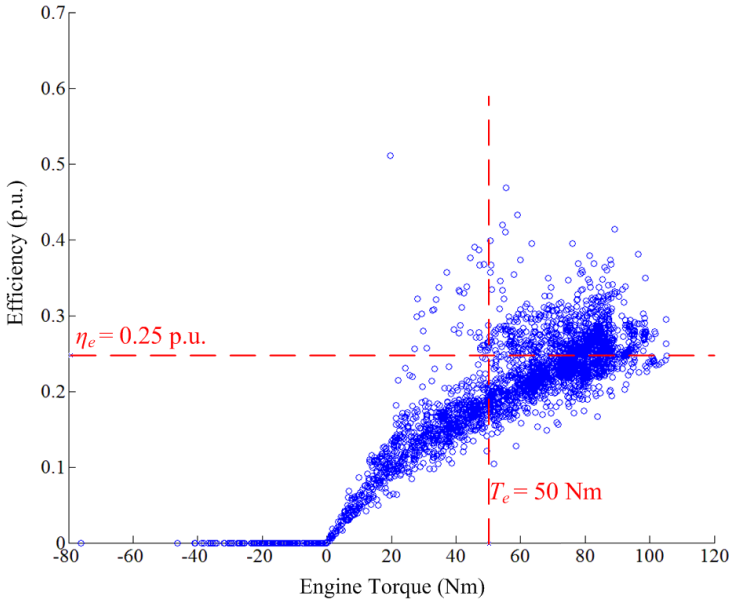

Figure 3.29 – Toyota Prius 2010 ICE efficiency of operation with respect to output torque on the UDDS.

The ICE efficiency identified by Figure 3.27 to Figure 3.29 is only an estimate and it is more the characteristics relative to a potential performance map that are being examined. The data can, however, be separated into approximate categories to determine a potential average operating efficiency according to the load placed on the ICE during the tested drive cycle. Figure 3.30 indicates the percentage of total data points that exhibit an operating efficiency less than some threshold efficiency η_e, indicated on the x-axis. For the point of this discussion 35% is near optimal efficiency, identifying an upper limit for ICE operation. Figure 3.30 concludes that the ICE efficiency is below the mid-point (e.g. η_e = 20%) 33.90% of the time and that the majority of operating points are below the optimal ICE efficiency having 66.28% of operation below 25% as determined in this analysis. Therefore average ICE operating efficiency can be improved by increasing the average torque and speed requested. This supports the consideration of high efficiency control of the ICE for improved average efficiency of the EMS in HEV and PHEV as featured in Chapters 4 and 5.

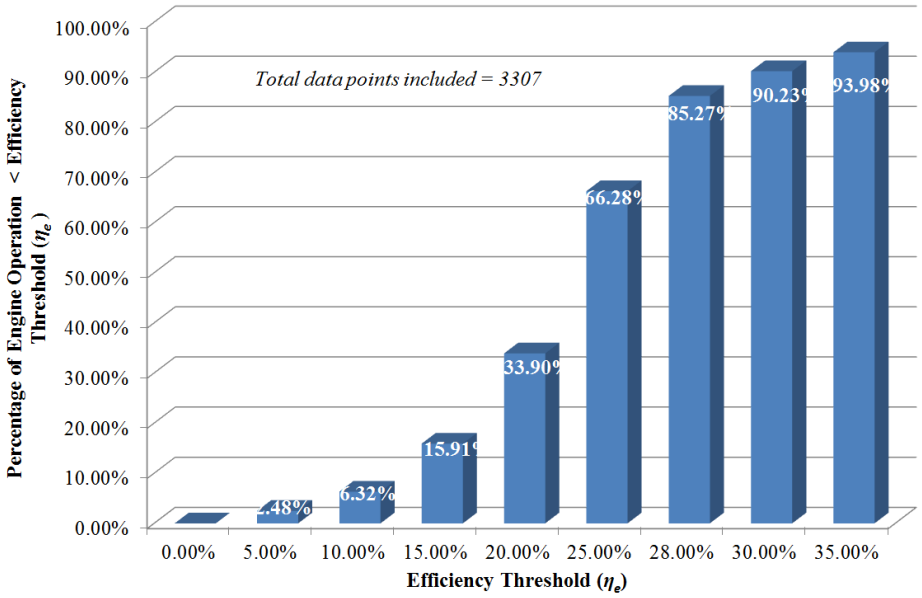

Figure 3.30 - Identifying characteristics of ICE operating efficiency.

3.6 Vehicle Component Models

The following Section defines the component models featured in the ADVISOR software package. The models are outlined in terms of general component characteristics such that the reader can replicate the overall results presented in this thesis. Here the electrical and mechanical losses are defined with respect to the ICE, M/G, ESS and drivetrain. The models presented here are largely based on the predefined models utilised in the ADVISOR software [49]. Within the ADVISOR software both electrical and mechanical losses include energy transfer losses with some additional considerations. Additional electrical losses include conversion losses, while additional mechanical losses include rotational inertia losses and slip. Each model is representative of the data presented in the previous Sections of this Chapter.

3.6.1 Internal Combustion Engine

Energy conversion losses of the ICE are incorporated using the performance map similar to the efficiency contours of Figure 3.21. The output torque and speed requested from the ICE is matched to a particular efficiency or fuel consumption rate from a look-up table. This allows the model to calculate approximate fuel consumption for varying drive profiles. The model checks the current settings of the drivetrain to determine the available ICE torque and then compares this against the requested torque. This comparison is the inclusion of the backward-forward facing approach to simulation as discussed in Section 3.2.3. Such models as discussed in Section 3.2 are considered accurate in representing whole systems, however, they omit transient responses that are otherwise present in real-world systems [157]. For

example the model interpolates two vectors of varying length one for output speed and another for output torque.

$$\overline{\omega}_e = \begin{bmatrix} \omega_{e1} \\ \omega_{e2} \\ \vdots \\ \omega_{en} \end{bmatrix} \quad \text{and} \quad \overline{T}_e = \begin{bmatrix} T_{e1} \\ T_{e2} \\ \vdots \\ T_{em} \end{bmatrix} \tag{3.33}$$

With $\omega_{en}>\ldots>\omega_{e2}>\omega_{e1}$ and $T_{em}>\ldots>T_{e2}>T_{e1}$ referencing an array of size n by m having fuel consumption rate or efficiency data recorded from operation of the ICE at the respective values of torque and speed.

$$\overline{\dot{m}}_f(T_e, \omega_e) = \begin{bmatrix} \dot{m}_{f11} & \dot{m}_{f12} & \cdots & \dot{m}_{f1m} \\ \dot{m}_{f21} & \ddots & \cdots & \dot{m}_{f2m} \\ \vdots & \vdots & \ddots & \vdots \\ \dot{m}_{fn1} & \dot{m}_{fn2} & \cdots & \dot{m}_{fnm} \end{bmatrix} \tag{3.34}$$

Each torque and speed relative to the fuel consumption rate is interpolated linearly to allow for the consideration of fuel consumption at all points in between those defined by equations 3.33 and 3.34. In addition, the input energy required for the ICE is modified by an inertial component such that the torque requested from the ICE includes the excess torque required to overcome any variation in speed.

$$T_e = T_e^* + J_e \frac{d\omega_e}{dt} \tag{3.35}$$

Where T_e^* is the requested torque, J_e is the inertial constant for the ICE and T_e and ω_e are the torque and speed output from the ICE as featured in equations 3.33 and 3.34. The resulting torque of equation 3.35 is used to determine the torque referenced for the look-up table of equation 3.34, with the resulting fuel consumption rate determining the instantaneous input power requirement of the ICE. The model is also influenced by temperature such that increased fuel consumption results from the ICE operating at cold start [49].

$$\dot{m}_{f,C} = \gamma \times \dot{m}_{f,H} \tag{3.36}$$

where

$$\gamma = \left(1 + \lambda^z\right) \tag{3.37}$$

and

$$\lambda = \frac{T_{tstat} - T_{coolant}}{T_{tstat} - 20} \tag{3.38}$$

Equation 3.36 indicates that all measurements for ICE operation in the ADVISOR software occur during 'hot' conditions with $\dot{m}_{f,H}$ being the fuel consumed during 'hot' operation of the ICE (i.e. $\dot{m}_{f,C}$ is the fuel consumption during 'cold' operation after scaling). A factor γ is used to normalise the operation according to the calculated temperature. The factor γ is varied according to the coefficient λ as identified in 3.38 and can be further scaled by the power z (equation 3.37). For scaling of fuel consumption z equals 1, however, for other characteristics of the ICE such as HC, NO or CO emissions z exhibits varying values determined from experimental data. T_{tstat} is the threshold thermostat temperature of the ICE for which the vehicle is considered to be operating at hot or cold temperatures. For this study, only the effect of temperature on fuel consumption is considered since the emissions data of the three test benches is not available.

3.6.2 Motor/generator

Similar to the ICE, the M/G has a look-up table for the efficiency of operation with respect to the torque and speed.

$$\overline{\omega}_{m/g} = \begin{bmatrix} \omega_{m/g1} \\ \omega_{m/g2} \\ \vdots \\ \omega_{m/gp} \end{bmatrix} \quad \text{and} \quad \overline{T}_{m/g} = \begin{bmatrix} T_{m/g1} \\ T_{m/g2} \\ \vdots \\ T_{m/gq} \end{bmatrix} \tag{3.39}$$

And

$$\overline{\eta}_{m/g}(T_{m/g}, \omega_{m/g}) = \begin{bmatrix} \eta_{11} & \eta_{12} & \cdots & \eta_{1q} \\ \eta_{21} & \ddots & \cdots & \eta_{2q} \\ \vdots & \vdots & \ddots & \vdots \\ \eta_{p1} & \eta_{p2} & \cdots & \eta_{pq} \end{bmatrix} \tag{3.40}$$

Leading to:

$$P_{m/g.in} = \frac{P_{m/g}{}^{*} + \omega_{m/g} J_{m/g} \dfrac{d\omega_{m/g}}{dt}}{\overline{\eta}_{m/g}(T_{m/g}, \omega_{m/g})} \tag{3.41}$$

where $P^{*}_{m/g}$ is the requested output power, $J_{m/g}$ is the rotational inertia factor representing inertia of the rotor and $\eta_{m/g}$ is the efficiency of the M/G. While the operating temperature of the M/G is determined as a function of output power and vehicle speed in the model, it does not influence the required input power [49]. Additionally, the backward/forward facing

approach to simulation is utilised in determining the limits of the M/G (available output torque and speed) in meeting the requested load as discussed in Section 3.2.3.

3.6.3 Energy Storage System

The model referred to is an open circuit voltage source with an internal resistance of the ESS. Leading to a discharge power of:

$$P_{ess} = V_{OC} I_{ess} - I_{ess}^2 R_{\text{int}} \tag{3.42}$$

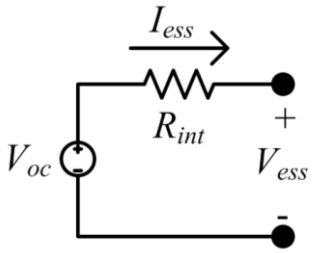

Figure 3.31 - Simple ESS model showing the open circuit voltage source and internal resistance.

This simple circuit allows for varying open circuit voltage levels in the source, as well as varying internal resistance according to the SOC, temperature and whether the ESS is charging or discharging. Look-up tables for V_{oc} and R_{int} with respect to the SOC and temperature are defined similar to the ICE and M/G. In addition, the coulomb efficiency of the ESS is considered for the power requirement for charging the ESS, such that energy stored in the ESS is reduced by the proportional coulomb efficiency in calculating the SOC.

$$I_{ess} = \begin{cases} I_{ess}^*, & for \quad I_{ess}^* > 0 \\ \eta_c I_{ess}^*, & for \quad I_{ess}^* \le 0 \end{cases} \tag{3.43}$$

I_{ess} is current drawn/absorbed by the ESS, I_{ess}^* is the requested signal and η_c is a constant representing the coulomb efficiency. Here the coulomb efficiency is applied once since it is a ratio of the amount of energy sent to the battery with respect to the amount of energy available from the battery after charging has occurred. Finally SOC is calculated as:

$$SOC = \frac{E_{ess,total} - V_{ess} Ah_{used}}{E_{ess,total}} \tag{3.44}$$

Equation 3.44 utilises the integral of the current to determine the Ah_{used}, such that positive I_{ess} current is drawn from the ESS and negative I_{ess} current is absorbed by the ESS.

3.6.4 Drivetrain Losses

Relative to the mechanical losses identified above the drivetrain losses include transfer of energy (performance map), rotational inertia and slip losses. For automatic and manual transmissions a performance map identifies the energy transfer losses between the propulsion device and the driven wheels. The PGS on the other hand is considered an ideal mechanical coupling with rotational inertia and slip contributing the losses. Two general equations for drivetrain losses are:

$$T_{in} = \frac{T_{out} + J\dfrac{d\omega_{out}}{dt}}{i \times \eta\left(T_{out}, \omega_{out}\right)} \tag{3.45}$$

And

$$\omega_{in} = i\left(1+s\right)\omega_{out} \tag{3.46}$$

where T_{in} and ω_{in} are the input and T_{out} and ω_{out} are the output torque and speed of drivetrain components, J is a constant rotational inertia, η is the efficiency with respect to the output torque and speed, s is the slip percentage and i represents any potential gear ratio that exists between the input and output of the device (e.g. equalling 1 for any direct coupling). Equation 3.45 and 3.46 determine general energy losses for any clutch, torque coupling, transmission, final drive and wheels.

3.6.5 Vehicle Specifications

From the analysis discussed in Sections 3.4 and 3.5 further specifications of the three test benches have been determined. The relative powertrain and drivetrain setup for each test bench was built in ADVISOR as discussed in Sections 3.2 and 3.3 with the powertrain specifications of Table 3.1. Simulating the vehicles for input and output energy considerations as calculated in Section 3.5 the parameters of Table 3.9 are refined through trial and error. In particular, it is possible to match the energy requirement for aero dynamic drag and rolling resistance in simulation to the total tractive power requirement of the vehicles. This comparison allowed for the accurate calculation of the rolling resistance coefficient, coefficient of aerodynamic drag and frontal area of the vehicle as represented in equation 3.1. While Section 3.4 determined that the tractive power of the measured data does not include a rolling resistance it was found that a small rolling resistance included in the ADVISOR simulation improved the error when compared to the measured tractive energy requirement of the vehicles. Due to equations 3.19 to 3.21 for the PGS only the numbers of teeth on the sun and ring gear are required.

Table 3.9 - Test bench simulation parameters determined from analysis of measured data.

Parameter	Toyota Prius 2010	Hyundai Sonata Hybrid 2011	Honda CR-Z 2010
Gear Ratios	S:30, R:78	[4.22, 2.64, 1.77, 1.35, 0.98, 0.75]	[3.62, 2.09, 1.44, 1.16, 0.94, 0.76]
Final Drive Ratio	4.2	3.08	3.21
Initial Conditions	Hot Start	Hot Start	Hot Start
Vehicle Mass (kg)	1531	1701	1329
Wheel Radius (m)	0.287	0.287	0.275
Rolling Resistance Coefficient	0.0024	0.004	0.00648
Coefficient of Aerodynamic Drag	0.3	0.24	0.25
Frontal Area (m^2)	1.745	1.835	2.427
Fuel Density	741	742	742

The results of Section 3.8 determine acceptable correlation of the measured and simulated models. Before demonstrating the three test benches the control strategies utilised in modelling the three vehicles are described.

3.7 Test Bench Control Strategies

Here the original controllers for the Toyota Prius 2010, Hyundai Sonata Hybrid 2011 and Honda CR-Z 2010 vehicles are defined ready for comparison with the developed controllers presented in Chapters 4 and 5. The vehicle configuration and powertrain ratings limit the control strategy the three test benches are capable of employing. The parallel configuration of the Hyundai and Honda when compared to the power-split configuration of the Toyota Prius, limit the flexibility in controlling the ICE. In the parallel configuration the ICE is directly coupled to the driven wheels which results with a lower average ICE efficiency. The Hyundai and Honda therefore have greater average fuel consumption for standardised drive cycles due to the limited flexibility in control. The performance resulting from the Hyundai and Honda is discussed in Section 2.4.2. In addition, the low power rating of the Honda leads to the ICE being on for all requested loads limiting the potential for fuel savings.

The control strategies of the three test benches seem to follow equivalent consumption minimisation strategy as considered from the analysis of Section 3.4 and 3.5. Due to the unknown parameters considered in the equivalent consumption minimisation strategy and therefore the exact ICE and ESS operating times the authors decided to utilise a set of rules to represent the original control strategy based on the analysis completed in Section 3.4 and 3.5. By comparison of the simulated signals with the measured signals as shown in Section

3.8, and the input and output energies of the vehicles the developed models demonstrate acceptable representations of the real-world vehicles.

3.7.1 Original Control Strategies

The ICE and M/Gs for each vehicle have been utilised to balance requested load according to:

$$P_L = P_e - P_{m/g} \tag{3.47}$$

Equation 3.47 indicates that when the ICE does not supply the full load the M/Gs combine with the ICE in hybrid mode. On the other hand when the ICE produces more power than the load the M/G absorbs energy to recharge the ESS. In the Hyundai and Honda the ICE torque is restricted by some percentage of the maximum brake torque the ICE can produce. This constraint ensures that the ICE operates at a minimum output torque in order to conserve fuel. Such a control strategy works in two ways; when requested torque is low and the SOC of the ESS is high the M/G can supply the load. Alternatively, the ICE operates at the minimum torque supplying the load and charging the ESS when the SOC is low. Table 3.10 identifies the control rules for the Hyundai and Honda test benches based on the described constraints. The measured signals are highlighted in bold type in Table 3.10. *V* is the vehicle velocity, SOC is the measured SOC, T_e^* is the requested ICE torque and $T_{m/g}^*$ is the requested M/G torque. The inequalities of the input signals in Table 3.10 define the thresholds for when the respective outputs will be set for T_e^* and $T_{m/g}^*$. The constants $p_{e,min}$ and $p_{e,opt}$ are percentages of maximum brake torque the ICE can develop while $p_{m/g,max}$ limits the maximum brake torque the M/G can produce as a percentage of maximum brake torque. In addition to the torque constraints of the ICE, V_{ZEV} determines the vehicle speed threshold below which the two test benches operate as electric vehicles. Each of the rules of Table 3.10 holds as long as the SOC remains between the high and low limit. As an example if the vehicle velocity is greater than V_{ZEV} and the requested load torque (T_L^*/i_g) is less than $T_{e,max}p_{e,min}$ then T_e^* is set to 0 and $T_{m/g}^*$ is set to $T_L^*/i_g k_1$, where k_1 represents the gear ratio between the input of the final drive and output of the M/G.

Table 3.10 - Hyundai Sonata Hybrid 2011 and Honda CR-Z 2010 control rules.

Input Signals		Output Signals	
Vehicle Velocity (*V*)	$SOC_{low}<\boldsymbol{SOC}<SOC_{high}$	**ICE Torque Request (T_e^*)**	**M/G Torque Request ($T_{m/g}^*$)**
$\boldsymbol{V}\leq V_{ZEV}$	$T_L^*/i_g < T_{e,max}p_{e,min}$	0	$T_L^*/i_g k_1$
	$T_L^*/i_g > T_{e,max}p_{e,min}$	T_L^*/i_g	0
$\boldsymbol{V}>V_{ZEV}$	$T_L^*/i_g < T_{e,max}p_{e,opt}$	$T_{e,max}p_{e,opt}$	$(T_{e,max}\omega_e p_{e,opt} - T_L^* \omega_L)/\omega_{m/g}$
	$T_L^*/i_g > T_{e,max}p_{e,opt}$	$T_{e,max}p_{e,opt}$	$(T_L^* \omega_L - T_{e,max}\omega_e p_{e,opt})/\omega_{m/g}$
$\boldsymbol{V}>0$	$T_L^*/i_g k_1 < T_{m/g,max}p_{m/g,max}$	0	$T_L^*/i_g k_1$
	$T_L^*/i_g k_1 > T_{m/g,max}p_{m.g,max}$	$T_L^*/i_g - k_1 T_{m/g,max}p_{m/g,max}$	$T_{m/g,max}p_{m/g,max}$

Due to the PGS of the Toyota Prius the ICE is restricted to the optimal operating line having a unique speed ratio for optimal operating efficiency at any load power requested [91]. This control strategy in combination with the rules of Table 3.11 describes the main control strategy of the Toyota Prius 2010.

Table 3.11 - Toyota Prius 2010 control rules

Input Signals		Output Signals	
SOC	**Vehicle Velocity (*V*)**	**ICE Power Request (P_e^*)**	**M/G Power Request ($P_{m/g}^*$)**
$\boldsymbol{SOC}>SOC_{target}$	$\boldsymbol{V}>V_{ZEV}$	P_L^*	0
	$\boldsymbol{V}\leq V_{ZEV}$	0	P_L^*
$SOC\leq SOC_{target}$	$\boldsymbol{V}>V_{ZEV}$	$P_L^* + P_{chg}^*$	P_{chg}^*
	$\boldsymbol{V}\leq V_{ZEV}$	0	P_L^*

For the ADVISOR software a general algorithm to determine the optimal operating line is featured as follows. Algorithm 3.1 assumes that the M/G1 torque and speed range is high enough to accommodate the ICE operating torque and speed at any power request. In the case that M/G1 has a torque or speed constraint this must be included in the torque and speed ranges maximum and minimum values for the system.

Algorithm 3.1: Optimal operating line of ICE (Adapted from the ADVISOR software [49])

1: define *resolution*

2: get $(\overline{T}_e, \overline{\omega}_e)$ // $\overline{T}_e$ and $\overline{\omega}_e$ are vectors with the lengths *m* and *n* containing the ICE torque and speed ranges

3: Create array $\overline{P}_e = \overline{\omega}_e \times \overline{T}_e$ //This array is the ICE output power, indexed horizontally by $\overline{T}_e$ and vertically by ω_e having dimensions *n* by *m*.

4: define array $\overline{P}_{e,in} = \overline{\dot{m}}_f(T_e, \omega_e) \times Q_{HV}$ //fuel consumption rate map in g/s and lower heating value of the fuel in J/g. $\overline{\dot{m}}_f$ is indexed horizontally by $\overline{T}_e$ and vertically by $\overline{\omega}_e$ and is a pre-existing array in the ICE control unit for estimating fuel consumption relative to output torque and speed.

5: define array $\overline{\eta}_e = \overline{P}_e ./ \overline{P}_{e,in}$ //element-wise division of the two arrays which maintains the horizontal and vertical index for $\overline{T}_e$ *and* $\overline{\omega}_e$ respectively.

6: define $\omega_{e,min} = \min(\omega_e)$, and $\omega_{e,max} = \max(\omega_e)$.

7: define $\overline{\omega}_{e,map} = [\omega_{e,min}: ((\omega_{e,max} - \omega_{e,min})/resolution): \omega_{e,max}]$. //defines a new vector for the ICE speed with the defined resolution, interpolating the measured speeds.

8: define $\overline{T}_{e,\max-map} = interp1(\overline{\omega}_e, T_{e,max}, \overline{\omega}_{e,map})$ //*interp1*(… ,… ,…) is a MATLAB function that interpolates the values of the second vector $T_{e,max}$ (which originally has the same number of elements as the first vector $\overline{\omega}_e$) to match the same number of elements as the third vector $\overline{\omega}_{e,map}$. This means that $\overline{T}_{e,\max-map}$ is now indexed by $\overline{\omega}_{e,map}$ with total number of elements equal to *resolution*. Note that the maximum and minimum values of the first and third vectors must be the same as defined at 6 and 7.

9: define $\overline{P}_{e,\max} = \overline{T}_{e,\max-map} .* \overline{\omega}_{e,map}$ //defining the maximum power output by the ICE at each speed in $\overline{\omega}_{e,map}$.

10: define $P_{e,min} = \min(\overline{T}_e) * \omega_{e,min}$. //minimum power for each case should be zero due to the ICE operating as a motor only.

11: define $\overline{P}_{e,map} = [P_{e,min}: ((P_{e,max} - P_{e,min})/resolution): P_{e,max}]$ //defines a new vector for the ICE output power that can be indexed by the previously defined $\overline{\omega}_{e,map}$.

12: define count_$P_{e,map}$ = length($\overline{P}_{e,map}$) - 1 //length is a MATLAB function that returns the length of a vector.

13: define count_$\omega_{e,map}$ = length ($\overline{\omega}_{e,map}$) – 1

14: for P_{e,map_index} = 1 to count_$P_{e,map}$ do {

15: $\overline{T}_{e,Pe,map} = \overline{P}_{e,map}(P_{e,map\_index}) ./ \overline{\omega}_{e,map}$ //calculate torques at power levels for each speed of $\overline{\omega}_{e,map}$.

16: $\overline{T}_{e,Pe,map} = \min(\overline{T}_{e,Pe,map}, \overline{T}_{e,\max-map})$ //check that all calculated torques are below the maximum torque for each speed in $\overline{\omega}_{e,map}$.

17: $T_{e,Pe,map} = \max(\overline{T}_{e,Pe,map}, \min(\overline{T}_e))$ //check that all calculated torques are above the minimum torque the ICE is known to develop for each speed in $\overline{\omega}_{e,map}$.

18: for ω_{e,map_index} = 1 to count_$\omega_{e,map}$ do

19: $\overline{\eta}_{e,\omega e,map\_index}(\omega_{e,map\_index}) = interp2(\overline{\omega}_e, \overline{T}_e, \overline{\eta}_e^T, \overline{\omega}_{e,map}(\omega_{e,map\_index}),$

$\overline{T}_{e,Pe,map}(\omega_{e,map\_index})$) //*interp2*(… ,… ,… ,… ,…) is a MATLAB function that interpolates the elements of an array (third entry $\overline{\eta}_e^T$, with dimensions equivalent to the first ($\overline{\omega}_e$) and second entry ($\overline{T}_e$)) outputting an array with a larger number of elements (determined by the dimensions of the fourth ($\overline{\omega}_{e,map}(\omega_{e,map\_index})$) and fifth ($\overline{T}_{e,Pe,map}(\omega_{e,map\_index})$)) entries).

20: end for

21: $\eta_{e,\omega e,map\_index\_max} = \max(\eta_{e,\omega e,map\_index})$

22: $\overline{\eta}_{e,\omega e,map\_index\_norm} = \eta_{e,\omega e,map\_index\_max} ./ \overline{\eta}_{e,\omega e,map\_index}$ //provides a means for checking the optimal efficiency of operation at some power in $\overline{P}_{e,map}$.

23: $\omega_{e,best\_index}$ = min(find($\overline{\eta}_{e,\omega e,map\_index\_norm}$=min($\overline{\eta}_{e,\omega e,map\_index\_norm}$)) //find(…=…) is a MATLAB function that returns indexes of the left hand side vector that satisfy the conditions specified in the input to the function.

24: $\overline{T}_{e,best}(P_{e,map\_index})$ = $\overline{T}_{e,Pe,map}(\omega_{e,best\_index})$ //record the optimal torque @ $\overline{P}_{e,map}$ (P_{e,map_index})

25: $\overline{\omega}_{e,best}(P_{e,map\_index})$ = $\overline{\omega}_{e,map}(\omega_{e,best\_index})$ //record the optimal speed @ $\overline{P}_{e,map}$ (P_{e,map_index})

26: end for

27: P_{e,max_index} = min(find($\overline{P}_{e,\max}$ =max($\overline{P}_{e,\max}$)))

28: $\overline{P}_{e,opt}$ = [0 $P_{e,map}$(1: count_$P_{e,map}$) $P_{e,max}$(P_{e,max_index})]

29: $\overline{\omega}_{e,opt}$ = [$\omega_{e,best}$(1) $\overline{\omega}_{e,best}$ $\overline{\omega}_{e,map}(P_{e,max\_index})$]

30: $\overline{T}_{e,opt}$ = [0 $\overline{T}_{e,best}$ $\overline{T}_{e,\max-map}(P_{e,max\_index})$]

Equation 3.48 identifies the vectors resulting from Algorithm 3.1:

$$\overline{\omega}_{e,opt} = \begin{bmatrix} \omega_{e,opt1} \\ \omega_{e,opt2} \\ \vdots \\ \omega_{e,opt-i} \end{bmatrix}, \qquad \overline{T}_{e,opt} = \begin{bmatrix} T_{e,opt1} \\ T_{e,opt2} \\ \vdots \\ T_{e,opt-i} \end{bmatrix} \qquad \text{and} \qquad \overline{P}_{e,opt} = \begin{bmatrix} P_{e,opt1} \\ P_{e,opt2} \\ \vdots \\ P_{e,opt-i} \end{bmatrix} \tag{3.48}$$

With $\omega_{e,opt-i}>\ldots>\omega_{e,opt2}>\omega_{e,opt1}$, $T_{e,opt-i}>\ldots>T_{e,opt2}>T_{e,opt1}$, $P_{e,opt-i}>\ldots>P_{e,opt2}>P_{e,opt1}$ and i is the length of the vectors as defined by *resolution* in algorithm 3.1. With the definition of algorithm 3.1 the EMS controller uses the resulting vector combination as a look-up for the optimal torque ($T_{e,opt}$) and speed ($\omega_{e,opt}$) at the requested power ($P_{e,opt}$) from the ICE.

$$\overline{P}_{e,opt}(P_L) \rightarrow T_e = \overline{T}_{e,opt}(P_L) \qquad \text{and} \qquad \omega_e = \overline{\omega}_{e,opt}(P_L) \tag{3.49}$$

P_L is entered into $\overline{P}_{e,opt}$ to determine the index for selecting the desired speed of the ICE. Once the ICE speed is determined the torque can either be calculated or selected from the

optimal torque vector defined in equation 3.48. Table 3.12 outlines the selected values for the control strategies defined in Table 3.10 and Table 3.11. ICE idle speed, target SOC, velocity for zero emissions vehicle mode, ICE downshift and upshift, motor torque limit, ICE minimum torque, and ICE optimal torque control parameters are determined from the analysis in a similar fashion to that discussed in in Sections 3.4 and 3.5 for the three test benches. The ESS SOC limits are based on the pre-existing constraints in the ADVISOR software models.

Table 3.12 - Test bench control strategy parameters.

Control Parameter	Symbol	Toyota Prius 2010	Hyundai Sonata Hybrid 2011	Honda CR-Z 2010
ICE Idle Speed (rpm)	ω_{idle}	1200	700	898
High SOC Limit (%)	SOC_{high}	75	70	80
Low SOC Limit (%)	SOC_{low}	45	60	20
Target SOC (%)	SOC_{target}	60	N/A	N/A
ICE minimum SOC limit	SOC_{ICE}	50	N/A	N/A
Velocity for EV mode (km/h)	V_{ZEV}	45	18	0
ICE Downshift Speed (rpm)	ω_{dwn}	N/A	797	1260
ICE Upshift Speed (rpm)	ω_{up}	N/A	1500	2160
Motor Torque Limit (%)	$p_{m,max}$	100	100	32
ICE Minimum Torque (%)	$p_{e,min}$	N/A	20	N/A
ICE Optimal Torque (%)	$p_{e,opt}$	N/A	60	N/A
HEV Type	-	Full	Mild	Micro

3.8 Model Verification

In order to demonstrate the accuracy of the developed test benches in the ADVISOR software the input and output efficiencies, overall efficiency and fuel consumption from simulation are compared against the measured data. The three test benches were verified on two drive cycles, the UDDS and the HWFET for which the measured data is available [118]. In addition, the simulated and measured signals are compared over time to show similar component operation.

Table 3.13 compares the results for the three test benches. The error in the fuel consumption is 3.87% more on the UDDS drive cycle suggesting that the simulated model consumes more fuel energy than indicated by the measured data. This error resulted from the Toyota Prius control strategy being required to find a balance between operation during city (UDDS) and highway (HWFET) driving scenarios. However, the maximum error of 3.87% demonstrates the low error in the simulated model when compared to the measured data.

Comparison of the operating signals (measured and simulated) on the standardised drive cycles suggests that the three vehicles are operating as required. Signals compared include the wheel speed, tractive power, ICE speed, total fuel energy consumed, ESS SOC and ESS power output for each of the vehicles. Again rather than including all the signal comparisons at this point in the thesis only the Toyota Prius 2010 signals are shown for the UDDS, the compared signals for the Hyundai Sonata Hybrid 2011 and Honda CR-Z 2010 are found in Appendix A.1.

Uncertainty of the control strategy utilised is evident in the ESS SOC and ESS power output of Figure 3.33 and Figure 3.37. Due to the rule based controller representing the original controller of the Toyota Prius there is a noticeable difference between the charge and discharge of the measured and simulated ESS data. The correlation of the wheel speed for simulated and measured signals in Figure 3.32 does not suggest that the selected wheel radius is the same as the actual Toyota Prius 2010 wheel radius. It does, however, demonstrate that the simple speed conversion from vehicle speed to wheel speed can be assumed to have the same ratio. The main point to consider is the ratio between the ICE and wheels since this determines the relationships for torque and speed. The analysis of Sections 3.4 and 3.5 in determining the ratio between the ICE and wheels is essential in realistically representing the vehicles in simulation. While the selected wheel radius, final drive and PGS ratios may not be individually correct, the comparison of ICE speed, fuel consumption and tractive power (Figure 3.34, Figure 3.35 and Figure 3.36 respectively) indicates that the overall ratio is similar in the simulated vehicle.

Table 3.13 - Comparison of simulated and measured data.

Drive Cycle	Component Parameter	Toyota Prius 2010		Hyundai Sonata Hybrid 2011		Honda CR-Z 2010	
		Measured	Simulated	Measured	Simulated	Measured	Simulated
UDDS	Tractive Energy (Aero + Rolling) (kJ)	1249.850	1257.000	1460.037	1494.017	1880.040	1879.193
	Energy Used (Fuel Energy – ESS Energy) (kJ)	12059.941	12182.495	18816.294	18802.500	23035.423	23081.07
	Overall Efficiency (%)	10.36	10. 31	7.76	7.95	8.16	8.14
	Fuel Consumption (L/100km)	3.10	3.22	4.92	4.89	6.04	6.06
HWFET	Tractive Energy (Aero + Rolling) (kJ)	3332.530	3275.794	3430.303	3357.123	4037.890	4378.479
	Energy Used (Fuel Energy – ESS Energy) (kJ)	17655.660	17188.000	21174.387	21078.79	23760.145	23243.05
	Overall Efficiency (%)	18.88	19.06	16.20	15.93	16.99	18.84
	Fuel Consumption (L/100km)	3.36	3.29	4.05	4.04	4.48	4.41

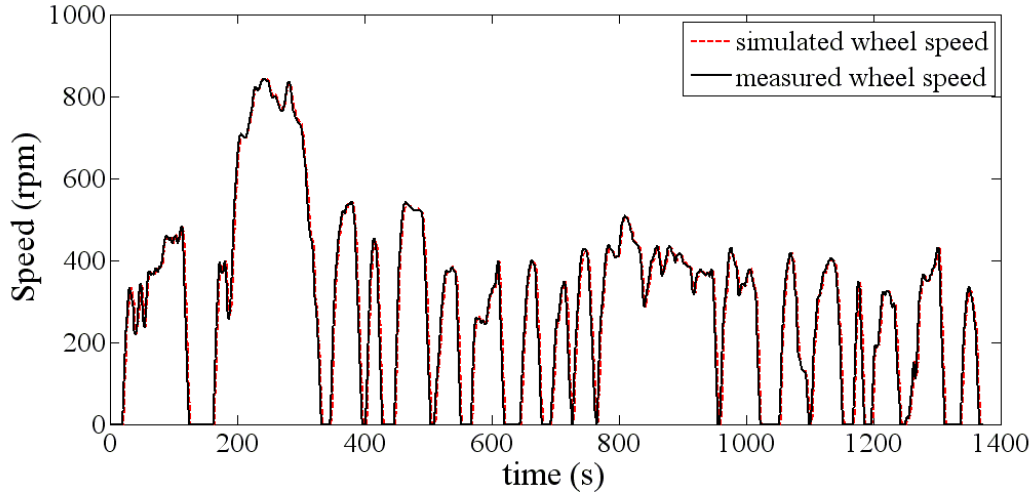

Figure 3.32 - Toyota Prius 2010 wheel speed - simulated versus measured signals operating on the UDDS.

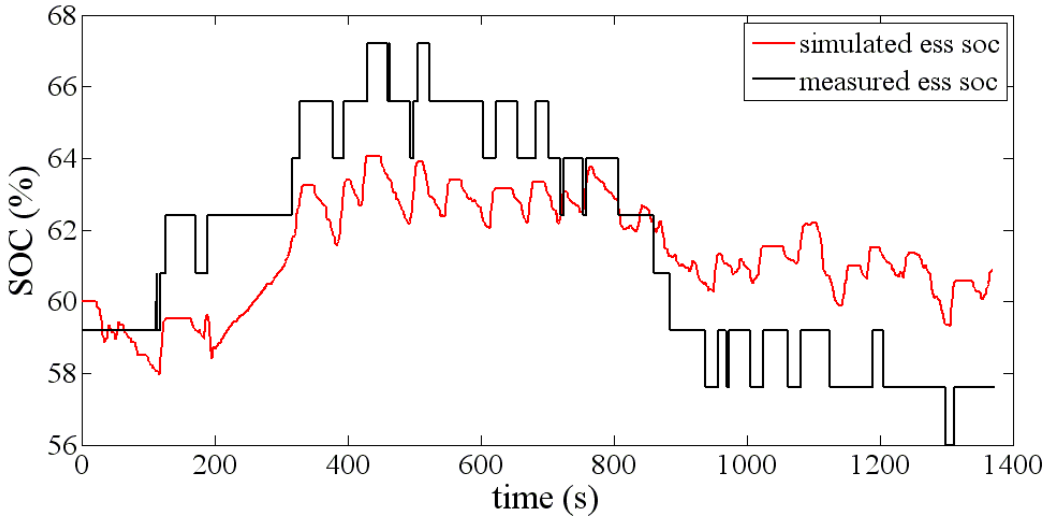

Figure 3.33 - Toyota Prius 2010 ESS SOC - simulated versus measured signals operating on the UDDS.

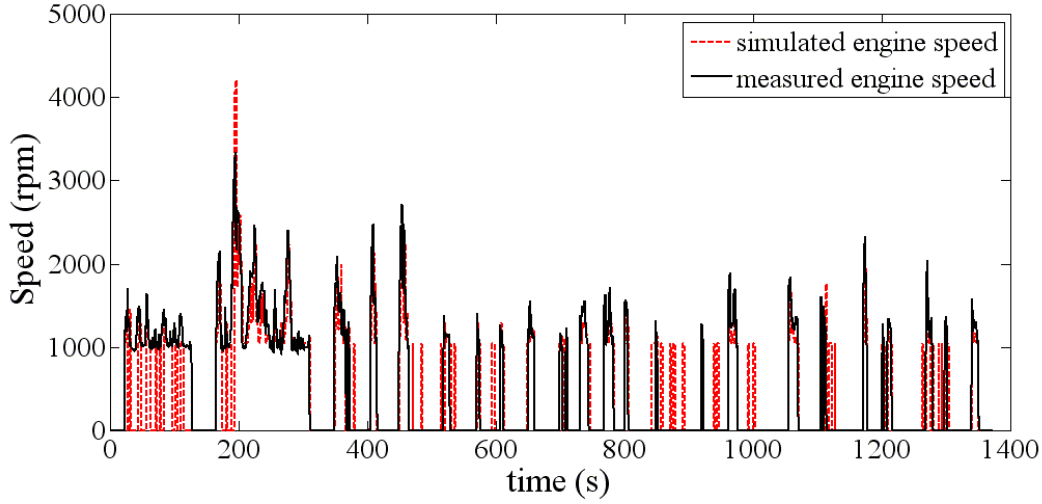

Figure 3.34 - Toyota Prius 2010 ICE speed - simulated versus measured signals operating on the UDDS.

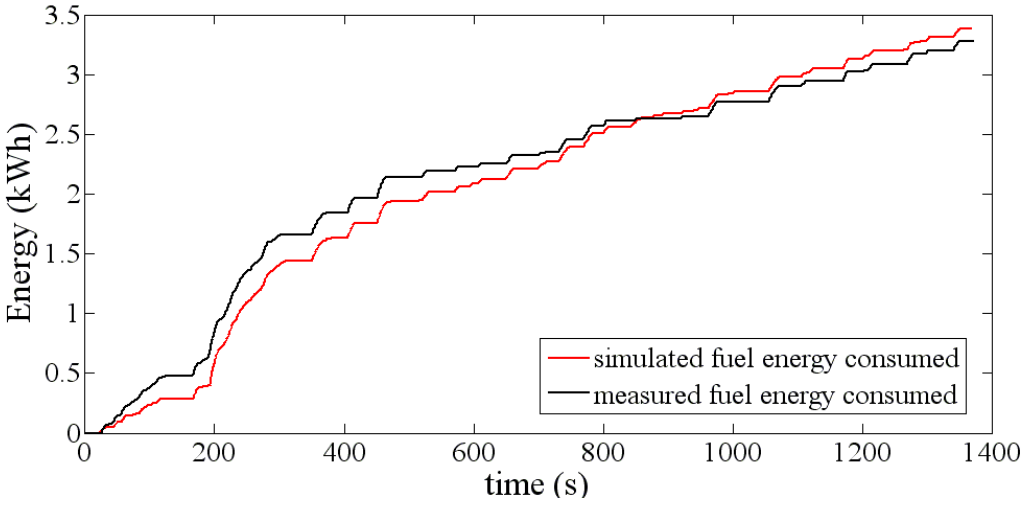

Figure 3.35 - Toyota Prius 2010 fuel energy consumed - simulated versus measured signals operating on the UDDS.

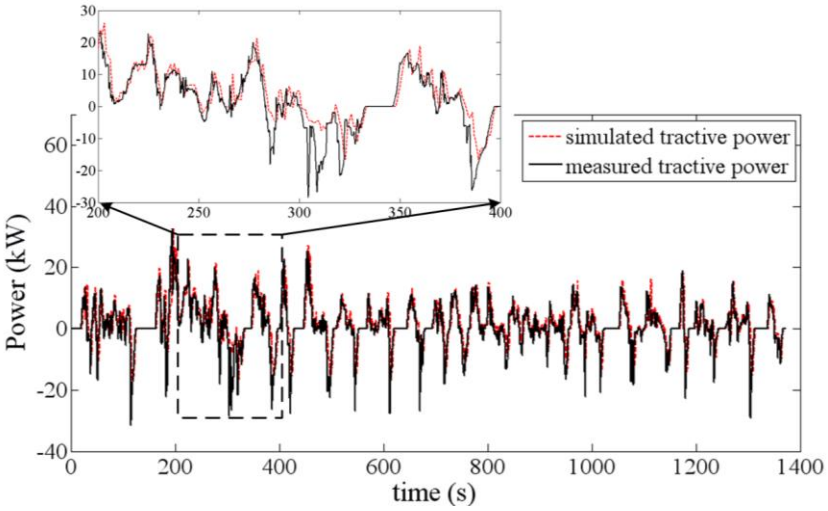

Figure 3.36 - Toyota Prius 2010 tractive power - simulated versus measured signals operating on the UDDS.

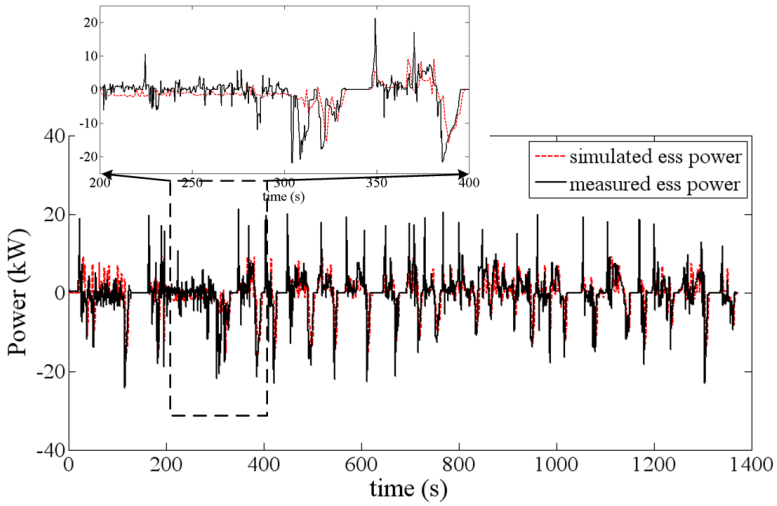

Figure 3.37 - Toyota Prius 2010 ESS power output - simulated versus measured signals operating on the UDDS.

3.9 Summary of ESV Modelling

For the modelling presented in this thesis three test benches are developed in the ADVISOR software package, which is a MATLAB/Simulink add-on. This software conforms to the backward-forward facing approach to simulation. This means that it considers both backward and forward facing simulation techniques when evaluating the models. The forward facing approach is more accurate than the backward facing approach for real-time simulation, however, the forward facing approach takes a significant amount of time to simulate. For the ADVISOR model the backward facing elements determine the required input signals and thereby the input energy consumed during driving. The forward facing elements enforce the constraints of the components for driving whilst ensuring that the vehicle meets the required trace speed during driving. The backward/forward facing approach to simulation has proven accuracy, is utilised by a number of researchers and is much faster than the forward facing approach alone.

Data obtained from the Downloadable Dynamometer Database at Advanced Powertrain Research Facility in the Argonne National Laboratory is analysed to confirm the specifications of the vehicles and to define the existing vehicles' control strategies. Firstly the measured tractive power requirement is compared against a known method for tractive power calculation. The results from this comparison suggested that the chassis dynamometer does not include components for rolling resistance or inertia of the moving mass of the vehicle (mass factor equal to unity). This measured data is not a fair comparison to the real-world conditions of driving, however, the data reflects the operation of the vehicles over a defined drive profile. Therefore creating a model based on this measured data serves as a bench mark for comparison of different methods of control. The only difference being that the tractive energy requirement (i.e. output power) is less when it comes to the chassis dynamometer as compared with a real-world scenario.

After defining the mechanical coupling between the ICE and driven wheels it is possible to compare approximate output power of the propulsion devices to the measured input for increased understanding of the control strategy. In comparing energy supplied and consumed by the powertrain and drivetrain of the vehicles, measured ESS energy is subtracted from measured fuel energy. This convention ensures that energy sent to the ESS and losses induced by charging the ESS are accounted for as part of the ICE loading. This comparison is demonstrated for the Toyota Prius, distinguishing modes of operation and potential average efficiencies of operation. For the Toyota Prius hybrid, electric and regenerative braking modes of operation are identified having average efficiencies of 28.78%, 61.87% and 79.45% respectively. Operation during these modes does not represent the overall efficiency of the vehicle at 10.36% on the UDDS, however, it suggests that significant losses

are introduced by accessory loads, ESS SOC maintenance and transient operations of the vehicle.

Further analysis of the modes of operation reveals that mismatch exists between signals measured at input and the signals measured at output. Possible causes identified include time delay between input and output and the high number of transient operations. Therefore the individual operations of the vehicle as measured by the sensors are somewhat inhibited due to the real-world dynamics of the vehicle. According to the separation of modes in Section 3.5.5, 63.82% of the measured data over the UDDS resembles conditions expected by each of the modes of operation. This means that 36.18% of the total measured data is received during a transition from one mode to the next or during large transient operations of the vehicle. The measured transients are therefore an approximate representation of the vehicles operations. The consideration for mismatch is relative to the time at which each measurement is taken and therefore overall quantities such as efficiency or fuel consumption are acceptable bench marks for comparison of the simulated and measured data. Examining the measured data through the analysis completed in this Chapter does, however, confirm the following about the three existing vehicles' controllers:

- The ICE starts once the vehicle has accelerated above some minimum vehicle velocity
- The ICE idles during negative transients if the ICE was previously on.
- Regenerative braking occurs for all negative tractive power
- M/G operation during ICE shutdown and low vehicle velocity
- SOC is maintained to some target, or between a high and low SOC limit
- The approximate efficiency of operation during ICE, motoring and regenerative braking modes of operation
- There are limitations in the data such as missing ICE start-up transients and time delays between input and output
- Operation of the ICE in the Toyota Prius according to the optimal operating line also referred to as VSC in Section 4.3.2
- The ICE typically starts for tractive power levels greater than 10 kW in the Toyota Prius 2010
- The Hyundai Sonata Hybrid restricts ICE operation to above a percentage of maximum brake torque (e.g. $T_e > 0.2T_{e,max}$)

Keeping in mind that the signals and therefore individual operating points of the vehicle are potentially mismatched the approximate ICE operation over the drive cycle provides an insight into potential performance improvements. It is assumed that measured fuel power

greater than 90% of the total power delivered at input represents ICE only mode of operation. This consideration allows for the estimation of the torques placed on the ICE at the measured ICE speeds. Analysing this data reveals low ICE operating efficiency over the UDDS even though operation is limited to the optimal operating line. Observing the approximated torques at measure ICE speed at least 60% of ICE operation over the UDDS occurs at efficiencies below 25% while 30% occur at efficiencies below 20%. Considering that ICEs are capable of efficiencies greater than 30% this analysis suggests there is potential for improvement.

Adapting the above control considerations to the energy loss models available in the ADVISOR software the vehicles' models are varied by comparison of the simulated and measured signals. In the process of developing the models in the ADVISOR software a method for calculating the optimal operating line was required for the ICE as identified with Algorithm 3.1. Initially the three vehicle models' specifications were experimented with in order to determine the exact values for the simulation and to accurately represent the existing vehicles. Once the specifications had been determined for the UDDS drive cycle the vehicles were tested and compared on the HWFET. Additional trial and error testing determined the final values of specifications for the vehicles that best represented operations on both drive cycles. This included varying specifications such as those featured in Table 3.2, Table 3.9 and Table 3.12 until the input, output, overall efficiency and fuel consumption had minimal error. Finally, results of the input, output, overall efficiency and fuel consumption reveal that the maximum error observed on the Toyota Prius 2010 is less than 3.87%.

CHAPTER FOUR

Design of a High Efficiency Controller in PHEV

4.1 Introduction

Three vehicle models were developed in the ADVISOR software in the previous Chapter, for use as test benches in evaluating the proposed high efficiency controller of this Chapter. The original controller developed from the detailed analysis of the measured data for each of the three vehicles determines a fair bench mark for the performance evaluation of the novel controller presented here. The three vehicle models in simulation are shown to represent real-world operation within 4% of the measured performance values. The four performance quantities used for comparison include, input (fuel and electrical) and output (tractive) energy, overall efficiency and fuel consumption over two standardised drive cycles.

Section 2.2.1 highlighted the low average efficiency of operation of the ICE in comparison to the efficiency of operation of the M/Gs and ESS. This was confirmed for an ICE operating in parallel connected hybrid vehicles. These parallel connected hybrid vehicles have greater average fuel consumption than the power-split connected topology descibed in Section 2.4.2 and again in Section 3.8. Following the development of the three test benches, the motivation for high efficiency control of ESVs is identified through analysis of the Toyota Prius measured data. In particular, this analysis identified that even with the ICE control constrained to the optimal operating line average efficiency of operation is low (Section 3.5.5). This Chapter acknowledges that while high efficiency control of the ICE will improve average ICE efficiency, it may lead to increased losses in other components on the vehicle and thus the overall efficiency must also be examined. However, high efficiency control of the ICE is the starting point for improving the overall efficiency of PHEVs.

In addition to the high efficiency controller, rules are defined in order to maintain the SOC of the ESS. These control rules also help to make energy management decisions when requested drivetrain power is outside of a defined high efficiency region for the ICE. This high efficiency region restricts output torque and speed operating points to efficiencies greater than a desired minimum. A method for calibrating the high efficiency controller is discussed with respect to the fuel consumption of the vehicle and the SOC of the ESS. This discussion realises the importance of selecting the optimal high efficiency region for the ICE

to operate within. Operation of the novel control strategy is demonstrated for simulation over the UDDS before quantifying the performance improvement.

From the bench mark detailed in Chapter 3, a percentage improvement in the form of fuel consumption reductions is determined relative to the designed controller on the UDDS and HWFET drive cycles previously used. In addition, the new European drive cycle (NEDC) is added for a third drive scenario. Initially, for city drive scenarios the novel control strategy determines up to 12% fuel consumption reductions, while improvement to highway driving is minimal (between 0 to 3%). Secondly, the drivability of the three vehicles is examined through the consideration of the total number of ICE and gear shift events using the original and designed high efficiency controller. Finally further investigation of the high efficiency controller's operation in the Toyota Prius reveals the potential for more fuel consumption reductions. This analysis prompts the investigation of the high efficiency region on-the-go; this is described in Chapter 5. The focus for this Chapter, however, is the definition of the non-predictive high efficiency control for PHEV.

4.2 Energy Management System Controller

Typically an EMS controller determines the proportion of power to supply from the ICE or M/G(s) with the alternative device balancing the requested load power. For example, in the case of an EMS controller that determines the ICE power requirement the following equation represents the power balance of energy sources:

$$P_L^* = P_e - P_{m/g} \tag{4.1}$$

where P_L^* is the instantaneous requested load power, P_e the determined ICE output power that balances with the output power supplied by the M/Gs ($P_{m/g}$). Let T_e^* denote commanded ICE output torque and T_e measured ICE output torque. The same notation is used for other commands (requested signals) and measured signals respectively. It is assumed that the ICE satisfies a specified amount of the requested load power with the M/Gs balancing the remainder of the load.

Figure 4.1 outlines the generalized control system for the PHEV and HEV. The user controls the accelerator pedal which is proportional to the maximum brake torque ($T_{e,max} + T_{m/g,max}$) the vehicle can produce. At the equivalent to wide-open-throttle (WOT) with the accelerator fully depressed, maximum brake torque is requested from the system. Each process block identifies the location of a measured or requested signal throughout the vehicle topology. The output torque of the ICE (T_e), M/Gs ($T_{m/g}$) and load (T_L) as shown in Figure 4.1 are assumed to be referred to the shaft of the ICE. The mechanical coupling between the M/G

and ICE is represented by the ratio k_1. The requested load torque (T_L^*), measured load speed (ω_L) and SOC of the ESS are inputs to the EMS controller for determining the optimal ICE brake torque (T_e^*) and speed (ω_e^*) commands. The fuel, M/G and transmission controllers are slave to the EMS controller, utilising the identified output signals from the EMS controller to locally control each respective device. From Figure 4.1 and with reference to equation 4.1, the load torque and speed with respect to the ICE and M/Gs are given as:

$$T_L = i_g\left(T_e - k_1 T_{m/g}\right) \tag{4.2}$$

And

$$\omega_L = \frac{\omega_e}{i_g} = \frac{\omega_{m/g}}{i_g k_1} \tag{4.3}$$

Equation 4.2 and 4.3 represent the ideal case, establishing the fundamental relationship between the ICE, M/Gs and load. This is for the consideration of the designed EMS controller for improving the performance of each of the models defined in Chapter 3.

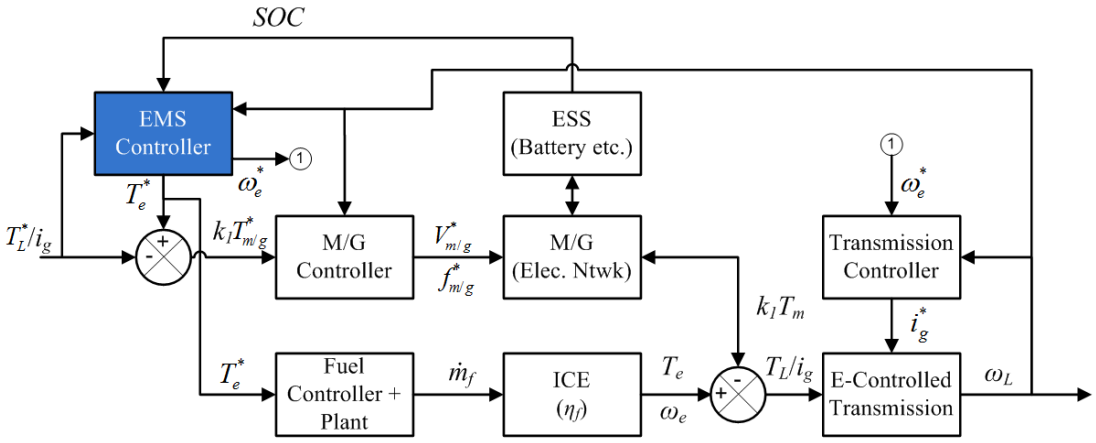

Figure 4.1 - General block diagram for the control system of a PHEV and HEV.

4.3 Maximising ICE Efficiency of Operation

The ICE being the primary power source in both parallel and power-split topologies leads to the need for conserving fossil fuel while maintaining the ESS SOC according to some control strategy. There are three fundamental techniques for ICE control in parallel and power-split connected PHEV and HEV. These include PBS, VSC and combined PBS with VSC.

4.3.1 Power Balancing Strategy

As mention in Chapter 2 a mechanical coupling device is required in order to achieve the balancing of power between at least two propulsion devices. Parallel and power-split

topologies for example exhibit the necessary mechanical connection between the ICE and M/Gs to achieve PBS. In dynamical systems the operating speed of the ICE is proportional to the wheel speed of a vehicle as a result of the brake torque developed. This means that the ICE developed torque (T_e) required to meet the load power ($P_L^*=P_e$) is proportional to the fuel rate fed into the ICE, this can be represented by:

$$T_e = k\dot{m}_f \tag{4.4}$$

where k represents constants unique to individual ICE [54] and $\dot{m}_f$ is the fuel rate. Referring to Figure 4.2, an example scenario for the discussed PBS is illustrated. T_{e1} is the requested brake torque from the drivetrain of the vehicle, occurring at the speed ω_{e1} determined by the drivetrain coupled to the ICE. By supplying a fuel rate of $\dot{m}_{f1}$ to the ICE, the load torque demanded by the drivetrain is satisfied. The problem here is that the requested operating point is not at the most efficient operating conditions for the ICE. If the SOC of the ESS is below maximum and the losses incurred from charging are less than the potential improvement to the whole system efficiency [10], then the fuel rate can be increased to $\dot{m}_{f2}$ resulting with a brake torque of T_{e2}. The excess power ($P_{e2} - P_{e1}$) generated by increasing the fuel rate is absorbed by the M/G resulting in a more efficient outcome for the whole system. According to the example ICE efficiency map in Figure 4.2 this improves the efficiency of the ICE from 26% to 32%. As mentioned, the benefit of using this control strategy is dependent on the efficiency of charging/discharging the ESS. If the energy consumed by the ICE and electrical network, in moving the operating point, is greater than that consumed by the original load request then relocating the ICE operating point is unnecessary. The alternative to PBS in high efficiency control of the ICE is VSC.

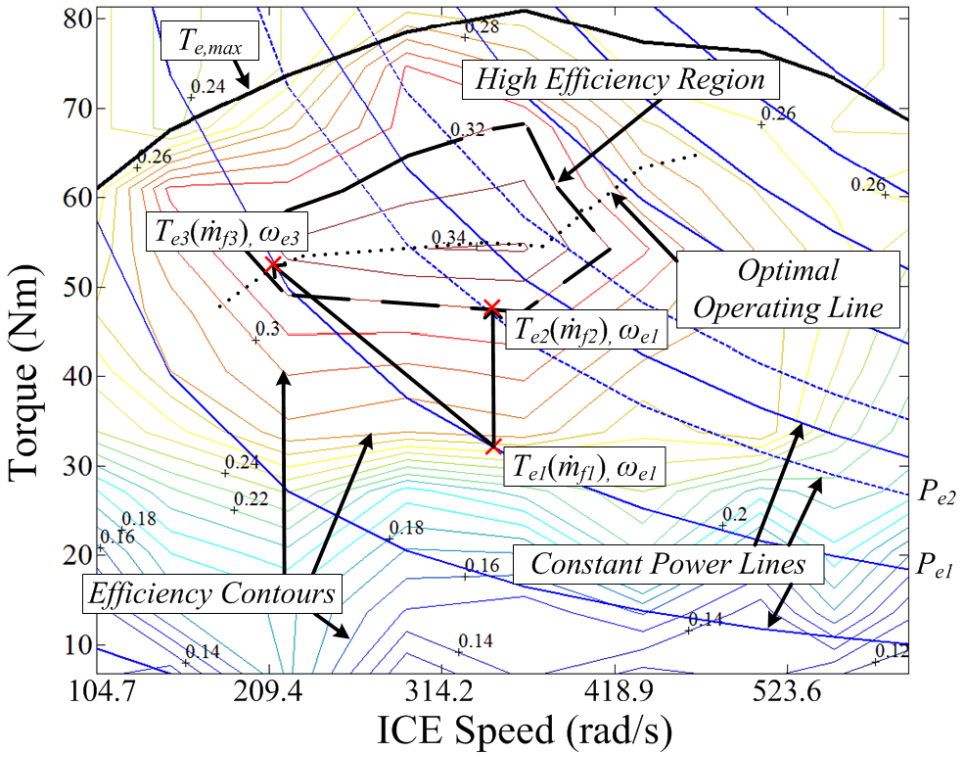

Figure 4.2 - Example ICE efficiency map illustrating PBS and VSC for high efficiency control of the ICE. Movement from ($T_{e1}(\dot{m}_{f1}),\omega_{e1}$) to ($T_{e2}(\dot{m}_{f2}),\omega_{e1}$) demonstrates PBS and requires increase in ICE power. Movement from ($T_{e1}(\dot{m}_{f1}),\omega_{e1}$) to ($T_{e3}(\dot{m}_{f3}),\omega_{e3}$) demonstrates VSC and requires no increase in ICE power.

4.3.2 Variable Speed Control

VSC realises an independent operating speed for the ICE with respect to the drivetrain. This form of control restricts the ICE to the optimal operating line as defined in [91]; also known as best fuel efficiency line [98]. There are a number of ways to achieve VSC of the ICE in a PHEV and an HEV [11, 34, 76, 93, 100, 105]. The CVT is at the centre of the VSC for parallel and power-split connected PHEVs and HEVs, such devices allow the power source to operate at infinite speed ratios relative to the drivetrain. The total number of power sources integrated on a topology determines the type of CVT employed. The PGS featured in the Toyota Prius allows for the connection of three power sources to the drivetrain, using two M/Gs to control the operation of the ICE [5, 100]. This coupling of two M/Gs in a drivetrain realizes an electric variable transmission [34, 93]. This introduces the option of transferring energy using the mechanical or electrical energy paths in the drivetrain. Having the option of mechanical or electrical energy paths to meet a requested load increases flexibility in control and improves the potential for fuel consumption reduction. The conversion of energy from mechanical to electrical and to mechanical again by using an electric variable transmission in PHEV and HEV does, however, have increased losses similar to the series topology referred to in Section 2.3.1 [105].

Figure 4.2 also provides an example of VSC. The optimal operating line identifies the maximum efficiency the ICE will operate at for a given power request. Each point on the power lines (e.g. P_{e1}) that intercepts the optimal operating line identifies the best efficiency for satisfying that power with the ICE. Consider the torque requested from the drivetrain at an ICE speed of ω_{e1} to be T_{e1}, thereby expecting to produce the power P_{e1} at the output shaft of the ICE. Using VSC the speed of the ICE is varied to ω_{e3} and with an unchanged power requested the torque (T_{e3}) at the new ICE speed is calculated and satisfied by varying the fuel rate ($\dot{m}_{f1}$ to $\dot{m}_{f3}$).

The difference between VSC and the PBS in terms of energy management is that for VSC there is no need to increase the power generated by the ICE. Using VSC all energy generated by the ICE will be utilized to satisfy the present load requirements. The PBS on the other hand leads to charging or discharging the ESS. The decision to charge or discharge the ESS during energy management remains one of the most challenging control problems for fuel consumption reduction in PHEV and HEV.

4.3.3 Combined PBS and VSC

Through the combination of the PBS and VSC the potential for increased ICE efficiency of operation using the proposed method is realized. Referring to Figure 4.3 as an example, each ICE efficiency map has a maximum efficiency point ($\eta_{e,max}$) for the ICE operation relative to a specific brake torque ($T_{\eta e,max}$) and speed ($\omega_{\eta e,max}$). The maximum efficiency point is the most desirable operating point of the ICE, such that the ratio of mechanical energy output from the ICE with respect to the fuel energy consumed is maximised. Using PBS and VSC a controller is able to select between two methods for relocating an otherwise low ICE operating efficiency point to a higher efficiency point. This increases the flexibility in energy management of PHEVs and HEVs. In Figure 4.3 the previously defined high efficiency region corresponding to a specific efficiency contour (i.e. 32% in Figure 4.2) is used. It then follows that any operation of the ICE should satisfy the inequality of equation 4.7, with the requested load being satisfied by the ICE alone:

$$T_e^* = \frac{T_L^*}{i_g} \tag{4.5}$$

$$\omega_e = i_g \omega_L \tag{4.6}$$

$$\eta\left(T_e^*, \omega_e\right) \geq \eta_{e,low} \tag{4.7}$$

The efficiency (η_e) of a requested brake torque (T_e^*) and measured drivetrain speed (ω_e) is estimated using the performance maps (similar to that shown in Figure 4.3) allowing the

controller to make a calculated decision for optimal ICE operation. By defining the inequality of equation 4.7 the balance between fuel consumption and efficiency of operation is explored; $\eta_{e,low}$ is varied in simulation to determine the optimal high efficiency region for each scenario. A scenario varies with vehicle topology and road conditions, which can thus be integrated with trip based information for improved optimisation [127].

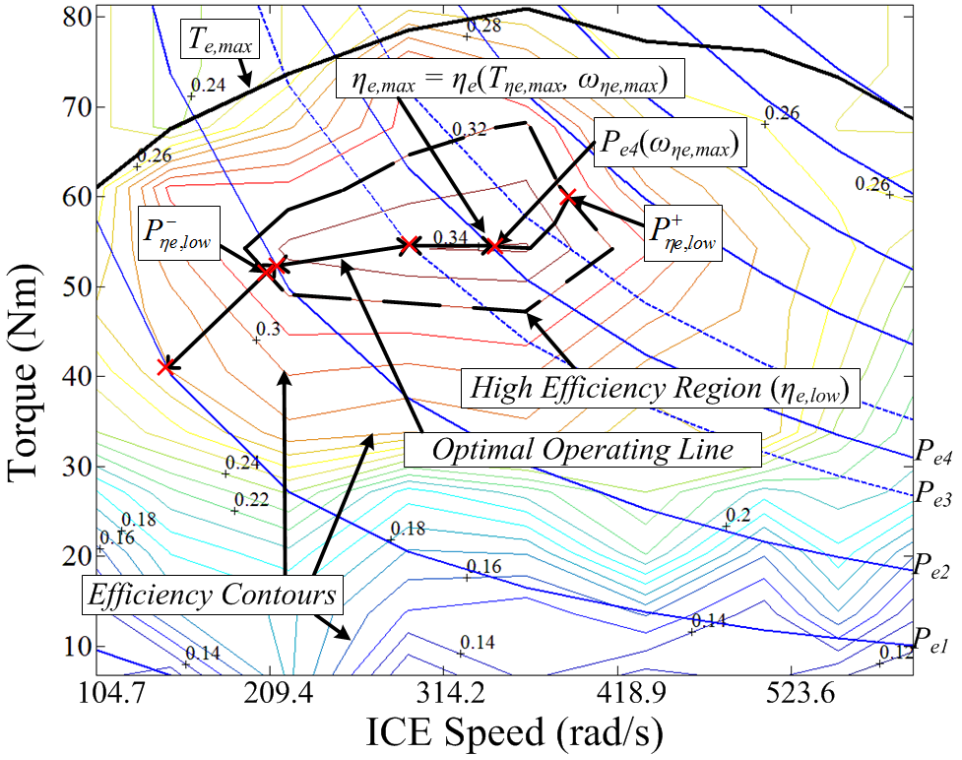

Figure 4.3 - Example ICE efficiency map illustrating combined PBS and VSC for high efficiency control of the ICE.

P_{e1} to P_{e4} identified on the bottom right of Figure 4.3, represent arbitrary power magnitude lines. If a power magnitude of P_{e1}, P_{e2}, P_{e3} or P_{e4} is requested from the ICE, theoretically the controller can choose to satisfy this requested power anywhere along the respective power line. The goal, however, is to maximise the ICE efficiency of operation using PBS and VSC. In the case shown in Figure 4.3 it is evident that a requested power magnitude equal to P_{e1} is undesirable since all operating torques and speeds along the P_{e1} power line are outside the high efficiency region even at its maximum efficiency (using VSC only). To maintain the desired efficiency of operation P_{e1} must be relocated to the high efficinecy region using PBS and VSC (e.g. P_{e2}). On the other hand if a power equal to P_{e4} is requested the controller relocates the requested operating point from anywhere on the P_{e4} constant power line using VSC to achieve the maximum efficiency. For example the optimal operating speed of the ICE for a power request of P_{e4} is $\omega_{\eta e,max}$, where:

$$P_{e4}(\omega_{\eta e,\max}) = P_{\eta e,\max} = T_{\eta e,\max}\omega_{\eta e,\max} \tag{4.8}$$

And

$$\eta_{e,\max} = \eta_e\left(T_{\eta e,\max}, \omega_{\eta e,\max}\right) \tag{4.9}$$

P_{e2} and P_{e3} power magnitudes requested from the ICE, as shown in Figure 4.3, will be satisfied by the ICE given that any operating torque and speed (T_{e2}, ω_{e2} or T_{e3}, ω_{e3}) that lie outside the high efficiency region can be relocated to the optimal operating line within the high efficnecy region using VSC. Finally, consider the points at which the optimal operating line intercepts the high efficiency region at the known upper ($P^{+}_{\eta e,low}$) and lower ($P^{-}_{\eta e,low}$) boundaries. In addition to checking the inequality of equation 4.7, the controller utilizes these power values ($P^{+}_{\eta e,low}$ and $P^{-}_{\eta e,low}$) to request efficient operation from the ICE with the M/G balancing the remaining power requirement. The use of the upper and lower boundaries identified in Figure 4.3 is introduced in Section 4.6 and demonstrated in Section 4.9.1.

4.4 ESS SOC Control

The PBS and VSC defined above determine the methods for maximising ICE efficiency of operation while the ESS SOC control is determined by the EMS employed. Constraints can be placed on the ESS SOC in order to maintain safe operating limits of the ESS, these constraints are due to the characteristics of the ESS employed. Some of the various types of ESS are discussed in Section 2.2.2. The ESS considered for the developed control strategy and therefore utilised on the three test benches is a battery bank. Here two methods for monitoring the SOC of the ESS are presented to identify the means for ESS SOC control relative to the proposed controller. These include SOC swing and a target SOC which as identified introduce varying limitations to the operation of PHEV and HEV.

4.4.1 SOC Swing

The concept of a SOC swing for the ESS provides two levels of control. Primarily the aim is to limit the operating region of the ESS to some high and low SOC such that overcharging and undercharging concerns are taken care of [20, 164]. Following the safe operation of the ESS, the EMS must determine the availability for charging or discharging the ESS and therefore the operation of the ICE. Additionally, SOC swing concerns have the ability to prolong the life of the ESS [94]. Such SOC swing considerations limit ICE operation to predetermined charge and discharge periods during normal driving. Referring to Figure 4.4 for example the SOC swing determines when the ICE must be switched on in order to maintain the ESS SOC between the limits SOC_{low} and SOC_{high} [33, 60].

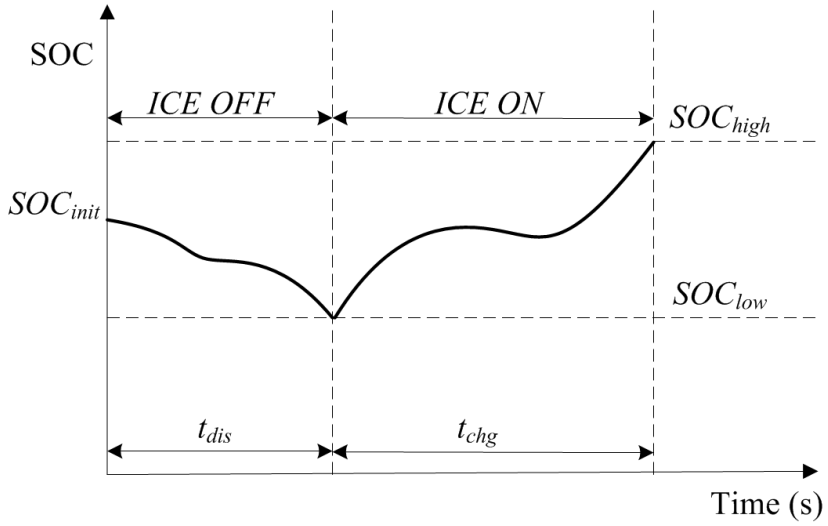

Figure 4.4 – SOC swing example identifying the charge and discharge period.

In the case shown in Figure 4.4 a charge depletion/charge sustenance [33] strategy is assumed to illustrate the SOC limits of the ESS. During charge depletion (t_{dis}) the ICE is switched off and the ESS is supplying the drivetrain load.

$$P_L^* = \eta_d \eta_t \eta_{m/g} \eta_c P_{ess} \tag{4.10}$$

On the other hand during charge sustenance the ICE is switched on to supply the drivetrain load with an increased power requested from the ICE for charging the ESS.

$$P_L^* = \eta_d \eta_t \left(P_e - \eta_{m/g}^{-1} \eta_c^{-1} P_{ess} \right) \tag{4.11}$$

Alternatively, blended charge depletion observes the discharge of the ESS while the ICE is operating in order to minimise fuel consumption for the full drive cycle. Blended charge depletion is typically utilised in a PHEV where the initial SOC (SOC_{init}) is set by charging the vehicle from the grid [7, 33].

4.4.2 SOC Target

A second means to achieve charge depletion/charge sustenance is to employ a target SOC (SOC_{target}) while utilising a cost function to determine operation of the ICE. Using this approach the ESS power requested for charge/discharge is dependent on the following equation, however, charging can only occur while the ICE is supplying power to the load.

$$P_{ess}(t) = \frac{\left(SOC_{target} - SOC(t-1) \right) I_{chg} V_{bus}(t-1)}{\eta_{m/g} \eta_c} \tag{4.12}$$

An EMS controller for example receives the measurement of the SOC and using equation 4.12 calculates the required power to charge/discharge to/from the ESS based on the

maximum charge current (I_{chg}) the ESS can safely handle. The bus voltage (V_{bus}) and M/G efficiency ($\eta_{m/g}$) can also be measured from the vehicle's previous operations. Operation of a PHEV or HEV utilising some target SOC is illustrated in Figure 4.5. ICE on/off periods are determined by the EMS controller such that charging/discharging occurs more frequently than in the case of Figure 4.4, and the SOC oscillates about the target (SOC_{target}). Due to the EMS employed by the vehicle it may be more efficient for the vehicle if no energy is charged or discharged from the ESS as illustrated for one case in Figure 4.5.

In the case of using the SOC_{target} method for charge/discharge of the ESS it may be beneficial to also employ SOC_{low} and SOC_{high} to maintain ESS SOC limits. Limiting the maximum depth of discharge to 10% and maintaining a high SOC has been known to improve the life cycle of ESS [165]. The benefit of employing the target SOC using equation 4.12 results from the increased ESS efficiency of operation due to the minimised charge and discharge currents [11, 89]. Both of these ESS SOC management strategies contribute to the optimal control of PHEV and HEV using the high efficiency control proposed in this Chapter.

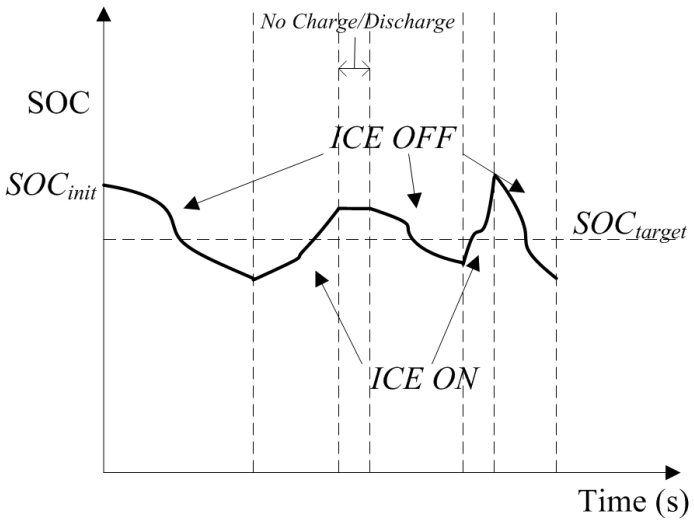

Figure 4.5 - ESS SOC variation over an arbitrary drive cycle with respect to SOC_{target}.

4.5 High Efficiency Control versus Fuel Consumption Minimisation

For an ICE in a PHEV or HEV there are two alternative methods for reducing fuel consumption: high efficiency control [100] and fuel consumption minimisation [10, 26]. Firstly the equivalent consumption minimisation strategy is an example of fuel consumption minimisation [47, 61, 100]. Equivalent consumption minimisation strategy estimates the equivalent fuel and electrical energy required to supply a requested load via the use of a cost function. ICE operating times are restricted and fuel consumption rates are minimised

according to this cost function to ensure overall fuel consumed is reduced in comparison to a defined bench mark [47, 61]. In some cases ICE operating times are dependent on the ESS SOC such that the previously defined SOC_{high} and SOC_{low} limits apply [89]. In addition, predictive methods have shown to improve the performance of the equivalent consumption minimisation strategy or similar strategies by attempting to determine future load requirements and allowing for varying levels of load scheduling [65] of the ICE and ESS [11, 32]. While fuel consumption minimisation strategies have shown a reduction in fuel consumption in comparison to the bench mark the concern is that ICE operation is occurring during inefficient conditions. Instead of operating the ICE in the high efficiency region of Figure 4.3 the control strategy forces the ICE to operate at low power levels in order to conserve fuel [10]. This is observed in Section 3.5.5 with the analysis of the Toyota Prius` ICE efficiency of operation revealing low average efficiency. For this reason high efficiency control of the ICE is potentially more beneficial to fuel consumption reduction through improved energy conversion efficiency.

Using the combined PBS and VSC as described in Section 4.3.3 the requested load power is relocated from low efficiency ICE operating regions to the high efficiency region. An example of this high efficiency region is illustrated in Figure 4.3. This relocation of low efficiency of operation of the ICE attempts to maximise the fuel utilisation while remaining within the operating limitations of the ESS. The constraints placed on the ICE ensure that the load is met efficiently while the ESS balances the load: absorbing or supplying the difference. Such control strategies have concern for consuming more fuel than is required for a given drive period since there is uncertainty in future load requirements [4, 5]. For example if the ICE charges the ESS during the drive period to above the initial SOC and this energy is not utilised throughout the drive period then the energy is considered wasted, especially in PHEV [10, 33]. The challenge for high efficiency control of the ICE is therefore balancing fuel consumption with efficient operation of the ICE. For the proposed controller this is achieved by identifying the optimal high efficiency region relative to the combined PBS and VSC of Section 4.3.3.

4.6 Constraints for High Efficiency Controller

In order to determine the optimal balance between the ICE and ESS in terms of energy consumption, the proposed controller relies on a set of operating constraints. The combination of PBS and VSC with the ESS SOC management identified in Sections 4.3.3 and 4.4 optimise the power level of the ICE and ESS, however, additional information is required to determine optimal charge and discharge times. In effect the combination of equations outlined in Sections 4.3.3 and 4.4 are the cost functions representing fuel and

electric energy of the HEV or PHEV. The purpose of the constraints defined here is to ensure undesirable operating conditions are mitigated.

Control decisions need to include load power requests that lie outside the high efficiency region of the ICE. Due to the inequality of equation 4.7 in Section 4.3.3 the ICE will operate for load requests that fall within the high efficiency region which also includes a component of charge or discharge power from the ESS relative to equations 4.11 and 4.12. The issue in this case is how the controller should respond if the requested power is outside the high efficiency region. Table 4.1 identifies the control considerations for input signals *SOC*, T_e^*, ω_e^* and P_L^* as presented in Figure 4.1. Each inequality of Table 4.1 is for positive load torque (T_L^*) requested. The variables $P_{\eta e,low}^+$ and $P_{\eta e,low}^-$ are defined in Figure 4.3. In the event that load torque is negative (i.e. deceleration) the ICE will shut down, allowing the M/G to absorb power and resulting with deceleration of the vehicle. In the event that requested deceleration is greater than the power rating of the M/G the mechanical brakes will absorb the excess requirement. ICE on/off is the same as defined for the original controllers in Section 3.7.1 with ICE starting energy consumption being due to inertial resistance. The use of the target SOC (SOC_{target}) identifies the median for which the ESS is aiming to achieve (i.e. rules 1 to 8). The SOC high (SOC_{high}) and low (SOC_{low}) limits ensure that the ESS SOC never overcharges or over discharges the ESS (i.e. rules 9 to 16). Equation 4.1 defines the power balance between the load (P_L^*), ICE (P_e) and M/G ($P_{m/g}$) which is the basis for the rules of Table 4.1.

During acceleration of the vehicle, requested ICE brake torque (T_e^*) and speed (ω_e^*) are determined from the requested load power P_L^* and measured load speed (ω_L) using equations 4.2 and 4.3. If load speed is zero then ICE idle speed (ω_{idle}) is utilized. With respect to each input signal of Table 4.1, the columns identify an inequality for comparison by the controller. For each output of requested ICE (P_e^*) and M/G ($P_{m/g}^*$) power the corresponding inequalities on each row must hold true. The requested output power signals determine the brake torque and speed signals of Figure 4.1.

As an example on how to interpret Table 4.1, consider the input conditions $SOC>SOC_{target}$, $\eta_e(T_e^*, \omega_e^*)<\eta_{e,low}$, and $P_L^*>P(\eta_{e,max})$. The input signals must satisfy the identified conditions in order for the output signals to be set as $P_e^* = P_{\eta e,low}^+$ and $P_{m/g}^* = P_L^* - P_{\eta e,low}^+$. The entries of Table 4.1 identified in this example are highlighted in bold type text in the table, and are equivalent to rule 3. A further limitation of the vehicles is the maximum torque the M/Gs ($T_{m/g,max}$) can supply/absorb at any given moment. If the M/G cannot satisfy the requested

load torque (example $T_L^* > T_{m/g,max}$ at $\omega_{m/g}=k_1\omega_e$) then the controller approaches the high efficiency region by setting the M/G to the maximum torque (motoring or generating as needed) and using the ICE to balance the load. This alternative scenario is highlighted in Table 4.1 by the motor limitations column, with the override output signals columns resulting for each respective ICE and M/G command.

The controller also minimizes fuel consumption by ensuring no unnecessary charging occurs. Unnecessary charging occurs during conditions such as $SOC>SOC_{target}$, $\eta_e(T_e^*, \omega_e^*)<\eta_{e,low}$, and $P_L^* < P(\eta_{e,max})$, since there is no need to operate the ICE if the M/G can supply the load. On the other hand if $|P_L^*|>|T_{m/g,max}\,\omega_{m/g}^*|$, then the ICE satisfies the load, due to the requested load power being larger than the M/G can supply (rule 4). The alternative in this case observes the ICE being brought up to the high efficiency region and the M/G charging the ESS by balancing the excess ICE output power generated (rule 8). Such operation may be beneficial to ICE average efficiency, however, it does not mean it is beneficial to overall efficiency. Storing energy in the ESS costs energy and may lead to increased fuel consumption. This consideration for unnecessary charging also applies to the high SOC rules.

Table 4.1 – Additional control rules for optimal ICE and ESS operation.

Input Signals (Left hand side of Inequality)			**Rule No.**	**Output Signals**		**Motor Limitation**	**Override Output Signals**	
SOC	**Operating Efficiency** $\eta_e(T_e^*, \omega_e^*)$	**Load Power** P_L^*		**Initial ICE Power Request** $P_e^* = T_e^* \times \omega_e^*$	**Initial M/G Power Request** $P_{m/g}^* = T_{m/g}^* \times \omega_{m/g}^*$	**Maximum M/G Torque** $\lvert T_{m/g,max} \rvert$	**ICE Power Request if M/G is Limited** P_e^*	**M/G Power Request if M/G is Limited** P_m^*
$>SOC_{target}$	$>\eta_{e,low}$	$>P_e(\eta_{e,max})$	1	P_L^*	0	N/A	N/A	N/A
		$< P_e(\eta_{e,max})$	2	P_L^*	0	N/A	N/A	N/A
	$< \eta_{e,low}$	$>P_e(\eta_{e,max})$	3	$P_{\eta e,low}^+$	$P_{\eta e,low}^+ - P_L^*$	$< \lvert P_{\eta e,low}^+ - P_L^* \rvert / \omega_{m/g}$	$P_L^* - T_{m/g,max}\omega_{m/g}$	$- T_{m/g,max}\omega_{m/g}$
		$< P_e(\eta_{e,max})$	4	0	$-P_L^*$	$< \lvert P_L^* \rvert / \omega_{m/g}$	P_L^*	*0*
$<SOC_{target}$	$> \eta_{e,low}$	$> P_e(\eta_{e,max})$	5	P_L^*	0	N/A	N/A	N/A
		$< P_e(\eta_{e,max})$	6	P_L^*	0	N/A	N/A	N/A
	$< \eta_{e,low}$	$> P_e(\eta_{e,max})$	7	$P_{\eta e,low}^+$	$P_{\eta e,low}^+ - P_L^*$	$< \lvert P_{\eta e,low}^+ - P_L^* \rvert / \omega_{m/g}$	$P_L^* - T_{m/g,max}\omega_{m/g}$	$- T_{m/g,max}\omega_{m/g}$
		$< P_e(\eta_{e,max})$	8	$P_{\eta e,low}^-$	$P_{\eta e,low}^- - P_L^*$	$< \lvert P_{\eta e,low}^- - P_L^* \rvert / \omega_{m/g}$	$P_L^* + T_{m/g,max}\omega_{m/g}$	$T_{m/g,max}\omega_{m/g}$
$<SOC_{low}$	$> \eta_{e,low}$	$> P_e(\eta_{e,max})$	9	P_L^*	0	N/A	N/A	N/A
		$< P_e(\eta_{e,max})$	10	P_L^*	0	N/A	N/A	N/A
	$< \eta_{e,low}$	$> P_e(\eta_{e,max})$	11	P_L^*	0	N/A	N/A	N/A
		$< P_e(\eta_{e,max})$	12	$P_{\eta e,low}^-$	$P_{\eta e,low}^- - P_L^*$	$< \lvert P_{\eta e,low}^- - P_L^* \rvert / \omega_{m/g}$	$P_L^* + T_{m/g,max}\omega_{m/g}$	$T_{m/g,max}\omega_{m/g}$
$>SOC_{high}$	$> \eta_{e,low}$	$> P_e(\eta_{e,max})$	13	P_L^*	0	N/A	N/A	N/A
		$< P_e(\eta_{e,max})$	14	P_L^*	0	N/A	N/A	N/A
	$< \eta_{e,low}$	$> P_e(\eta_{e,max})$	15	$P_{\eta e,low}^+$	$P_{\eta e,low}^+ - P_L^*$	$< \lvert P_{\eta e,low}^+ - P_L^* \rvert / \omega_{m/g}$	$P_L^* - T_{m/g,max}\omega_{m/g}$	$-T_{m/g,max}\omega_{m/g}$
		$< P_e(\eta_{e,max})$	16	0	P_L^*	$< \lvert P_L^* \rvert / \omega_{m/g}$	P_L^*	0

The controller accounts for the losses in the electrical network by the predetermined $\eta_{e,low}$. The combination of restricting charge periods of the ESS and the selection of the optimal $\eta_{e,low}$ for each vehicle leads to minimized fuel consumption over each drive period. Minimized fuel consumption results from the optimal $\eta_{e,low}$ which corresponds to reduced losses experienced in the whole system. The selection of $\eta_{e,low}$ in combination with equation 4.12 realises minimal losses in the electrical network.

4.7 Calibration of the High Efficiency Region

The aim for the controller defined in this Chapter is to operate the ICE within some high efficiency region in order to conserve fuel. Operating the ICE within a high efficiency region leads to increased average power output. If the average requested load power is less than the average power generated by the ICE the ESS will absorb the difference. If the ESS SOC is already above SOC_{target} charging is unnecessary, therefore any fuel consumed during such conditions is potentially wasted [8]. Optimal $\eta_{e,low}$ is determined in simulation by comparison of minimising fuel consumption while ensuring that the ESS SOC is maintained. By starting with $\eta_{e,low}$ equal to a fraction of the maximum ICE efficiency ($\eta_{e,max}$) and working towards this maximum ICE efficiency point (Figure 4.3) the relationship between ESS final SOC and fuel consumption identified in Figure 4.6 will result. This characteristic is observed because of the restrictions placed on the ICE [10].

Referring to Figure 4.6 as an example of calibrating the high efficiency controller, start with $\eta_{e,low} = 0.6 \times \eta_{e,max}$ and approach $\eta_{e,max}$ in increments of $\Delta\eta_{e,max} = 0.05$. It was noticed that as $\eta_{e,low}$ approaches $\eta_{e,max}$ the fuel consumption and final ESS SOC increase. As mentioned previously this demonstrates the increased ICE output energy being stored in the ESS. Note however that there is a point where the fuel consumption is a minimum. This also coincides with a lower ESS final SOC such that the controller is forcing the powertrain to rely more heavily on the ESS as opposed to the ICE. In this case there is some optimal for which the final ESS SOC is similar to the initial ESS SOC and the fuel consumption is a minimum. The aim is determining the $\eta_{e,low}$ value that achieves this optimal.

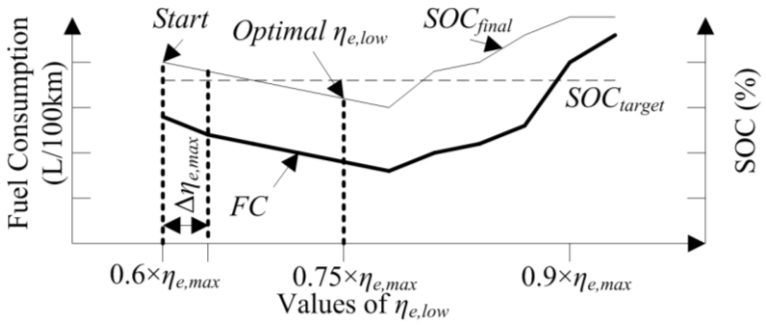

Figure 4.6 - Selection of the optimal $\eta_{e,low}$ value based on the average fuel consumption and final ESS SOC.

In Figure 4.6 an arbitrary optimal $\eta_{e,low}$ is identified such that the final ESS SOC is just below the target (or initial SOC) and the fuel consumption is close to the minimum. In the case of the three existing vehicles this method was utilised to determine the optimal $\eta_{e,low}$ value on the UDDS for reduced fuel consumption and maintaining the final ESS SOC. Each vehicle is then tested at the selected $\eta_{e,low}$ value on the HWFET and the NEDC. The results are presented in Section 4.9 in comparison to the previously developed models of Chapter 3. Firstly a method for determining the $\eta_{e,low}$ value for control of ICE in PHEV and HEV is outlined.

4.8 Algorithm for Implementing $\eta_{e,low}$

In order to define the high efficiency region in MATLAB/Simulink an algorithm was used to read and extrapolate the ICE fuel consumption rate maps present in the ADVISOR software. The notation utilised for equations is relative to the MATLAB code defined in an M-file, where appropriate '//' is used for annotations to further explain each line. Algorithm 4.1 is added to Algorithm 3.1, with all variables and loops defined at the appropriate locations based on the existing code of Algorithm 3.1.

Algorithm 4.1: Determining $\eta_{e,low}$ (Lines numbers refer to Algorithm 3.1)

1: define $\eta_{e,low}$

…

11:

12: define $P^{+}_{\eta e,low}$ = min($\overline{P}_{e,map}$) //define the starting point in the search for the maximum acceptable power for $\eta_{e,low}$. This determines a starting point for calculating $P^{+}_{\eta e,low}$.

13: define $P^{-}_{\eta e,low}$ = max($\overline{P}_{e,map}$) //define the starting point in the search for the minimum acceptable power for $\eta_{e,low}$. This determines a starting point for calculating $P^{-}_{\eta e,low}$.

…

25:

26: if $\eta_{e,\omega e,map\_index\_max} \geq \eta_{e,low}$ then

27: if $\overline{P}_{e,map}$ (P_{e,map_index}) < $P^{-}_{\eta e,low}$ then

28: $P^{-}_{\eta e,low}$ = $\overline{P}_{e,map}$ (P_{e,map_index})

29: $\omega_{e,P\eta e,low}{}^{-}$ = $\overline{\omega}_{e,best}$ (P_{e,map_index})

30: end if

31: if $\overline{P}_{e,map}$ (P_{e,map_index}) > $P^{+}_{\eta e,low}$ then

32: $P^{+}_{\eta e,low}$ = $\overline{P}_{e,map}$ (P_{e,map_index})

33: $\omega_{e,P\eta e,low}{}^{+}$ = $\overline{\omega}_{e,best}$ (P_{e,map_index})

34: end if

35: end if

…

4.9 Results

The performance of the high efficiency controller is examined in this Section by comparison with the original controller developed in Chapter 3. Outcomes of the fuel consumption, drivability, acceleration performance and reasons for these results are discussed. Firstly, the operation of the high efficiency controller is demonstrated on the UDDS with respect to the rules of Table 4.1.

4.9.1 Example Operations of High Efficiency Control

The high efficiency controller operation is defined in Table 4.1, here the operation with respect to rules 1 to 8 are explained with reference to the Toyota Prius 2010 and the UDDS. Rules 9 to 16 are not demonstrated during this example since the SOC does not reach either the high (SOC_{high}) or low (SOC_{low}) limits. The main point for rules 9 to 16, however, is simply to maintain ESS SOC to within some SOC swing as discussed in Section 4.4.1.

Starting from the top left of Figure 4.7, the time period Δt_a is an example of rule 8 from Table 4.1. The SOC is less than the target SOC (SOC_{target}), the requested load power occurs at efficiencies outside the high efficiency region and the power level is low. This means that the proposed controller will request $P^{-}_{\eta e,low}$ from the ICE forcing M/G1 to absorb the difference between load power (P^{*}_{L}) and the requested output power of the ICE ($P^{*}_{e} = P^{-}_{\eta e,low}$). During the indicated time period this is not always the case since there is some deceleration occurring. Δt_b is an example of rules 5 and 6 since the SOC is less than SOC_{target} and power absorbed/supplied from the M/Gs is zero meaning that only the ICE is supplying power ($P^{*}_{e} = P^{*}_{L}$). Δt_c is an example of rule 3, such that SOC is greater than SOC_{target}, and power requested occurs above the high efficiency region leading to the selection of $P^{+}_{\eta e,low}$ with the M/Gs balancing the remaining load and drawing power from the ESS. Due to low power levels requested from the EMS, and SOC being higher than SOC_{target}, the period Δt_d observes the ICE remaining off while M/G2 supplies the requested load; representing rule 4. Δt_e is the opposite of Δt_b such that SOC is above SOC_{target} and the ICE is operated within the high efficiency region. Finally Δt_f identifies the override scenario of rule 7, this is a switch between the motor limitation override and the defined output signals of Table 4.1. Initially SOC is below SOC_{target} and a high load power requested from the EMS forces M/G2 to supply power at $T_{m/g,max}$ with the ICE balancing the remaining load. Once the vehicle begins to pick up speed, the ICE is able to operate within the high efficiency region due to the reduction in requested load power. The ICE output power is set at $P^{+}_{\eta e,low}$ with the M/Gs

balancing the remaining load. The main point to note is that the proposed controller is achieving PBS and VSC with reference to the defined high efficiency region.

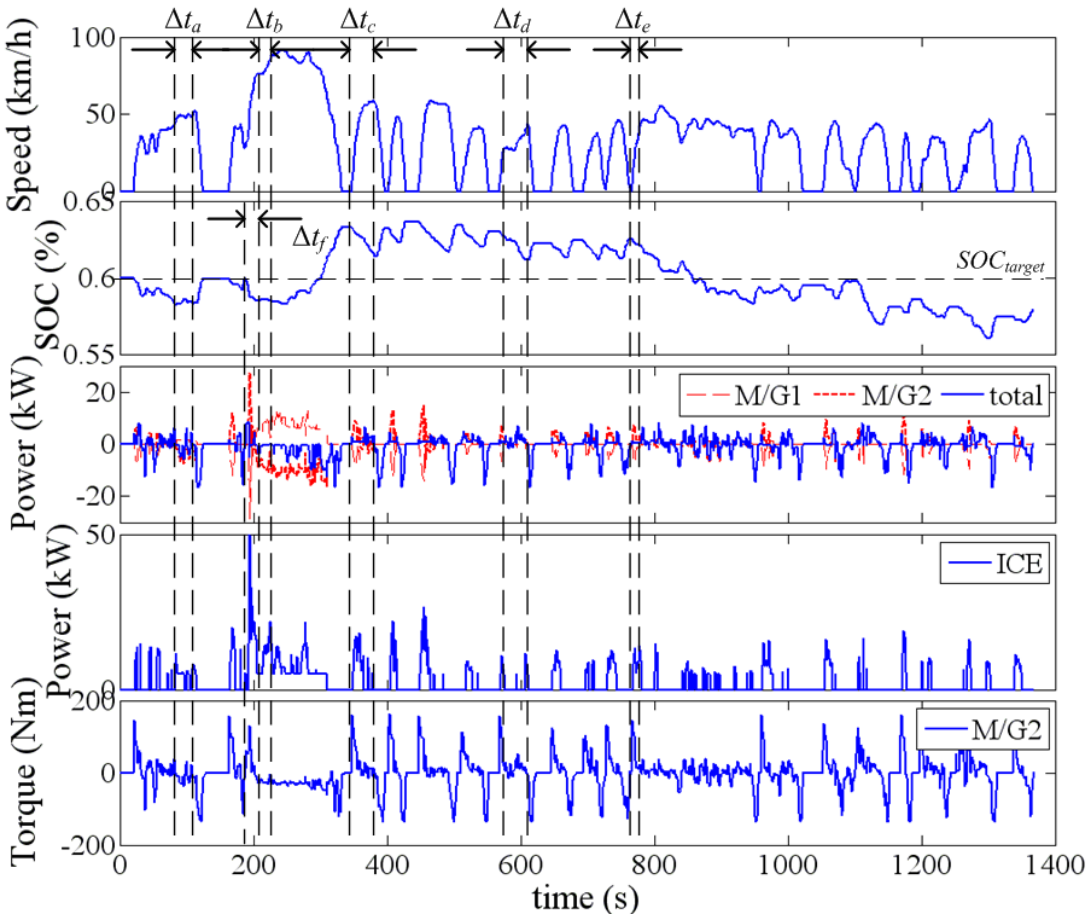

Figure 4.7 – Example operation of the high efficiency controller on the Toyota Prius 2010 for the UDDS drive cycle. From top to bottom: vehicle speed (km/h), ESS SOC (%), M/G1, M/G2 and total M/G output power (kW), ICE output power (kW) and M/G2 output torque.

4.9.2 Fuel Consumption and ESS final SOC

The results of employing the high efficiency controller in the three test benches are listed in Table 4.2. The majority of the base control methods outlined in Sections 3.4 and 3.5 are maintained such that the three test benches operate with the same real-world limitations. The difference here is the control strategy used to determine the operation of the ICE and M/Gs. The UDDS and NEDC represent city (urban) driving while the HWFET represents highway (extra urban) driving. In Table 4.2 the high efficiency controller has been given the acronym HEC. Under the heading HEC in Table 4.2 the optimal selected $\eta_{e,low}$ value is given for each test bench. This $\eta_{e,low}$ value has been selected according to the procedure outlined in Section 4.7.

Table 4.2 - High efficiency controller performance comparison.

Drive Cycle	Component Parameter	Toyota Prius 2010		Hyundai Sonata Hybrid 2011		Honda CR-Z 2010	
		Original	HEC ($\eta_{e,low}$ =28)	Original	HEC ($\eta_{e,low}$ =30)	Original	HEC ($\eta_{e,low}$ =32)
UDDS	Avg ICE Eff. (%)	31.14	31.87	28.19	29.62	18.74	22.37
	Avg Mot. Eff. (%)	82.95	83.76	82.91	84.04	83.92	69.85
	ESS Init. SOC (%)	60	60	60	60	70	70
	ESS Final SOC (%)	60.86	57.85	60.45	60.5	75.39	80.03
	ICE Events	56	57	71	63	20	20
	Gear Events	N/A	N/A	146	158	96	202
	Overall Eff. (%)	10.31	10.73	7.95	8.30	8.14	9.34
	Fuel Cons. (L/100km)	3.22	3.05	4.89	4.68	6.06	5.31
	Fuel Cons. Improvement (%)	-	**5.28**	-	**4.29**	-	**12.38**
HWFET	Avg ICE Eff. (%)	29.24	30.53	28.82	29.32	25.31	26.22
	Avg Mot. Eff. (%)	84.97	87.36	85.27	87.19	84.56	47.78
	ESS Init. SOC (%)	65	65	70	70	70	70
	ESS Final SOC (%)	68.26	66.4	73	77.56	70.35	76.18
	ICE Events	5	5	69	67	1	1
	Gear Events	N/A	N/A	12	12	20	7
	Overall Eff. (%)	19.06	19.31	15.93	15.93	18.82	19.29
	Fuel Cons. (L/100km)	3.29	3.17	4.04	4.03	4.41	4.33
	Fuel Cons. Improvement (%)	-	**3.65**	-	**0.2**	-	**1.81**
NEDC	Avg ICE Eff. (%)	30.19	31.73	29.53	29.69	20.40	23.43
	Avg Mot. Eff. (%)	77.25	77.95	82.89	82.26	81.77	72.31
	ESS Init. SOC (%)	60	60	60	60	70	70
	ESS Final SOC (%)	63.56	63.21	72.62	70.61	72.73	79.25
	ICE Events	11	20	74	55	13	13
	Gear Events	N/A	N/A	74	68	40	76
	Overall Eff. (%)	13.69	14.71	10.98	11.47	11.53	13.05
	Fuel Cons. (L/100km)	3.52	3.27	4.82	4.59	5.71	5.08
	Fuel Cons. Improvement (%)	-	**7.10**	-	**4.77**	-	**11.03**
Acceleration Perf.	0-96.4km/h (sec)	10.7	13.4	7.5	10.6	9.5	13.7

The final ESS SOC indicates the true benefit observed by the reported fuel consumption improvement as seen in Table 4.2. With the final ESS SOC being above the initial ESS SOC at the end of driving the reported fuel consumption improvement is as stated. On the other hand if the final ESS SOC is below the initial ESS SOC this means that the controller has forced the vehicle to become more reliant on the stored energy. In such a case it is observed as the relocation of the load from the ICE to the ESS and does not constitute an improvement to the fuel consumption. ESS SOC correction must therefore be performed in order to determine the true fuel consumption improvement [33].

For example the test bench for the Toyota Prius observed the final ESS SOC for the high efficiency controller at 2.15% below the initial SOC over the UDDS with a fuel consumption reduction of 5.28 %. This indicates that the high efficiency controller is consuming less fuel over the UDDS, however, it is transferring some of the load to the ESS. This suggests that the operation may in fact be relocating the load to the more efficient power source rather than actually conserving fuel. SOC correction in the fuel consumption is achieved using the following equation:

$$\Delta FC = \frac{100E_{ess}\left(SOC_{init} - SOC_{final}\right)}{1000\eta_e^{opt}\eta_{m/g}\eta_{chg}Q_{HV}\rho_f d} \tag{4.13}$$

This leads to the addition of ΔFC = 0.10 L/100km at the end of driving to increase the final SOC from 57.85 to 60% in the Toyota Prius. The improvement for the fuel consumption therefore reduces from 5.28% to 2.17% over the considered drive period. For the remaining tests listed in Table 4.2 the final SOC is above the initial SOC and thus there is no cause for concern relative to the ESS SOC. The next consideration is how the high efficiency controller will effect normal driving this is quantified in terms of the drivability and a study presented in [38].

4.9.3 **Drivability**

By comparing the original controller and the high efficiency controller's ICE and gear events and with reference to the study completed in [38] the effect on drivability is discussed. One ICE event is defined as the ICE switching on then off again throughout the driving period, while one gear event is the shifting of the fixed gears up or down. The Toyota Prius having the PGS has smooth gear transitions, thus the gear events are not quantifiable. The effects of the high efficiency controller on drivability in the Toyota Prius are examined for the ICE events only. The total numbers of ICE and gear events are listed in Table 4.2.

Reference [38] indicates that a low number of both ICE and gear events is desirable, however, that for the demonstrated cases there is a range for optimality. For tests completed

on the Federal Test Procedure (FTP) which is an extended version of the UDDS, a variation of 25% in the total number of ICE events realises an increase of 2% in the final average fuel consumption. This variation in fuel consumption is with respect to a test bench utilising a fuel consumption minimisation strategy similar to the Toyota Prius 2010 considered here. Additionally, for the two drive cycles (FTP and NEDC) tested in [38], a variation of up to 75% in the total number of gear events leads to an increase of up to 5% in the fuel consumption.

Relating the results presented in [38] to those presented in this paper, there are three cases in Table 4.2 that may have concerns. Firstly, the Toyota Prius' operation on the NEDC increases the number of ICE events from 11 to 20 with the use of the high efficiency controller. In comparison to the total ICE events per kilometre of the FTP cycle presented in [38] the increase from 11 ICE events over 10.93 km (NEDC) to 20 ICE events is minimal. This equates to less than 3 ICE events per kilometre. The test vehicle utilised in [38] by comparison has up to 5 ICE events per kilometre on the FTP. In addition, from the perspective of time the high efficiency controller has an ICE event every 60 seconds (NEDC ~1200 seconds) in comparison to the test vehicle in [38] having an ICE event every 23 seconds (FTP ~2000 seconds). Alternatively the optimal region for the total number of ICE events that achieves best performance [38] for the NEDC is between 15 and 25 ICE events. Assuming this applies to all ESVs that contain an ESS and an ICE the increase in the total number of ICE events (from 11 to 20) is potentially improving the operation of the vehicle.

The second point for concern comes from the total number of gear events for the Honda CR-Z. As shown in Table 4.2 on the UDDS and NEDC the total number of gear events for the Honda have increased by over 100% which according to the results of [38] may lead to an increased fuel consumption of up to 10%. A 10% increase in the determined fuel consumption for the Honda CR-Z realises 5.84 L/100km and 5.59 L/100km for the UDDS and NEDC drive cycles respectively. In comparison to the original controller this is still an improvement of 3.63% and 2.10% on both of these drive cycles respectively (as compared with 6.06 L/100km and 5.71 L/100km from the original controller). Alternatively, if the increased number of ICE and gear events is a concern for the high efficiency controller, reducing the selected $\eta_{e,low}$ value will lead to a reduction in the total number of events. Note that any change in the $\eta_{e,low}$ value has a quadratic relationship to the final fuel consumption such that varying the $\eta_{e,low}$ value too much will lead to an increase in the fuel consumption. The study completed in [38] highlights the potential impacts for employing the high efficiency controller on the drivability of the three test vehicles. This analysis ultimately suggests that the use of the proposed controller is beneficial to the drivability of the three

existing vehicles and at the very least (in terms of drivability) performs similarly to the original controller.

4.9.4 Acceleration Performance

Restricting the ICE operation to the high efficiency region reduces the maximum output torque the vehicle is able to achieve at any given time. There are two causes of this limitation. Firstly the high efficiency region may restrict the maximum torque from the ICE at any speed to the high efficiency region which can be below the maximum rated brake torque of the ICE. This means that in order to conserve fuel the output power will not exceed $P^{+}_{\eta e,low}$ such that the output torque at the wheels is lower than the rated torque (and therefore rated power) of the vehicle. On the other hand the optimal speed selected for the requested power may be limited by the ICEs maximum torque. For example the optimal speed at some low requested power (P_{e1}) is shown in Figure 4.8, if at the next time step a power level of P_{e3} is requested from the ICE the scenario identified by Figure 4.8 will result.

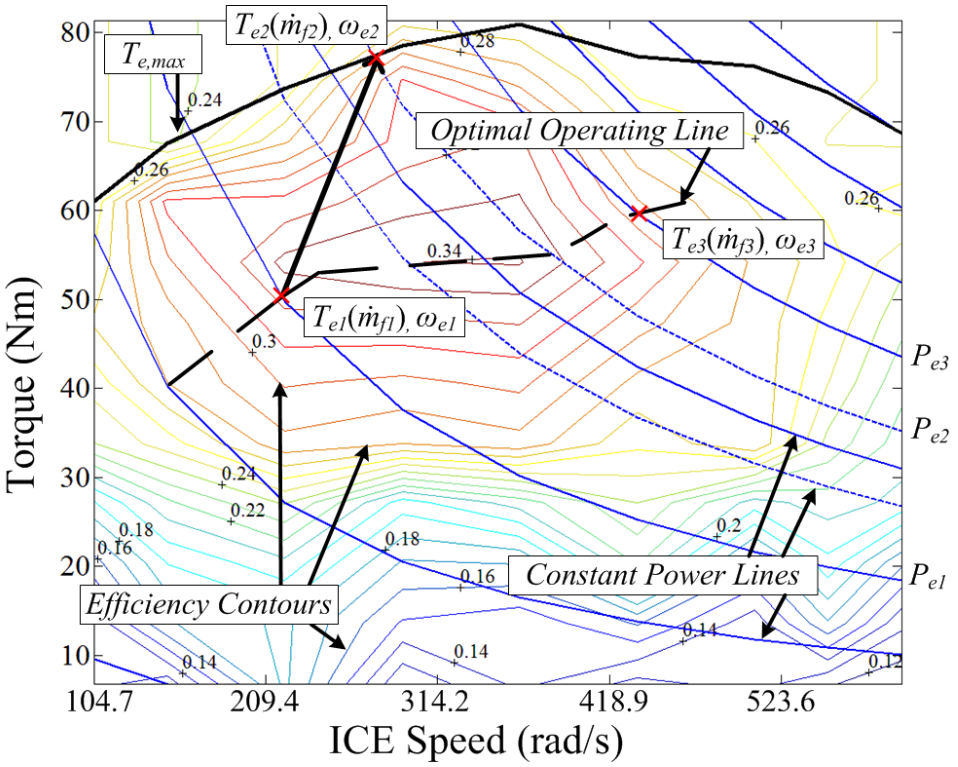

Figure 4.8 - Delay in VSC due to mechanical inertia of PGS

The EMS controller will observe the requested power and calculate the desired speed at ω_{e3} according to the optimal operating line. The transmission control unit (Figure 4.1) will receive the requested speed and begin to vary the ICE output speed to the desired speed. The issue, however, is that there is a delay in achieving the desired speed at P_{e3} using the transmission control unit. As the transmission approaches the desired speed the ICE begins

to develop the requested torque to meet the desired power at the current speed (ω_{e2}). A torque of T_{e2} would result since the ICE is aiming to supply the maximum power at the current speed ω_{e2} (or maximum torque at the current speed). The developed power is therefore P_{e2} which is less than the requested output power of P_{e3}. This means that the torque available at the wheels is temporarily limited until the transmission control unit can achieve the desired speed (ω_{e3}) and thus the acceleration performance of the vehicle is reduced according to this delay.

This delay or restricted output torque is represented in the comparison of the original controller with the high efficiency controller acceleration times in Table 4.2. The high efficiency controller adds up to 4.2 seconds to the acceleration performance of the vehicles in accelerating from 0 to 96.4 km/h (60 mph). For this reason the authors envisage that the high efficiency controller might be offered as an alternative to a 'normal' mode such as 'economy'. Currently 'economy' modes do not affect the performance of a vehicle in the manner discussed in this Chapter, instead they increase response times of the vehicle and reduce the accessory loads of the whole system [166]. The consumer would then have the choice of which mode of operation best suits their needs.

4.9.5 Evidence for High Efficiency Control leading to Fuel Consumption Reduction

Table 4.2 highlights that by using the high efficiency controller the fuel consumption is reduced by up to 12.38%. There is, however, limited improvement during the tested highway driving scenario (between 0.2 and 3.65%). This low improvement is due to the already large loads placed on the ICE and therefore limited availability of a more efficient operating point. In addition, the Honda and Hyundai topologies have limited capacity for PBS (Section 4.3.1) due to the small motor sizes in comparison to the size of the ICE. This ratio of M/G to ICE power rating is referred to as the HF [106], as discussed in Section 2.6.2 and determines a limited overall benefit to fuel consumption. The ICE operates within the high efficiency region most of the time and torques requested from driving in the highway scenario are too large to be redirected to the electrical network. The high efficiency controller is therefore more suitable for city driving scenarios as presented in this Chapter.

On the topic of HF of HEVs there are some interesting points to note about the performance of the three existing vehicles. Chan et al [4] refers to the HF in a different light considering the micro, mild and full hybrid systems of HEV. In particular, it is noted in [4] that an increasing HF leads to increased fuel savings as discussed in Section 2.6.2. For the three existing vehicles discussed in this Chapter, the Toyota Prius is a full hybrid and the Hyundai and Honda are both mild hybrids. Considering the low power rating of the Honda's M/G it is

almost categorised as a micro hybrid. With respect to the defined HF this may be part of the reason the Toyota Prius is capable of achieving such low fuel consumption. This is in addition to the Toyota Prius being power-split compared with the parallel connected Hyundai and Honda.

Figure 4.10 to Figure 4.14 outline the operation of the ICE of each of the test benches with and without the high efficiency controller. The comparison is made for the vehicles operating on the UDDS. It is clear from the visual comparison of the two images for the three cases that the ICE operation is being restricted to higher torque and/or speeds in order to maximise the fuel utilisation. This is achieved in the Toyota Prius 2010 through the use of the combined PBS and VSC as described in Section 4.3.3 For the Hyundai and Honda test vehicles, however, VSC is limited due to the fixed gear transmissions [10]. Instead the transmission controller aims to maintain higher gears (lower gear ratios) in order to maximise the torque output from the ICE. This is observed by the increase in the operating torque in Figure 4.12 and Figure 4.14. In addition, because of the low power rating of the Honda's M/G the ICE must remain on for the full duration of driving. This means that while the high efficiency controller aims to increase the ICE output torque, operation is limited by the need to satisfy all load requirements using the ICE. Figure 4.14 identifies the requirement for the ICE to supply low power levels in addition to the improved efficiency of operation on the Honda CR-Z 2010 test bench. While there are limitations based on the M/G power ratings in the case of the Hyundai and Honda test benches, it is apparent that the high efficiency controller is capable of improving the fuel consumption on varying vehicle topologies as seen in Table 4.2.

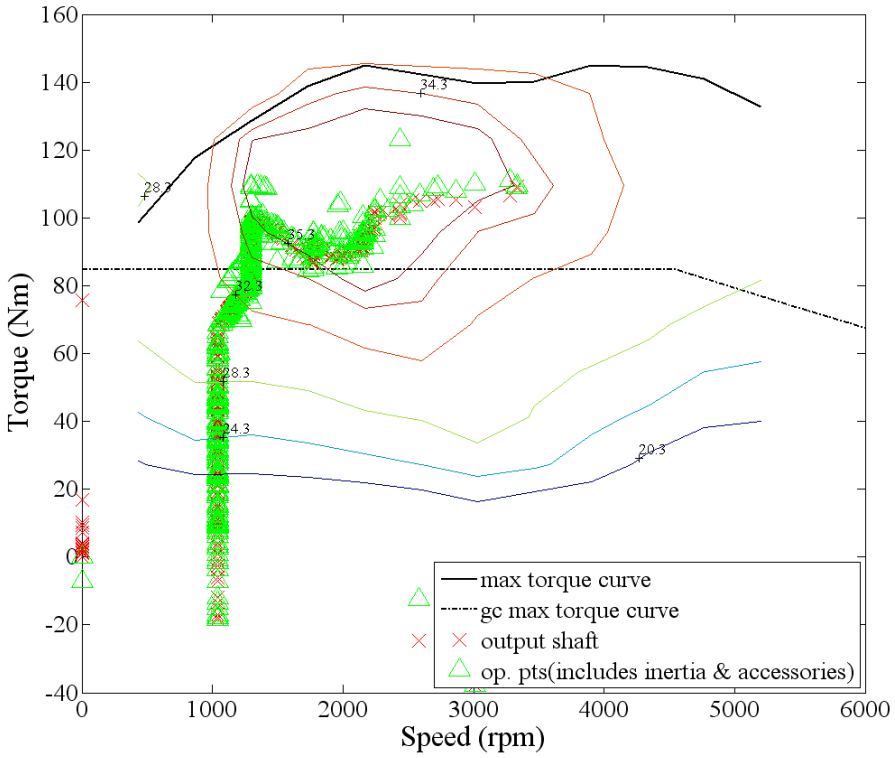

Figure 4.9 - ICE operating points for Toyota Prius 2010 using original controller. Operation is restricted to the optimal operating line.

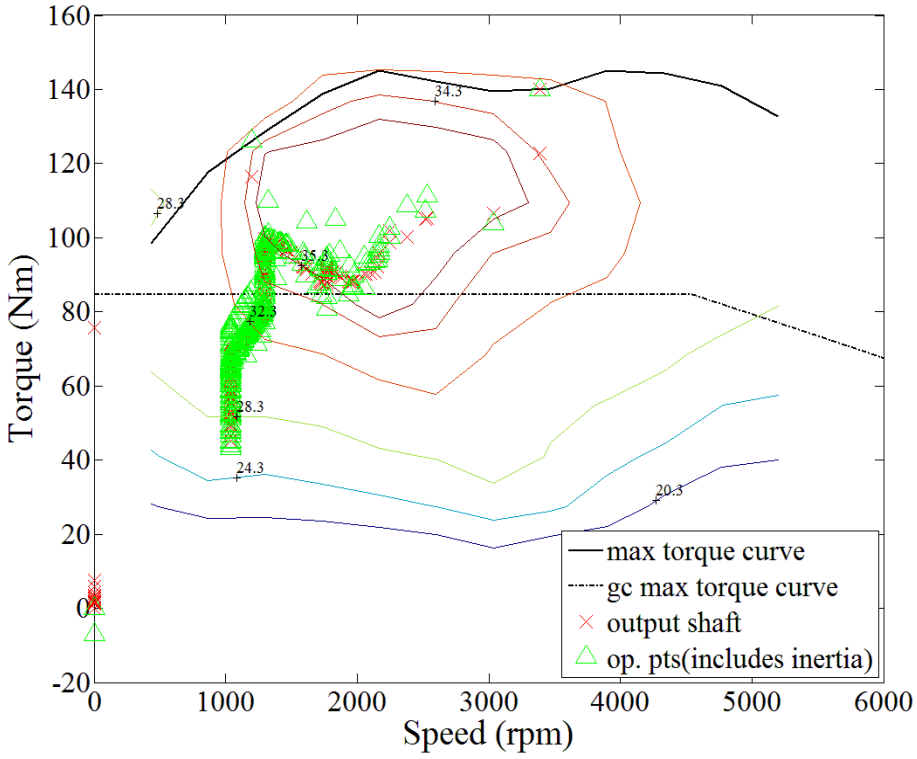

Figure 4.10 - ICE operating points for Toyota Prius 2010 using high efficiency controller. Operation is restricted to the high efficiency region in addition to the optimal operating line.

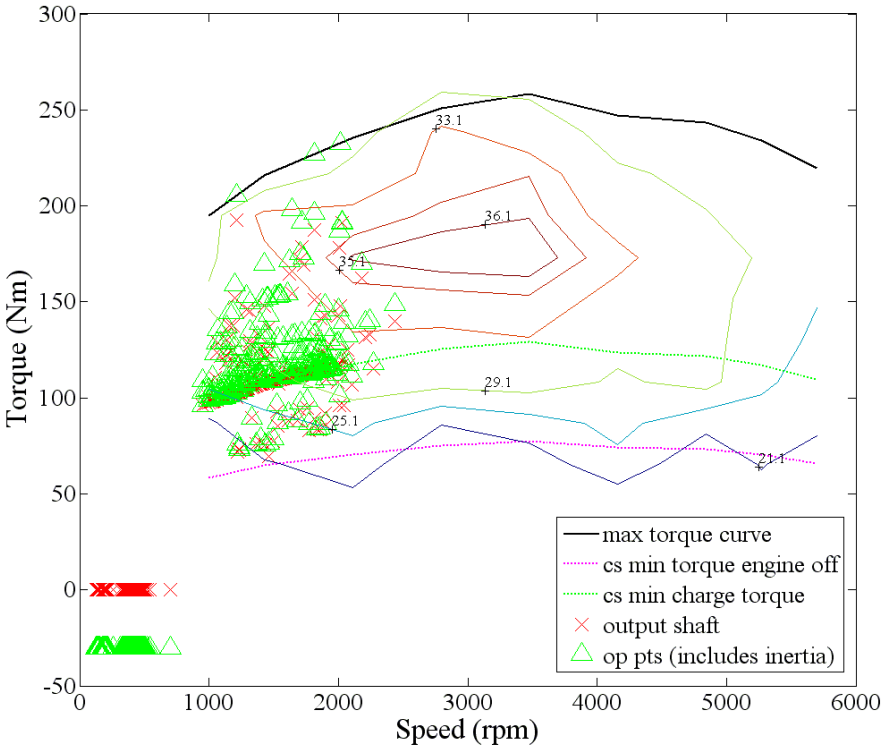

Figure 4.11 - ICE operating points for Hyundai Sonata Hybrid 2011 using original controller. Operation is restricted by a minimum on/off and minimum charge torque.

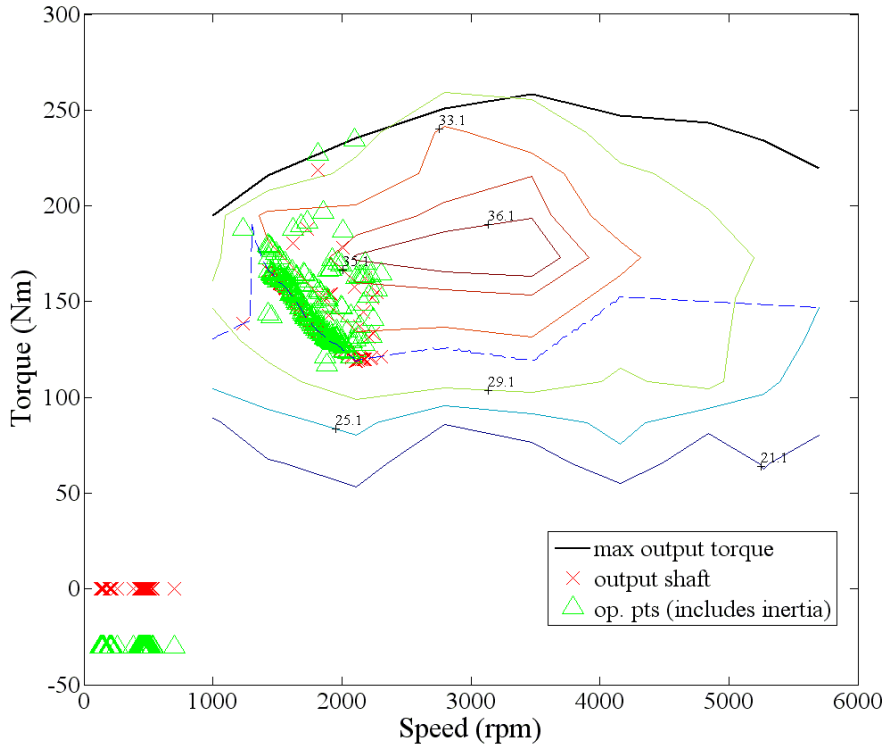

Figure 4.12 - ICE operating points for Hyundai Sonata Hybrid 2011 using high efficiency controller. Operation is restricted by the high efficiency region as indicated by the blue dotted line.

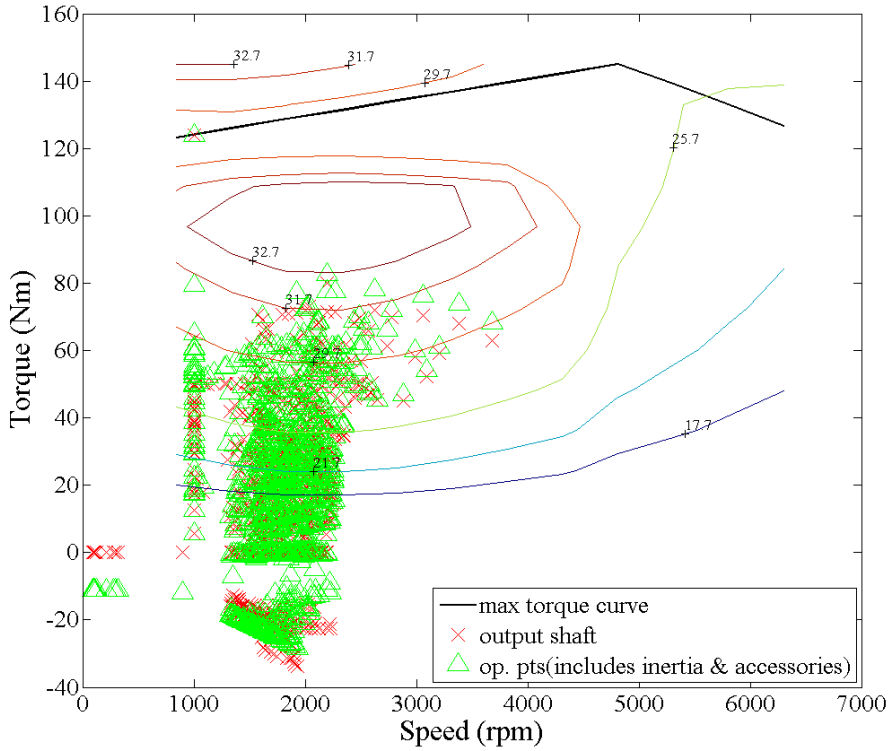

Figure 4.13 - ICE operating points for Honda CR-Z 2010 using original controller. Operation is restricted to maximum and minimum speeds for gear changes.

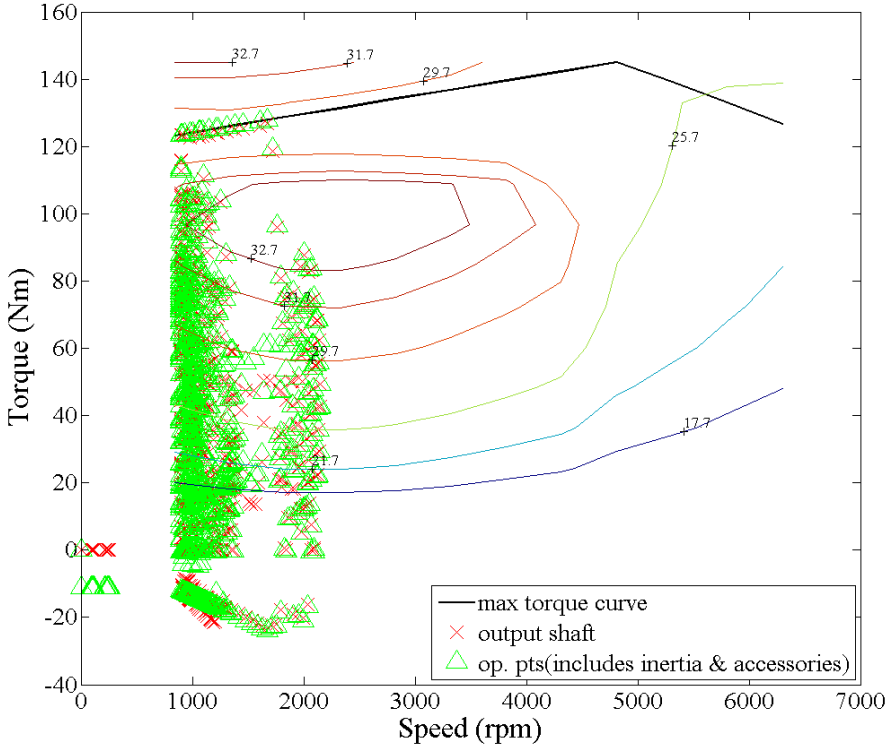

Figure 4.14 - ICE operating points for Honda CR-Z 2010 using high efficiency controller. Operation is restricted to the high efficiency region where possible.

4.9.6 Concerns for High Efficiency Controller

Upon further analysis of the high efficiency controller defined in this Chapter there are areas for potential improvement. Figure 4.15 to Figure 4.17 show the initial SOC (SOC_{init}), final SOC (SOC_{final}) and fuel consumption improvement for varying values of $\eta_{e,low}$ when compared against the original controller using the high efficiency controller. Firstly, Figure 4.15 to Figure 4.17 support the calibration method discussed in Section 4.7 observing that if you start with $\eta_{e,low}$ equal to some low percentage of maximum ICE efficiency ($\eta_{e,max}$) and increase by an incremental amount ($\Delta\eta_{e,low}$) the discussed relationship (Section 4.7) between ESS final SOC and ICE average fuel consumption results. For example consider the case with $\eta_{e,low}$ = 0.29, final SOC of the ESS when driving on the UDDS is too low to be considered an improvement to the average fuel consumption at SOC_{final} = 55.41%. This is instead relying more heavily on the stored energy. Therefore $\eta_{e,low}$ = 0.28 is selected since there is a greater percentage of energy stored in the ESS for the fuel consumption reductions that have occurred. Table 4.2 identifies the SOC_{init} for the HWFET in the original controller is 65% which is due to the measured data of the Toyota Prius having an initial SOC of 65%. SOC_{target} for the HWFET is remaining at 60% for the energy management controller meaning that if the final SOC is above SOC_{target} there is no cause for concern. In effect if SOC_{final} is greater than SOC_{target} the EMS has consumed more fuel energy than is required. This then leads to the selection of $\eta_{e,low}$ for varying drive profiles.

Without the correct calibration of the high efficiency controller the EMS will consume more fuel than the original controller. Figure 4.15 and Figure 4.17 identify that the UDDS and NEDC have similar optimal values for the high efficiency region at $\eta_{e,low}$ = 0.28 while Figure 4.16 indicates that the optimal for the HWFET is $\eta_{e,low}$ = 0.2. Note that the fuel consumption improvement at the selected $\eta_{e,low}$ = 0.28 on the HWFET is half of the fuel consumption improvement at $\eta_{e,low}$ = 0.2. Section 2.2.4 and 3.5 outline that the ICE supplies the average load power requirement of the drive cycle and the ESS provides the transient load requirements. Figure 4.15 to Figure 4.17 indicate that the final SOC increases with increasing $\eta_{e,low}$ value. The ESS in the case of $\eta_{e,low} \geq 0.3$ absorbs the higher average power developed by the ICE leading to an increased final SOC. This means that the reason for increased fuel consumption on the HWFET with a higher $\eta_{e,low}$ value is due to the increased average power demand from the ICE and therefore less opportunity to utilise the ESS stored energy. This is also discussed in Sections 4.5 and 4.7.

According to equation 3.1 in Section 3.4 the component contributing to average power demand in drive cycles is the vehicle velocity. Therefore the proposed high efficiency controller was modified to account for the varying average vehicle velocity by having two

alternative $\eta_{e,low}$ values. Including the same rules as identified in Table 4.1 the following inequality is also utilised to determine the value of $\eta_{e,low}$.

$$\eta_{e,low} = \begin{cases} \eta_{e,low1}, & for\ V > V_2 \\ \eta_{e,low2}, & for\ V \le V_2 \end{cases} \tag{4.14}$$

Where $\eta_{e,low1}$ and $\eta_{e,low2}$ are selected as 0.2 and 0.28 respectively according to the results of Figure 4.15, Figure 4.16 and Figure 4.17, and V_2 is selected at 12 m/s using trial and error in simulation for the best results. Table 4.3 indicates that by adding the consideration for vehicle velocity to the high efficiency controller (HEC), improvement occurs to the HWFET with minimal side effects to the city driving scenarios. HEC-V in Table 4.3 identifies the results for the high efficiency controller including the control of equation 4.14. The only noticeable side effect is a small increase in the consumption of ESS energy on the UDDS and NEDC. This analysis lead to the understanding that the load required from the vehicle can inform the controller of the optimal high efficiency region to select. For example in the above case the vehicle velocity is used to select the sub-optimal high efficiency region for the UDDS, HWFET and NEDC.

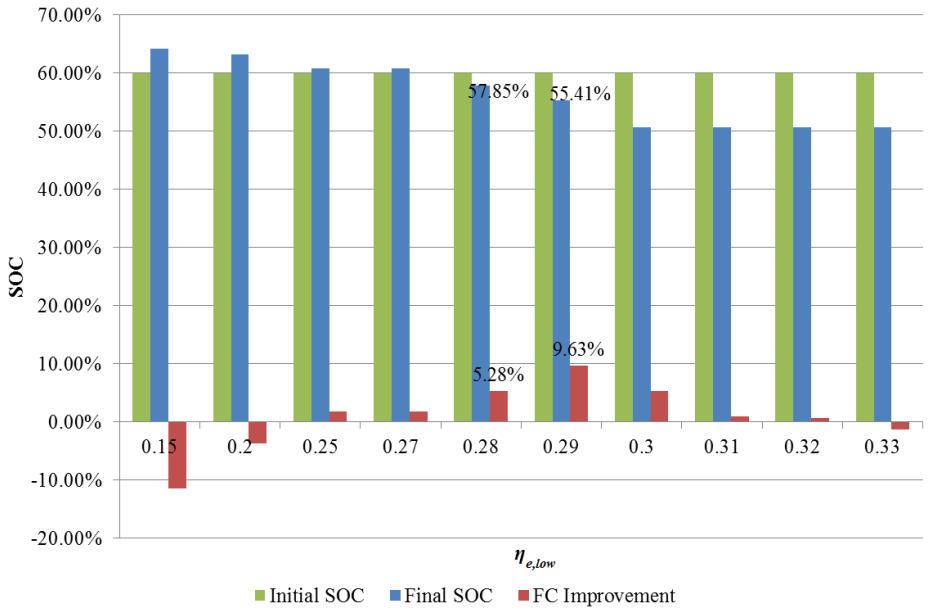

Figure 4.15 - Varying high efficiency region ($\eta_{e,low}$) on the Toyota Prius 2010 over the UDDS drive cycle.

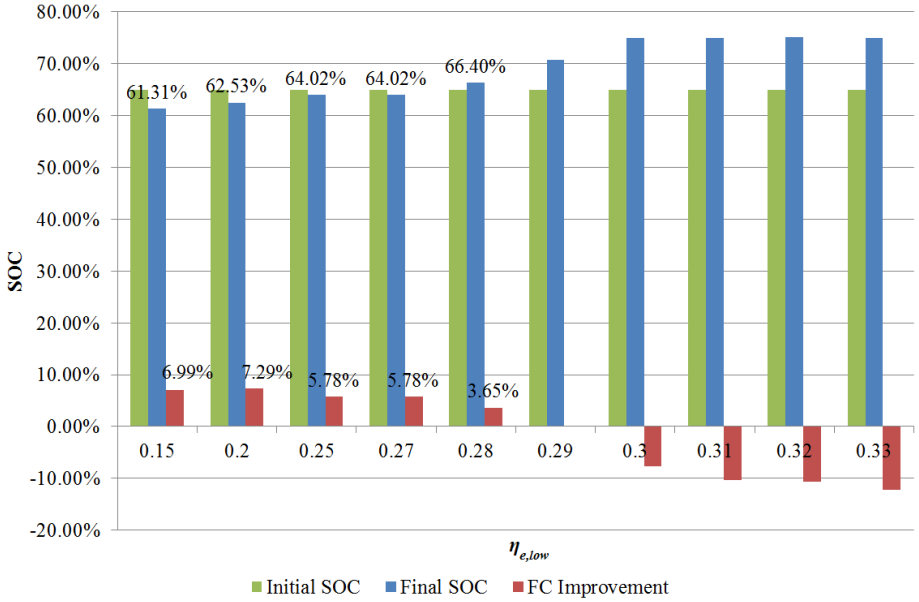

Figure 4.16 - Varying high efficiency region ($\eta_{e,low}$) on the Toyotas Prius 2010 over the HWFET drive cycle.

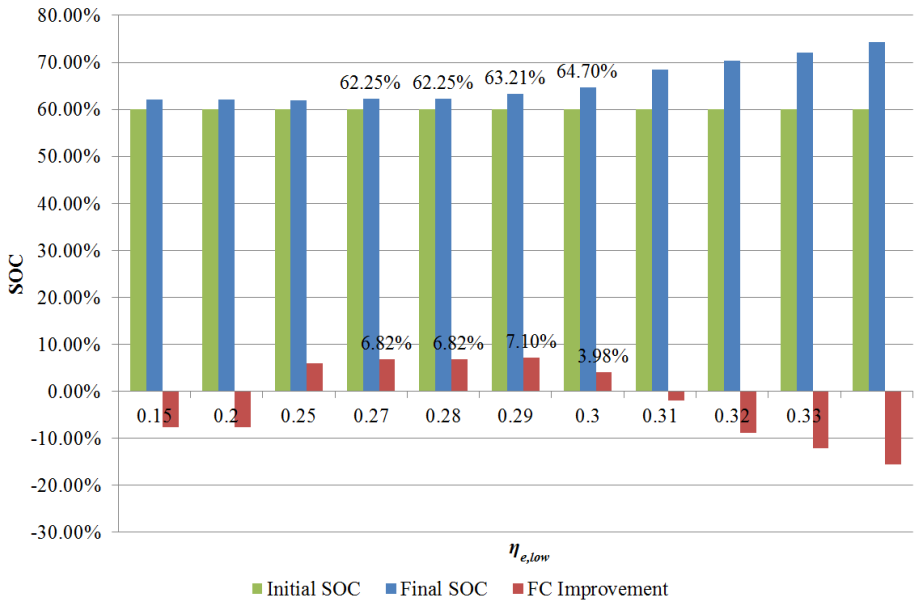

Figure 4.17 - Varying high efficiency region ($\eta_{e,low}$) on Toyota Prius 2010 over the NEDC drive cycle.

Table 4.3 - Comparison of high efficiency controller performance: varying with respect to vehicle velocity.

Drive Cycle	Component Parameter	Toyota Prius 2010		
		Original	HEC	HEC-V
UDDS	Initial SOC (%)	60	60	60
	Final SOC (%)	60.86	57.85	56.89
	Overall Eff. (%)	10.31	10.73	10.67
	Fuel Cons. (L/100km)	3.22	3.05	3.05
	Fuel Cons. Improvement (%)	-	**5.28**	**5.28**
HWFET	Initial SOC (%)	65	65	60
	Final SOC (%)	68.26	66.4	62.08
	Overall Eff. (%)	19.06	19.31	19.97
	Fuel Cons. (L/100km)	3.29	3.17	3.11
	Fuel Cons. Improvement (%)	-	**3.65**	**5.47**
NEDC	Initial SOC (%)	60	60	60
	Final SOC (%)	63.56	63.21	61.62
	Overall Eff. (%)	13.69	14.71	14.61
	Fuel Cons. (L/100km)	3.52	3.27	3.27
	Fuel Cons. Improvement (%)	-	**7.10**	**7.10**

4.10 Summary of High Efficiency Control

Motivation for the high efficiency controller of this Chapter was established in Chapter 3. Initially, the fundamental means for controlling HEVs is defined with the power balance of the ICE and M/Gs. This lead to a discussion for the control signals represented in the selected topologies that ensure the desired operation of ESVs. For the purpose of control, requested and measured signals of ESVs using a block diagram are distinguished, separating steady-state (measured) from input signals (requested). Acknowledging the existing control methods of PBS and VSC a means for achieving high efficiency control is established. Using the ICE performance map a predefined value of $\eta_{e,low}$ constrains operation of the ICE to a specified region, maintaining higher average ICE efficiency. ICE developed power is then balanced with the ESS and drivetrain load, according to the ESS target SOC. This is an important consideration for the reduced fuel consumption using the high efficiency controller, since the constraints placed on the ICE by using the $\eta_{e,low}$ value lead to increased average power. Power developed by the ICE that is not consumed by the drivetrain will be absorbed by the ESS. This may result with unnecessary charging of the ESS and therefore increased fuel consumption.

For improved performance resulting from the operation of the high efficiency controller, a set of rules in addition to those existing on the three test benches are required. These additional control rules ensure that the ICE switches on when required and more importantly determine what to do when the requested power is outside the high efficiency region. Once the desired operation is defined the ICE controller is calibrated according to the final average fuel consumption and ESS final SOC. This calibration results with the selection of the optimal $\eta_{e,low}$ value. High efficient ICE performance is demonstrated on the Toyota Prius over the UDDS, identifying periods of operation subject to the developed control rules. Performance quantities of the high efficiency controller are compared against the original controller as presented for the three test benches of Chapter 3.

The results indicate that the fuel consumption is reduced by up to 12% with maintained ESS target SOC. It was noted that due to the fixed gear transmissions on the Hyundai and Honda test benches that the potential for fuel consumption reductions is limited. Without the ability for VSC of the ICE low efficiency operating conditions cannot be relocated to high efficiency operating conditions very easily. This means that the controller must compromise between increasing ICE output torque and meeting the requested load. As mentioned unnecessary charging of the ESS will lead to increased fuel consumption, negatively impacting performance.

The total number of ICE and gear shift events quantifies the effect on the drivability. Overall, the concerns for drivability are minimal if not beneficial to vehicle operation through use of the high efficiency controller. This consideration is due to the test benches having a similar number of ICE and gear shift events when using either the original or high efficiency controller. A secondary concern for the proposed high efficiency controller is that the acceleration performances of the vehicles are increased. To allow the user the option of a fast acceleration or reduced fuel consumption a solution is to offer the high efficiency controller as an alternative to normal operating mode (i.e. economy mode). Finally, a comparison of the operating points of the three models' ICEs confirms the reasons for fuel consumption reductions using the high efficiency controller. The Toyota Prius in particular demonstrates the potential for the high efficiency controller to increase average ICE efficiency with all operating points occurring within the predefined high efficiency region.

Further investigation of the high efficiency controller's operation having varying $\eta_{e,low}$ values revealed the importance of calibration. This was carried out on the Toyota Prius for the three tested drive cycles. Specifically, the analysis determined that for highway driving it is best to place fewer restrictions on the ICE for improved fuel consumption reductions. This was attributed to the higher average tractive power requested from the powertrain such that the ESS has less opportunity to supply the load. Generally once the Toyota Prius exceeds a minimum vehicle velocity the ICE will remain on as identified in Section 3.5.4. The ESS absorbs any excess power developed by the ICE which is restricted to the previous high efficiency region ($\eta_{e,low}$ = 0.28). The ESS, however, is not capable of utilising this stored energy during the remainder of the drive cycle. This means that fuel is consumed unnecessarily during driving on the HWFET (i.e. highway driving). Modifying the controller to account for a varying high efficiency region based on the vehicle velocity lead to improved fuel consumption on the HWFET with minimal adverse effects on the city drive profiles (UDDS and NEDC). Fuel consumption improvement rose from 3.65% to 5.47% on the HWFET, with fuel consumption on the UDDS and NEDC remaining unchanged. This outcome then encourages the consideration for determining $\eta_{e,low}$ on-the-go, identifying the motivations for the controller featured in Chapter 5.

CHAPTER FIVE

Design of a Predictive Controller for PHEV

5.1 Introduction

Having defined the high efficiency controller in Chapter 4 the potential for fuel consumption reductions is realised in PHEV with power-split and parallel configurations. The use of a predefined high efficiency region to restrict operation of the ICE, however, limits the capability for optimal performance over varying drive scenarios. Here calibration of the high efficiency controller is realised on-the-go through the use of predictive control. In particular, the focus is on predicting the energy requirements of a planned driving route to aid with the selection of the $\eta_{e,low}$ value defined in Chapter 4.

The predictive method identified here is considered a fundamental approach, serving to demonstrate the use of GPS [127, 167, 168] or intelligent transportation system [167] information in the designed EMS controller. The amount of information included in such predictive methods determines the accuracy of the prediction with increasing amounts leading to better accuracy and a high computational requirement [7, 36]. Thereby, increased computational requirements lead to increased costs of the system [36]. With the aim for reducing the computational burden of predictive control, the proposed predictive method uses the expected driving requirements in an attempt to calculate the future tractive energy requirement of a planned driving route. This future energy requirement in combination with the estimated time of arrival (or trip time) autonomously selects the optimal $\eta_{e,low}$.

Following the autonomous selection of the high efficiency region for the ICE, the ESS charge and discharge is determined based on the average tractive power requirement of the planned driving route, the total expected tractive energy of driving and the consumed tractive energy. This approach to ICE and ESS operation is based on the initial consideration of power density and energy density of each respective power source. The ICE is utilised for average power supply having a high energy density and low average efficiency, while the ESS is utilised for transient power supply having high efficiency of operation and low energy density. Results of the proposed approach demonstrate the ability of the controller to maximise the use of stored energy while minimising fuel consumption for the three drive scenarios identified previously (UDDS, HWFET and NEDC).

Since the Toyota Prius 2010 has the best flexibility in control it has been selected for the study presented in this Chapter. It is envisaged that the controller is capable of similar performance on the Hyundai and Honda test benches, however, the fixed gear transmissions of the parallel configurations (Sections 3.3.2 and 3.3.3) limits the application of the autonomous control. For a fair comparison the original and non-predictive controllers are modified to operate as PHEV. This observes the two controllers operating as described in Chapters 3 and 4, and then entering a charge depletion mode closer to the planned destination for increased ESS reliance. Operation as a PHEV assumes that the original and non-predictive controllers are capable of monitoring the estimated time of arrival in order to determine when to enter charge depletion mode. The predictive controller is thus analysed for operation as an HEV and PHEV. Consideration as an HEV reveals the fuel consumption reductions comparison for the three controllers having SOC corrections at the end of driving using the ICE. Alternatively, for SOC correction when using the developed controller in PHEVs electricity is used via the grid connection.

Operation as a HEV results with improved fuel consumption of up to 4% using the predictive controller in comparison to the original controller. On the other hand operation as a PHEV determines fuel consumption reductions up to 22% when compared against the original controller. A final consideration for the performance analysis is the impact of error in predicting the tractive energy requirement or total trip time of a drive cycle since there is uncertainty in everyday driving conditions. With a 20% error in the total trip time this may lead to a variation in the average fuel consumption of 0.62% at the end of driving. This consideration demonstrates the robust nature of the proposed controller in using the predicted information. The main point to note from this analysis is that the predictive controller calculates the energy requirement of a drive scenario in order to maximise the use of stored energy with the expectation for grid charging at the end of driving.

5.2 Predicting Drive Cycle Energy Requirements

Through the use of GPS and intelligent transportation systems, drivers have the convenience of planning trips ahead of time. Using the same information as available to the driver the controller featured here can predict the energy requirements of a planned driving route in order to help with energy management decisions of the ICE and ESS. Section 3.4 evaluated a known equation for estimating drive cycle energy requirements of a vehicle having a specific mass and wheel radius. This information is useful if individual transients of a drive cycle are known. For the case of planned driving routes there is a significant amount of uncertainty such as traffic conditions and driver behaviour. The approximate energy requirement of the drive cycle is therefore expected to have some error in comparison to the actual energy requirement of the drive cycle. Here a method for determining the energy requirement is

presented as a means to demonstrate the use of this knowledge in the developed controller. There are a number of methods for predicting the energy requirements of driving each of which can be utilised in the proposed controller. The more information the predictive controller utilises the more complex it becomes [32]. The focus here is that the high efficiency controller will benefit from future knowledge in the demonstrated manner.

5.2.1 Proposed Method for Predictive Control

Referring to equation 3.1 in Section 3.4 it is possible to utilise the vehicle velocity and specifications to calculate the energy requirement of everyday driving. This estimated energy can then be applied to the ICE operation such that the ICE supplies the average power demand as discussed in Sections 2.2.4 and 3.5. Consider the use of equation 3.1 to predict the average power requirement of a planned trip with respect to the average vehicle velocity. This consideration leads to equation 5.1:

$$P_{av} = V_{av}\left(Mgf_r + \frac{1}{2}\rho C_D A_f V_{av}^2 \right) \tag{5.1}$$

where P_{av} is the average tractive power required from the vehicle and V_{av} is the average vehicle velocity. As detailed in Section 3.4 M is the vehicle mass, g is the gravitational acceleration, f_r is the rolling resistance coefficient, ρ is the air density, C_D is the coefficient of aerodynamic drag and A_f is the frontal area of the vehicle. Using GPS or intelligent transportation systems an estimated trip time (t_{trip}) then determines an approximate energy requirement from equation 5.1.

$$E_{total} = P_{av} t_{trip} \tag{5.2}$$

Equation 5.2 follows from the integration of power with respect to time. There is, however, concern with equation 5.1 eliminating the elements representing the rotational inertia of components in the energy requirements of the vehicle. This is due to the fact that with an average vehicle velocity transients of a drive cycle are zero and thus the acceleration and deceleration of the vehicle is unknown. Since the average velocity is represented in the first two components and the variance of this velocity is excluded a component is required to estimate the total energy spent based on the average acceleration and deceleration of the vehicle over the driving period.

$$P_{av} = V_{av}\left(Mgf_r + \frac{1}{2}\rho C_D A_f V_{av}^2 + \alpha_{av}\beta_{av} \right) \tag{5.3}$$

The factors α_{av} and β_{av} are constants and vary according to the drive conditions such as driver behaviour and traffic conditions. In reality the average power requirement of driving may be

determined from the relationship of a driver's acceleration and deceleration to the past recorded total energy requirement of driving [26, 127]. In this way future driving conditions are accounted for with computational requirements dependent on the sampling of planned driving routes. This component therefore represents the inertial losses of the vehicle. The more frequent the sampling of α_{av} and β_{av} the closer the approximation will be to the real energy requirements of a drive cycle.

For the purpose of the predictive control in this study the whole drive cycle is considered as a single sample. This shows a worst case scenario of the predictive controller. It is envisaged that increasing the sampling frequency for this energy comparison will lead to a more accurate prediction of the total energy requirement. The concern for increasing the sample frequency, however, is the increased computational requirements of the controller. The reason for displaying a worst case scenario is to demonstrate the ability of the predictive controller to overcome the error in estimating future energy requirements and thus the overcharge or over discharge of the ESS. Therefore in this study, α_{av} and β_{av} are approximated from the standardised drive cycles based on the required energy calculated using equation 5.1 in comparison to equation 3.1. The difference in energy and the difference in average power are then related using the absolute average acceleration/deceleration of the vehicle for each case. This identifies a means for the variation in α_{av} and β_{av} according to the driving conditions mentioned previously. The drive cycles considered include those listed in Table 5.1.

Table 5.1 - List of drive cycles utilised for determining α_{av} and β_{av}. Drive cycles are displayed in appendix A.3.

Drive Cycle	Abbreviation	Distance (km)	Time (s)
Urban dynamo driving schedule	UDDS	11.989	1370
Highway fuel economy test	HWFET	16.505	766
US Environmental Protection Agency 's supplemental federal test procedure	US06	12.886	600
New European drive cycle	NEDC	10.930	1184
Unified driving schedule – emissions test	LA92	15.796	1435
West Virginia city driving schedule	WVUCITY	5.318	1408
Drive cycle for bus route 36 in Nuremberg, Germany	NurembergR36	4.312	1084
An aggressive driving schedule determined in combination with the federal test procedure	HL07	10.050	421

Firstly α_{av} is approximated according to the difference in total power by using equation 5.1 and equation 3.1 to calculate the energy requirement of the drive cycles listed in Table 5.1. Using a linear approximation the absolute acceleration/deceleration defines the approximate

difference between the actual tractive energy requirement and the estimated energy requirement. This difference is identified in equation 5.4:

$$\alpha_j = \frac{P_{av,act}(j) - P_{av,est}(j)}{\bar{a}_j} \tag{5.4}$$

with $P_{av,act}$ being the tractive power requirement of equation 3.1 and $P_{av,est}$ being the tractive power requirement of equation 5.1. The value of α_j for each drive cycle considered for the analysis from Table 5.1 determines a unique α value with j = 1 ,2 ,…, N representing a different drive cycle such that N number of drive cycles are included. The absolute average acceleration/deceleration for each drive cycle is represented by a_j with the absolute average value of equation 5.4 calculated as:

$$\bar{a}_j = \frac{1}{T}\int_0^T |a(t)|dt = \frac{1}{n}\sum_{i=1}^{n}\left|\frac{\Delta V_i}{\Delta t_i}\right| \tag{5.5}$$

Where V in equation 5.5 is the velocity and therefore ΔV_i is the ith derivative of the velocity. This means that for each α_j of equation 5.4 there is a unique $\bar{a}_j$ calculated using equation 5.5, where i = 1, 2, …, n, similar to the power balancing problem of equation 3.47 in Section 3.7.1, at each time step except that i must be considered as a discrete time constant with respect to the drive cycle and represents the sample time of the acceleration relative to the full driving period T. In addition, $\bar{a}_j$ can be determined based on past information and varied according to the conditions of specific segments of the planned driving route.

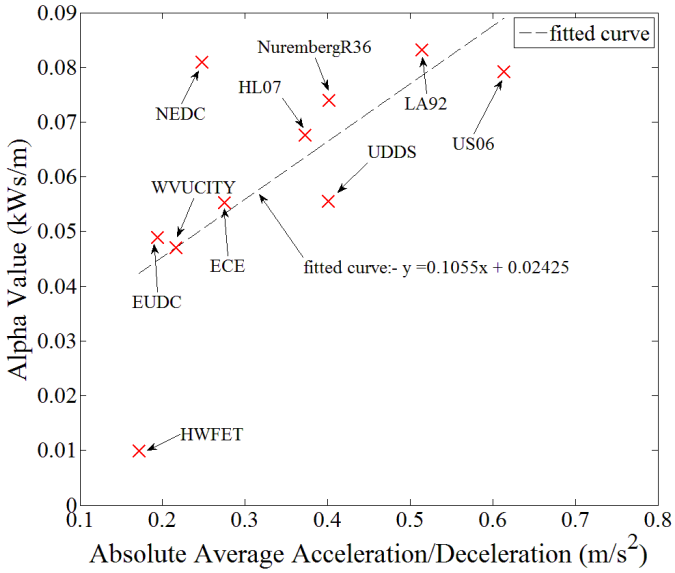

Figure 5.1 - Estimating α_j for a given drive cycle with respect to the absolute average acceleration/deceleration ($\bar{a}$).

Fitting a linear trend line to the data of Figure 5.1 determines the approximate α_{av} such that:

$$\alpha_{av} = 0.1055\bar{a} + 0.02425 \tag{5.6}$$

Similarly β_{av} is calculated according to:

$$\beta_j = \frac{1}{K}\frac{E_{total,act}(j) - E_{total,est}(j)}{\bar{a}_j} \tag{5.7}$$

where K is a constant that reduces β_j to unity allowing the correction of predicted energy values when using α_{av} and β_{av} in equation 5.3. K is determined based on the resulting average of the differences between total energy using equation 3.1 and equation 5.1 for the sample space of N number of drive cycles. In the case of equation 5.7 the total energy requirement over the drive cycle is determined from the integral of the tractive power resulting from equation 3.1 with respect to time.

$$E_{total} = \int_0^T P(t)dt = \sum_{i=1}^{n} P_i \Delta t_i \tag{5.8}$$

P_i is calculated according to equation 3.1 ($E_{total,act}$) or 5.1 ($E_{total,est}$) at each discrete time step i throughout the drive cycle. Equation 5.7 in comparison to the absolute average acceleration/deceleration then results with the approximation of β_{av} as shown in Figure 5.2.

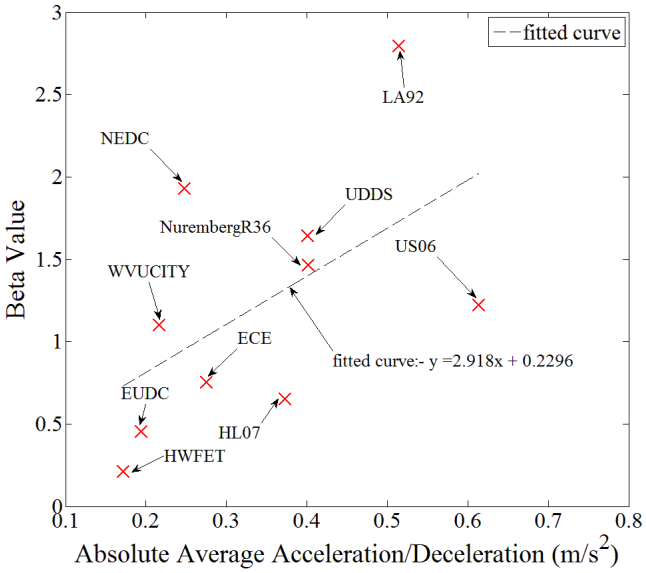

Figure 5.2 – Estimating β_j for a given drive cycle with respect to the absolute average acceleration/deceleration $\bar{a}$.

From Figure 5.2 the resulting estimation β_{av} is:

$$\beta_{av} = 2.918\bar{a} + 0.2296 \tag{5.9}$$

Then using the average vehicle velocity and absolute average acceleration/deceleration the total energy requirements for a planned trip are estimated.

5.2.2 Error in Prediction

Utilising the approximation of equation 5.3 and comparing against the energy calculated using equation 3.1 the results are listed in Table 5.2. The error in predicting the energy requirement is a result of the available sensitivity in sampling the expected transients of the drive cycle. This result is apparent from the consideration of discrete methods of integration versus continuous integration, the smaller the increment the greater the accuracy of the discrete integral [169]. Note that for the NEDC drive cycle identified in Table 5.2 the error in the energy prediction is 38.7 % however taking the urban and extra urban segments of the drive cycle leads to reduced error. The 4xECE represents the urban segment with an error of 14.1% and the EUDC represents the extra urban segment with an error of 20.9%. While this large error for the energy approximation may be a concern it is shown in the proposed predictive controller that there are measures of redundancy in place to help with fuel consumption minimisation (Sections 5.7.3 and 5.7.4). With increased accuracy in the energy prediction it is expected that there will be increased fuel savings.

Table 5.2 demonstrates that it is possible to predict the tractive energy requirement of standardised drive cycles with respect to average vehicle velocity and absolute average acceleration/deceleration. Such methods will provide a basis for interpreting the information available from GPS and intelligent transportation systems in the process of EMS control strategies. This application of the energy prediction is demonstrated with the predictive controller developed in this Chapter.

Table 5.2 – Predicting drive cycle tractive energy requirement from average vehicle velocity and absolute average acceleration/deceleration.

Drive Cycle	Predicted Tractive Energy (kWh)	Tractive Energy (kWh)	Error (%)
UDDS	0.538	0.521	-3.4
HWFET	1.077	1.029	-4.7
US06	1.359	1.250	-8.7
NEDC	0.343	0.559	38.7
4xECE*	0.104	0.121	14.1
EUDC*	0.346	0.438	20.9
LA92	0.955	0.984	3
WVUCITY	0.138	0.163	15.4
NurembergR36	0.172	0.179	4
HL07	0.900	0.983	8.4

5.3 ICE On/Off Strategy Using Predictive Control

Using a comparison of the expected tractive energy such as that calculated using equation 5.8 and 5.3 with the energy consumed over a drive period allows for the consideration of ICE on/off times. Firstly observe the fundamental requirements of the ICE and M/G in a PHEV and HEV during hybrid mode of operation. Ideally the fuel energy consumed by the ICE should be directly proportional to the tractive energy requirement of the vehicle such that the net energy charged or discharged from the ESS is zero.

$$E_L(T) = \eta_{sys} E_f(T) \tag{5.10}$$

T is the final time for the driving period with the fuel (E_f) and tractive (E_L) energy being proportional by some average efficiency of the system (η_{sys}). Equation 5.10 is true if and only if:

$$SOC_{init} = SOC_{final} \rightarrow SOC(0) = SOC(T) \tag{5.11}$$

with

$$E_{ess}(T) = 0 \tag{5.12}$$

There are losses during the charge and discharge of the ESS which are included in the system efficiency (η_{sys}) and therefore energy losses are with respect to the fuel consumption. The definition of equations 5.10 to 5.12 for the hybrid mode of operation in the PHEV or HEV realises the fundamental approach to the problem for energy management.

Expanding on the fundamental considerations of equations 5.10 and 5.12 in light of the constraint that energy discharged over a time period T must be replenished by the ICE the following is introduced. Referring to equation 2.2 for the hybrid mode from Section 2.2.6 the relationship for energy consumption of the ICE and M/G mathematically define the tractive power. During an ideal scenario the ICE supplies the average tractive power with the ESS supplying the transient loads. In addition, intermittent operation of the ICE with a minimum number of ICE start/stops requires that the ICE switches off for a discharge period of the ESS and then on for a charge period. This means that the energy available in the ESS must be utilised before the ICE is switched on to charge the ESS to the maximum again. On the other hand during a charge period the ICE must remain on until the energy stored in the ESS is at the maximum.

Figure 5.3 identifies the consideration for the ICE on/off times as described above. The tractive energy required to drive the vehicle as represented by E_L is supplied by the M/G during t_{off} and then during t_{on} it is supplied by both the ICE and M/G. The determination of

ΔE is dependent on the amount of energy that can be charged/discharged to/from the ESS to ensure equation 5.11 and 5.12 hold. This also maintains that t_{on} and t_{off} add to equal T.

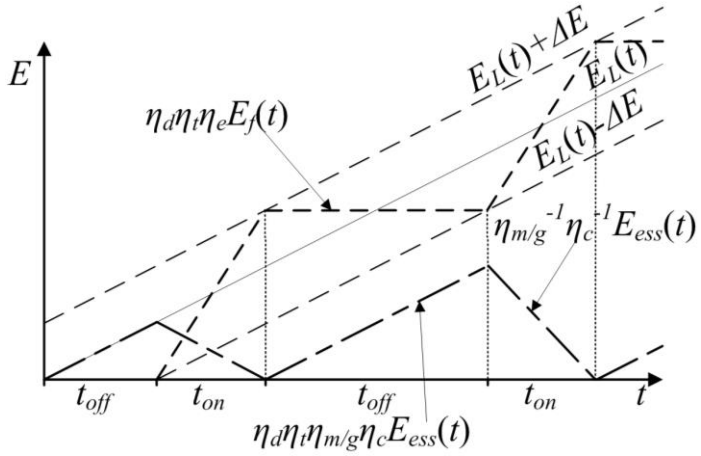

Figure 5.3 - Tractive energy consumed relative to fuel energy consumed.

From Figure 5.3 the period of t_{off} determines consumption of energy from the ESS alone with the equation:

$$P_L(t) = -\eta_d \eta_t \eta_{m/g} \eta_c \frac{dE_{ess}(t)}{dt} \tag{5.13}$$

As decided by equation 2.2 in Section 2.2.6. It is therefore considered that the total energy drawn from the ESS during t_{off} is:

$$E_{L_{toff}} = \int_0^{t_{off}} P_L(t)dt = \int_0^{t_{off}} -\eta_d \eta_t \eta_{m/g} \eta_c \frac{dE_{ess}(t)}{dt} dt \tag{5.14}$$

Resulting with:

$$E_{L_{toff}} = -\eta_d \eta_t \eta_{m/g} \eta_c E_{ess}(t_{off}) \tag{5.15}$$

Equation 5.14 and 5.15 at this stage of the definition assumes constant average efficiency of components for the period 0 to t_{off}, and that a deficit is occurring in the stored energy of the ESS. This allows the controller to determine approximate future operations with respect to ΔE. Additionally equation 5.15 determines that the energy measured at the wheels during t_{off} is the net energy consumed from the ESS minus losses, such as that considered from Sections 3.4 and 3.5 in the power balance between the ICE and ESS. Then during t_{on}:

$$P_L(t) = \eta_d \eta_t \left(\eta_e \frac{dE_f(t)}{dt} - \eta_{m/g}^{-1} \eta_c^{-1} \frac{dE_{ess}(t)}{dt} \right) \tag{5.16}$$

In the case of equation 5.16 the ICE is used to satisfy the load while the ESS is predominantly charged by the ICE. Similar to total energy discharged during t_{off} the scenario for t_{on} becomes:

$$E_{L_{ton}} = \int_0^{t_{on}} P_L(t)dt = \int_0^{t_{on}} \eta_d \eta_t \left(\eta_e \frac{dE_f(t)}{dt} - \eta_{m/g}^{-1} \eta_c^{-1} \frac{dE_{ess}(t)}{dt} \right) dt \tag{5.17}$$

Again assuming constant average efficiencies for t_{on}:

$$E_{L_{ton}} = \eta_d \eta_t \left(\eta_e E_f(t_{on}) - \eta_{m/g}^{-1} \eta_c^{-1} E_{ess}(t_{on}) \right) \tag{5.18}$$

Equation 5.18 is observed during t_{on} in Figure 5.3. Having defined the period $T = t_{on} + t_{off}$ it follows that at the end of t_{off} the SOC (SOC(t_{off})) will have reached some low limit which coincides with the start of t_{on}. Additionally the end of t_{on} indicates that the SOC (SOC(t_{off}+t_{on})) has reached some high limit which coincides with the start of a charge/discharge period T and therefore the next period (i.e. SOC(t_{off}+t_{on}) = SOC(T) = SOC(0)).

By the same consideration $E_L(t)$-ΔE is at the end of t_{off} and start of t_{on} and $E_L(t)$+ΔE is at the end of t_{on} and start of t_{off}. ΔE is therefore the common parameter between equation 5.14 and 5.17 like a simple on/off switch as is the requirement for ICE operation. From Figure 5.3 ΔE is defined as:

$$2\Delta E = \int_0^{t_{off}} -\eta_d \eta_t \eta_{m/g} \eta_c \frac{dE_{ess}(t)}{dt} dt \tag{5.19}$$

Leading to:

$$2\Delta E = -\eta_d \eta_t \eta_{m/g} \eta_c E_{ess}(t_{off}) + E_L(0) \tag{5.20}$$

or

$$2\Delta E = \int_{t_{off}}^{T} \eta_d \eta_t \left(\eta_e \frac{dE_f(t)}{dt} - \eta_{m/g}^{-1} \eta_c^{-1} \frac{dE_{ess}(t)}{dt} \right) dt \tag{5.21}$$

becoming:

$$2\Delta E = \eta_d \eta_t \left(\eta_e E_f(T) - \eta_{m/g}^{-1} \eta_c^{-1} E_{ess}(T) \right) - E_L(t_{off}) \tag{5.22}$$

Then according to the constraints of equation 5.11 and 5.12 and the established powertrain operation over the period T:

$$E_L(0) = 0 \tag{5.23}$$

And

$$E_L(t_{off}) = E_{Ltoff} \tag{5.24}$$

With the substitution of equation 5.15 into 5.22:

$$2\Delta E = \eta_d \eta_t \left(\eta_e E_f(T) - \eta_{m/g}^{-1} \eta_c^{-1} E_{ess}(T)\right) + \eta_d \eta_t \eta_{m/g} \eta_c E_{ess}(t_{off}) \tag{5.25}$$

Equation 5.25 highlights that in order for equations 5.11 and 5.12 to hold the energy drawn from the ESS during t_{off} must be replenished during t_{on} in addition to the load. The definition of equation 5.25 identifies that ΔE determines the on and off times of the ICE for optimal drivability (i.e. minimal number of ICE start/stops).

Furthermore, inclusion of the average efficiency of operation for the defined period T determines the dependence of ΔE on the losses of the powertrain. From 5.14, 5.17 and 5.25:

$$2\Delta E = \int_{t_{off}}^{T} \eta_d \eta_t \left(\eta_e \frac{dE_f(t)}{dt} - \eta_{m/g}^{-1} \eta_c^{-1} \frac{dE_{ess}(t)}{dt} \right) dt + \int_0^{t_{off}} \eta_d \eta_t \eta_{m/g} \eta_c \frac{dE_{ess}(t)}{dt} dt \tag{5.26}$$

Then to generalise:

$$2\Delta E = \eta_d \eta_t \left[\int_{t_{off}}^{T} \eta_e(t) \frac{dE_f(t)}{dt} dt - \int_{t_{off}}^{T} \eta_{m/g}^{b}(t) \eta_c^{b}(t) \frac{dE_{ess}(t)}{dt} dt \right.$$

$$\left. + \int_0^{t_{off}} \eta_{m/g}^{b}(t) \eta_c^{b}(t) \frac{dE_{ess}(t)}{dt} dt \right] \tag{5.27}$$

where b = 1 for discharging and b = -1 for charging. Equation 5.27 indicates that if the electrical network is ideal ΔE is dependent on fuel consumption only, however, due to the varying efficiencies of the ESS and M/G with respect to the requested loads the losses incurred from charging and discharging must be considered for the energy of the system to balance within one full cycle T. Identifying the differences of the charging and discharging with respect to time, equation 5.27 may be simplified to:

$$2\Delta E = \eta_d \eta_t \int_{t_{off}}^{T} \eta_e(t) \frac{dE_f(t)}{dt} dt - E_{losses}(t) \tag{5.28}$$

It is also possible to estimate $E_{losses}(t)$ based on the average efficiencies of charging and discharging the ESS during t_{off} and t_{on} which would reduce the accuracy of equation 5.27, however, it allows for the variation of ΔE on-the-go. The selection of ΔE above therefore determines the on/off times of the ICE, however, more information is required in order to determine an optimal value of ΔE based on the constraints of the powertrain. For example the available stored energy is determined by the SOC swing available from the ESS such as that discussed in Section 4.4.1.

5.4 Further Constraints for ICE On/Off

Accounting for the operation of the ICE during the previously defined period T identified in Figure 5.3, the ΔE is determined with respect to the available energy stored in the ESS. The ICE is capable of producing an output power of:

$$0 < P_e \leq P_{e,\max} \tag{5.29}$$

at any given time t. For the case of the high efficiency controller of Chapter 4, however, the ICE operating power is limited by the selected $\eta_{e,low}$ such that:

$$P^-_{\eta e,low} \leq P_e \leq P^+_{\eta e,low} \tag{5.30}$$

Where $P^-_{\eta e,low}$ is the minimum power and $P^+_{\eta e,low}$ is the maximum power the ICE is allowed to operate at to achieve the minimum efficiency $\eta_{e,low}$. Equation 5.30 identifies that if the requested load power is within the high efficiency region the ICE is able to supply the load directly during t_{on}:

$$P_L(t) = \eta_d \eta_t \eta_e \frac{dE_f(t)}{dt} = \eta_d \eta_t P_e(t) \tag{5.31}$$

In addition, for P_L less than $P^-_{\eta e,low}$ the following occurs with respect to equation 4.1:

$$P_{m/g}(t) = P_e(t) - P_L(t) \tag{5.32}$$

with

$$P_e(t) = P^-_{\eta e,low} \tag{5.33}$$

Meaning that the power absorbed by the M/G is less than or equal to $P^-_{\eta e,low}$, for example:

$$P_L(t) = 0; \qquad P_{m/g}(t) = P_e(t) = P^-_{\eta e,low} \tag{5.34}$$

Such that equation 5.34 defines the constraints for the $\eta_{e,low}$ at any given time. The ESS must be able to absorb:

$$P_{ess,\max}(t) = \eta_{m/g} \eta_c P_{m/g,\max} \geq \eta_{m/g} \eta_c P^-_{\eta e,low} \tag{5.35}$$

Relative to the maximum instantaneous power the M/G and ESS can absorb at any given time the ESS may have a minimum charge time in place to ensure prolonged ESS life [44, 170]. Referring to Figure 5.4, a charging scenario of the ESS is shown with respect to a predefined SOC swing (ΔSOC) and a target SOC (SOC_{target}) such as that discussed in Sections 4.4.1 and 4.4.2. Instead of calculating how far the SOC is from the SOC_{target} to determine the required charge the controller operates between the maximum (SOC_{target} +

ΔSOC) and minimum (SOC_{target} - ΔSOC). This period of charge and discharge is determined by the method of ICE on/off described in Section 5.3, however, it is also dependent on whether the ESS can absorb the maximum charge power developed by the ICE.

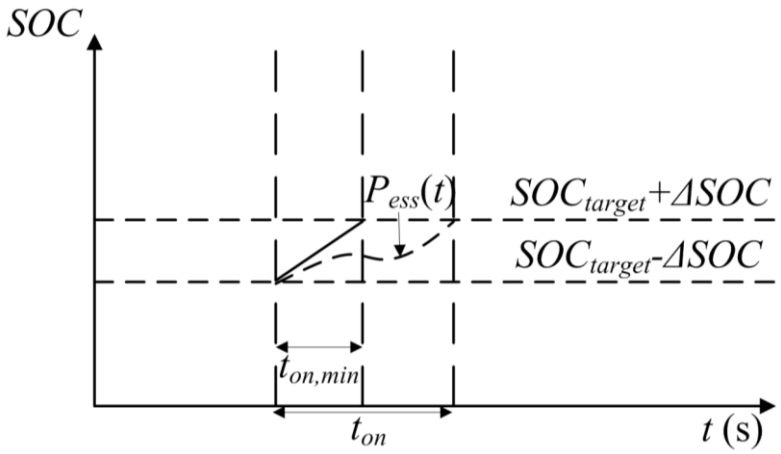

Figure 5.4 - Constraint for charging ESS.

Figure 5.4 relates the SOC of the ESS to the defined t_{on} for ICE on/off. This relationship highlights that in order to maintain some minimum on time of the ICE the ΔSOC must coincide with the developed ICE power of equation 5.35 such that:

$$2\Delta SOC = \frac{P_{ess,\max}(t)t_{on,\min}}{E_{ess,total}} = \frac{\eta_{m/g}\eta_c P^{-}_{\eta e,low} t_{on,\min}}{E_{ess,total}} \tag{5.36}$$

Equation 5.36 identifies that the minimum ICE on time ($t_{on,min}$) is dependent on the maximum charge power the ICE sends to the ESS. The maximum charge power is either determined by the ESS specifications such as a maximum RMS current (I_{RMS}) or the minimum operating power of the ICE ($\eta_{m/g}\eta_c P^{-}_{\eta e,low}$). This highlights that the constraints introduced by the specifications of the ESS may influence the selection of $\eta_{e,low}$ (from Section 4.3.3) depending on the topology and the components utilised. If the ESS is comprised of a battery and ultracapacitor, larger transients can be absorbed by the ESS over short time periods, without the ultracapacitor the capacity for absorbing large transients is reduced [103]. On the other hand the ΔSOC restricts the discharge power of the ESS as identified in Figure 5.5.

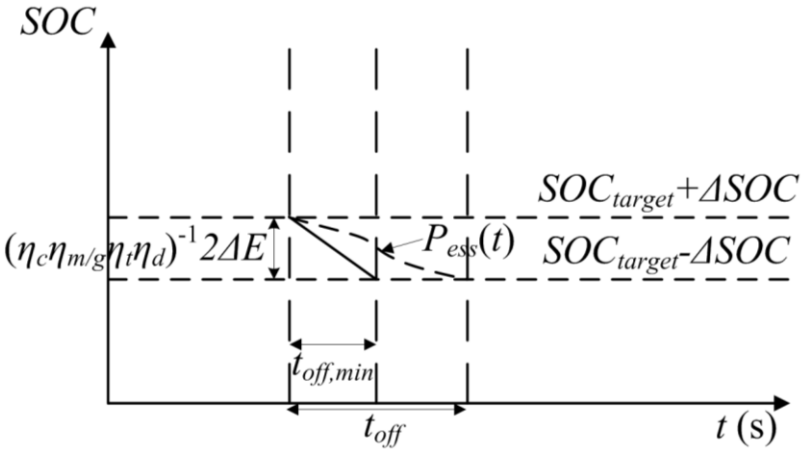

Figure 5.5 – Constraint for discharging ESS.

Figure 5.5 provides the alternative constraints for t_{off} such that ΔSOC determines the available stored energy and therefore the ΔE during ESS discharge. Ideally the ICE will remain off until the SOC reaches the defined lower limit. Figure 5.5 therefore introduces the constraint of equation 5.37:

$$\frac{2\Delta E}{\eta_d\eta_t\eta_{m/g}\eta_c} \leq 2\Delta SOC \tag{5.37}$$

Once the SOC of the ESS has fallen below the low limit (SOC_{target}-ΔSOC) the ICE will start again. It is the required tractive energy during t_{off} that determines the ΔSOC for the control system which is then utilised to calculate approximate ICE on/off frequency as well as on/off times (t_{on} and t_{off}). The average tractive power (P_{av} in Section 5.2.1) required from the ICE and ESS for a given trip helps predict when the ICE needs to turn on according to the following inequality:

$$\frac{\left(P_{av}t_{off} - \Delta E\right)}{\eta_d\eta_t\eta_{m/g}\eta_c} > \left(SOC(t) - \Delta SOC\right)E_{ess,total} \tag{5.38}$$

Leading to:

$$t_{off} = \frac{\eta_d\eta_t\eta_{m/g}\eta_c\left(SOC(0) - \Delta SOC\right)E_{ess,total} + \Delta E}{P_{av}} \tag{5.39}$$

Where SOC(0) is the initial SOC of the ESS at the start of driving or once the ICE has been switched off after a charge period (t_{on}). P_{av} as discussed in Section 5.2.1 is determine from the expected driving route using the average vehicle velocity and absolute average acceleration/deceleration with respect to GPS or intelligent transportation system information and recorded vehicle data. Equation 5.39 also implies that:

$$\Delta E = \eta_d\eta_t\eta_{m/g}\eta_c\left(SOC(0) - \Delta SOC\right)E_{ess,total} \tag{5.40}$$

Equation 5.40 holds for the period t_{off} assuming that at t = 0, the energy consumed by the vehicle ($E_L(0)$) is equal to the SOC_{target} which is the requirement for the constraints of equation 5.11 and 5.12. It is therefore considered that equation 5.39 is a direct result of equation 5.37 in defining the relationship between ΔSOC and ΔE. Once the controller can calculate the ICE off time it has a means for determining the ICE on time and required $\eta_{e,low}$ with respect to the predicted energy (E^*_{total}) and in comparison to equation 5.34. Following the same procedure t_{on} is defined similarly to equation 5.38:

$$\left(P_{av}t_{on} + \Delta E\right) > \eta_d \eta_t \int_{t_{off}}^{T} \eta_e(t) \frac{dE_f(t)}{dt} dt \tag{5.41}$$

Evaluating to:

$$\frac{\left(P_{av}t_{on} + \Delta E\right)}{\eta_{d,av}\eta_{t,av}\eta_{e,av}} > \left(E_f(T) - E_f(t_{off})\right) \tag{5.42}$$

This is also equal to:

$$\frac{\left(P_{av}t_{on} + \Delta E\right)}{\eta_{d,av}\eta_{t,av}\eta_{e,av}} > \left(E_f(t_{on}) + E_f(t_{off}) - E_f(t_{off})\right) \tag{5.43}$$

And

$$\frac{\left(P_{av}t_{on} + \Delta E\right)}{\eta_{d,av}\eta_{t,av}\eta_{e,av}} > E_f(t_{on}) \tag{5.44}$$

As long as the inequality of equation 5.43 holds the ICE should remain on. This means that for the full period of the drive cycle the charge cycle needs to determine an approximate $E_f(t_{on})$ according to:

$$E_f(t_{on}) = \frac{P_{av}t_{on}}{\eta_{d,av}\eta_{t,av}\eta_{e,av}} + \frac{\left(SOC(0) - \Delta SOC\right)E_{ess,total}}{\eta_{e,av}\eta_{m/g,av}\eta_{c,av}} \tag{5.45}$$

Equation 5.45 then relates back to equation 5.21 if average efficiency and power values accurately represent vehicle operations during real-world driving conditions. Equation 5.45 demonstrates that for minimum fuel consumption during t_{on} the powertrain and drivetrain of the vehicle should achieve maximum efficiency of operation. This strategy in combination with the ESS SOC maintenance defines the importance of operating the ICE in a high efficiency region.

5.5 Control Equations

The three main control equations resulting from the mathematical investigation of Section 5.3 relative to the constraints of Section 5.4 and the measurements available from the test vehicles of Chapter 3, including:

$$\int_0^{t_{off}} \eta_{m/g}^{-1}\eta_c^{-1}\frac{dE_{ess}(t)}{dt}dt = \left(SOC(0) - \Delta SOC\right)E_{ess,total} = \Delta E \tag{5.46}$$

$$\int_{t_{off}}^{T} P_L(t)dt = P_{av}t_{on} \tag{5.47}$$

$$\int_{t_{off}}^{T} P_f(t)dt = E_f(t_{on}) \tag{5.48}$$

Equations 5.46 to 5.48 lead to the definition of the objective function:

$$\text{Objective: minimise } J = E_f(t_{on}) \tag{5.49}$$

With the constraints:

$$\text{Subject to: } \begin{cases} P_{ess,\min}(t) \le P_{ess}(t) \le P_{ess,\max}(t) \\ P_{m/g,\min}(t) \le P_{m/g}(t) \le P_{m/g,\max}(t) \\ P^{-}_{\eta e,low} \le P_e(t) \le P^{+}_{\eta e,low} \\ P_{ess,\max}(t) \ge \eta_{m/g}\eta_c P^{-}_{\eta e,low} \\ E_L + \Delta E > \eta_d\eta_t\eta_e E_f(t_{on}) \\ SOC_{low} \le SOC(t) \le SOC_{high} \end{cases} \tag{5.50}$$

Equation 5.49 determines the objective function for the proposed predictive controller in terms of the constraints defined by equation 5.50. The constraints of equation 5.50 indicates that for any load request the power ratings of the ESS and M/G restrict optimisation such that they must be able to meet the maximum requested load power during ICE shutdown. If the power ratings for either the ESS or the M/G are too low the vehicle will not be able to sustain the required load. In addition, the high efficiency region defined by $\eta_{e,low}$ and therefore $P^{-}_{\eta e,low}$ and $P^{+}_{\eta e,low}$ restricts ICE operation aiding with the minimisation of equation 5.49. For the objective function to hold (as defined in Section 5.4) the power limit of the ESS ($P_{ess,max}(t)$) must exceed the minimum power ($\eta_c\eta_{m/g}P^{-}_{\eta e,low}$) the high efficiency control forces the ICE to develop in the event that requested load is zero. ICE on/off is controlled by the SOC limits as discussed in Section 5.4. Finally, for the ICE to remain on during t_{on}, the fuel energy consumed ($\eta_d\eta_t\eta_e E_f(t_{on})$) in comparison to the expected tractive energy requirement must not exceed the upper limit (E_L+ΔE). If the fuel energy consumed does exceed the upper

limit the ICE will switch off. In most cases the upper limit is defined by SOC_{high} of the ESS since the SOC swing (i.e. SOC_{high}-SOC_{low}) of the ESS is the ultimate constraint for ICE operation as defined here. The defining factor for the objective function is the selection of the high efficiency region over time and thus the value of $\eta_{e,low}$.

5.6 Approximating $\eta_{e,low}$ on-the-go.

Utilising SOC swing alone the charge and discharge of the vehicle is determined according to the total driving time. Using the estimated trip energy and total energy in one SOC swing ($2\Delta SOC$) an approximate number of charge/discharge cycles may be determined. To ensure that the initial SOC (SOC_{init} = $SOC(0)$) is maintained a half discharge cycle must also be considered in the estimation. This leads to:

$$f_e = \frac{\dfrac{E_{total}^{*}}{\eta_{d,av}\eta_{t,av}\eta_{m/g,av}\eta_{c,av}} - \Delta SOC \times E_{ess,total}}{2\Delta SOC \times E_{ess,total}} + 0.5 \tag{5.51}$$

Where f_e is the frequency of ICE on/off periods, E_{total}^{*} is the estimated total tractive energy using t_{trip}^{*} and P_{av} from Section 5.2.1. The charge/discharge period is then approximated as:

$$T = \frac{t_{trip}^{*}}{f_e} \tag{5.52}$$

Using the period for each charge/discharge the ICE on time (t_{on}) is known at the start of a charging period to achieve the constraints of equation 5.11 and 5.12 such that:

$$T = t_{on} + t_{off} \tag{5.53}$$

Leading to:

$$t_{on} = T - t_{off} = \frac{t_{trip}^{*}}{f_e} - t_{off} \tag{5.54}$$

This will ensure that regardless of the discharge time taken the total time of the charge/discharge will be equal to T allowing a minimum number of ICE start/stops. This approximation is a simplification of the control problem, and therefore it may lead to unrealistic charging expectations especially if t_{off} exceeds T. The approximation, however, determines the required $P_{\eta e,low}^{-}$ with respect to the constraints of the objective function (equation 5.50).

For the intermittent ICE operation defined here it is expected that the ICE will remain on until the fuel energy consumed exceeds the considered upper limit. Assuming that the initial

SOC (SOC_{init} = SOC(0)) is the target SOC (SOC_{target}), and the average power requirement for the load will vary about P_{av} equally over a drive cycle, the charge period (t_{on}) by rearranging equation 5.45 with respect to the objective function determines the average ICE power:

$$P_{e,av} = P^{-}_{\eta e,low} = \frac{\left[\frac{P_{av}t_{on}}{\eta_{d,av}\eta_{t,av}\eta_{e,av}} + \frac{2\Delta SOC \times E_{ess,total}}{\eta_{m/g,av}\eta_{c,av}}\right]}{t_{on}} \tag{5.55}$$

With $P_{av}t_{on}$ being the tractive energy required during t_{on} and the SOC component being the energy required to recharge the ESS over the period t_{on}. The average efficiency values of η_e, η_t, η_d, η_c and $\eta_{m/g}$ are estimated from past driving information (during t_{on}) at the expected speeds from the initial trip energy analysis. Alternatively these average efficiencies may be based on recent moving average values so as to account for recent transients. The assumption is that the efficiencies will be consistent due to the small windows of operation the controller enforces onto the ICE. From equation 5.54 t_{on} is known at the beginning of the ICE on period then following the recording of trip energy according to the constraints of equation 5.50 the ICE will switch off either when $E_f(t_{on})$ exceeds $E_L+\Delta E$ or when the SOC_{high} limit is reached. Note that $P^{-}_{\eta e,low}$ is directly related to $\eta_{e,low}$ and thus the value defining the high efficiency region is calculated on-the-go.

5.7 Implementing Predictive Control Strategy

The optimal control for a typical test bench is outlined in Figure 5.6. The load power (P_L^*) requested at the wheels of the vehicle is converted into the potential ICE power (P_e^*) requirement. The controller then determines the optimal operating torque (T_e^*) and speed (ω_e^*) the ICE is required to supply based on some constraints. By limiting the ICE to some desired operating region the ESS charge (P_{ess}^*) requirement and mechanical losses ($P_{J(t-1)}$)of the drivetrain are considered for the requested load. Finally, the recorded average ICE power ($P_{e,av}$) is utilised to determine the optimal $\eta_{e,low}$ value with respect to the recorded fuel consumption ($\dot{m}_{f(t-1)} \rightarrow E_f(t_{on})$).

Having defined the objective function and associated constraints for optimal control in Section 5.5 the implementation of the high efficiency control for the ICE must adhere to the real-world limitations of the vehicle configuration utilised. Therefore, the proposed predictive control must be evaluated on a real-world model for comparison of performance using the measured data. Here the Toyota Prius is utilised since this is a power-split topology that demonstrates the most flexibility in control of the three test benches available. In addition, the power ratings of the M/G on both the Hyundai and Honda limit the ability to

switch the ICE off, such that load requirements would need to be satisfied by the ICE for the majority of tractive power requirements.

5.7.1 Constraints of the Toyota Prius 2010

During simulation of the Toyota Prius it was found that with periods of ICE shut down the power rating of the ESS and M/G failed to supply the load of large transients during acceleration. This was noted in the trace miss for the comparison of the requested vehicle speed and achieved vehicle speed, as shown in the appendices (Section A.4). For this reason the ICE is required to be on or available to be switched on in order for the test bench to meet the acceleration requirements. Therefore, the defined control strategy for ICE on/off must be altered to account for this. Since it is not possible to predict when the user requires the vehicle to accelerate at maximum power it is a difficult task to determine when the ICE is allowed to be switched off [91]. Figure 5.6 identifies that the ICE on/off control is primarily determined by the requested power. In addition, a number of rules are introduced inside the "Need ICE On?", block of Figure 5.6 to anticipate the ICE on requirement and make sure the vehicle can meet the vehicle speed trace. These rules are identified in Table 5.3 such that if all four inequalities are true the ICE will shut down.

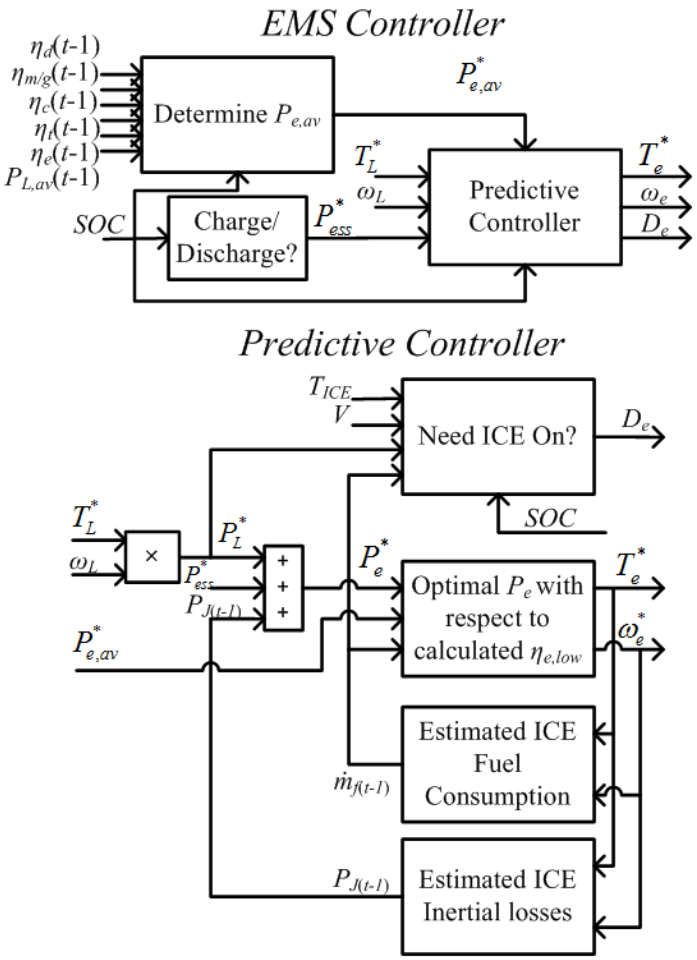

Figure 5.6 – EMS control structure identifying the signals required for the predictive controller.

Table 5.3 - ICE off rules for the Toyota Prius 2010.

Vehicle Parameter	Rule (True = ICE OFF)
Requested load power	$P^*_L < P^-_{\eta e,low}$
ESS SOC	$SOC > SOC_{low}$
Vehicle velocity	$V < V_{ZEV}$
ICE coolant temperature	$T_{ICE} \geq T_{HOT}$

Utilising the rules of Table 5.3, simulations of the Toyota Prius indicated that there are still some issues with meeting the vehicle speed trace. In order to solve this issue the requested acceleration and measured vehicle speed were utilised in order to have the ICE switch on at the required times.

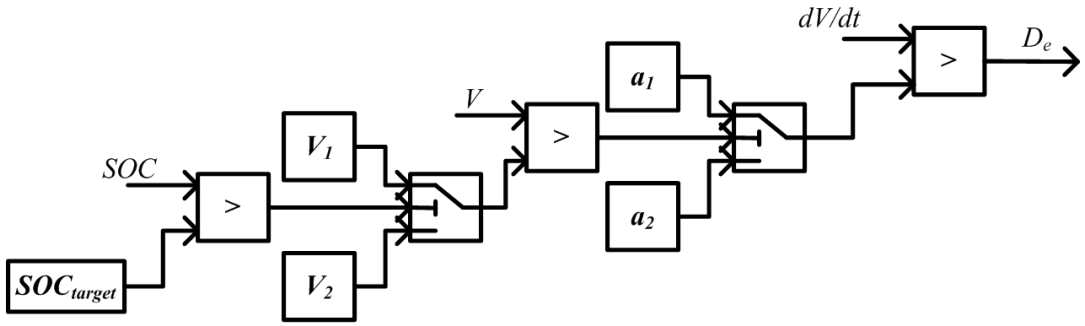

Figure 5.7 - ICE on/off strategy with respect to acceleration.

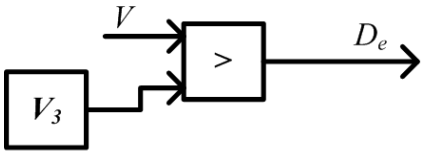

Figure 5.8 - ICE on/off strategy with respect to vehicle velocity.

Figure 5.7 and Figure 5.8 describe the ICE on/off constraints with respect to the vehicle velocity (V) and vehicle acceleration (a) for the Toyota Prius 2010, which are dependent on the rules in Table 5.3. This means that the rules of Table 5.3 must allow ICE on operation before considering the rules of Figure 5.7 and Figure 5.8. D_e is the enable signal for the ICE. Values of V_1, V_2, V_3, a_1 and a_2 are determined with trial and error on standardised drive cycles. The main requirement for their selection being that the vehicle must meet the vehicle speed trace over the drive period. The selection of each variable must adhere to the following inequalities otherwise the rules defined in Figure 5.7 and Figure 5.8 will not hold.

$$V_3 > V_1 > V_2 \text{ and } a_1 < a_2$$

The rules of Figure 5.7 resulted from an observation of the charge and discharge of the ESS and the consideration that increasing the torque for charging the ESS at high speed incurs a smaller change in the already high load torque requested [11]. The rule indicates that if the ESS requires charging and the vehicle speed is high enough then the ICE must be on to allow the charging of the ESS above the selected acceleration a_1. On the other hand the rule ensures that the ICE does not have to operate if the SOC is above SOC_{target}. Figure 5.8 provides an additional constraint for ICE operation at higher vehicle speed as opposed to V_{ZEV} which is for lower vehicle speeds. For the Toyota Prius 2010 the vehicle speed trace is met for the three tested drive cycles having the velocities V_1, V_2, and V_3 equal to 14, 12, and 18 m/s and acceleration a_1 and a_2 equal to 0 and 0.5 m/s^2 respectively. These rules for ICE on/off are independent of the predictive control strategy indicating that ICE operation in the Toyota Prius 2010 does not fit the defined control strategy of Section 5.4.

Since the ICE on/off control is dependent on the vehicle speed trace with the rules defined in Table 5.3, Figure 5.7 and Figure 5.8, it is no longer possible to maintain the t_{on} and t_{off} as described in Section 5.4. Using the same principle for fuel consumption reduction it is, however, possible to utilise the predictive energy for autonomous control of the high efficiency region while meeting the vehicle speed trace. The average ICE power output ($P_{e,av}$) featured in equation 5.55 in reality can be recorded at the output shaft of the ICE, however, in simulation it is recorded from the load power requested (P_L^*), ESS power requirement (P_{ess}^*) and inertial power losses ($P_J(t\text{-}1)$). Instead of having a distinct ICE on/off period the controller exhibits an approximate charge/discharge period where the ESS is periodically charging and discharging. This means that the average power for a charge/discharge period calculated using equation 5.52 must be met by the ICE. This average power requirement is calculated as:

$$P_{e,av}(t) = \frac{\dfrac{P_{L,av}(t)T}{\eta_d(t-1)\eta_t(t-1)\eta_e(t-1)} + \left(SOC_{target} - SOC(t)\right)E_{ess,total}\eta_{m/g}^{b}(t-1)\eta_c^{b}(t-1)}{T} \tag{5.56}$$

where the average ICE power ($P_{e,av}(t)$) requirement at time t recorded by the controller is obtained based on the estimated expected total energy of the drive cycle and the past consumed energy of the drivetrain.

$$P_{L,av}(t) = \frac{1}{t_{trip} - t}\left(E_{total}^{\ *} - \int_{t_o}^{t} P_L(t)dt\right) \tag{5.57}$$

And

$$P_L(t) = P_L(t-1) + P_J(t-1) \tag{5.58}$$

Equation 5.56 is the recorded average power requirement of the ICE relative to the previous time step. By comparing the average recorded load power consumed in equation 5.57 from the start of driving at t_0 to the current time (t), the controller calculates how much energy the ICE is required to produce before the end of the planned driving route. The right hand side of equation 5.56 identifies the required variation in the average ICE power requirement due to the ESS SOC. Monitoring the average load requirement in this way records any transients in the load, maintaining a record of the expected energy to be consumed in the future. Due to the ICE on/off rules defined above, the SOC of the ESS is no longer controlled according to the method discussed in Section 5.4. This means that required output power of the ESS ($P_{ess}^*(t)$) is no longer a part of the optimisation and another method is needed in order to maintain ESS SOC.

Similar to the controller presented in Chapter 4 the ESS SOC during driving is monitored with respect to the difference between the measure SOC and SOC_{target}. The charge/discharge block of Figure 5.6 utilises the following equation to determine the charge power required for the ESS.

$$P_{ess}^{*}(t) = \left(SOC_{target} - SOC(t-1)\right)P_{e,av}(t-1)\eta_{m/g}^{b}(t-1)\eta_{c}^{b}(t-1) \tag{5.59}$$

Note that $P_{ess}^{*}(t)$ in equation 5.59 is determined from the past recorded $P_{e,av}(t\text{-}1)$ of the ICE output power to ensure that the calculation of $P_{ess}^{*}(t)$ does not cause a singularity when evaluating equation 5.56 in simulation. $SOC(t\text{-}1)$ is the previously recorded SOC, $\eta_{m/g}$ is the M/G efficiency, η_c is the coulomb efficiency, b = -1 for charging and b=1 for discharging.

The consideration of equation 5.56 and 5.59 results from the ΔE discussion previously, where all energy consumed from the ESS in time t_{off} must be replenished during t_{on}. Instead of having t_{on} and t_{off} determined by ΔE or the SOC of the ESS, $\eta_{e,low}$ is used as the balancing parameter between ICE power developed and charge/discharge of the ESS. This consideration relies on the assumption that the difference between the average ICE power and actual load power is reflected in the SOC of the ESS. The current selected value of $\eta_{e,low}$ will set the constraints for the ICE, then using the feedback from the transient response (i.e. equation 5.59) future values of $\eta_{e,low}$ will be calculated and utilised accordingly.

5.7.2 Implementing Predictive Control in the Toyota Prius 2010

Translating this average ICE power to the high efficiency region requires knowledge of the ICE performance map such as the efficiency contours observed in the figures of Section 4.3. Here the average ICE power requirement of equation 5.56 is mapped to the available $\eta_{e,low}$ values as they occur in the performance map. The VSC defined in Section 4.3.2 identifies the optimal efficiency of the ICE to satisfy a given power level [98]. Similarly this concept is utilised to determine the specific $\eta_{e,low}$ value to select for ICE operation. Defining a vector containing a number of $\eta_{e,low}$ values and cross referencing these values using VSC on the ICE performance map a second vector contain ICE average power levels for equation 5.56 is established.

$$\overline{\eta}_{e,low} = \begin{bmatrix} \eta_{e,low(1)} \\ \eta_{e,low(2)} \\ \vdots \\ \eta_{e,low(n)} \end{bmatrix} \quad \leftrightarrow \quad \overline{P}_{e,av} = \begin{bmatrix} P_{e,av(1)} \\ P_{e,av(2)} \\ \vdots \\ P_{e,av(n)} \end{bmatrix} \tag{5.60}$$

With $\eta_{e,max} \geq \eta_{e,low(n)} > \ldots > \eta_{e,low(2)} > \eta_{e,low(1)} \geq 0$ and $P_{\eta e,max} \geq P_{e,av(n)} > \ldots > P_{e,av(2)} > P_{e,av(1)} \geq 0$, leading to corresponding pairs from each vector $\overline{\eta}_{e,low}$ and $\overline{P}_{e,av}$. The vectors in equation 5.60 allow equation 5.56 to be fed into a look-up table to output the corresponding $\eta^*_{e,low}$ value such as that shown in Figure 5.9.

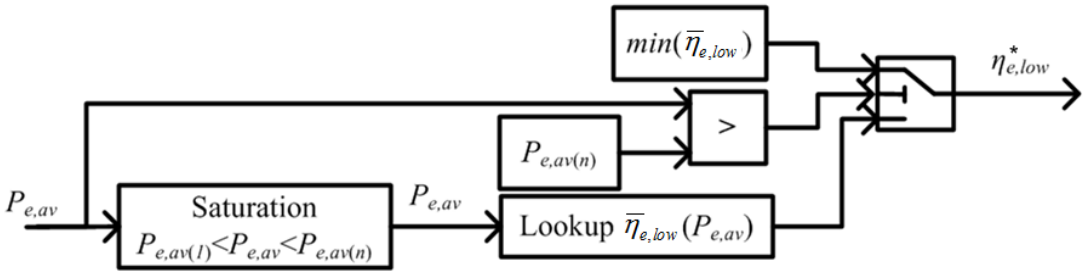

Figure 5.9 - Selecting optimal high efficiency region for ICE operation.

The selection of $\eta_{e,low}$ in the controller considered here is to avoid operating the ICE at low torques and speeds where the majority of inefficient operations occur [108]. It was previously noted that restricting the ICE for high power requests limited the acceleration performance of the vehicle while drawing more energy from the ESS at higher vehicle speeds unnecessarily (Sections 4.9.4 and 4.9.6). This operation lead to increased average fuel consumption since the ICE would have to regenerate energy consumed from the ESS. Figure 5.9 identifies that if the output power of the ICE exceeds the maximum average ICE power considered in mapping $\eta_{e,low}$ values, $\eta_{e,low}$ is set to the minimum.

Following the optimal selection of $\eta_{e,low}$ according to the procedure defined above the controller must still decide if a requested power is met by the ICE or ESS. Figure 5.10 identifies the additional control decisions considered for the selection of ICE output power based on $\eta_{e,low}$. Firstly, the predictive controller determines if the requested power lies within the high efficiency region calculated for the current load conditions. In the case that the requested power P_e^* is considered to fall within the high efficiency region it is passed straight through, this also relies on the need to have the SOC above SOC_{target}. In the event that SOC is below SOC_{target}, the vehicle speed is below the V_3 and the charge depletion mode (discussed in Section 5.7.4) is not active the controller will select the maximum of $P^-_{\eta e,low}$ and P_e^*. If SOC is greater than the target or the vehicle speed is greater than V_3 and the requested power is greater than the power developed at maximum efficiency ($P_{\eta e,max}$), then $P_e^* = P^+_{\eta e,low}$. Alternatively to this last case, if instead the SOC is low and the vehicle speed is above V_3, then the required charge power will be high as determined by equation 5.59 meaning that $P_{e,av}$ will be higher than the saturation (Figure 5.9), forcing $\eta_{e,low}$ to be selected as a minimum. This leaves the ICE unrestricted and allows it to supply maximum power to the

load. Finally, during charge depletion mode (the "CD mode?", block in Figure 5.10) the requested ICE power is set to zero if the SOC is greater than the target and the requested power is below the power developed at maximum ICE efficiency ($P_{\eta e,max}$).

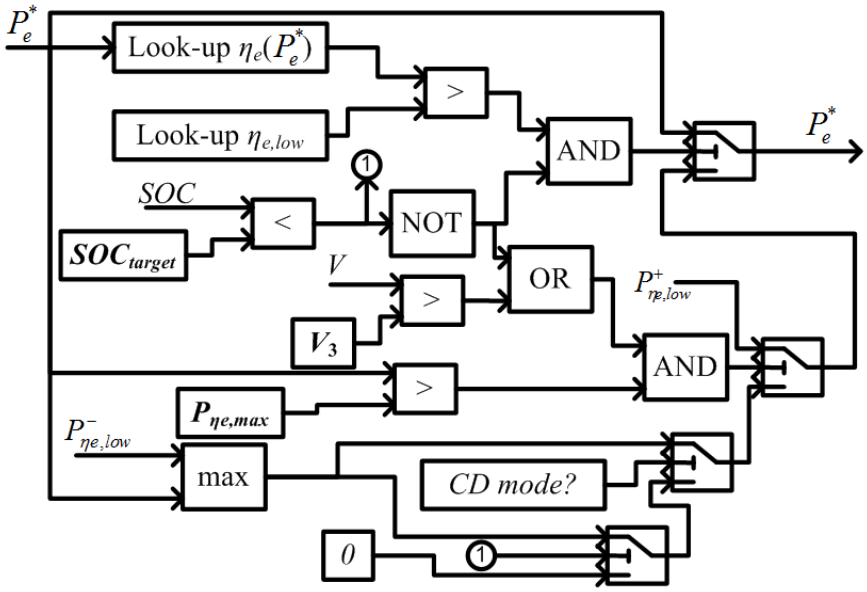

Figure 5.10 - Selecting ICE output power with respect to high efficiency control.

5.7.3 Avoiding Charge Sustenance mode in Blended Charge Depletion

To account for the over discharge of the ESS during driving a method for monitoring the SOC is introduced to anticipate increasing power requested from the ICE. This concern is discussed in Section 5.2.1 with Table 5.2 displaying a high error in the estimated energy for some drive cycles. By monitoring the average discharge power from the ESS and the remaining trip time (t_{trip}), the controller forces the ICE to recharge the ESS prior to an expected over discharge of the ESS. Using a set-reset (SR) flip-flop controller the expected over discharge towards the end of driving forces the ICE to charge the ESS according to:

$$\frac{\left(E_{ess,r}(t) - P_{ess,av}(t)\left(t_{trip} - t\right)\right)}{E_{ess,total}(t)} - SOC_{low} < 0.01 \qquad (5.61)$$

where $E_{ess,total}$ is the energy stored in the ESS at 100% SOC, $P_{ess,av}(t)$ is the average power consumed from the ESS over the current drive period from $t = 0$ to the current trip time (t), $E_{ess,r}$ is the remaining stored energy in the ESS, and in simulation is estimated as:

$$E_{ess,r}(t) = E_{ess,total}(t)SOC(t) = 3600 N_{ess} V_{ess} Ah_{ess} SOC(t) \qquad (5.62)$$

N_{ess} is the number of modules in the ESS, V_{ess} and Ah_{ess} are the average open circuit voltage the amp-hour rating of a single module and $SOC(t)$ is the measured SOC of the ESS. Using

equation 5.61 to determine the time to set the ICE to charge the ESS the controller has the ability to determine if the future energy requirement from the ESS is more than the stored energy remaining. The concern with setting the ICE to charge is anticipating when to begin discharging again so that the ICE does not consume more energy than is required for the remainder of the planned trip. Using the same principle the remaining energy required from the ESS is utilised to establish the minimum SOC required to satisfy the load until the end of driving. The reset of the SR flip-flop relies on:

$$\left(SOC(t)-SOC_{low}\right)E_{ess,total}(t) > P_{ess,av}(t)\left(t_{trip}-t\right) \tag{5.63}$$

Combining both equation 5.61 and 5.63 the set and reset respectively for ESS charging towards the end of driving is accounted for. Figure 5.11 identifies a method for creating an SR flip-flop in MATLAB. Using logic 'NOT OR' blocks (NOR) and memory blocks; the enable (*Q*) determines when to switch a device on or off with respect to the set and reset conditions.

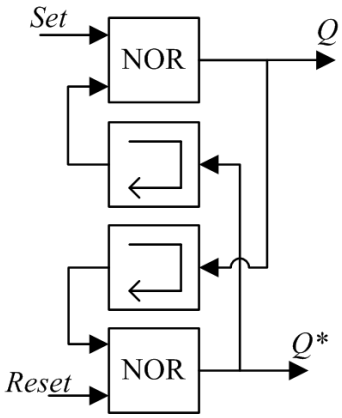

Figure 5.11 – Method for establishing an SR flip-flop using logic blocks in MATLAB.

The reason for using the SR flip-flop is because of the impulse set and reset. Once a condition has been met on either of the set or reset inputs, the output will remain in the previous state until the alternative condition is met. For example if the conditions for setting *Q* are met, *Q* becomes equal to logic 1 and remains set at 1 until the conditions of the reset are met at which time *Q* is reset to logic 0 (*Q** is the conjugate of *Q*). By this logic an SR flip-flop allows the continuous output of a signal according to a single event occurring at any given time. This means that once equation 5.61 is true the SR flip-flop will set the ICE to charge until equation 5.63 becomes true.

5.7.4 Charge Depletion mode at Final Stages of Driving

In addition to the over discharge of the ESS, the estimated energy requirement for driving as determined by the controller may be in excess, meaning that the ESS will not utilise all the stored energy and potentially consume more fuel energy than is necessary. Using the estimated trip time with respect to the SOC_{low} limit selected for the ESS and the average power requirement of the drive cycle, the controller estimates when to enter charge depletion mode.

$$\left(t_{trip} - t\right) < \frac{\left(SOC(t) - SOC_{low}\right)T}{2\Delta SOC} \tag{5.64}$$

Combining equation 5.64 with a second SR flip-flop the charge depletion mode reduces the SOC_{target} to ensure that at the end of driving the ESS approaches the SOC_{low} limit, utilising any available stored energy and further conserving fuel. For example equation 5.59 becomes:

$$P_{ess}(t)^{*} = \left(SOC_{low} - SOC(t-1)\right)P_{e,av}(t-1)\eta^{b}_{m/g}(t-1)\eta^{b}_{c}(t-1) \tag{5.65}$$

which proportionally reduces the demand on the ICE according to equation 5.56 (with $SOC_{target} = SOC_{low}$). The two considerations for over discharge or using excess stored energy at the end of driving help the controller to maximise the use of stored energy in the ESS of PHEV over a planned driving route whilst minimising fuel consumption. This outcome is demonstrated in comparison to the original controller and the developed non-predictive high efficiency controller discussed in Chapter 4.

5.8 Results

Following the analysis of the non-predictive high efficiency controller in Section 4.9, the autonomous control involved with selecting the high efficiency region using the predicted information demonstrates improved performance for PHEV. To show the improvement to efficiency of operation the predictive and non-predictive controllers are compared against the original controller with SOC corrections. This comparison identifies that the fuel consumed over the drive period is not being redistributed to the ESS. Alternatively, the operation of the predictive controller improves the utilisation of the ESS stored energy over the full drive cycle through the novel method of blended charge depletion. Finally, the error in predicting the total energy and trip time is demonstrated with respect to increased input energy consumption.

5.8.1 Modifications for PHEV Operation

In order to demonstrate a fair comparison of the original, non-predictive and predictive controllers the charge depletion mode defined in Section 5.7.4 is included in the original and

non-predictive controllers as well. Simply by monitoring the trip time (t_{trip}) relative to the SOC as discussed in Section 5.7.4 the target SOC at the end of driving is varied to the SOC_{low} limit in order to consume more ESS energy at the end of driving. Such operation is similar to the charge depletion mode typically seen at the start of driving in PHEV [7], however, the original controller does not operate in the described mode in the Toyota Prius 2010. This mode of operation highlights that the predictive controller is not simply relying more heavily on the ESS but instead it is calculating when to supply energy from the ESS in order to minimise fuel consumption. In effect the described mode for the original controller is providing an insight into how it would operate the Toyota Prius as a PHEV. The analysis that follows in this Section demonstrates that without the optimisation of the predictive controller described in this Chapter the original and non-predictive controllers have limited capability for utilising the ESS stored energy and minimising fuel consumption.

5.8.2 Operations of the Predictive Controller

During the drive period the predictive controller measures and estimates a number of quantities in the process of energy management. Section 5.2.1 discusses the calculation of the required energy (E^*_{total}) for a drive cycle based on the specifications of the vehicle, average vehicle velocity and the average absolute acceleration/deceleration of the vehicle over the drive period. This estimation of the required energy leads to the calculation of the average power requirement over the drive cycle which then helps in the selection of the high efficiency region (i.e. a value of $\eta_{e,low}$).

Figure 5.12 is an example of the estimated tractive power required from the Toyota Prius` ICE during operation for the UDDS over three continuous runs of the drive cycle. As discussed in Section 5.7.1 with equation 5.57 the average tractive power requirement (P_{av}) is approximated based on the estimated energy requirement (E^*_{total}) of the drive cycle. The developed power of the ICE is subtracted from the initial estimated energy requirement to determine remaining average tractive power estimates. This is evident from the decreasing average tractive power requirement over time during the drive cycle in Figure 5.12. Towards the end of the drive cycle erratic transients occur in the estimated tractive power, due to the low level of remaining tractive energy of equation 5.57 with respect to the load transients of the drive cycle. This highlights the importance of including the modes of Sections 5.7.3 and 5.7.4 such that the operation of the ICE is not reliant on the erratic behaviour of the average tractive power estimate toward the end of a planned trip.

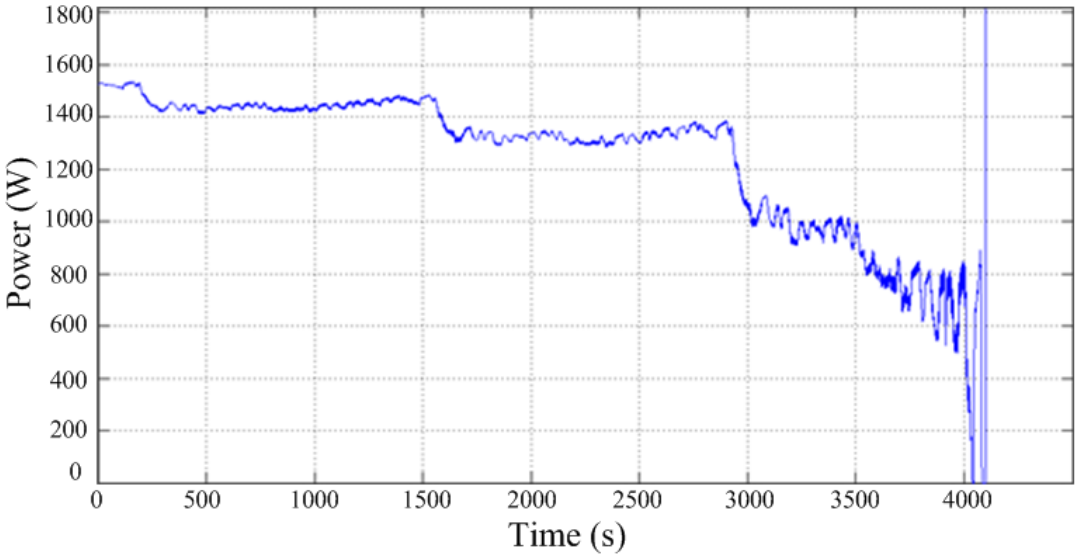

Figure 5.12 - Example of estimated tractive power (P_{av}) over three continuous runs of the UDDS.

Figure 5.13 is an example of predicting the high efficiency region over the UDDS with the $\eta_{e,low(1)}$ = 0.2 and $\eta_{e,low(n)}$ = 0.34 (Section 5.7.2). During the majority of time periods where the ICE is restricted to $\eta_{e,low}$ = 0.2 in Figure 5.13 the ICE is switched off, the recorded signal assumes that the ICE always operates such that when it does switch on it will have the minimum efficiency identified. An interesting point to note from Figure 5.13 is that the majority of ICE operation is restricted to the calibrated high efficiency region of the HEC-V controller in Section 4.9 with $\eta_{e,low}$ = 0.28, supporting the use in the non-predictive controller.

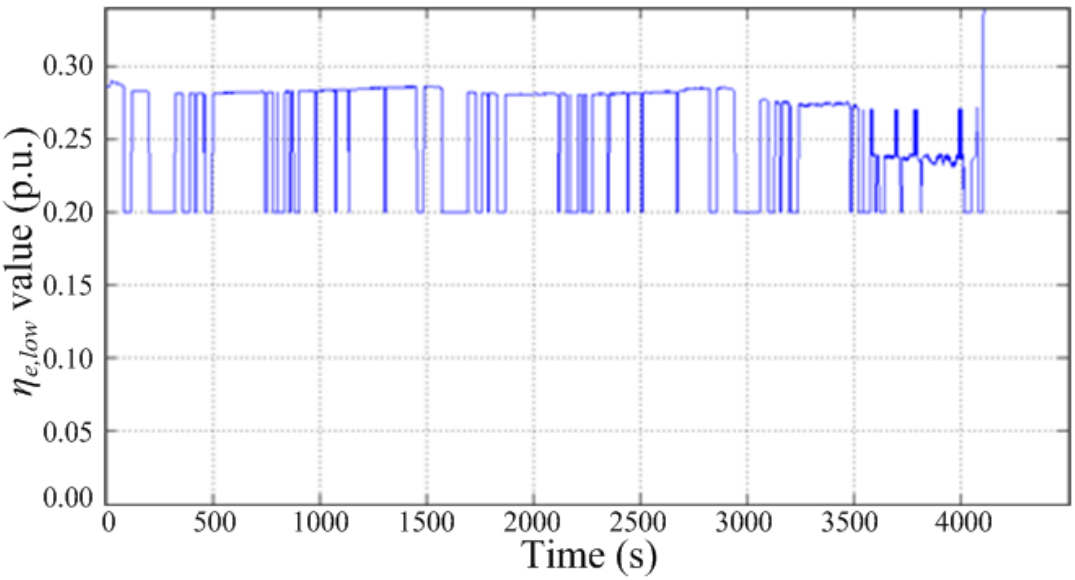

Figure 5.13 – Predicting $\eta_{e,low}$ from the average power requirement of Figure 5.12 over three continuous runs of the UDDS.

5.8.3 Preliminary Results for Controller Operations

Here the three controllers are intended to operate as PHEV in which case charging of the ESS occurs at the end of a driving period. However, to show a fair comparison of the three controllers SOC correction is utilised as if charging of the ESS occurs by the ICE. This endeavours to demonstrate that even though the predictive controller is more heavily reliant on the ESS stored energy it is minimising fuel consumption based on the energy requirements of the drive cycle. One of the main outcomes for this Section is that simply operating a HEV with increased reliance on the ESS does not lead to improved overall efficiency of the vehicle.

Table 5.4 identifies the performance of the three controllers before any corrections are considered. The first point to note is that the predictive controller is reducing the fuel consumption over city drive scenarios (UDDS and NEDC), however, it struggles on the highway driving scenario (HWFET). Secondly, in terms of the drivability as discussed in Section 4.9.3, with respect to the analysis completed in [38] the operation of the predictive controller on the NEDC is a potential concern.

Assuming that the same outcomes from [38] apply to hybrid vehicles in general the following is concluded. Operation observed an increase in the number of ICE events from 11 to 16 for the non-predictive controller and then up to 31 ICE events for the predictive controller. Over the full drive cycle this is just under 3 ICE events per kilometre for the predictive controller. Considering that the total number of ICE events reported in [38] on the federal test procedure (FTP) drive cycle observes up to 5 ICE events per kilometre the ICE is capable of sustaining the start/stop frequency as per the predictive controller. In addition, the predictive controller experiences one ICE event every 38 seconds compared against the test vehicle of [38], which experiences one ICE event every 23 seconds. For the UDDS and HWFET the total number of ICE events are similar or less than the original controller and therefore will not negatively affect performance [38]. The analysis completed in [38] suggests that operating the Toyota Prius 2010 with the predictive controller has little to no adverse effects on the drivability. This leads to the consideration of SOC corrections in demonstrating the improved operating efficiency using the predictive controller.

Table 5.4 - Operation of the three controllers with the inclusion of a charge depletion mode at the end of driving. Original is the controller developed from the measured data, HEC-V is the high efficiency controller from Section 4.9.6 and HEC Predictive is the predictive high efficiency controller described in this Chapter.

Drive Cycle	Component Parameter	Toyota Prius 2010		
		Original	HEC-V ($\eta_{e,low1}$ =20, $\eta_{e,low2}$ =28)	HEC Predictive
UDDS	Tractive Energy (kJ)	1256.73	1256.80	1256.71
	Energy Used (kJ)	12561.97	11508.11	10936.19
	Overall Efficiency (%)	10.00	10.92	11.49
	Fuel Cons. (L/100km)	3.22	2.91	2.68
	ICE Events	56	59	44
	Generating AVG Efficiency	86.50	87.11	87.53
	ESS AVG Charge Efficiency (%)	89.77	89.52	89.48
	ESS Initial SOC (%)	60.00	60.00	60.00
	ESS Final SOC (%)	53.79	51.31	45.72
	Fuel Cons. Improvement (%)	-	**9.67**	**16.73**
HWFET	Tractive Energy (kJ)	3275.89	3275.87	3275.87
	Energy Used (kJ)	17219.47	15838.85	16127.08
	Overall Efficiency (%)	19.02	20.68	20.31
	Fuel Cons. (L/100km)	3.29	2.95	3.00
	ICE Events	5	5	5
	Generating AVG Efficiency	90.15	89.78	89.71
	ESS AVG Charge Efficiency (%)	92.40	90.68	90.56
	ESS Initial SOC (%)	60	60.00	60.00
	ESS Final SOC (%)	60.39	52.11	51.64
	Fuel Cons. Improvement (%)	-	**10.52**	**9.00**
NEDC	Tractive Energy (kJ)	1643.56	1643.56	1643.55
	Energy Used (kJ)	11780.98	10416.85	10115.89
	Overall Efficiency (%)	13.95	15.78	16.25
	Fuel Cons. (L/100km)	3.39	2.85	2.64
	ICE Events	11	16	31
	Generating AVG Efficiency	87.62	85.62	88.12
	ESS AVG Charge Efficiency (%)	91.72	90.04	90.47
	ESS Initial SOC (%)	60	60.00	60.00
	ESS Final SOC (%)	59.77	49.78	41.52
	Fuel Cons. Improvement (%)	-	**16.04**	**22.26**
Acceleration Performance	0-100km/h (sec)	10.7	12.7	12.6

5.8.4 Operation of Controllers in HEV

Due to the inability of HEV to recharge the ESS from the grid at the end of driving the fuel consumption performance of controllers featured in recent research are subject to SOC corrections. This SOC correction demonstrates a fair comparison of each controllers operation such that fuel consumption reductions are due to factors other than the relocation of load requirements from the ICE to the ESS [44, 170]. The SOC correction is determined for increased average fuel consumption relative to the difference between the initial and final SOC [33].

$$\Delta FC = \frac{100 E_{ess,total}\left(SOC_{init} - SOC_{final}\right)}{1000 \eta_e^{opt} \eta_{m/g} \eta_{chg} Q_{HV} \rho_f d} \tag{5.66}$$

where ΔFC is the change in final fuel consumption due to recharging the ESS, $E_{ess,total}$ is the total capacity of the ESS, SOC_{init} is the initial SOC, and SOC_{final} is the final SOC, η_e^{opt} is the optimal ICE efficiency of operation at stand still, $\eta_{m/g}$ is the average M/G efficiency during charging, η_{chg} the average ESS charge efficiency (both $\eta_{m/g}$ and η_{chg} values are taken from Table 5.4), Q_{HV} the high heating value of the fuel, ρ_f the density of the fuel and d the distance covered by the vehicle during the drive test. The additional energy consumed from recharging the ESS using the ICE is calculated using:

$$\Delta E_{HEV} = \frac{E_{ess,total}\left(SOC_{init} - SOC_{final}\right)}{\eta_e^{opt} \eta_{m/g} \eta_{chg}} \tag{5.67}$$

with the new total energy used being:

$$E_{corrected} = E_f - E_{ess} + \Delta E_{HEV} \tag{5.68}$$

If final SOC is greater than the initial SOC the recorded fuel consumption from simulations remains unchanged. This is due to the consideration that once fossil fuel has been consumed it cannot be reformed or regenerated. Table 5.5 identifies the corrected energy consumption, overall efficiency and fuel consumption of the three controllers using the data of Table 5.4 and equations 5.66 to 5.68. Initially the results suggest that there is no benefit in using the HEC predictive controller in comparison to the original controller since the HEC predictive controller has increased fuel consumption on the NEDC.

Due to the optimisation approach in the predictive controller it relies more heavily on the ESS knowing that it does not need to conserve stored energy for later use. The increased fuel consumption in the predictive controller over the NEDC is therefore a result of consuming increased amounts of ESS energy during blended charge depletion as opposed to the vehicle operating inefficiently. The predictive controller observes that it is approaching the end of

the drive cycle and therefore does not need to maintain the ESS SOC for future tractive load requirements. This results in the decision to discharge energy from the ESS to satisfy load demand.

Table 5.5 - SOC correction using the ICE for the three controllers over a single run of each of the drive cycles.

Drive Cycle	Component Parameter	Original	HEC-V	HEC Predictive
UDDS	Energy Used (kJ)	13722.78	13125.72	13583.30
	Overall Eff. (%)	9.16	9.58	9.25
	Fuel Consumption (L/100km)	3.52	3.33	3.38
	Fuel Cons. Improvement (%)	-	**5.42**	**4.19**
HWFET	Energy Used (kJ)	17152.21	17245.09	17620.14
	Overall Eff. (%)	19.10	19.00	18.59
	Fuel Consumption (L/100km)	3.28	3.21	3.28
	Fuel Cons. Improvement (%)	-	**1.99**	**0.00**
NEDC	Energy Used (kJ)	11822.31	12340.78	13481.70
	Overall Eff. (%)	13.90	13.32	12.19
	Fuel Consumption (L/100km)	3.41	3.41	3.61
	Fuel Cons. Improvement (%)	-	**0.00**	**-5.96**

High efficiency control is demonstrated by increasing the distance driven by the vehicle for the same drive cycles. Table 5.6 lists the SOC correction for the three controllers' performance over three runs of each respective drive cycle. By simulating the three controllers for three runs of each drive cycle the distance travelled by the vehicle is increased. This means that the ESS stored energy must be conserved in order to maintain ESS SOC until the end of driving. Observing the improvement to fuel consumption of the two proposed controllers after SOC correction over the three runs of each drive cycle concerns for the efficiency of operation are mitigated.

On the other hand, Table 5.6 suggests that the autonomous optimisation using the predictive controller is not as efficient as the calibrated non-predictive controller. This indicates that for autonomous optimisation there is a small sacrifice to the efficiency of operation. In the case of the original controller it operates in normal mode of operation until the final stages of the drive cycle as discussed in Section 5.8.1. Then when it finally enters the charge depletion mode there is not enough tractive energy demand remaining in the current drive period to utilise the ESS energy. This results with the original controller consuming ESS energy without showing any benefit in reducing the average fuel consumption.

Table 5.6 – SOC correction using the ICE for the three controllers over three continuous runs of the respective drive cycles.

Drive Cycle	Component Parameter	Original	HEC-V	HEC Predictive
3x UDDS	Energy Used (kJ)	39809.22	37393.19	38970.05
	Overall Eff. (%)	9.47	10.08	9.67
	Fuel Consumption (L/100km)	3.46	3.24	3.31
	Fuel Cons. Improvement (%)	-	**6.35**	**4.32**
3x HWFET	Energy Used (kJ)	51540.68	49845.35	51045.62
	Overall Eff. (%)	19.07	19.72	19.25
	Fuel Consumption (L/100km)	3.28	3.15	3.22
	Fuel Cons. Improvement (%)	-	**4.12**	**2.04**
3x NEDC	Energy Used (kJ)	35420.10	34431.42	35216.67
	Overall Eff. (%)	13.92	14.32	14.00
	Fuel Consumption (L/100km)	3.40	3.26	3.30
	Fuel Cons. Improvement (%)	-	**4.13**	**3.00**

The results of Table 5.6 indicate that both the non-predictive and predictive controllers are achieving their targets of reduced fuel consumption. Over a long distance of driving there is a clear savings in the fuel consumption even when the SOC correction is undertaken by the ICE. The reason for increased fuel consumption in the single run of each drive cycle (for the predictive controller in Table 5.6) is because the controller has realised it can rely more heavily on the stored energy given the anticipated grid charging at the end of the planned driving route. The performance comparison of the three controllers operating in PHEV is determined through recharging the ESS from the grid.

5.8.5 Operation of Controllers in PHEV

For consideration as a PHEV the SOC correction is included by charging from the grid as a fair comparison of the energy requirement of each of the three controllers.

$$\Delta E_{PHEV} = \frac{E_{ess,total}\left(SOC_{init} - SOC_{final}\right)}{\eta_{chg}} \tag{5.69}$$

The calculated energy of equation 5.69 which is consumed from the grid in order to charge the ESS to the initial SOC after each respective drive cycle, is added to the total energy consumed during driving for calculation of the overall efficiency. Results are listed in Table 5.7 and Table 5.8. Any additional losses incurred from the grid will be the same for each controller since charging the ESS is independent of driving the vehicle. Table 5.7 and Table

5.8 suggest that the predictive controller is capable of reducing the fuel consumption more effectively in city driving scenarios.

This is due to the city driving scenario requiring lower power on average than the highway driving and therefore allowing for the use of ESS energy more frequently. For example the average tractive power for the HWFET is 4.3 kW over the full drive period, while the average tractive power for the UDDS and NEDC over the full drive period is 0.9 kW and 1.4 kW respectively. These average tractive power requirements are determined over the full drive period whereby the ICE is operating for some fraction of the total time. In addition, the average tractive power values identified above increase with losses of the drivetrain and powertrain. This means that in the case of the HWFET there is more chance for the average ICE requested power to exceed the maximum ICE power (max($\overline{P}_{e,av}$)) of the $\overline{\eta}_{e,low}$ look up table of equation 5.60 in Section 5.7.2. In such cases the controller will select the minimum value of the $\overline{\eta}_{e,low}$ look-up table ensuring that the ICE is unrestricted and allow for any acceleration transients that may occur at higher speeds. This leads to the potential for increased fuel consumption during highly transient loading. For the most part the results of Table 5.7 and Table 5.8 highlight that the predictive controller is capable of minimising fuel consumption over the drive period while maintaining efficient operation without the need for calibration.

Table 5.7 – SOC correction using the grid for the three controllers over a single run of each of the drive cycles.

Drive Cycle	Component Parameter	Original	HEC-V	HEC Predictive
UDDS	Energy Used (kJ)	12923.45	12015.37	11770.32
	Overall Eff. (%)	9.72	10.46	10.68
	Fuel Consumption (L/100km)	3.22	2.91	2.68
	Fuel Cons. Improvement (%)	-	**9.67**	**16.73**
HWFET	Energy Used (kJ)	17197.64	16293.36	16609.26
	Overall Eff. (%)	19.05	20.11	19.72
	Fuel Consumption (L/100km)	3.29	2.95	3.00
	Fuel Cons. Improvement (%)	-	**10.52**	**9.00**
NEDC	Energy Used (kJ)	11794.02	11009.88	11183.59
	Overall Eff. (%)	13.94	14.93	14.70
	Fuel Consumption (L/100km)	3.39	2.85	2.64
	Fuel Cons. Improvement (%)	-	**16.04**	**22.26**

Table 5.8 - SOC correction using the grid for the three controllers over three continuous runs of the respective drive cycles.

Drive Cycle	Component Parameter	Original	HEC-V	HEC Predictive
3x UDDS	Energy Used (kJ)	38860.71	36223.31	35952.46
	Overall Eff. (%)	9.70	10.41	10.49
	Fuel Consumption (L/100km)	3.33	3.09	2.92
	Fuel Cons. Improvement (%)	-	**7.44**	**12.46**
3x HWFET	Energy Used (kJ)	51586.25	48905.18	49814.96
	Overall Eff. (%)	19.05	20.10	19.73
	Fuel Consumption (L/100km)	3.29	3.06	3.10
	Fuel Cons. Improvement (%)	-	**6.94**	**5.69**
3x NEDC	Energy Used (kJ)	35390.51	33250.50	33177.13
	Overall Eff. (%)	13.93	14.83	14.86
	Fuel Consumption (L/100km)	3.40	3.10	3.01
	Fuel Cons. Improvement (%)	-	**8.88**	**11.37**

5.8.6 Error Tolerance in Predictive Control

Estimating the required energy and trip time of a planned route leaves room for uncertainty due to a number of reasons [127]. This Section offers a comparison of the predictive controller's ability to maintain minimum fuel consumption relative to errors in estimating the required energy and trip time of planned routes. Using GPS [127] and intelligent transportation systems [167] the ability of EMS controllers to estimate required energy and trip times of daily commutes is improved. There is minimal chance that the daily commute will vary significantly with respect to the final time or energy requirement of driving since speed limits are set and congestion is expected during peak times. With this in mind the tests completed here assume that no more than 20% error in the estimated quantities would occur for a planned trip.

Referring to Table 5.9, the error in predicting required energy (E^*_{total}) and trip time (t^*_{trip}) are applied to each of the drive cycles (UDDS, HWFET and NEDC) separately and the results are used to determine the MAPE (%) and variance (σ^2 in L/100km) in the fuel consumption. Table 5.9 identifies that for a 20% error in the estimated trip time of a planned route no more than ±0.62% variation will result in the final fuel consumption. For example the final fuel consumption of the predictive controller as it has performed on the UDDS (listed in Table 5.4) may be 2.68 ± 0.62% if the error in t_{trip} is ±20% respectively. With the consideration of

increased sensitivity for updating the predicted quantities E^*_{total} and t^*_{trip} using recorded tractive energy, GPS [127] or intelligent transportation system [171] information, the error in estimation will reduce thus Table 5.9 highlights a worst case scenario. The robust nature of the controller is due to the recalculation of P_{av} with respect to the approximate E^*_{total} and remaining trip time (t^*_{trip}). As the vehicle approaches the destination both values of E^*_{total} and t^*_{trip} reduce toward zero, providing an acceptable reference (P_{av}) for the selection of $\eta_{e,low}$ values on-the-go.

Table 5.9 – Error in fuel consumption due to uncertainty in predicted quantities.

Component Parameter	1 x Drive Cycle		3 x Drive Cycles	
	MAPE (%)	σ^2 (L/100km)	MAPE (%)	σ^2 (L/100km)
E^*_{total} **±10%**	0.01	0.0004	0.01	0.0003
E^*_{total} **±20%**	0.13	0.0035	0.06	0.0017
t^*_{trip} **±10%**	0.19	0.0055	0.41	0.0120
t^*_{trip} **±20%**	0.62	0.0182	0.36	0.0109

5.9 Summary of Predictive Control in PHEV

The use of GPS and intelligent transportation systems in EMS aids with the prediction of planned driving route information. In particular, the energy requirement of driving and the total trip time allow the EMS to predict ICE operation times and loads. Using the expected values of average vehicle velocity and absolute average acceleration/deceleration of the vehicle, the EMS estimates the tractive energy requirement. This approach demonstrates one of the possible methods for predictive control. It is expected that with increased frequency of sampling the future tractive energy requirements, that the accuracy of the predicted energy requirement will improve. Increased accuracy in predicting the energy requirement of driving will lead to greater potential for fuel savings using the defined EMS controller.

Use of the predicted energy requirement is applied to the EMS controller via the principles of ICE on/off and ESS SOC swing control. This is then utilised to select the $\eta_{e,low}$ value for the high efficiency control of the ICE. The ICE will supply average tractive power in addition to charging the ESS during the on phase, while the ESS will supply the load during the ICE off phase. This ensures that charging of the ESS is occurring during high efficiency of operation of the ICE and potentially reduces the total number of ICE events. For the implemented version of this controller on the Toyota Prius 2010 test bench the power rating of the M/Gs is not sufficient to sustain all requested drivetrain loads when the ICE is switched off. Thus the ICE on/off strategy must be altered in order to meet the power demand of the drivetrain and therefore the vehicle velocity trace of the drive cycles.

This leads to a charge and discharge phase of the ESS relative to the ICE output power requested. Defining an objective function for minimised fuel consumption with respect to the high efficiency region the controller aims to increase average powertrain efficiency while minimising fuel consumption over the entire drive period. In this case $\eta_{e,low}$ for the high efficiency control of the ICE is determined from the average tractive power requirement and expected operating efficiency of the drivetrain and powertrain components. Using a look-up table $\eta_{e,low}$ is selected by comparison with the known ICE power (P_e) at which the corresponding ICE performance map develops the desired efficiency ($\eta_e(P_e)$). Then optimal efficiency of operation for the ICE is achieved using VSC in combination with PBS as discussed in Section 4.3.3. Monitoring the SOC of the ESS with respect to E^*_{total} and t^*_{trip}, overcharge and over discharge are avoided maximising the use of stored energy and minimising fuel consumption. This is essential for optimal performance of PHEV.

Performance of the predictive controller is examined for two cases; a HEV with SOC correction using the ICE and a PHEV with SOC correction using the grid. For the HEV case SOC correction reveals that for short trips the predictive controller is consuming more fuel than necessary since it is relying more heavily on the ESS. This would be a concern if the predictive controller was not capable of maintaining the ESS SOC for longer trips. Extending the distance travelled by the Toyota Prius 2010 using the three controllers it is revealed that the predictive controller has reduced fuel consumption for operation as a HEV. For the HEV case fuel consumption improvement is observed at up to 6% and 4% for the non-predictive and predictive controllers respectively. The non-predictive controller outperforms the predictive controller for this case since the predictive controller has been calibrated for the selected drive profiles. In addition, the $\eta_{e,low}$ value selected in the calibrated non-predictive controller is supported by the calculated value of $\eta_{e,low}$ in the predictive controller (i.e. $\eta_{e,low}$ = 0.28 in Figure 5.13). As discussed in Section 4.9.6 incorrect calibration of the non-predictive controller may lead to unwanted levels of fuel consumption.

Operation as a PHEV with charging from the grid reveals the predictive controllers ability to minimise fuel consumption. The prediction of the tractive energy requirement for driving alerts the EMS that it no longer needs to maintain the ESS SOC. The control strategy ensures that the loads placed on the ICE are transferred to the ESS with the new target SOC (e.g. SOC_{target} = 30% instead of 60%). The results demonstrate up to 16% and 22% fuel consumption improvement for the non-predictive and predictive controllers respectively, during city drive scenarios. The predictive controller achieves efficiencies similar to the calibrated non-predictive controller through autonomous selection of $\eta_{e,low}$ as determined using the predicted energy requirement.

Finally, the error tolerance of the predictive controller is quantified through the effect on final fuel consumption. This analysis leads to the conclusion that for a large error in the predicted trip time (up to 20%) the variation in the fuel consumption will be less than 0.62% for short trips and reducing for longer trips (0.41% for 3 x Drive Cycles case). This is demonstrated for a worst case scenario, such that the energy requirement and trip time are predicted at the beginning of driving. With increased sampling frequency of the required tractive power and trip time the variation in the final average fuel consumption is expected to reduce. Considering the low MAPE as well as variance the EMS controller is already providing a robust reference point for the selection of $\eta_{e,low}$ values in light of the potential uncertainty in traffic and drive conditions. This analysis demonstrates the robust nature of the designed predictive controller.

CHAPTER SIX

Conclusions

6.1 Outcomes for Research Program

This thesis focussed on the design and control of both a non-predictive and predictive real-time optimisation based blended controller for high efficiency control of power-split PHEVs. The outcomes for the research program are summarised with respect to the research questions outline in Section 1.3.2. The original controller refers to the controller developed from the measured data of the three existing vehicles featured in Chapter 3. The non-predictive controller refers to that resulting from Chapter 4 which requires calibration for high efficiency control of the three test benches. Lastly, the predictive controller refers to that resulting from Chapter 5 utilising expected tractive energy requirements to autonomously calibrate the high efficiency control for operation on the power-split PHEV.

From the perspective of source-to-tank [7], Section 1.1 identified the World's available energy sources and current usage. This discussion highlighted that an alternative means to fossil energy consumption is required especially in the transportation sector. In particular, reports suggest that the World is still very reliant on fossil energy resources and will be for a significant period of time because of rising energy demands. An alternative offered in many research papers is the use of electrical energy in EVs since it is considered emissions free. This ideology for EVs is, however, unrealistic. The projection for total renewable energy sources used in the electricity sector is expected to rise from 20.6% to 24.6% from 2010 to 2040 with at least 60% of the total generated electricity coming from fossil fuel. In addition, 60 to 80% of the World's renewable energy (in the electricity sector) is sourced from hydropower over this period (2010 to 2040), requiring mountainous regions and high annual rain falls to sustain the high energy output before transferring this energy to where it is needed. In Australia in 2010 renewable energy sources made up 10% of the total generated electricity, with more than 90% sourced from fossil resources. Penetration of renewable energy generation in Australia's electricity sector is expected to exceed 20% by 2020, however, judging from World growth 10% over 10 years is optimistic. This indicates that the EV being emissions free during driving, is not enough to justify it as the best alternative to the conventional vehicle since the majority of EV stored energy is sourced from fossil resources.

Chapter Six: Conclusion

Observing the general uses of ESVs with respect to driving requirements reduces the scope for the best alternative to the conventional vehicle. There are four main alternative ESVs available for replacing the conventional ICE vehicle; EVs, fuel cell vehicles, HEVs and PHEVs. Initially it was observed that the use of EVs alone leaves a lot to be desired concerning the required performance in passenger vehicles. The EV limits the drive range while requiring large charge times to replenished on-board energy storage. The fuel cell vehicle while demonstrating the ability to prolong the energy storage suffers from waste energy required for hydrogen storage. In addition, the energy to volume density of hydrogen storage devices is lacking in comparison to ESS and fossil fuels making them an unattractive source of energy in transportation. HEV on the other hand utilise the ICE in combination with the ESS for improved average efficiency. By using the ICE to satisfy steady-state demands and the ESS to meet transient load requirements, the HEV offers more efficient operation than the conventional vehicle and fuel cell vehicle while having a larger drive range than the EV. Alternatively the PHEV is much the same as the HEV, except that it has a larger ESS. The PHEV is therefore able to operate as an EV for a short drive period before operating as a HEV. By this consideration it was noted that PHEV have the potential to operate as efficiently as EV without the concern for range anxiety.

Inspecting the powertrain and drivetrain connections, and modes of operation in HEV and PHEV various advantages and disadvantages are revealed in light of the vehicle configuration. The three main vehicle configurations include the series, parallel and power-split connections. The series connection determines ICE operation independent of the driven wheels, increasing average ICE efficiency. The concern for the series connection, however, is increased losses in the drivetrain resulting from the conversion of energy. The parallel connection offers increased efficiency in the drivetrain because of a direct mechanical coupling, however, the ICE is restricted by the vehicle speed. This leads to a lower average ICE efficiency. Alternatively, the power-split configuration provides independent ICE operation with the option for direct mechanical coupling to the wheels. Examining the energy outlook and alternative ESVs the power-split PHEV determines a pathway for transitioning the World into sustainable transportation.

Section 2.6 defined the relative means for sizing the components in HEV and PHEV for everyday driving using an example experimental setup. Typically component sizing relies on the use of standardised drive cycles such that these drive cycles represent the expected steady-state and transient operations expected from a vehicle. The power and energy density for an approximate mass and shape of the vehicle relative to standardised drive cycles determine the power rating of propulsion devices. In particular, it is expected that the ICE will provide the average power requirement of driving while the ESS and M/G will provide

the transient power requirements. Following the selection of propulsion device power rating specifications including torque, speed, input voltage, and input current with respect to the driven wheels, drivetrain requirements such as transmission and final drive gear ratios are determined. This sizing process is undertaken for a 2 by 2 power-split PHEV with a scale version of the NEDC. The 2 by 2 power-split PHEV is chosen since it excludes the expensive PGS while maintaining the flexibility in control demonstrated by the power-split connection. Following the calculation of component sizes the specifications are verified in simulation. This verification ensures that load power, tractive torque and the vehicle speed trace of the drive profile for which the vehicle is designed are met, while ensuring that the ESS has sufficient energy storage to support ICE operations.

For the discussion relating control strategies to the power-split PHEV four categories are considered. These include hybrid, multimode, rule-based blended and optimisation based blended controllers. The examination of recent research found in technical papers realised that optimisation-based blended control offers robust, flexible, efficient and accurate means for controlling PHEV and HEV. Global optimisation while it provides potential for fuel savings requires high computational requirements which limit the applications and portability. Real-time optimisation on the other hand has the ability to determine an optimal solution to current loading requirements while acknowledging future loads with the integration of driver information, traffic conditions and planned driving routes. There is, however, the concern of increased computational requirements in real-time control due to the inclusion of large amounts of driver and vehicle information. This research aims to maximise the benefits to fuel savings whilst minimising the computational requirements. This is achieved by considering real-time optimisation relative to input and output energy and thereby overall efficiency.

Research questions 1 to 3 determine the focus for the investigation of the controller in the EMS of an ESV; real-time optimisation-based blended control of the power-split PHEV. Further definition of the components inherent on such a vehicle configuration distinguishes the varying operating principles and characteristics. From the perspective of tank-to-wheels as defined in [7], the ICE, M/G, ESS and drivetrain are examined in light of their contributions to overall operation. The ICE offers sustained energy density as the primary propulsion device during hybrid operations, however, this occurs with inefficient consumption of fossil fuels and thereby significant emissions. The M/G and ESS offer limited energy density at high efficiency during all drive modes, while ESS life expectancy is low (less than 8 years). As a result of the discussion provided in Chapter 2 relative to the propulsion devices and potential control, the aim is to maximise efficiency of operation along with component life expectancy. Optimising these two main control problems using a

single EMS controller reveals a robust, computationally low and easily implementable method for improved performance in new and existing HEVs and PHEVs.

Following the investigation of the experimental setup, budget constraints meant that available software packages had to be used. ADVISOR, a MATLAB/Simulink add-on, which takes advantage of the backward-forward facing approach to simulation is utilised for the testing of vehicles and control strategies in this thesis. Three test benches are created in the ADVISOR software using measured data from three commercially available vehicles. The three vehicles are the Toyota Prius 2010, Hyundai Sonata Hybrid 2011 and Honda CR-Z 2010. The Toyota Prius 2010 is a power-split HEV while the Hyundai and Honda are both parallel HEVs. The selection of two parallel vehicles serves to demonstrate the application of the high efficiency control to various topologies, hence, identifying with a portable and robust controller. Investigating the tractive power requirement, ICE, ESS and M/G operations of the three vehicles leads to the confirmation of powertrain and drivetrain specifications before detailing the underlying control strategies.

Limitations of the measured data are acknowledged in order to make reasonable assumptions for simulation. It was noted from the comparison of a moving mass and the results obtained from the chassis dynamometer (Section 3.4) that the tractive power analysis measured on the chassis dynamometer is less than expected. While the measured data has discrepaencies in comparison to real world driving scenarios such as a reduced fuel consumption, the data provides a starting point for the development and evaluation of the controllers presented in this thesis. Through using the measured data it is known that the tractive power requested at the wheels of the vehicle will invoke a unique response from the drivetrain regardless of the resulting performance. If the simulation results reflect the same response of the existing vehicle then the measured data serves as an acceptable bench mark for developing models of the vehicles in simulation.

In addition, mismatch between measured signals is identified reducing the accuracy of transient information. As a result of the analysis of the measured data it was observed that some signals measured at input demonstrate the expected relationship to signals measured at output. This is thought to be due to the time delay between input and output of the dynamics of the mechanical system such that power in the fuel that is injected at ICE input will take time to reach the driven wheels. For each transient operation it was also noted that this time delay varied and thus it is difficult to match up the signals even if a constant time delay were introduced. By this consideration if the injected fuel is varied significantly then the measured data will show inconsistency between input and output. This meant that the measured data can only be used as a guide for the transient operation of the existing vehicles. The measured data does, however, contain all transients of the vehicle throughout the drive period and thus

the quantities of measured signals at input and received at output represent the performance of the vehicles accurately.

Analysis of the measured data helped to confirm the main control problem for investigation in this thesis. It is however possible to utilise the data to gain an idea of ICE operation. In particular the Toyota Prius is demonstrated to operate according to the optimal operating line using VSC. Following the operation of the ICE in the Toyota Prius, low average efficiency of the ICE is demonstrated using the measured data as a result of the lack of PBS occurring in ICE developed power. More than 60% of the ICE operation in the Toyota Prius over the UDDS is occurring at efficiencies below 25%. With demonstrated efficiencies of more than 30% in the Toyota Prius the data suggests that there is potential for fuel savings by increasing the average power requested from the ICE. This analysis supports the general concern about low ICE efficiency and leads to the motivation for the developed high efficiency controller.

In terms of a bench mark the three vehicles' original controllers are developed for comparison with the two designed controllers featured in this thesis. It is revealed from the analysis of the three vehicles that the original controllers perform similar to equivalent consumption minimisation strategies. However, due to the unknown objective function of the equivalent consumption minimisation strategy and the identified mismatch between input and output signals, it was decided to utilise a set of rules for the original controller. Referring to the measured data, overall performance of the original controllers is verified in simulation to within 3.87% error. Observing the signals of the three original controllers the reasons for errors are apparent, however, as a whole system the input and output energy, overall efficiency and fuel consumption over two drive cycles demonstrates that the three vehicles are accurately represented in simulation. By matching these performance totals of the simulated and measured data the three models are shown to be accurate representations of the three commercially available vehicles.

Chapter 4 identified the design of a high efficiency controller for PHEVs in light of the need for a real-time optimisation based blended controller. In response to research questions 7 and 8 investigations began with a focus on maximising efficiency of the ICE relative to two existing ICE control methods; VSC and PBS. Local optimisation of the ICE resulted from the concern for low average ICE efficiency, however, as discussed in Section 4.5, high efficiency control of one propulsion device alone does not constitute high efficiency control of the whole system. Therefore, additional control constraints were introduced in order to meet the tractive power requirements of driving and to maintain ESS SOC.

Maintaining ESS SOC as a secondary objective in the designed controller determines the basis for prolonging ESS life expectancy. Research into the life expectancy of ESSs (especially batteries) indicates that a small SOC swing is beneficial as outlined in Section 4.4.1 (first introduced in Section 2.2). Therefore, it is envisaged that operating the ESS to within a specific SOC swing will minimise the total number of charge/discharge cycles. For requested tractive power that lies outside the high efficiency region defined for the ICE, the determining rules delegate whether to relocate operation to the high efficiency region or whether to supply using the ESS. This decision is based on the power balancing that occurs between the ICE and ESS. Power requested for charging the ESS is generally much smaller than the tractive power requirement, thus charging during tractive power supply is more beneficial to ESS operation than charging the ESS alone. In addition, by restricting ICE operation to the high efficiency region and balancing tractive power using the ESS, the EMS controller observes minimal losses when consuming fossil fuel. This is the underlying consideration for high efficiency control in PHEV.

The designed controller is robust, computationally low, and easily implemented on the three test benches for improved performance. Performance of the designed high efficiency controller is evaluated with respect to fuel consumption, overall efficiency and drivability. Effects on noise, vibration and harshness and emissions reductions are expected to be minimised or accounted for outside of the optimisation. Noise, vibration and harshness are considered a control problem for local optimisation such that global optimisation is applied with noise, vibration and harshness constraints. These constraints for example include delay times for component torque and speed transition, and inertia of components. Emissions on the other hand are expected to be reduced by the high efficiency operation of the ICE since prior research has demonstrated increased emissions at low ICE torque and speed conditions. Fuel consumption is reduced by up to 12% with maintained ESS SOC. The total number of ICE and gear shift events quantifies the effect on the drivability. The analysis shows that the three test benches have a similar number of ICE and gear shift events for the original and designed controllers suggesting that drivability is unchanged.

The importance of calibration of the high efficiency controller presented in Chapter 4 is realised from the analysis of operation with varying the high efficiency region (i.e. different values of $\eta_{e,low}$). Varying the selected value of $\eta_{e,low}$ by one or two increments ($\Delta\eta_{e,low} = 0.01$) fuel consumption or ESS final SOC vary significantly. This analysis also demonstrated the need for varying $\eta_{e,low}$ according to the speed of the vehicle such that fewer restrictions should be placed on the ICE at higher speeds. Employing two values of $\eta_{e,low}$ with a threshold of 12 m/s for vehicle velocity, realised improved performance on the HWFET drive cycle with minimal adverse effects resulting on the UDDS and NEDC. With improved

fuel consumption for a suboptimal selection of $\eta_{e,low}$ it was considered that the high efficiency region for ICE operation is tuneable with respect to the tractive power requirements on-the-go.

Predictive control endeavours to notify the EMS controller of future driving events and the cost they may have to the HEV or PHEV. One of the more common predictions made is the energy requirement for driving such that the EMS controller knows in advance when to utilise the ESS stored energy and when to conserve it. Information needed for calculating the energy requirement of driving includes driver behaviour, traffic conditions and the planned driving route. At a more complicated level individual power requirements are determined in an attempt to accurately project loading for the EMS controller. High levels of accuracy in predicting future energy requirements demands large amounts of information and processing power, ultimately leading to a computationally complex and expensive EMS controller. Therefore a computationally low predictive controller is proposed for the autonomous calibration of the high efficiency controller of Chapter 4.

Through the use of technology such as GPS or intelligent transportation systems the designed predictive controller is capable of forecasting the total tractive energy requirement of a planned driving route. The predictive control described in this thesis uses expected average vehicle velocity and absolute average acceleration/deceleration. These quantities are estimated with respect to expected traffic conditions, driver behaviour, speed limits and estimated time of arrival and then used to calculate the total tractive energy requirement of the drive cycle. The result is a predictive real-time optimisation-based blended controller employing blended charge depletion of the ESS from the initial SOC to a defined minimum SOC.

Using the estimated total tractive energy requirement in comparison to the consumed energy during driving the designed predictive controller calculates the average tractive power requirement of driving and uses this to determine the high efficiency region of the ICE. A look-up table provides a link between the ICE performance map and the requested output power for selecting the $\eta_{e,low}$ value for the high efficiency region on-the-go. The optimal $\eta_{e,low}$ value also corresponds to the optimal operating line for maximised efficiency at the requested power level using VSC. Using the predicted average tractive power requirement with respect to the estimated time of arrival the EMS controller is capable of maintaining ESS SOC until the end of a planned driving route. In addition, overcharge and over discharge considerations help to maximise the use of stored energy as well as maintaining ESS SOC until the end of driving.

Implementing charge depletion/charge sustenance strategies for the original and non-predictive controllers featured in Chapter 4, provides a fair comparison for the operation of the predictive EMS controller. The charge depletion/charge sustenance strategy maintains normal operation of the two controllers until the end of the planned driving route relative to the charge depletion mode identified in Section 5.7.4. By operating the original and non-predictive controllers with a charge depletion mode at the end of driving, operation as a PHEV is demonstrated. This means that the ESS is more heavily relied upon at the end of driving in an attempt to minimise fuel consumption. The results for the three controllers are compared relative to operation as a HEV and PHEV respectively. Operation as a HEV is realised by SOC correction at the end of driving using the ICE, while operation as a PHEV is realised by SOC correction using the grid.

Comparison of the three controllers realises that an arbitrary charge depletion mode does not provide optimal operation and may cause increased energy consumption. Instead the calculated blended charge depletion of the predictive controller must be utilised in order to yield optimal performance in the power-split PHEV. Firstly, for HEV mode of operation the calibrated non-predictive controller (HEC-V) determines greater fuel consumption reductions than the predictive controller. The non-predictive controller is capable of up to 6%, while the predictive controller achieves 4% fuel consumption improvement. This is due to the robust nature of the calibrated high efficiency region of the non-predictive controller. Having two set high efficiency regions to select from, the non-predictive controller is able to maintain high efficiency control regardless of the transients required from the vehicle. The calibrated non-predictive controller is, however, limited to this optimal performance on the specified drive cycles and there is no guarantee that performance will be the same on other drive cycles. On the other hand the predictive controller determines optimal operation on-the-go. The predictive controller thereby introduces a small time delay which may lead to increased fuel consumption. This is demonstrated by the reduced fuel consumption improvement when compared to the non-predictive controller. This may be the cost of autonomous control over specific drive cycles, however, such predictive control is applicable to a number of varying drive scenarios (i.e. without calibration). This comparison demonstrates the robust nature of the predictive control such that it does not require large amounts of *a priori* knowledge and that it is capable of minimising fuel consumption to a similar extent as an optimally calibrated non-predictive controller.

Operation as a PHEV reveals the predictive controller's ability to maximise the use of ESS stored energy. Initially it was observed that during the HEV SOC corrections using the ICE, the predictive controller utilised more fuel than the original controller for short trips. This is due to the predictive controller's ability to determine when it was safe to rely more heavily

on the ESS stored energy. For short trips this means using more ESS energy with the expectation of grid charging at the end of driving. In doing so the predictive controller is capable of minimising fuel consumption by up to 22% in comparison to the non-predictive controller having up to 16% fuel consumption reduction. The autonomous calibration of the predictive controller therefore helps to maximise the use of stored energy over a planned driving route.

This thesis has identified two alternative real-time optimisation based blended controllers for the high efficiency control of power-split PHEVs. It is envisaged that due to the non-predictive controllers application to the parallel connected test benches featured in this thesis that predictive control can be achieved with similar changes as discussed for the power-split connected topology. The defined approach to high efficiency control as well as the add-on for predictive control have robust operation, low computational requirements, flexibility in control, low calibration and are applicable to a number of existing ESVs. Using measured data from existing commercially available vehicles models are developed for three test benches in simulation, which also serves to provide a realistic bench mark for comparison. Simulations on the featured test benches demonstrate reduced fuel consumption and thereby emissions, with minimal expected adverse effects on drivability for both the non-predictive and predictive high efficiency controllers.

6.2 Future Research

There are a number of areas identified in this research program for further research; three of the most prominent areas resulting from the work completed are featured here. Firstly, it was noted in Section 5.8 that for different drive cycles the resulting fuel consumption improvement is varying significantly between the non-predictive and predictive controllers. This highlights that there may be a concern for the accuracy of the predicted information as outlined in Table 3.4 of Chapter 3. Therefore, a comparison of the predictive control strategy using the described method against the increased number of road segments discussed in Section 5.2 is required. The predictive control approach featured in this thesis realised a worse-case scenario such that only total energy for the whole drive cycle is determined as opposed to splitting the planned driving route into segments. The aim for such research would be to improve the fuel consumption reductions using the increased sensitivity of future predicted information. Then taking advantage of the self-correction of the proposed controller in this thesis, the future work could utilise a specific time window for recalculation of E_{total} and t_{trip} for comparison with the consumed energy. The obvious constraint for this type of controller is the computational complexity for example how often the controller will

need to sample the future energy requirements in order to improve fuel consumption. This however, would demonstrate an interesting study for the proposed predictive controller.

Secondly, an experimental setup to test the proposed control in a real-world test bench similar to that discussed in Section 2.6. The experimental setup described in Section 2.6 is a 2 by 2 power-split PHEV (or dual drive power-split PHEV). This vehicle configuration as mentioned excludes the expensive PGS of the Toyota Prius. While simulations of the topology have been undertaken there is no guarantee of the real-world operations until experimental results have been confirmed. The design for the final experimental setup is featured in the appendices and is expected to conform to necessary standards for passenger vehicle design. This was one of the reasons that lead to the experimental setup exceeding the budget constraints for this research program.

The above experimental setup also relates to the consideration of a vehicle configuration to test the control strategy outlined in Section 5.3. Using the ICE to supply steady-state power demand and the ESS transient power demands it is envisaged that ICE on/off times are minimised in addition to fuel consumption. This strategy observes calculated ICE on/off periods relative to the ESS charge and discharge constraints. During ICE operation high efficiency control is achieved in the process of meeting tractive power demands as well as ESS charge requirements. Once the ESS is charged to a defined high limit the ICE switches off for the electric mode of operation. The key difference between typical charge depletion/charge sustenance strategies and the described strategy is that it realises high efficiency operation of the ICE in order to maximise the use of stored energy for a planned driving route. The main reason for not employing this control strategy in this research program is due to the undefined test bench. Research is required into whether or not it is possible to design a 2 by 2 power-split PHEV since there are challenges involved with maintaining equilibrium between the independently driven front and rear axles of the vehicle. While this is easy enough to achieve in simulation there is no guarantee that results will be replicable in an experimental environment due to the uncertainty in operation.

Bibliography

[1] D. Abbott, "Keeping the Energy Debate Clean: How Do We Supply the World's Energy Needs?," *Proc. of the IEEE*, vol. 98, pp. 42-66, Jan. 2010.

[2] U.S. Energy Information Administration (EIA), "International Energy Outlook 2013," Office of Energy Analysis, U.S. Department of Energy, Washington, DC, Jul. 2013.

[3] Bureau of Resources and Energy Economics, "Energy in Australia 2012," BREE, Canberra, ACT, Feb 2012.

[4] C. C. Chan, A. Bouscayrol, & K. Chen, "Electric, Hybrid, and Fuel-Cell Vehicles: Architectures and Modeling," *IEEE Trans. on Vehicular Technology*, vol. 59, pp. 589-598, Feb. 2010.

[5] M. Ehsani, Y. Gao, & A. Emadi, *Modern electric, hybrid electric, and fuel cell vehicles : fundamentals, theory, and design*, 2nd ed. Boca Raton: CRC Press, 2010.

[6] U. Bossel, "Does a Hydrogen Economy Make Sense?," *Proc. of the IEEE*, vol. 94, pp. 1826-1837, Oct. 2006.

[7] S. G. Wirasingha, R. Gremban, & A. Emadi, "Source-to-Wheel (STW) Analysis of Plug-in Hybrid Electric Vehicles," *Smart Grid, IEEE Transactions on*, vol. PP, pp. 1-1, 2011.

[8] S. G. Wirasingha, & A. Emadi, "Classification and Review of Control Strategies for Plug-In Hybrid Electric Vehicles," *Vehicular Technology, IEEE Transactions on*, vol. 60, pp. 111-122, 2011.

[9] J. T. B. A. Kessels, M. W. T. Koot, P. P. J. van den Bosch, & D. B. Kok, "Online Energy Management for Hybrid Electric Vehicles," *Vehicular Technology, IEEE Transactions on*, vol. 57, pp. 3428-3440, 2008.

[10] S. Adhikari, S. K. Halgamuge, & H. C. Watson, "An Online Power-Balancing Strategy for a Parallel Hybrid Electric Vehicle Assisted by an Integrated Starter Generator," *Vehicular Technology, IEEE Transactions on*, vol. 59, pp. 2689-2699, 2010.

[11] Z. Menyang, Y. Yan, & C. C. Mi, "Analytical Approach for the Power Management of Blended-Mode Plug-In Hybrid Electric Vehicles," *Vehicular Technology, IEEE Transactions on*, vol. 61, pp. 1554-1566, 2012.

[12] S. Barsali, M. Ceraolo, & A. Possenti, "Techniques to Control Electricity Generation in a Series Hybrid Electrical Vehicle," *IEEE Trans. on Energy Conversion*, vol. 17, pp. 260-266, Jun. 2002.

[13] S. Barsali, C. Miulli, and A. Possenti, "A control strategy to minimize fuel consumption of series hybrid electric vehicles," *Energy Conversion, IEEE Transactions on*, vol. 19, pp. 187-195, 2004.

Bibliography

[14] Q. Wang, W. Liang, M. Kuang, & R. McGee, "Vehicle System Controls for a Series Hybrid Powertrain," in *Advanced Hybrid Vehicle Powertrains, World Congress*, SAE, Detroit, MI, Paper 2011-01-0860, 2011.

[15] H. Borhan, A. Vahidi, A. M. Phillips, M. L. Kuang, I. V. Kolmanovsky *et al.*, "MPC-Based Energy Management of a Power-Split Hybrid Electric Vehicle," *Control Systems Technology, IEEE Transactions on*, vol. PP, pp. 1-11, 2011.

[16] N. Kim, & A. Rousseau "Comparison between Rule-Based and Instantaneous Optimization for a Single-Mode, Power-Split HEV," in *Advanced Hybrid Vehicle Powertrains, World Congress*, SAE, Detroit, MI, Paper 2011-01-0873, 2011.

[17] B. Mashadi, & S. A. M. Emadi, "Dual-Mode Power-Split Transmission for Hybrid Electric Vehicles," *Vehicular Technology, IEEE Transactions on*, vol. 59, pp. 3223-3232, 2010.

[18] S. S. Williamson, & A. Emadi,, "Comparative assessment of hybrid electric and fuel-cell vehicles based on comprehensive well-wheels efficiency analysis," *IEEE Trans. on Vehicular Technology*, vol. 54, p. 6, 2005.

[19] A. Von Jouanne, I. Husain, A. Wallace, & A. Yokochi. (2005, Jul.-Aug.) Gone with the wind: Innovative hydrogen/fuel cell electric vehicle infrastructure based on wind energy sources. *IEEE Industry Applications Magazine*. 12-19.

[20] A. F. Burke, "Batteries and Ultracapacitors for Electric, Hybrid, and Fuel Cell Vehicles," *Proceedings of the IEEE*, vol. 95, pp. 806-820, 2007.

[21] S. Amjad, S. Neelakrishnan, & R. Rudramoorthy, "Review of design considerations and technological challenges for successful development and deployment of plug-in hybrid electric vehicles," *Renewable and Sustainable Energy Reviews*, vol. 14, pp. 1104-1110, 2010.

[22] K. M. Rahman, N. R. Patel, T. G. Ward, J. M. Nagashima, F. Caricchi, et al., "Applications of Direct-Drive Wheel Motor for Fuel Cell Electric and Hybrid Electric Vehicle Propulsion System," *IEEE Trans. on Industry Applications*, vol. 42, pp. 1185-1192, Sept.-Oct. 2006.

[23] G. M. Masters, *Renewable and Efficient Electric Power Systems*, 1st ed. Hoboken, NJ: John Wiley & Sons, 2004.

[24] Daily Wire Community. (2011, May). *What is the carbon tax*. Available: http://www.carbontax.net.au/category/what-is-the-carbon-tax/

[25] Department of Climate Change and Energy Efficiency 2012, "Australia's emissions projections 2012," DCCEE, Canberra, ACT.

[26] Z. Chen, & A. Vahidi, "Route Preview in Energy Management of Plug-in Hybrid Vehicles," *Control Systems Technology, IEEE Transactions on*, vol. 20, pp. 546-553, 2012.

[27] X. He, T. Maxwell, & M. E. Parten, "Development of a Hybrid Electric Vehicle With a Hydrogen-Fueled IC Engine," *IEEE Trans. on Vehicular Technology*, vol. 55, pp. 1693-1703, Nov. 2006.

[28] M. Van Wieringen, & R. Pop-Iliev, "Development of a Dual-Fuel Power Generation System for an Extended Range Plug-in Hybrid Electric Vehicle," *IEEE Trans. on Industrial Electronics*, vol. 57, pp. 641-648, Feb. 2010.

[29] P. Fajri, & B. Asaei, "Plug-in Hybrid Conversion of a Series Hybrid Electric Vehicle and Simulation Comparison," in *Conf. Rec. IEEE 11th Int. Conf. on Optimization of Electrical and Electronic Equipment*, Brasov, 2008, pp. 287-292.

[30] C. C. Lin, H. Peng, J. W. Grizzle, & J.-M. Kang, "Power Management Strategy for a Parallel Hybrid Electric Truck," *IEEE Trans. on Control System Technology*, vol. 11, pp. 839-849, Nov. 2003.

[31] J. Liu, & H. Peng,, "Modeling and Control of a Power-Split Hybrid Vehicle," *IEEE Trans. on Control System Technology*, vol. 16, pp. 1242-1251, Nov. 2008.

[32] Y. Fengjun, W. Junmin, and H. Kaisheng, "Hybrid Electric Vehicle Model Predictive Control Torque-Split Strategy Incorporating Engine Transient Characteristics," *Vehicular Technology, IEEE Transactions on*, vol. 61, pp. 2458-2467, 2012.

[33] S. J. Moura, H. K. Fathy, D. S. Callaway, & J. L. Stein, "A stochastic optimal control approach for power management in plug-In hybrid electric vehicles," *Control Systems Technology, IEEE Transactions on*, vol. 19, pp. 545-555, 2011.

[34] K. Jeongmin, K. Talchol, M. Byungsoon, H. Sungho, & K. Hyunsoo, "Mode Control Strategy for a Two-Mode Hybrid Electric Vehicle Using Electrically Variable Transmission (EVT) and Fixed-Gear Mode," *Vehicular Technology, IEEE Transactions on*, vol. 60, pp. 793-803, 2011.

[35] A. Emadi, S. S. Williamson, & A. Khaligh, "Power electronics intensive solutions for advanced electric, hybrid electric, and fuel cell vehicular power systems," *Power Electronics, IEEE Transactions on*, vol. 21, pp. 567-577, 2006.

[36] P. Pisu, & G. Rizzoni, "A Comparative Study of Supervisory Control Strategies for Hybrid Electric Vehicles," *IEEE Trans. on Control System Technology*, vol. 15, pp. 506-518, May 2007.

[37] F. Jehlik, "Methodology and analysis of determining plug-In hybrid engine thermal state and resulting efficiency," in *Advanced Hybrid Vehicle Powertrains, World Congress*, SAE, Detroit, MI, Paper 2009-01-1308, 2009.

[38] D. F. Opila, X. Wang, R. McGee, R. B. Gillespie, J. A. Cook, and J. W. Grizzle, "An Energy Management Controller to Optimally Trade Off Fuel Economy and Drivability for Hybrid Vehicles," *Control Systems Technology, IEEE Transactions on*, vol. 20, pp. 1490-1505, 2012.

[39] B. Geng, J. Mills, & D. Sun, "Two-Stage Energy Management Control of Fuel Cell Plug-In Hybrid Electric Vehicles Considering Fuel Cell Longevity," *Vehicular Technology, IEEE Transactions on*, vol. 61, pp. 498-508, 2012.

[40] T. Hofman, S. Ebbesen, and L. Guzzella, "Topology Optimization for Hybrid Electric Vehicles With Automated Transmissions," *Vehicular Technology, IEEE Transactions on*, vol. 61, pp. 2442-2451, 2012.

Bibliography

[41] B. Zhang, C. Mi, & M. Zhang, "Charge Depleting Control Strategies and Fuel Optimization of Blended-Mode Plug-in Hybrid Electric Vehicles," *Vehicular Technology, IEEE Transactions on*, vol. PP, pp. 1-1, 2011.

[42] T. C. Moore, & A. B. Lovins, "Vehicle Design Strategies to Meet and Exceed PNGV Goals," in *Future Transportation Technology Conference*, SAE, Costa Mesa, CA, Paper 951906, 1995.

[43] U.S. Department of Energy. (2013, 15 July 2013). *Download Fuel Economy Data*. Available: http://www.fueleconomy.gov/feg/download.shtml

[44] S. J. Moura, J. L. Stein, and H. K. Fathy, "Battery-Health Conscious Power Management in Plug-In Hybrid Electric Vehicles via Electrochemical Modeling and Stochastic Control," *Control Systems Technology, IEEE Transactions on*, vol. 21, pp. 679-694, 2013.

[45] M. Zandi, A. Payman, J. P. Martin, S. Pierfederici, B. Davat *et al.*, "Energy Management of a Fuel Cell/Supercapacitor/Battery Power Source for Electric Vehicular Applications," *Vehicular Technology, IEEE Transactions on*, vol. 60, pp. 433-443, 2011.

[46] S. Delprat, J. Lauber, T. M. Guerra, & J. Rimaux, "Control of a parallel hybrid powertrain: optimal control," *Vehicular Technology, IEEE Transactions on*, vol. 53, pp. 872-881, 2004.

[47] C. Musardo, G. Rizzoni, Y. Guezennec & B. Staccia, "A-ECMS: an adaptive algorithm for hybrid electric vehicle energy management," *Eur. J. Control*, vol. 11, pp. 509-524, 2005.

[48] S. Overington, & S. Rajakaruna, "Review of PHEV and HEV operation and control research for future direction," in *Power Electronics for Distributed Generation (PEDG 2012)*, Aalborg, Denmark, 2012.

[49] K. B. Wipke, M. R. Cuddy, & S. D. Burch, "ADVISOR 2.1: User-Friendly Advanced Powertrain Simulation Using A Combined Backward/Forward Approach," *IEEE Trans. on Vehicular Technology*, vol. 48, pp. 1751-1761, Nov. 1999.

[50] P. Mulhall, S. M. Lukic, S. G. Wirasingha, Y.-J. Lee, & A. Emadi, "Solar-Assisted Electric Auto Rickshaw Three-Wheeler," *IEEE Trans. on Vehicular Technology*, vol. 59, pp. 2298-2307, 11 Mar. 2010.

[51] W. Lei, E. G. Collins, & L. Hui, "Optimal Design and Real-Time Control for Energy Management in Electric Vehicles," *Vehicular Technology, IEEE Transactions on*, vol. 60, pp. 1419-1429, 2011.

[52] N. Woonki, P. Taesik, K. Taehyung, & K. Sangshin, "Light Fuel-Cell Hybrid Electric Vehicles Based on Predictive Controllers," *Vehicular Technology, IEEE Transactions on*, vol. 60, pp. 89-97, 2011.

[53] Y. Xibo and W. Jiabin, "Torque Distribution Strategy for a Front- and Rear-Wheel-Driven Electric Vehicle," *Vehicular Technology, IEEE Transactions on*, vol. 61, pp. 3365-3374, 2012.

[54] J. B. Heywood, *Internal Combustion Engine Fundamentals*. New York: McGraw-Hill, 1988.

[55] S. S. Williamson, M. Lukic, & A. Emadi, "Comprehensive Drive Train Efficiency Analysis of Hybrid Electric and Fuel Cell Vehicles Based on Motor-Controller Efficiency Modeling," *IEEE Trans. on Power Electronics*, vol. 21, pp. 730-740, May 2006.

[56] M. Bassett, I. Thatcher, A. Bisordi, J. Hall, N. Fraser, *et al.*, "Design of a Dedicated Range Extender Engine," in *Advanced Hybrid Vehicle Powertrains, World Congress*, SAE, Detroit, MI, Paper 2011-01-0862, 2011.

[57] Z. Zhu, A. Yablonski, H. Mearns, & W. Wayne, "Defining the Hybrid Drive System for the WVU ClearVue Crossover Sport Utility Vehicle," in *Advanced Hybrid Vehicle Powertrains, World Congress*, SAE, Detroit, MI, Paper 2010-01-0841, 2010.

[58] W. Colonna, "The 4L60 Evolution," *Motor Age*, vol. 132, pp. 24-24,28,30,32, Jul 2013 2013.

[59] M. Bertoluzzo, G. Buja, V. Cossalter, A. Doria, & D. Mazzaro. (2008, Sept.) Getting Around in Electric Vehicles. *IEEE Industrial Electronics Magazine*. 10-18.

[60] S. S. Raghavan and A. Khaligh, "Electrification Potential Factor: Energy-Based Value Proposition Analysis of Plug-In Hybrid Electric Vehicles," *Vehicular Technology, IEEE Transactions on*, vol. 61, pp. 1052-1059, 2012.

[61] V. Sezer, M. Gokasan, and S. Bogosyan, "A Novel ECMS and Combined Cost Map Approach for High-Efficiency Series Hybrid Electric Vehicles," *Vehicular Technology, IEEE Transactions on*, vol. 60, pp. 3557-3570, 2011.

[62] J. Dixon, I. Nakashima, E. F. Arcos, & M. Ortuzar, "Electric Vehicle Using a Combination of Ultracapacitors and ZEBRA Battery," *IEEE Trans. on Industrial Electronics*, vol. 57, pp. 943-949, Mar. 2010.

[63] D. Wu, D. C. Aliprantis, & K. Gkritza, "Electric Energy and Power Consumption by Light-Duty Plug-In Electric Vehicles," *Power Systems, IEEE Transactions on*, vol. 26, pp. 738-746, 2011.

[64] L. Wang, E. G. Collins & H. Li, "Optimal Design and Real-Time Control for Energy Management in Electric Vehicles," *Vehicular Technology, IEEE Transactions on*, vol. 60, pp. 1419-1429, 2011.

[65] A. Y. Saber, & G. K. Venayagamoorthy, "Plug-in Vehicles and Renewable Energy Sources for Cost and Emission Reductions," *Industrial Electronics, IEEE Transactions on*, vol. 58, pp. 1229-1238, 2011.

[66] O. Briat, J. M. Vinassa, W. Lajnef, S. Azzopardi, & E. Woirgard "Principle, design and experimental validation of a flywheel-battery hybrid source for heavy-duty electric vehicles," *IET Electr. Power Appl.*, vol. 1, pp. 665-674, Sept. 2007.

[67] J. R. A. Beale, "Stored energy transmission for road vehicles," *Electronics and Power*, vol. 25, pp. 323-328, 1979.

[68] M. Woon, X. Lin, A. Ivanco, A. Moskalik, C. Gray, et al., "Energy Management Options for an Electric Vehicle with Hydraulic Regeneration System," in *Advanced Hybrid Vehicle Powertrains, World Congress*, SAE, Detroit, MI, Paper 2011-01-0868, 2011.

[69] Y. Li, H. Chen, X. Zhang, C.Tan, & Y. Ding,, "Renewable energy carriers: Hydrogen or liquid air/nitrogen?," *Applied Thermal Engineering,* vol. 30, pp. 1985-1990, 2010.

[70] C. C. Chan, Y. S. Wong, A. Bouscayrol, & K. Chen, "Powering Sustainable Mobility: Roadmaps of Electric, Hybrid, and Fuel Cell Vehicles," *Proc. of the IEEE,* vol. 97, pp. 603-607, Apr. 2009.

[71] M. Zackrisson, L. Avellán, & J. Orlenius, "Life cycle assessment of lithium-ion batteries for plug-in hybrid electric vehicles - Critical issues," *Journal of Cleaner Production,* vol. 18, pp. 1519-1529, 2010.

[72] A. Brooker, M. Thornton, & J. Rugh, "Technology Improvement Pathways to Cost-effective Vehicle Electrification," in *Advanced Hybrid Vehicle Powertrains, World Congress*, SAE, Detroit, MI, Paper 2010-01-0824, 2010.

[73] Z. Amjadi, & S. S. Williamson, "Power-Electronics-Based Solutions for Plug-in Hybrid Electric Vehicle Energy Storage and Management Systems," *IEEE Trans. on Industrial Electronics,* vol. 57, pp. 608-616, Feb. 2010.

[74] A. Smith, N. Bucknor, H. Yang, & Y. He "Controls Development for Clutch-Assisted Engine Starts in a Parallel Hybrid Electric Vehicle," in *Advanced Hybrid Vehicle Powertrains, World Congress*, SAE, Detroit, MI, Paper 2011-01-0870, 2011.

[75] D. Martin, & E. Badillo, "Ratio-Metric Hesitation Fuel Detection and Compensation in Power Split Hybrid Electric Vehicles," in *Advanced Hybrid Vehicle Powertrains, World Congress*, SAE, Detroit, MI, Paper 2011-01-0882, 2011.

[76] J. Moyers, S. Akehurst, D. Parker, & S. Schaaf, "The Application of the Milner CVT as a Novel Power Splitting Transmission for Hybrid Vehicles," in *Advanced Hybrid Vehicle Powertrains, World Congress*, SAE, Detroit, MI, Paper 2011-01-0890, 2011.

[77] A. E. Fitzgerald, C. Kingsley, S.D. Umans, *Electric Machinery,* Sixth ed. New York, USA: McGraw-Hill, 2003.

[78] C. C. Chan, K. T. Chau, J. Z. Jiang, W. Xia, M. Zhu, and R. Zhang, "Novel permanent magnet motor drives for electric vehicles," *Industrial Electronics, IEEE Transactions on,* vol. 43, pp. 331-339, 1996.

[79] C. C. Chan, "An overview of electric vehicle technology," *Proceedings of the IEEE,* vol. 81, pp. 1202-1213, 1993.

[80] K. Kiyota, H. Sugimoto, and A. Chiba, "Comparing Electric Motors: An Analysis Using Four Standard Driving Schedules," *Industry Applications Magazine, IEEE,* vol. 20, pp. 12-20, 2014.

[81] A. Emadi, Y. J. Lee, & K. Rajashekara, "Power Electronics and Motor Drives in Electric, Hybrid Electric, and Plug-In Hybrid Electric Vehicles," *IEEE Trans. on Industrial Electronics,* vol. 55, pp. 2237-2245, Jun. 2008.

[82] L. Wang, & H. Li, "Maximum Fuel Economy-Oriented Power Management Design for a Fuel Cell Vehicle Using Battery and Ultracapacitor," *IEEE Trans. on Industry Applications,* vol. 46, pp. 1011-1020, May 2010.

[83] E. Schaltz, A. Khaligh, & P. O. Rasmussen, "Influence of Battery/Ultracapacitor Energy-Storage Sizing on Battery Lifetime in a Fuel Cell Hybrid Electric Vehicle," *IEEE Trans. on Vehicular Technology,* vol. 58, pp. 3882-3890, Oct. 2009.

[84] H. Chiu, & L.-W. Lin, "A Bi-directional DC-DC Converter for Fuel Cell Electric Vehicle Driving System," *IEEE Trans. on Power Electronics,* vol. 21, pp. 950-958, Jul. 2006.

[85] J. T. Pukrushpan, A. G. Stefanopoulou, S. Varigonda, L. M. Pedersen, S. Ghosh, et al., "Control of Natural Gas Catalytic Partial Oxidation for Hydrogen Generation in Fuel Cell Applications," *IEEE Trans. on Control System Technology,* vol. 13, pp. 3-14, Jan. 2005.

[86] N. Lior, "Energy resources and use: The present (2008) situation and possible sustainable paths to the future," *Energy,* vol. 35, pp. 2631-2638, 2010.

[87] A. B. C. Eisenhut, "Batteries and Ultracapacitors for Electric, Hybrid, and Fuel Cell Vehicles," *Proc. of the IEEE,* vol. 95, pp. 806-820, 30 Apr. 2007.

[88] D. Rotenberg, A. Vahidi, & I. Kolmanovsky, "Ultracapacitor Assisted Powertrains: Modeling, Control, Sizing, and the Impact on Fuel Economy," *Control Systems Technology, IEEE Transactions on,* vol. 19, pp. 576-589, 2011.

[89] B. Zhang, C. C. Mi & M. Zhang, "Charge-Depleting Control Strategies and Fuel Optimization of Blended-Mode Plug-In Hybrid Electric Vehicles," *Vehicular Technology, IEEE Transactions on,* vol. 60, pp. 1516-1525, 2011.

[90] M. Komatsu, & T. Takaoka, "Development of Toyota Plug-In Hybrid System," in *Advanced Hybrid Vehicle Powertrains, World Congress,* SAE, Detroit, MI, Paper 2011-01-0874, 2011.

[91] I. Aharon and A. Kuperman, "Topological Overview of Powertrains for Battery-Powered Vehicles With Range Extenders," *Power Electronics, IEEE Transactions on,* vol. 26, pp. 868-876, 2011.

[92] R. Carlson, H. Lohse-Busch, M. Duoba, & N. Shidore "Drive Cycle Fuel Consumption Variability of Plug-In Hybrid Electric Vehicles Due to Aggressive Driving," in *Advanced Hybrid Vehicle Powertrains, World Congress,* SAE, Detroit, MI, Paper 2009-01-1335, 2009.

[93] C. Li, Z. Futang, Z. Minmin, H. Yi, Y. Chengliang, & P. Huei, "Design and Analysis of an Electrical Variable Transmission for a Series-Parallel Hybrid Electric Vehicle," *Vehicular Technology, IEEE Transactions on,* vol. 60, pp. 2354-2363, 2011.

[94] D. Mehr, M. Michalak, S. Erlien, & G. Bower "Optimization and Testing of a Through the Road Parallel, Hybrid-Electric, Crossover Sports Utility Vehicle," in *Advanced Hybrid Vehicle Powertrains, World Congress,* SAE, Detroit, MI, Paper 2009-01-1318, 2009.

[95] V. Atluri, K. Koprubasi, R. Gupta, & N. Brinkman, "Analytical Evaluation of Propulsion System Architectures for Future Urban Vehicles," in *Advanced Hybrid Vehicle Powertrains, World Congress,* SAE, Detroit, MI, Paper 2011-01-0861, 2011.

[96] General Motors Ltd. (2013, Oct 3). Volt/14. *Introducing the best of both worlds*. Available:

http://www.chevrolet.com/content/dam/Chevrolet/northamerica/usa/nscwebsite/en/Home/Vehicles/Cars/2014_Volt/Model_Overview/02_pdfs/MY2014%20Volt%20Spec%20Sheet_PDF-X1a_hi-res.pdf

[97] N. Mohan, T. M. Undeland, & W. P. Robbins, *Power electronics : converters, applications, and design*, 3rd ed. Hoboken, N.J.: J. Wiley, 2003.

[98] K. Hayasaki, T. Abe, K. Tanishima, & K. Chujo "Development of a Parallel Hybrid System for RWD Vehicles," in *Advanced Hybrid Vehicle Powertrains, World Congress*, SAE, Detroit, MI, Paper 2011-01-0884, 2011.

[99] G. Qiuming, L. Yaoyu, & P. Zhong-Ren, "Power management of plug-in hybrid electric vehicles using neural network based trip modeling," in *Proc. Amer. Control Conf.*, St. Louis, MO, Jun. 2009, pp. 4601-4606.

[100] C. Yuan, R. Trigui, C. Espanet, A. Bouscayrol, & C. Shumei, "Specifications and Design of a PM Electric Variable Transmission for Toyota Prius II," *Vehicular Technology, IEEE Transactions on*, vol. 60, pp. 4106-4114, 2011.

[101] T. Donateo, Pacella, D., and Laforgia, D., , "Development of an Energy Management Strategy for Plug-in Series Hybrid Electric Vehicle Based on the Prediction of the Future Driving Cycles by ICT Technologies and Optimized Maps," in *Advanced Hybrid Vehicle Powertrains, World Congress*, SAE, Detroit, MI, Paper 2011-01-0892, 2011.

[102] J. Meisel, "An Analytic Foundation for the Two-Mode Hybrid-Electric Powertrain with a Comparison to the Single-Mode Toyota Prius THS-II Powertrain," in *Advanced Hybrid Vehicle Powertrains, World Congress*, SAE, Detroit, MI, Paper 2009-01-1321, 2009.

[103] Z. Amjadi and S. S. Williamson, "Prototype Design and Controller Implementation for a Battery-Ultracapacitor Hybrid Electric Vehicle Energy Storage System," *Smart Grid, IEEE Transactions on*, vol. 3, pp. 332-340, 2012.

[104] D. Karbowski, S. Pagerit, J. Kwon, A. Rousseau, & K.-F. Frieherr von Pechmann, ""Fair" Comparison of Powertrain Configurations for Plug-In Hybrid Operation Using Global Optimization," in *Advanced Hybrid Vehicle Powertrains, World Congress*, SAE, Detroit, MI, Paper 2009-01-1334, 2009.

[105] J. M. Miller, "Hybrid Electric Vehicle Propulsion System Architectures of the e-CVT Type," *IEEE Trans. on Power Electronics*, vol. 21, pp. 756-767, May 2006.

[106] S. G. Wirasingha, & A. Emadi, "Pihef: Plug-In Hybrid Electric Factor," *Vehicular Technology, IEEE Transactions on*, vol. 60, pp. 1279-1284, 2011.

[107] L. Shaofeng, S. Hillmansen, & C. Roberts, "A Power-Management Strategy for Multiple-Unit Railroad Vehicles," *Vehicular Technology, IEEE Transactions on*, vol. 60, pp. 406-420, 2011.

[108] A. R. Salisa, N. Zhang, & J. G. Zhu, "A Comparative Analysis of Fuel Economy and Emissions Between a Conventional HEV and the UTS PHEV," *Vehicular Technology, IEEE Transactions on*, vol. 60, pp. 44-54, 2011.

[109] Y. Xiaofang and W. Yaonan, "A Novel Electronic-Throttle-Valve Controller Based on Approximate Model Method," *Industrial Electronics, IEEE Transactions on*, vol. 56, pp. 883-890, 2009.

[110] P. Guarneri, G. Rocca, and M. Gobbi, "A Neural-Network-Based Model for the Dynamic Simulation of the Tire/Suspension System While Traversing Road Irregularities," *Neural Networks, IEEE Transactions on*, vol. 19, pp. 1549-1563, 2008.

[111] K. Donghyun, H. Sungho, and K. Hyunsoo, "Vehicle Stability Enhancement of Four-Wheel-Drive Hybrid Electric Vehicle Using Rear Motor Control," *Vehicular Technology, IEEE Transactions on*, vol. 57, pp. 727-735, 2008.

[112] S. Abuelsamid. (2010, Oct 3). Next-gen Volt could use diesel, two-cylinder or rotary range extender *Auto News*. Available: http://www.autoblog.com/2010/05/26/next-gen-chevrolet-could-use-diesel-two-cylinder-or-rotary-rang/

[113] GM Holden Ltd. (2013, Oct 3). *Long Range Electric Holden Volt*. Available: http://www.holden.com.au/cars/volt#/overview

[114] J. Voelcker, "Chevy Volt sparks a series of plug-in hybrids [Update]," *Spectrum, IEEE*, vol. 48, pp. 16-18, 2011.

[115] M. Miller, A. Holmes, B. Conlon, B., & P. Savagian, "The GM "Voltec" 4ET50 Multi-Mode Electric Transaxle," in *Advanced Hybrid Vehicle Powertrains, World Congress*, SAE, Detroit, MI, Paper 2011-01-0887, 2011.

[116] S. Abe, and M. Murata, , "Development of IMA Motor for 2006 Civic Hybrid," *SAE Technical Paper 2006-01-1505*, 2006.

[117] Honda. (2013, 28 Aug). *New Release CR-Z*. Available: http://crz.honda.com.au/features_engaging-drive.aspx

[118] H. Lohse-Busch, K. Stutenberg, M. Duoba, E. Rask, F. Jehlik, et. al. Downloadable Dynamometer Database [Online]. Available: http://www.transportation.anl.gov/D3/index.html

[119] S. Ashley. (2011, Oct 3). New York debuts for Sonata Hybrid and Turbo. *Automotive Engineering International - Online*. Available: http://articles.sae.org/8001/

[120] Toyota Motor Corporation Australia Limited. (2012). *Camry NG Features Hybrid Overview*. Available: http://www.toyota.com.au/camry/features/hybrid

[121] P. Weissler. (2011, Oct 3). Prius plug-in hybrid put to the test. *Automotive Engineering International - Online*. Available: http://articles.sae.org/9326/

[122] D. Kum, H. Peng, & N. K. Bucknor, "Optimal Energy and Catalyst Temperature Management of Plug-in Hybrid Electric Vehicles for Minimum Fuel Consumption and Tail-Pipe Emissions," *Control Systems Technology, IEEE Transactions on*, vol. PP, pp. 1-1, 2011.

[123] L. Hyeoun-Dong, K. Euh-Suh, S. Seung-Ki, K. Joohn-Sheok, M. Kamiya *et al.*, "Torque control strategy for a parallel-hybrid vehicle using fuzzy logic," *Industry Applications Magazine, IEEE*, vol. 6, pp. 33-38, 2000.

[124] L. Hyeoun-Dong, & S. Seung-Ki, "Fuzzy-logic-based torque control strategy for parallel-type hybrid electric vehicle," *Industrial Electronics, IEEE Transactions on*, vol. 45, pp. 625-632, 1998.

[125] A. Farkas, & R. Bonert, "Ultracapacitors as Sole Energy Storage Device in Hybrid Electric Cars?," in *Conf. Rec. IEEE Power Electronics in Transportation Proc.*, Dearborn, MI, 1993, pp. 97-101.

[126] M. Carlini, R. Impero Abenavoli, H. Kormanski, & K. Rudzinska, "A hybrid electric propulsion system for a forest vehicle," in *Energy Conversion Engineering Conference, 1997. IECEC-97., Proceedings of the 32nd Intersociety*, 1997, pp. 2019-2023 vol.3.

[127] G. Qiuming, L. Yaoyu, & P. Zhong-Ren, "Trip-Based Optimal Power Management of Plug-in Hybrid Electric Vehicles," *Vehicular Technology, IEEE Transactions on*, vol. 57, pp. 3393-3401, 2008.

[128] T. A. Burress, C. L. Coomer, S. L. Campbell, A. A. Wereszczak, J. P. Cunningham, *et al.*, "Evaluation of the 2008 LEXUS LS 600 h hybrid synergy drive system," Oak Ridge National Laboratory (ORNL), Oak Ridge, TNJan. 2009.

[129] B. M. Baumann, G. Washington, B. C. Glenn, & G. Rizzoni, "Mechatronic design and control of hybrid electric vehicles," *Mechatronics, IEEE/ASME Transactions on*, vol. 5, pp. 58-72, 2000.

[130] R. B. J. Sepe, C. M. Morrison, J. M. Miller, & A. R. Gale, "HEV S/G [hybrid electric vehicle starter/generator]," *Industry Applications Magazine, IEEE*, vol. 9, pp. 38-43, 2003.

[131] F. U. Syed, M. L. Kuang, M. Smith, S. Okubo, & H. Ying, "Fuzzy Gain-Scheduling Proportional-Integral Control for Improving Engine Power and Speed Behaviour in a Hybrid Electric Vehicle," *IEEE Trans. on Vehicular Technology*, vol. 58, pp. 69-82, Jan. 2009.

[132] D. Ambuhl, & L. Guzzella, "Predictive reference signal generator for hybrid electric vehicles," *Vehicular Technology, IEEE Transactions on*, vol. 58, pp. 4730-4740, 2009.

[133] O. Dingel, J. Ross, I. Trivic, N. Cavina & M. Rioli, "Model-based assessment of hybrid powertrain solutions," in *Proc. 10th Int. Conf. Engines & Vehicles*, Naples, Italy, Sept. 2011, pp. 1-23.

[134] J. G. Vlachogiannis, "Probabilistic Constrained Load Flow Considering Integration of Wind Power Generation and Electric Vehicles," *Power Systems, IEEE Transactions on*, vol. 24, pp. 1808-1817, 2009.

[135] J. Moreno, M. E. Ortuzar, & J. W. Dixon, "Energy-Management System for a Hybrid Electric Vehicle, Using Ultracapacitors and Neural Networks," *IEEE Trans. on Industrial Electronics*, vol. 53, pp. 614-623, Apr. 2006.

[136] F. Syed, S. Nallapa, A. Dobryden, C. Grand, R. McGee, *et al.*, "Design and Analysis of an Adaptive Real-Time Advisory System for Improving Real World Fuel Economy in a Hybrid Electric Vehicle," in *Advanced Hybrid Vehicle Powertrains, World Congress*, SAE, Detroit, MI, Paper 2010-01-0835, 2010.

[137] C. Yuan, C. Keyu, C. C. Chan, A. Bouscayrol, & S. Cui, "Global modeling and control strategy simulation," *Vehicular Technology Magazine, IEEE*, vol. 4, pp. 73-79, 2009.

[138] T. Huajin, W. Larry, D. Zhao Yang, & Y. Rui, "Adaptive and Learning Control for SI Engine Model With Uncertainties," *Mechatronics, IEEE/ASME Transactions on*, vol. 14, pp. 93-104, 2009.

[139] A. Zaremba, & M. Jennings "Purge Modeling for New Propulsion System Technology Applications," in *Advanced Hybrid Vehicle Powertrains, World Congress*, SAE, Detroit, MI, Paper 2011-01-0858, 2011.

[140] J. Gibbs, & T. Tabor, "On Board Jump Start for Belted Alternator Starter Hybrids," in *Advanced Hybrid Vehicle Powertrains, World Congress*, SAE, Detroit, MI, Paper 2011-01-0867, 2011.

[141] C. Bo-Chiuan, W. Yuh-Yih, W. Yi-Lin, & L. Chan-Chiao, "Adaptive Power Split Control for a Hybrid Electric Scooter," *Vehicular Technology, IEEE Transactions on*, vol. 60, pp. 1430-1437, 2011.

[142] W. Lianghong, W. Yaonan, Y. Xiaofang, & C. Zhenlong, "Multiobjective Optimization of HEV Fuel Economy and Emissions Using the Self-Adaptive Differential Evolution Algorithm," *Vehicular Technology, IEEE Transactions on*, vol. 60, pp. 2458-2470, 2011.

[143] H. Xi, T. Ying, & H. Xingui, "An Intelligent Multifeature Statistical Approach for the Discrimination of Driving Conditions of a Hybrid Electric Vehicle," *Intelligent Transportation Systems, IEEE Transactions on*, vol. 12, pp. 453-465, 2011.

[144] A. Hajizadeh, & M. A. Golkar, "Fuzzy neural control of a hybrid fuel cell/battery distributed power generation system," *IET Renew. Power Gener.*, vol. 3, pp. 402-414, Dec. 2009.

[145] B. A. Skinner, G. T. Parks, & P. R. Palmer, "Comparison of Submarine Drive Topologies Using Multiobjective Genetic Algorithms," *Vehicular Technology, IEEE Transactions on*, vol. 58, pp. 57-68, 2009.

[146] W. Lhomme, R. Trigui, P. Delarue, B. Jeanneret, A. Bouscayrol, et al., "Switched Causal Modeling of Transmission With Clutch in Hybrid Electric Vehicles," *IEEE Trans. on Vehicular Technology*, vol. 57, pp. 2081-2088, Jul. 2008.

[147] B. Geng, J. Mills, & D. Sun, "Management Control of Microturbine Powered Plug-in Hybrid Electric Vehicles Using Telemetry Equivalent Consumption Minimization Strategy," *Vehicular Technology, IEEE Transactions on*, vol. PP, pp. 1-1, 2011.

[148] J. Che, P. Tsou, L. Rose & M. Jennings, "Modeling and simulation of the dual drive hybrid electric propulsion system," in *Control and Optimization in Hybrid Powertrains, World Congress*, SAE, Detroit, MI, Paper 2009-01-0147, 2009.

[149] F. Syed, M. Yamazaki, V. Nallapa, & M. Kuang "Energy Management in a Dual-Drive Hybrid Powertrain," in *Advanced Hybrid Vehicle Powertrains, World Congress*, SAE, Detroit, MI, Paper 2009-01-1329, 2009.

[150] I. A. Albert, E. Kahrimanovic, & A. Emadi, "Diesel sport utility vehicles with hybrid electric drive trains," *IEEE Trans. on Vehicular Technology*, vol. 53, pp. 1247-1256, 2004.

[151] Xtreme Imports WA Pty. Ltd. (2012). *250DB*. Available: http://www.xtrememoto.com.au/250db.html

[152] S. Overington, S. Rajakaruna, & S. Islam, "Design of the Experimental Setup for a Plug-in Hybrid Electric Vehicle," in *Australasian Universities Power Engineering Conference 2012*, Bali, Indonesia, 2012.

[153] S. Overington, & S. Rajakaruna, "A modified method for the sizing of the plug-in hybrid electric vehicle propulsion devices," in *Australasian Universities Power Engineering Conference (AUPEC)*, 2011, pp. 1-7.

[154] P. Setlur, J. R. Wagner, D. M. Dawson, and B. Samuels, "Nonlinear control of a continuously variable transmission (CVT)," *Control Systems Technology, IEEE Transactions on*, vol. 11, pp. 101-108, 2003.

[155] Z. Amjadi, & S. S. Williamson, "Modeling, Simulation, and Control of an Advanced Luo Converter for Plug-In Hybrid Electric Vehicle Energy-Storage System," *Vehicular Technology, IEEE Transactions on*, vol. 60, pp. 64-75, 2011.

[156] Z. Hui, L. M. Tolbert & B. Ozpineci, "Impact of SiC Devices on Hybrid Electric and Plug-In Hybrid Electric Vehicles," *Industry Applications, IEEE Transactions on*, vol. 47, pp. 912-921, 2011.

[157] D. Feroldi, M. Serra, & J. Riera, "Design and Analysis of Fuel-Cell Hybrid Systems Oriented to Automotive Applications," *IEEE Trans. on Vehicular Technology*, vol. 58, pp. 4720-4729, Nov. 2009.

[158] A. G. Simpson, "Parametric Modelling of Energy Consumption in Road Vehicles," Doctor of Philosophy, School of Information Technology and Electrical Engineering, University of Queensland, Brisbane, 2005.

[159] M. Gokasan, S. Bogosyan, & D. J. Goering, "Sliding mode based powertrain control for efficiency improvement in series hybrid-electric vehicles," *Power Electronics, IEEE Transactions on*, vol. 21, pp. 779-790, 2006.

[160] T. Lee, Z. Baraket, T. Gordon, & Z. Filipi, "Characterizing One-day Missions of PHEVs Based on Representative Synthetic Driving Cycles," in *Advanced Hybrid Vehicle Powertrains, World Congress*, SAE, Detroit, MI, Paper 2011-01-0885, 2011.

[161] S. S. Williamson, A. Emadi, and K. Rajashekara, "Comprehensive Efficiency Modeling of Electric Traction Motor Drives for Hybrid Electric Vehicle Propulsion Applications," *Vehicular Technology, IEEE Transactions on*, vol. 56, pp. 1561-1572, 2007.

[162] A. C. Baisden, & A. Emadi, "ADVISOR-Based Model of a Battery and an Ultra-Capacitor Energy Source for Hybrid Electric Vehicles," *IEEE Trans. on Vehicular Technology*, vol. 53, pp. 199-205, Jan. 2004.

[163] N. Daiheng, & D. Henclewood, "Simple Engine Models for VII-Enabled In-Vehicle Applications," *Vehicular Technology, IEEE Transactions on*, vol. 57, pp. 2695-2702, 2008.

[164] M. Duoba, R. Carlson, & D. Bocci "Calculating Results and Performance Parameters for PHEVs," in *Advanced Hybrid Vehicle Powertrains, World Congress*, SAE, Detroit, MI, Paper 2009-01-1328, 2009.

[165] A. Affanni, A. Bellini, G. Franceschini, P. Guglielmi, & C. Tassoni, "Battery choice and management for new-generation electric vehicles," *Industrial Electronics, IEEE Transactions on*, vol. 52, pp. 1343-1349, 2005.

[166] uknown. (2009, July). *Toyota Prius User-Guide*. Available: http://john1701a.com/prius/documents/Prius_User-Guide_iconic.pdf

[167] P. Tulpule, V. Marano, G. Rizzoni, R. McGee, & H. Yu, "A Statistical Approach to Assess the Impact of Road Events on PHEV Performance using Real World Data," in *Advanced Hybrid Vehicle Powertrains, World Congress*, SAE, Detroit, MI, Paper 2011-01-0875, 2011.

[168] Q. Gong, S. Midlam-Mohler, V. Marano, & G. Rizzoni "An Iterative Markov Chain Approach for Generating Vehicle Driving Cycles," in *Advanced Hybrid Vehicle Powertrains, World Congress*, SAE, Detroit, MI, Paper 2011-01-0880, 2011.

[169] K. Singh, *Engineering mathematics through applications*. Basingstoke: Palgrave Macmillan, 2003.

[170] B. S. Bhangu, P. Bentley, D. A. Stone, & C. M. Bingham, "Nonlinear observers for predicting state-of-charge and state-of-health of lead-acid batteries for hybrid-electric vehicles," *Vehicular Technology, IEEE Transactions on*, vol. 54, pp. 783-794, 2005.

[171] G. Qiuming, L. Yaoyu, & P. Zhong-Ren, "Trip based power management of plug-in hybrid electric vehicle with two-scale dynamic programming," in *Proc. IEEE Vehicle Power Propulsion Conf.*, Arlington, TX, Sep. 2007, pp. 12-19.

Every reasonable effort has been made to acknowledge the owners of copyrighted material. I would be pleased to hear from any copyright owner who has been omitted or incorrectly acknowledged.

Appendices

A.1 Original Controllers for Test Vehicles

A.1.1 Toyota Prius Operation on HWFET

Table A.1 – Toyota Prius 2010 specifications as used in the ADVISOR software

Description	Symbol	Value	Unit
Mass	M	1531	kg
Rolling Resistance Coefficient	f_r	0.0024	-
Air Density	ρ	1.2	kg/m^3
Coefficient of Aerodynamic Drag	C_D	0.3	-
Frontal Area of Vehicle	A_f	1.745	m^2
Gravitational Acceleration	g	9.81	m/s^2
Wheel Radius	r_d	0.287	m

The following demonstrates the signals and specifications utilised for the Toyota Prius 2010 test vehicle on the HWFET drive cycle.

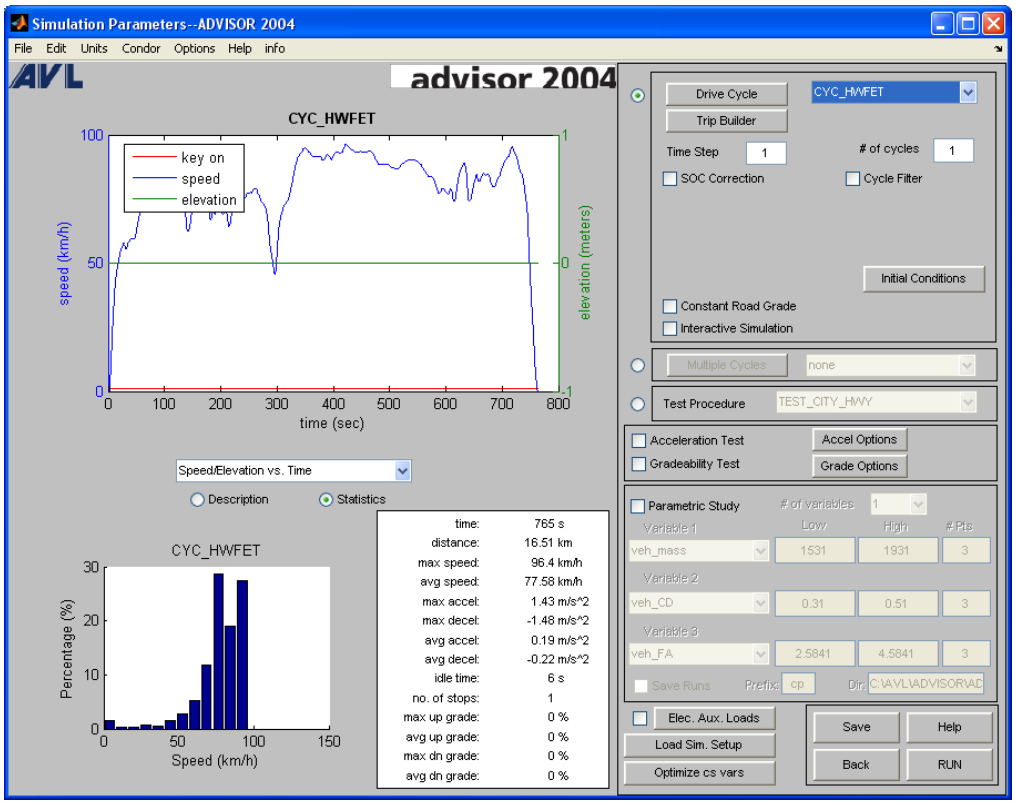

Figure A.1 - HWFET drive profile used for testing the developed model.

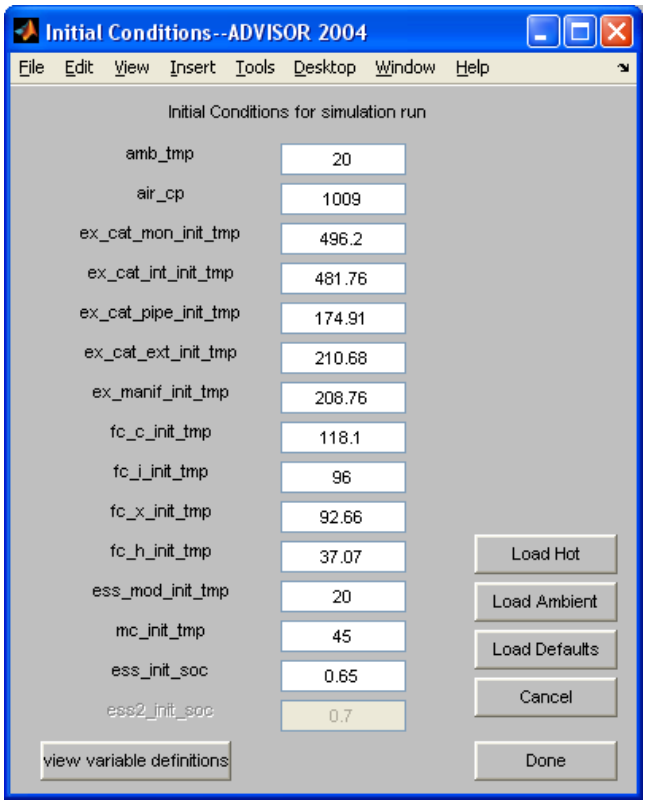

Figure A.2 - Initial conditions for hot start.

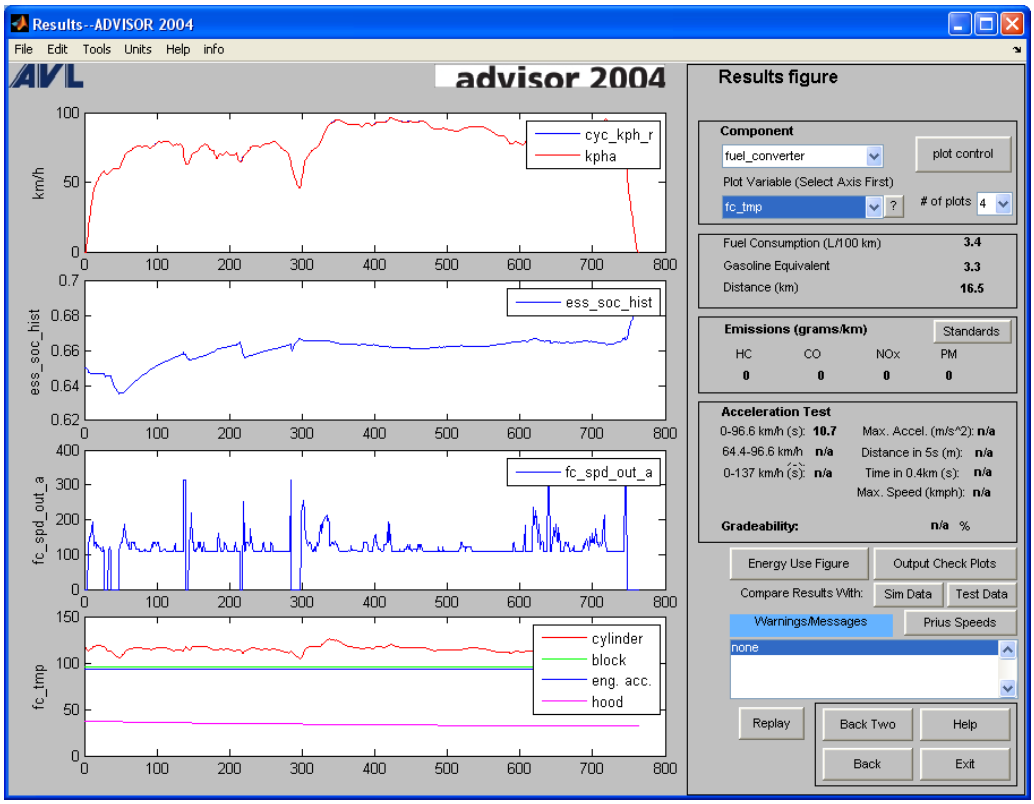

Figure A.3 - Results of the Toyota Prius 2010 model for the HWFET. Measured data indicates that fuel consumption is 3.36 L/100km.

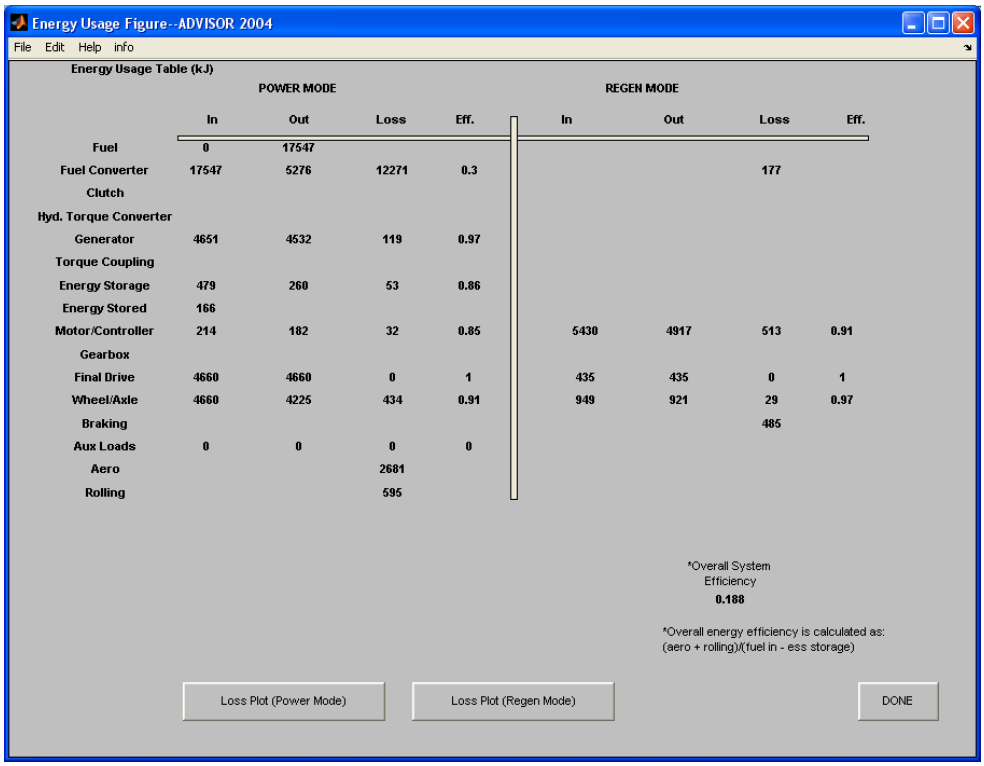

Figure A.4 - Energy usage figure identifying the efficiency of components in the powertrain and drivetrain for the Toyota Prius 2010.

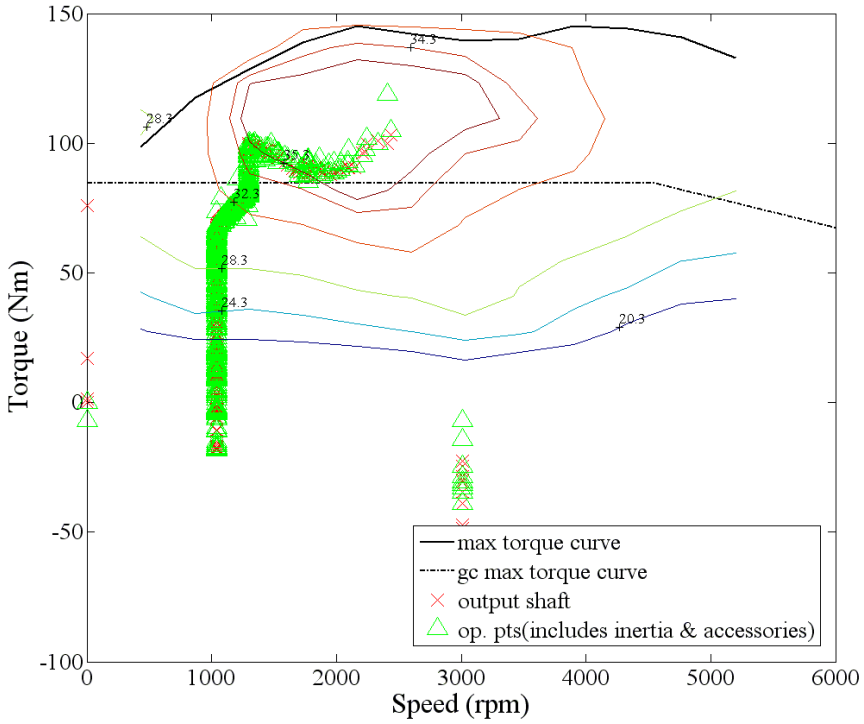

Figure A.5 - ICE operating points for the HWFET. Operation is according to the VSC described in Section 4.3.2.

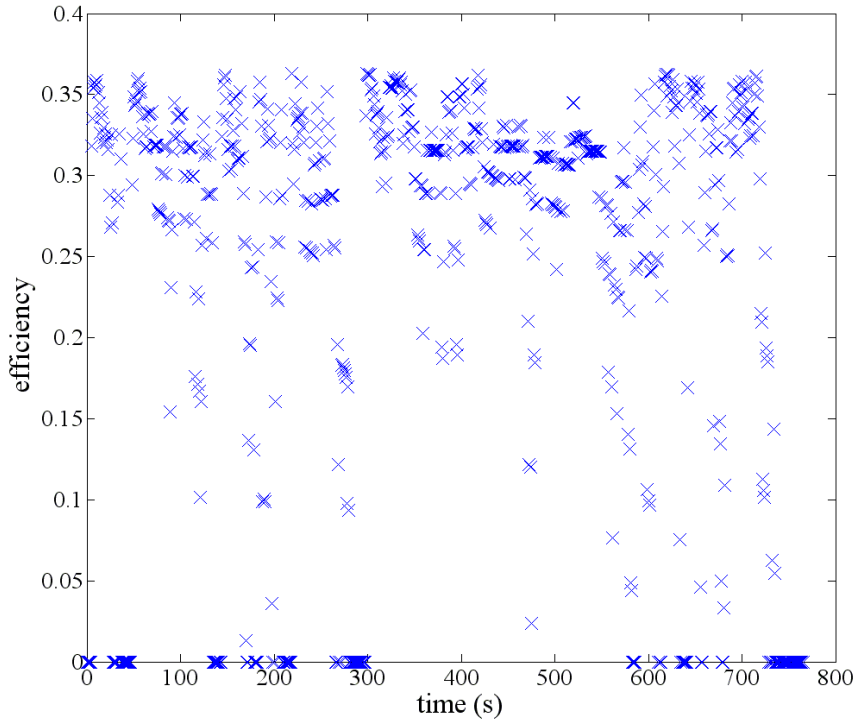

Figure A.6 - ICE efficiency over the HWFET. Average ICE efficiency is 29.24%.

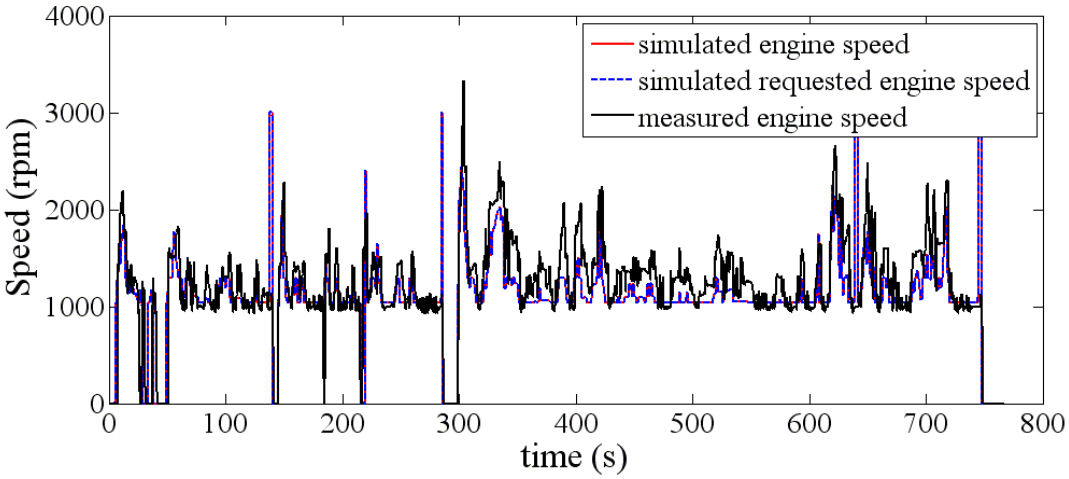

Figure A.7 - ICE speed for the HWFET.

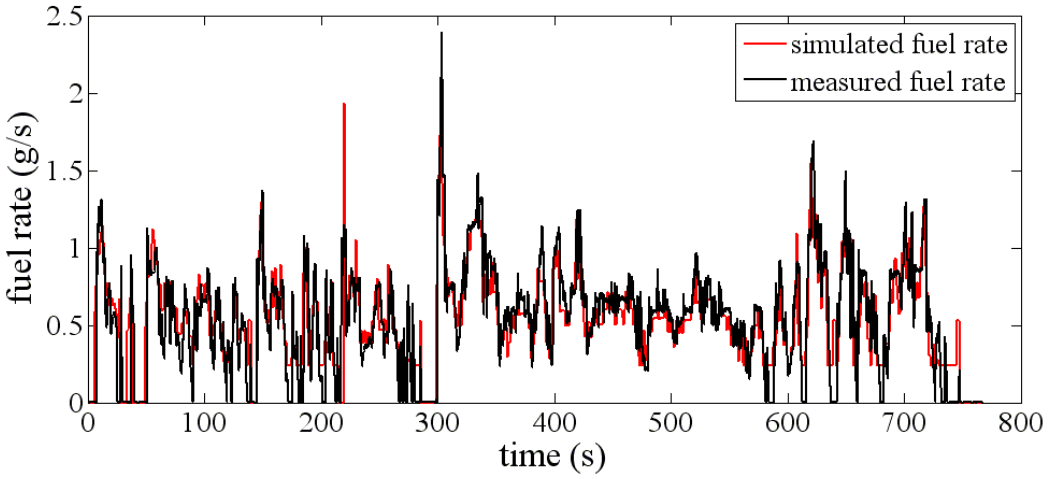

Figure A.8 - Fuel rate for the HWFET.

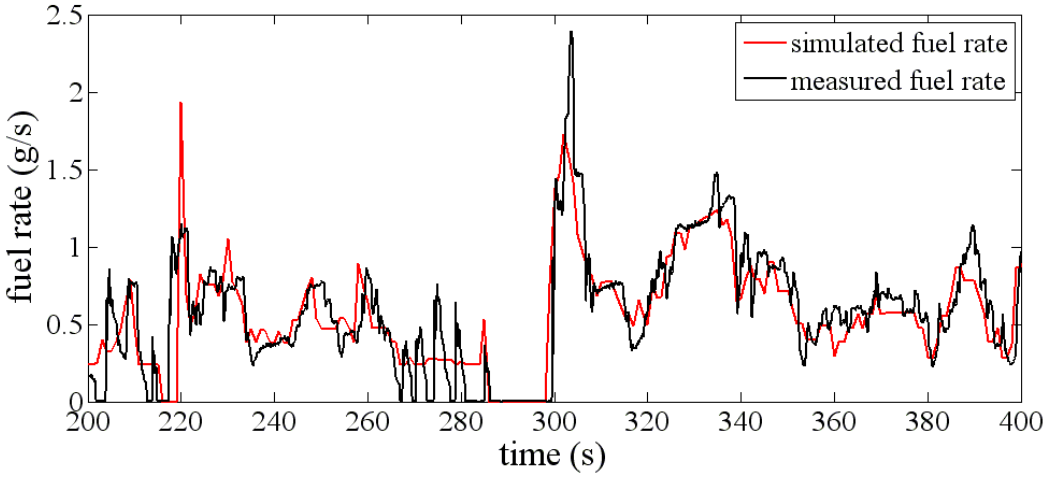

Figure A.9 - Fuel rate for the HWFET for a smaller time segment.

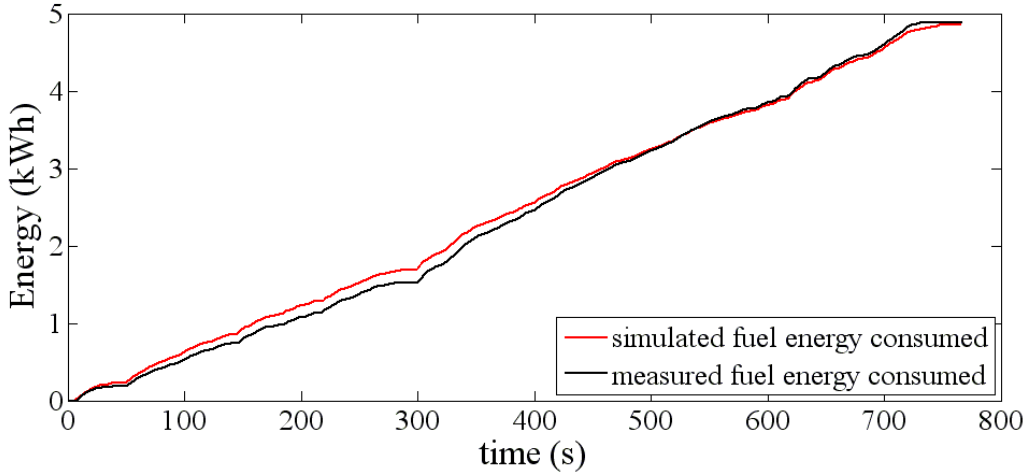

Figure A.10 - Total fuel consumption for the HWFET.

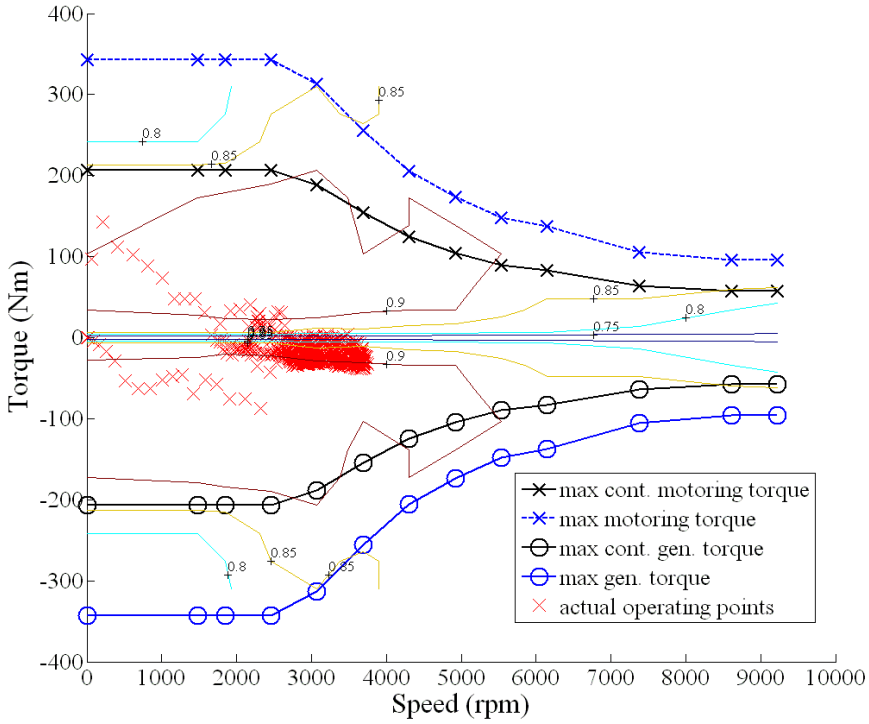

Figure A.11 – M/G2 coupled to ring gear.

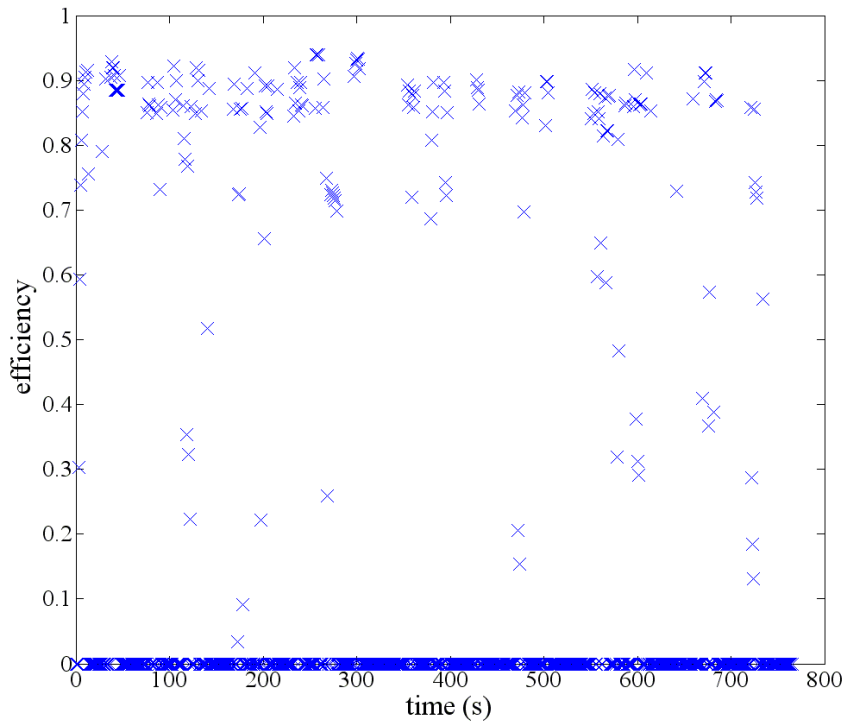

Figure A.12 – M/G2 efficiency over the HWFET. Motoring average efficiency is 84.97%.

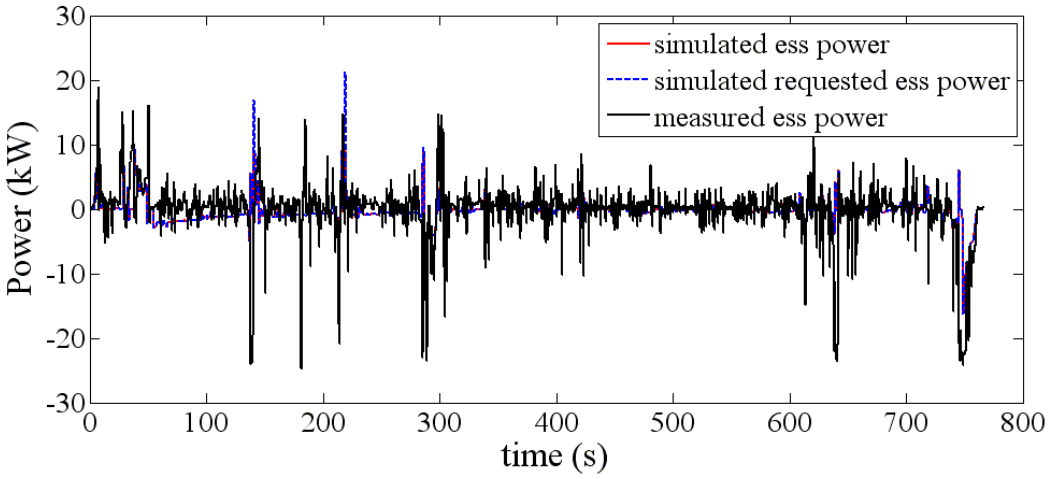

Figure A.13 - ESS power consumption for the HWFET.

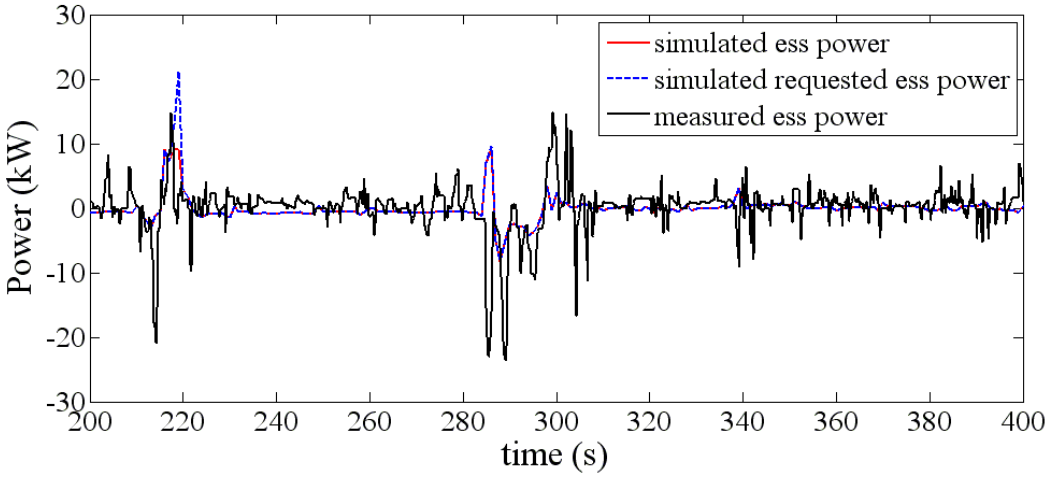

Figure A.14 - ESS power consumption for the HWFET for a smaller time segment.

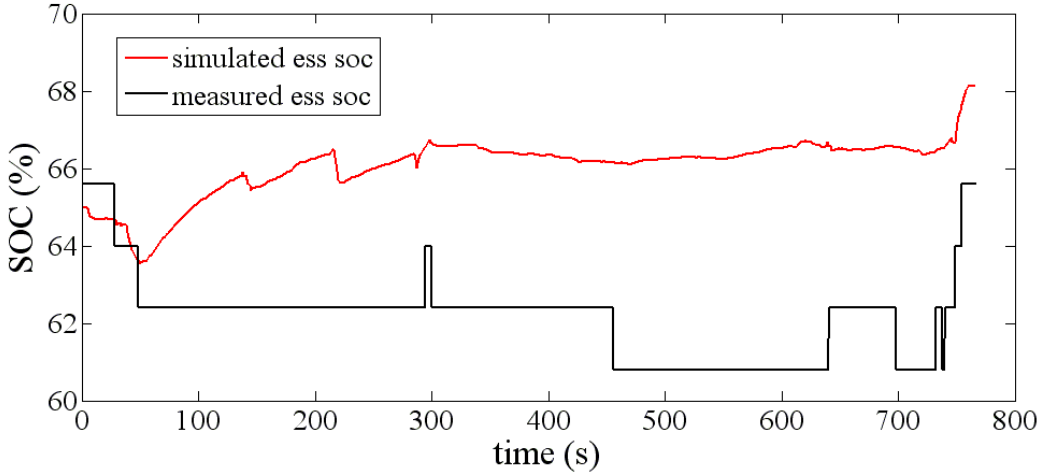

Figure A.15 - ESS SOC for the HWFET.

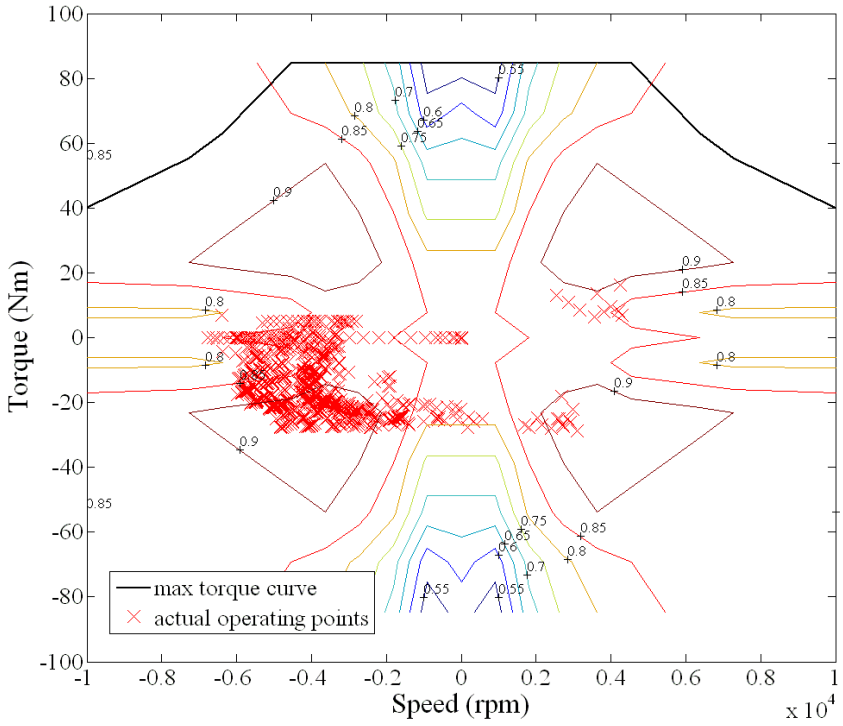

Figure A.16 – M/G1 operating points coupled to the sun gear. Average M/G1 efficiency is displayed as generator efficiency in Figure A.4.

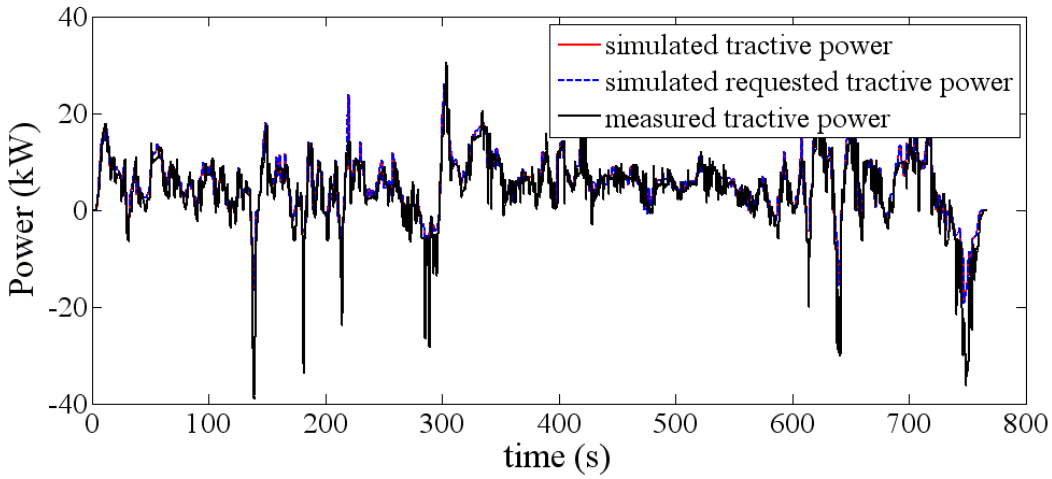

Figure A.17 - Tractive power for the HWFET.

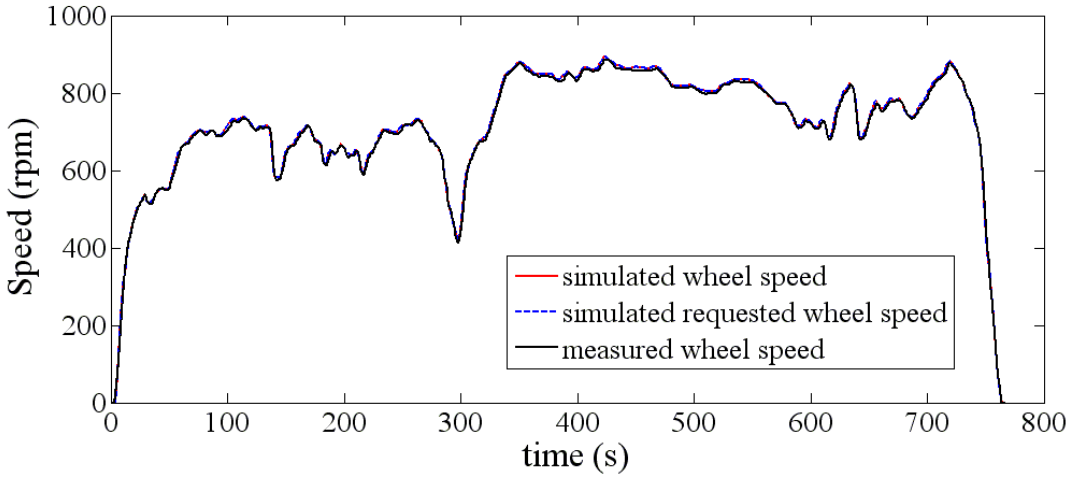

Figure A.18 - Wheel speed for the HWFET.

A.1.2 Hyundai Sonata Hybrid Operation on UDDS

Table A.2 – Hyundai Sonata Hybrid 2011 specifications as used in the ADVISOR software.

Description	Symbol	Value	Unit
Mass	M	1701	kg
Rolling Resistance Coefficient	f_r	0.004	-
Air Density	ρ	1.2	kg/m^3
Coefficient of Aerodynamic Drag	C_D	0.24	-
Frontal Area of Vehicle	A_f	1.835	m^2
Gravitational Acceleration	g	9.81	m/s^2
Wheel Radius	r_d	0.287	m

The following demonstrates the signals and specifications utilised for the Hyundai Sonata Hybrid 2011 test vehicle on the UDDS drive cycle.

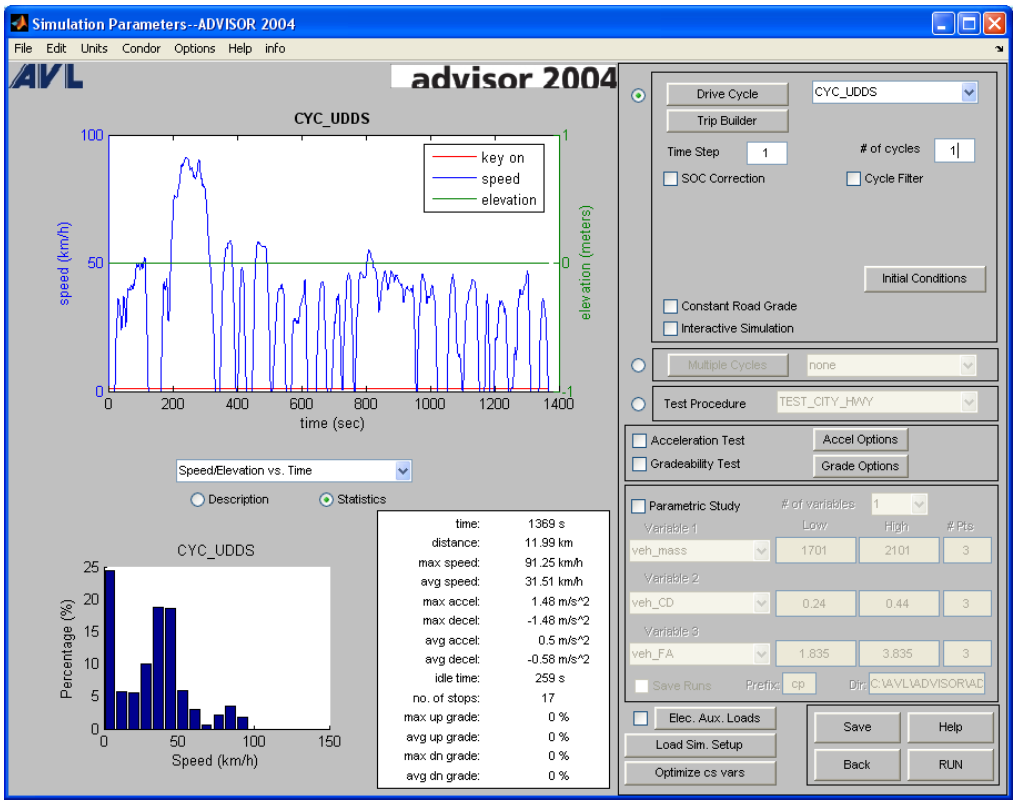

Figure A.19 - UDDS drive profile used for testing the developed model.

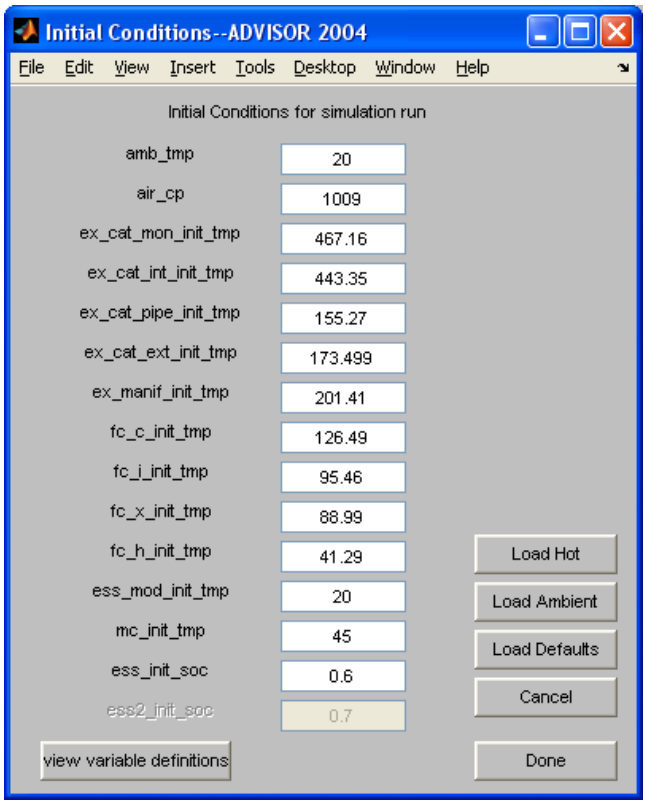

Figure A.20 - Initial conditions specified for the simulations to ensure hot start testing.

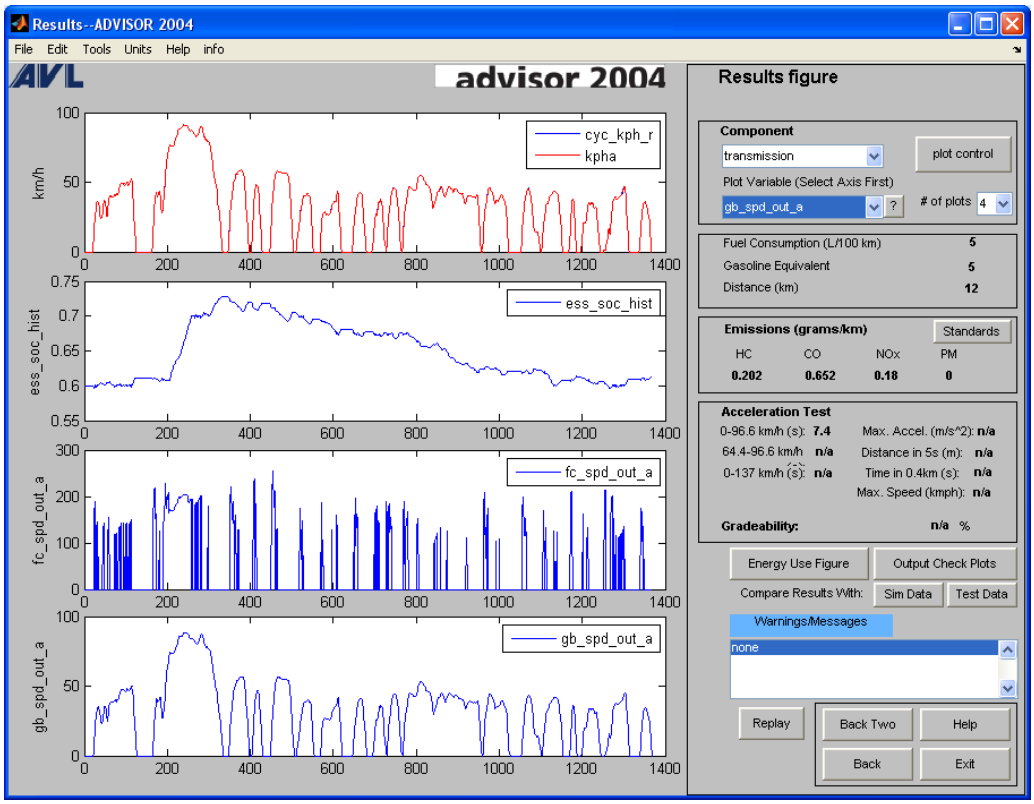

Figure A.21 - Results of the Hyundai Sonata Hybrid 2011 model for the UDDS. Measured data indicates that fuel consumption is 4.92 L/100km best achieved is 5 L/100km. By varying some of the vehicle parameters 4.89 L/100km was achieved.

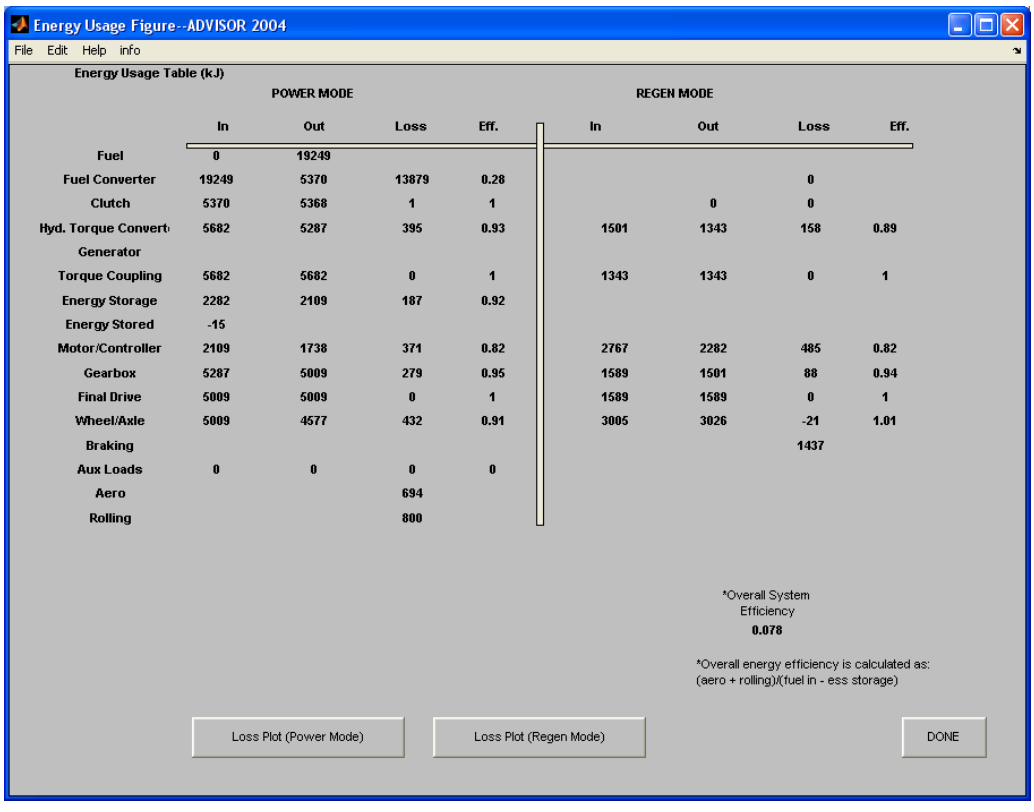

Figure A.22 - Energy usage figure identifying the efficiency of components in the powertrain and drivetrain for the Hyundai Sonata Hybrid 2011 on the UDDS.

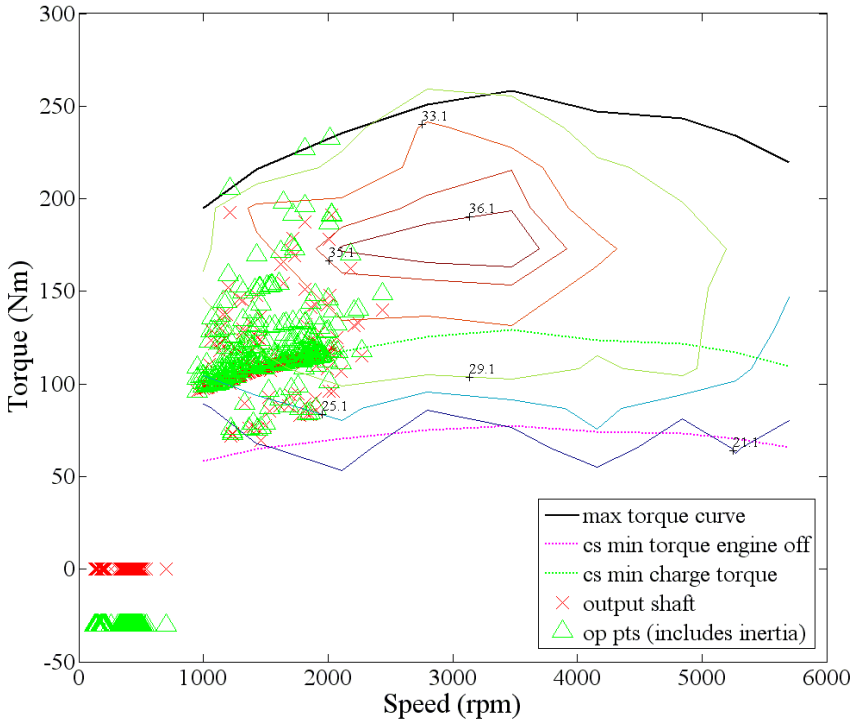

Figure A.23 - ICE operating points for the UDDS.

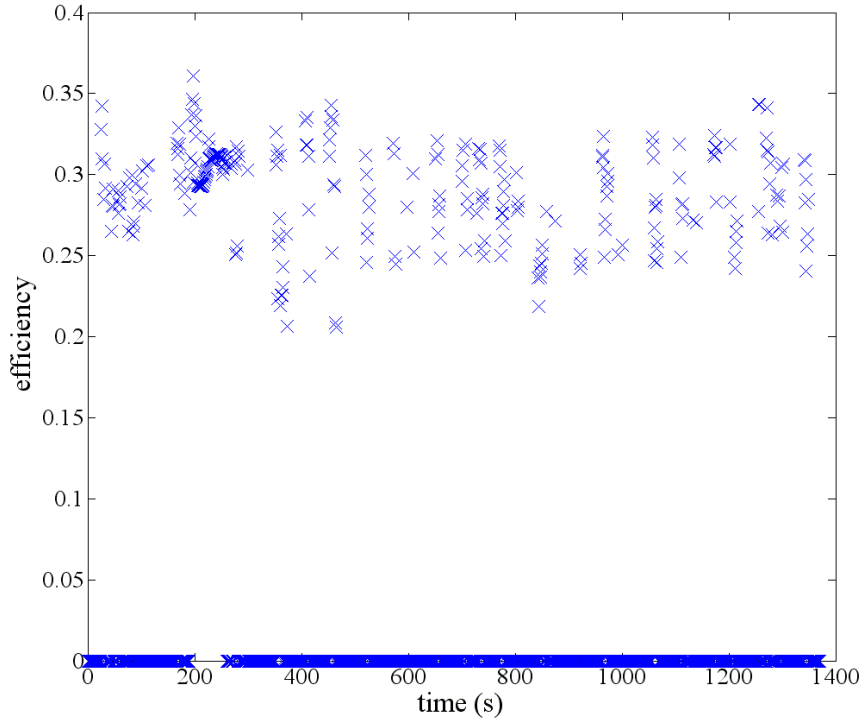

Figure A.24 - ICE efficiency over the UDDS, Average ICE efficiency is 26.9%.

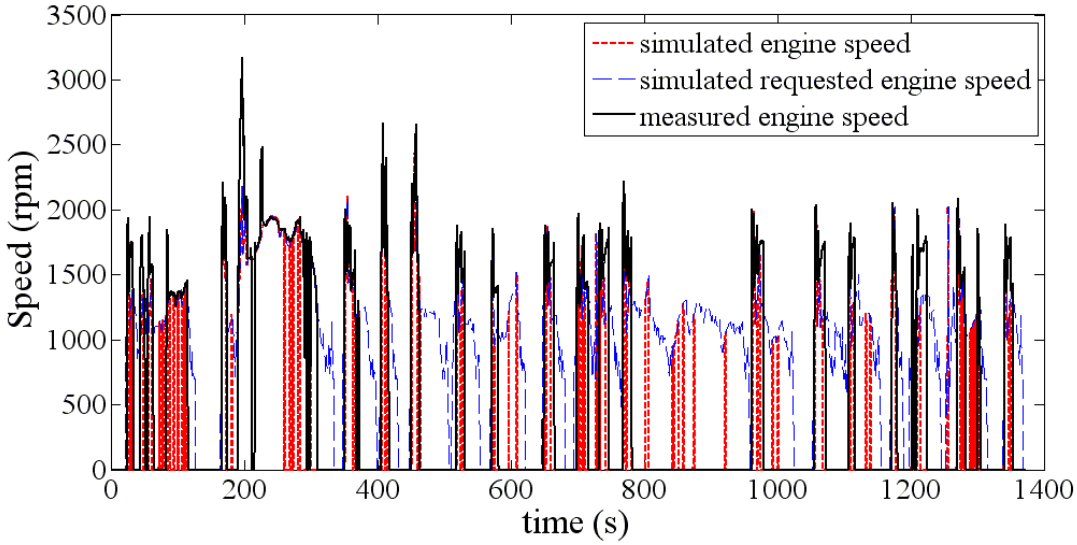

Figure A.25 - ICE speed over the UDDS. Control strategy for ICE on/off operation is unknown, strategy used in simulation is dependent on vehicle speed, acceleration and tractive torque relative to the SOC of the ESS. Gear ratios seem to be correct.

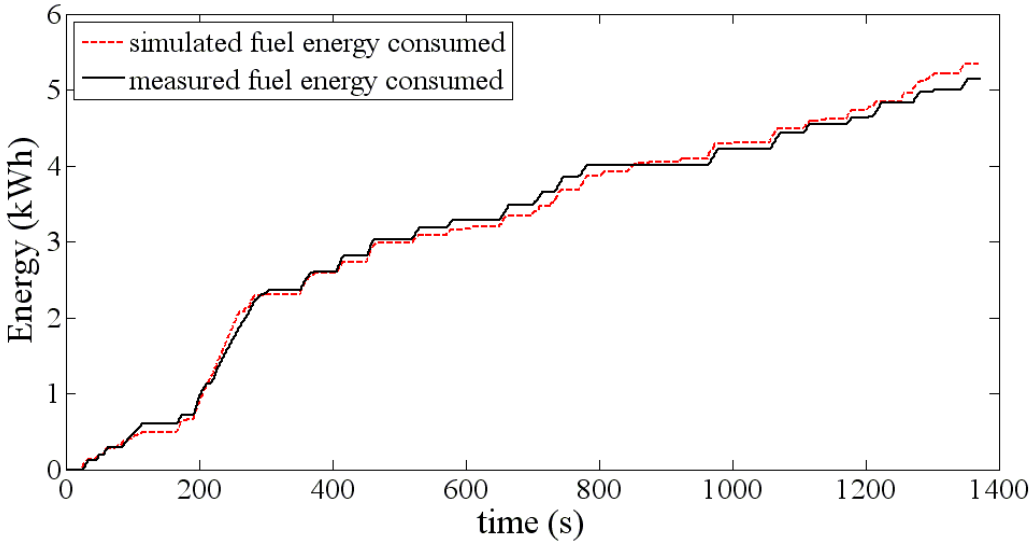

Figure A.26 - Total fuel consumption for the UDDS drive profile. While ICE speed operation is seen to be varying somewhat fuel consumption is relatively the same over the drive cycle.

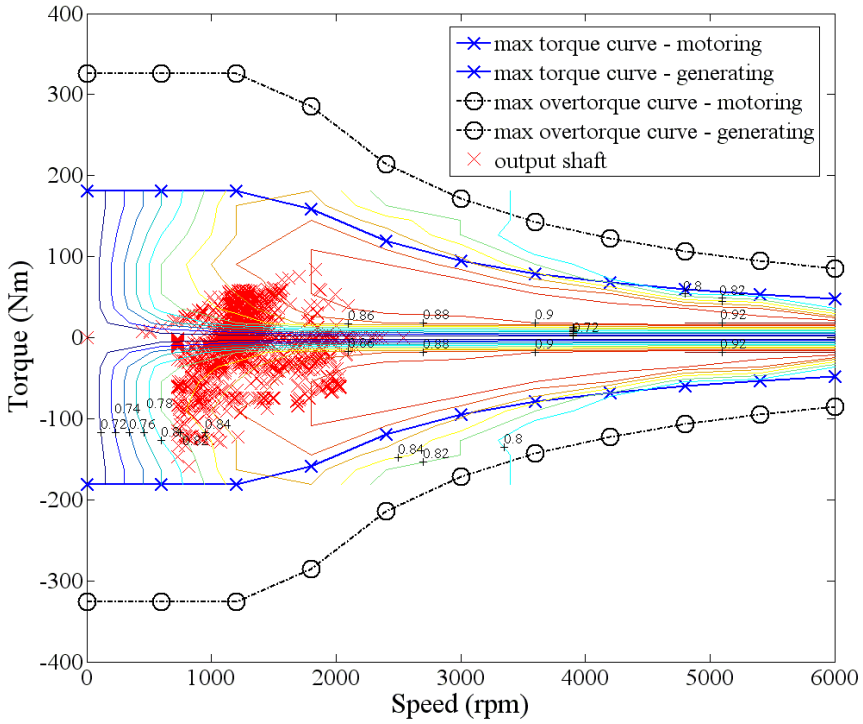

Figure A.27 – M/G operating points for the parallel topology adjacent to the ICE and before the transmission on the UDDS drive cycle.

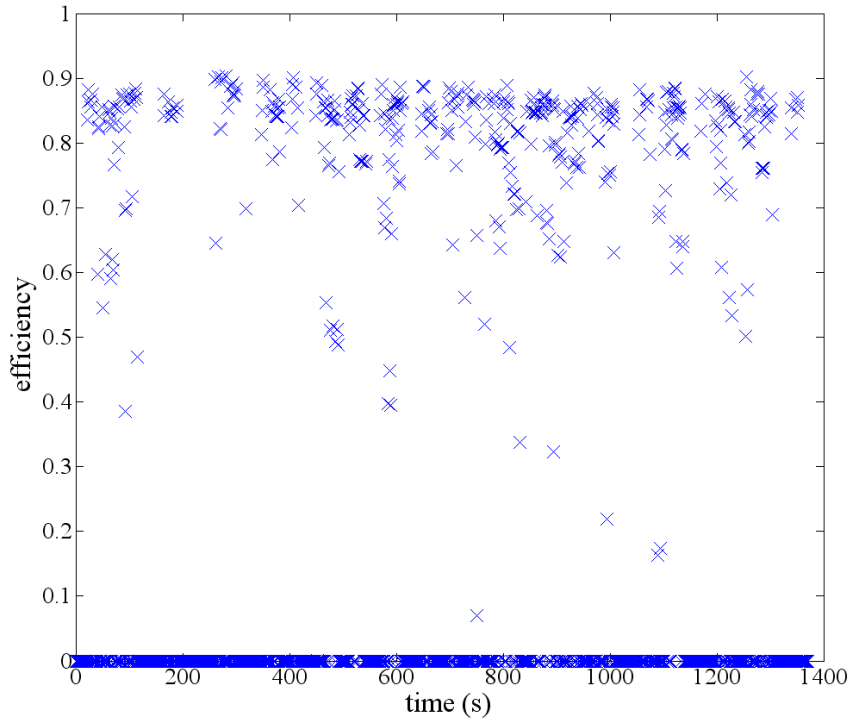

Figure A.28 – M/G efficiency over the UDDS. Motoring average efficiency is 82.4%.

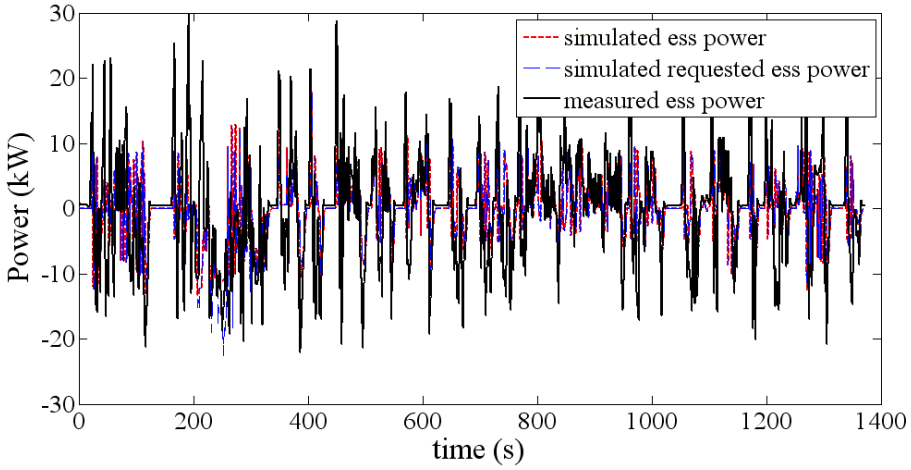

Figure A.29 - ESS power consumption over the UDDS.

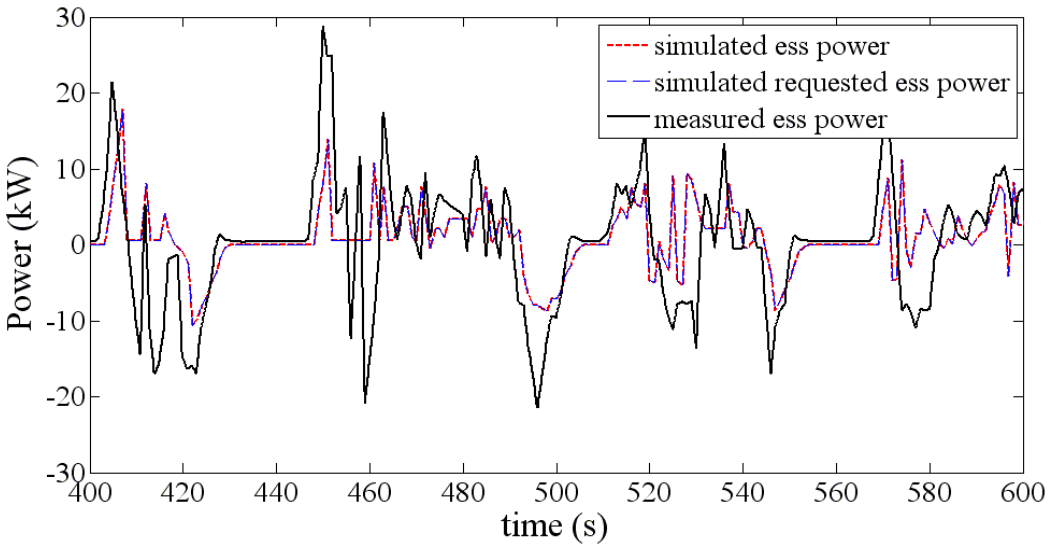

Figure A.30 - ESS power consumption over the UDDS for a smaller segment of time.

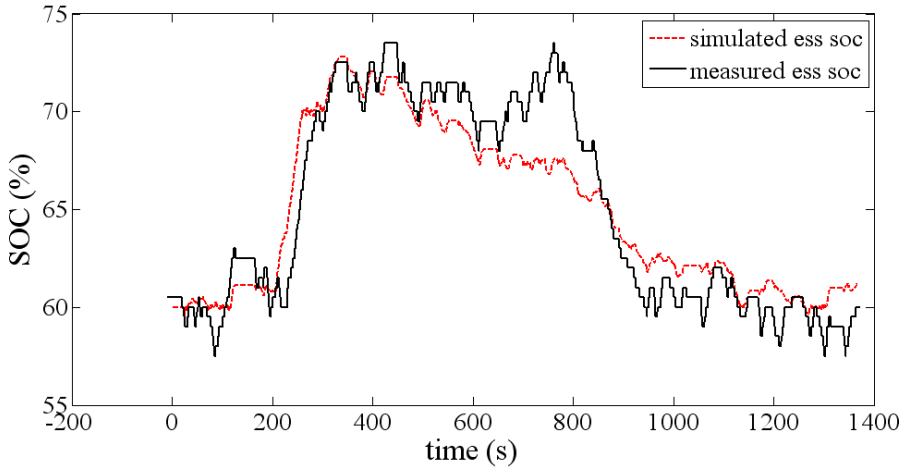

Figure A.31 – ESS SOC over the UDDS. Charge/discharge is similar; variations could not be mitigated without more information regarding the vehicle's control strategy.

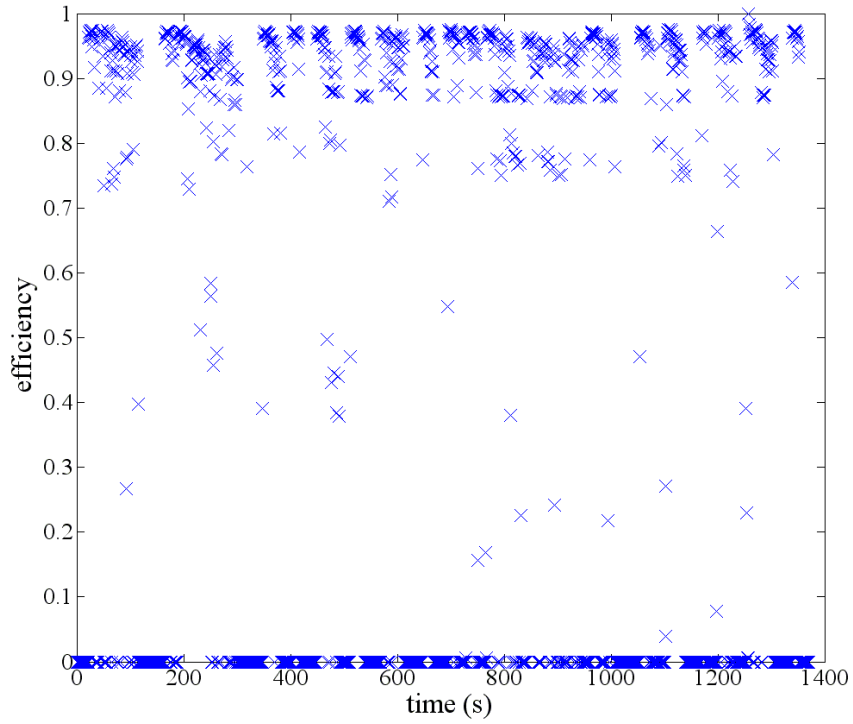

Figure A.32 - Drivetrain efficiency for the Hyundai Sonata Hybrid 2011 on the UDDS. Average drivetrain efficiency is 94.7%.

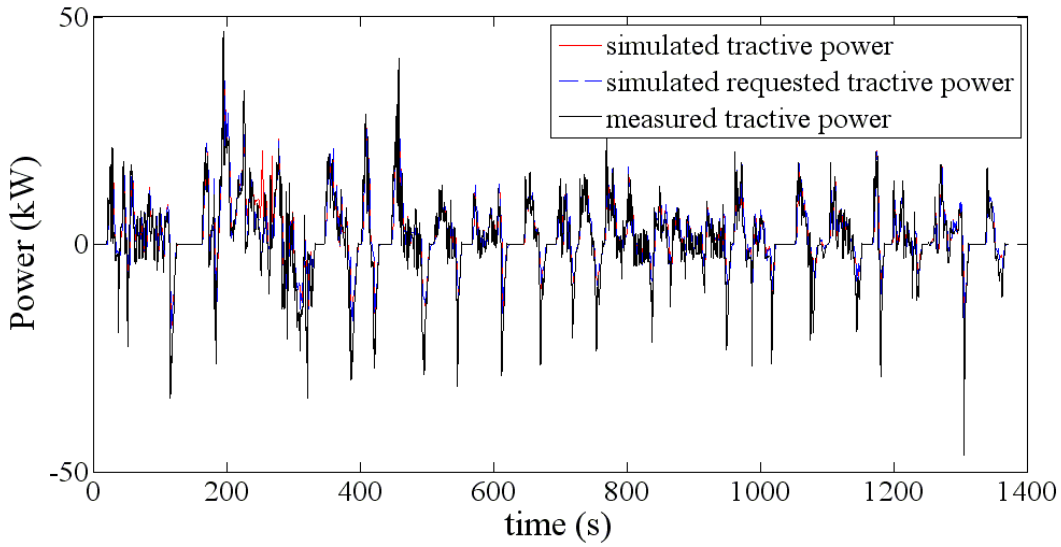

Figure A.33 - Tractive power requirement over the UDDS.

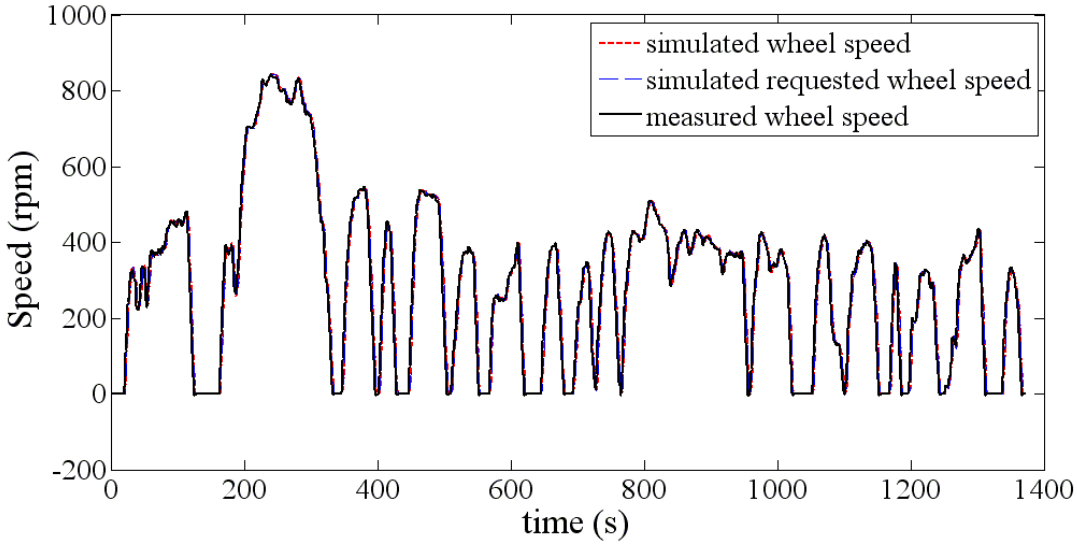

Figure A.34 - Wheel speed over the UDDS. Vehicle chassis dynamometer speed is used to calculate wheel speed using a wheel radius of 0.287 m.

A.1.3 Hyundai Sonata Hybrid Operating on HWFET

The following demonstrates the signals and specifications utilised for the Hyundai Sonata Hybrid 2011 test vehicle on the HWFET drive cycle.

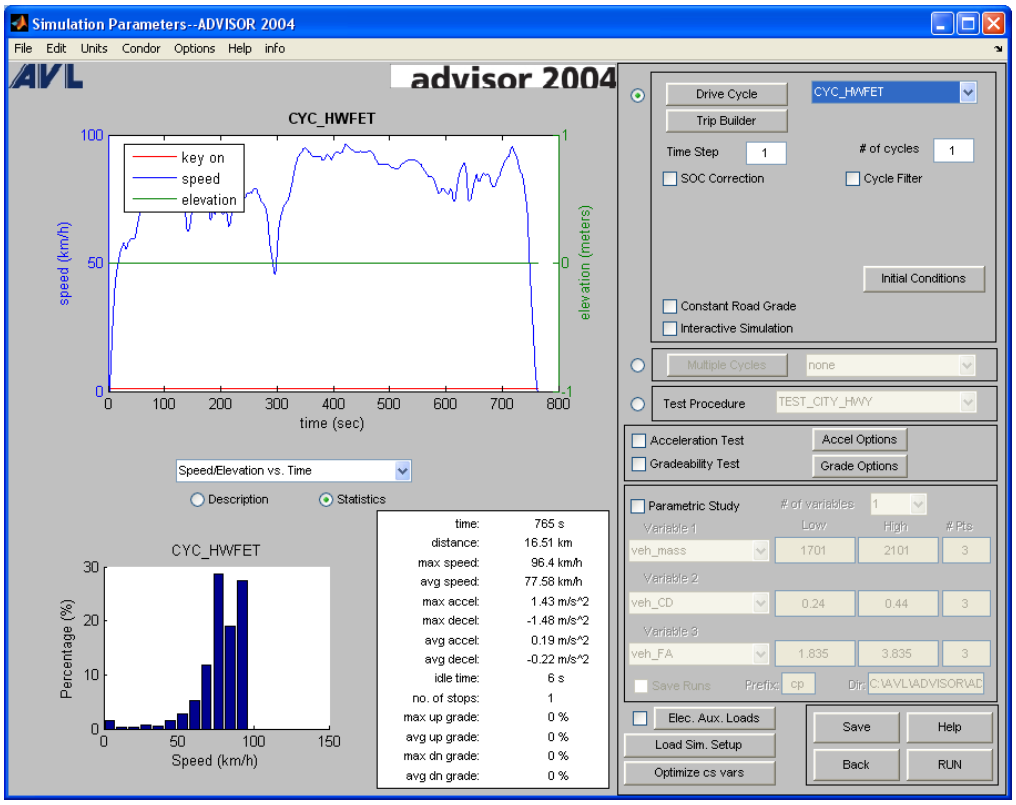

Figure A.35 - HWFET drive profile used for testing the developed model.

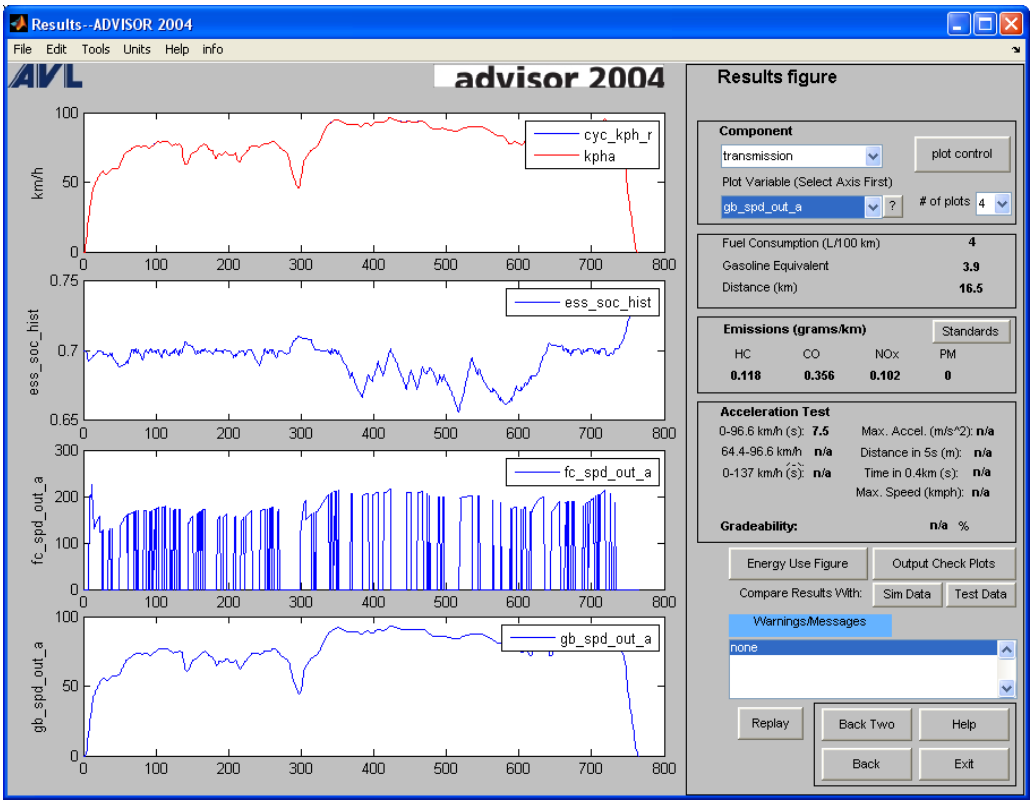

Figure A.36 - Results of the Hyundai Sonata Hybrid 2011 model for the HWFET. Measured data indicates that fuel consumption is 4.048 L/100km.

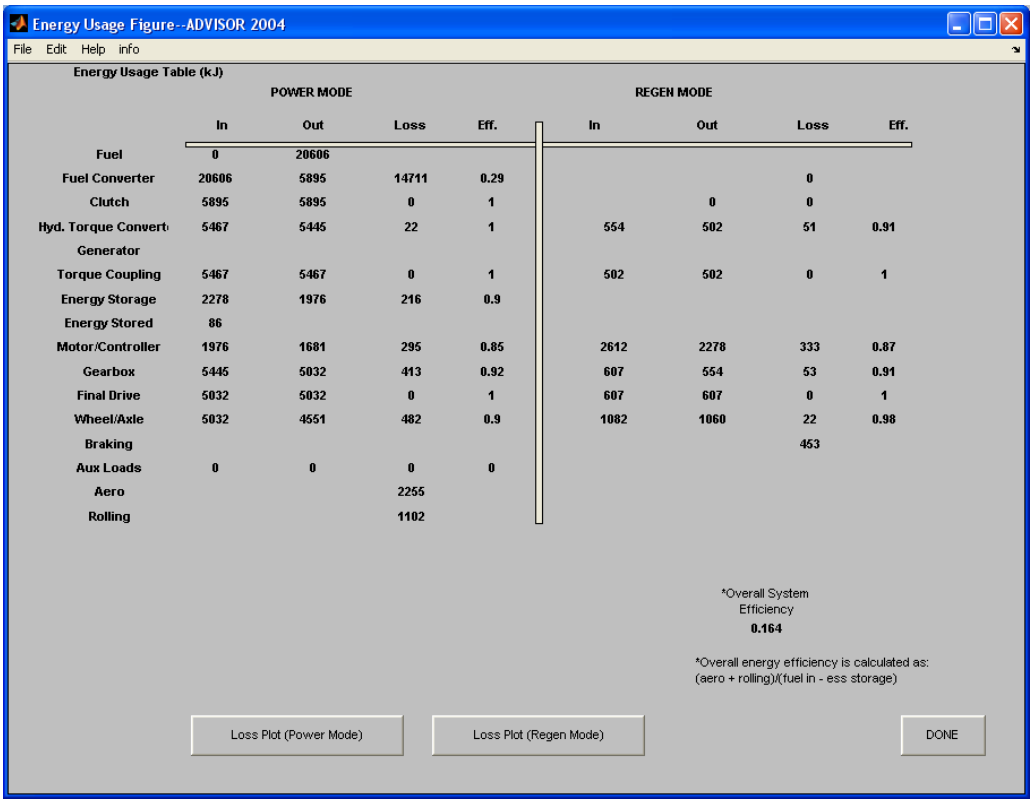

Figure A.37 - Energy usage figure identifying the efficiency of components.

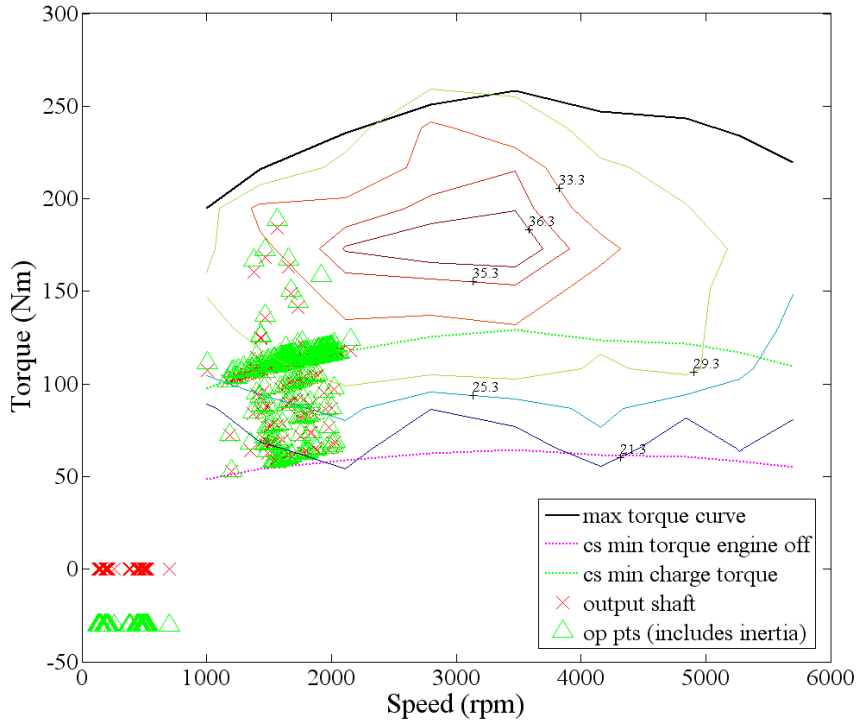

Figure A.38 - ICE operating points for the HWFET.

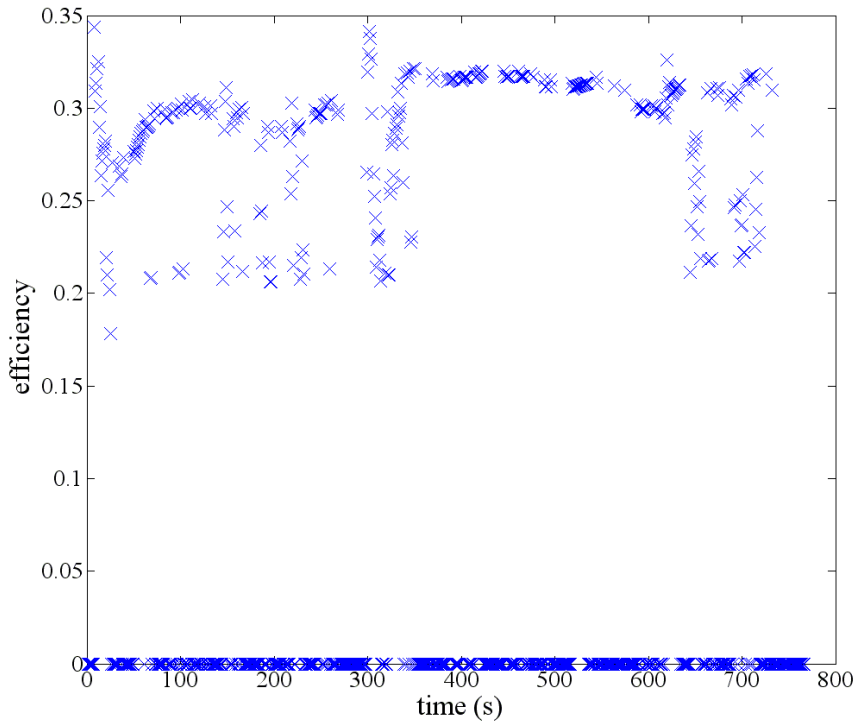

Figure A.39 - ICE efficiency over the HWFET, Average ICE efficiency is 27.7%.

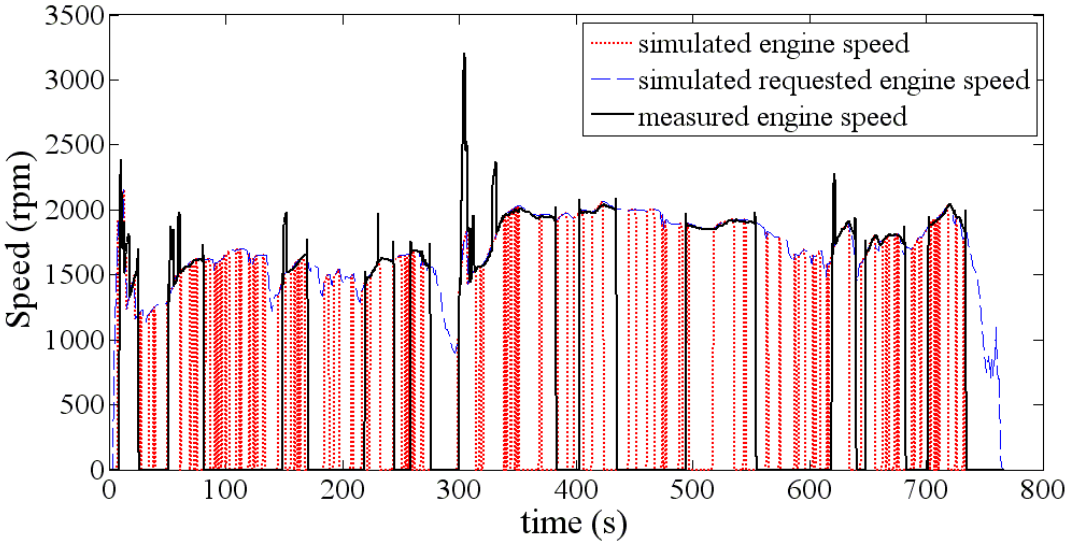

Figure A.40 - ICE speed over the HWFET. It is uncertain as to the exact ICE on/off strategy utilised. The frequency of ICE on/off suggests that the ICE has a minimum on time and remains on while charging the ESS to a set limit.

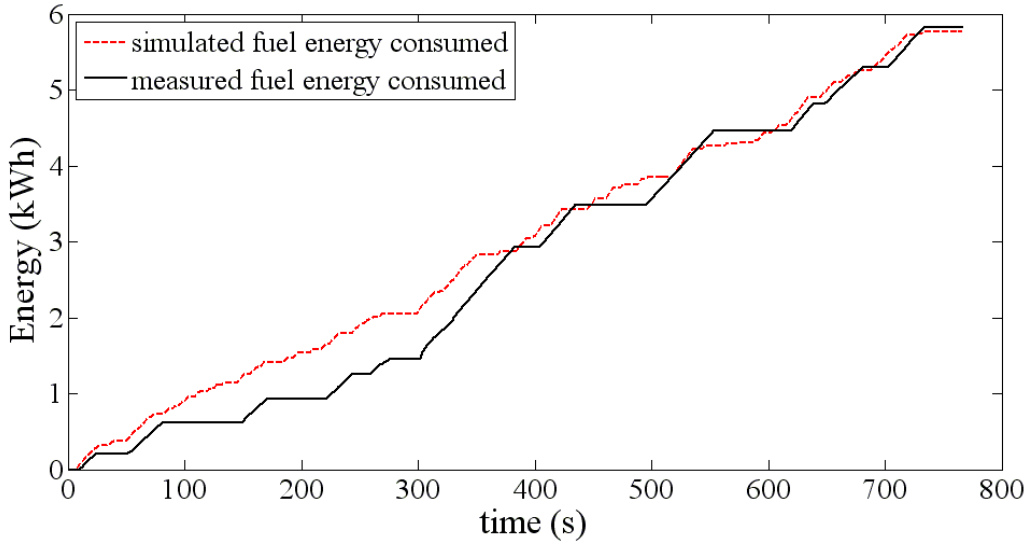

Figure A.41 - Total fuel consumption over the HWFET. Periods of fuel consumption vary for the simulated model however total fuel consumption is similar.

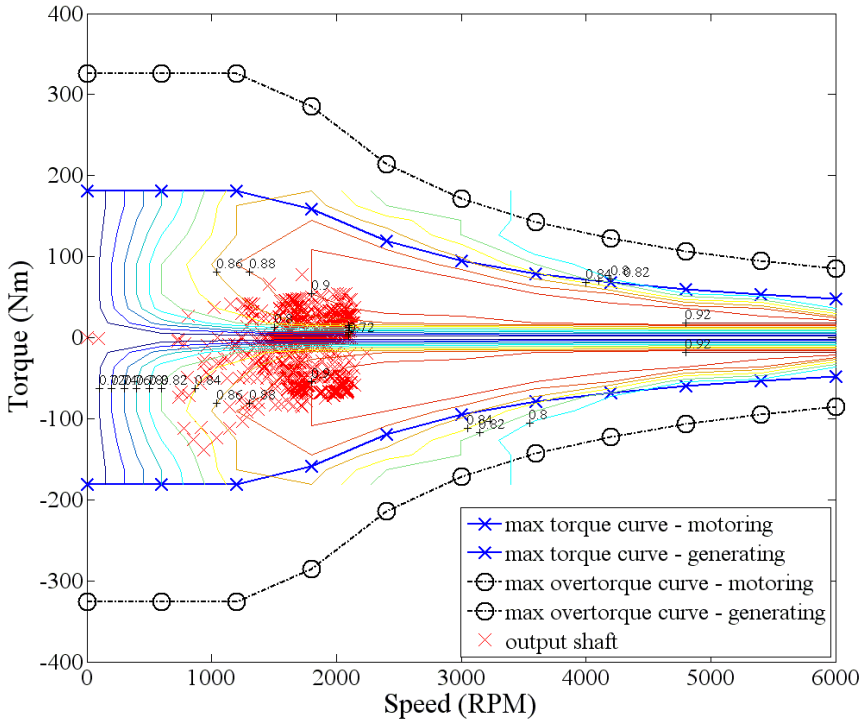

Figure A.42 – M/G operating points for the parallel topology adjacent to the ICE and before the transmission on the HWFET.

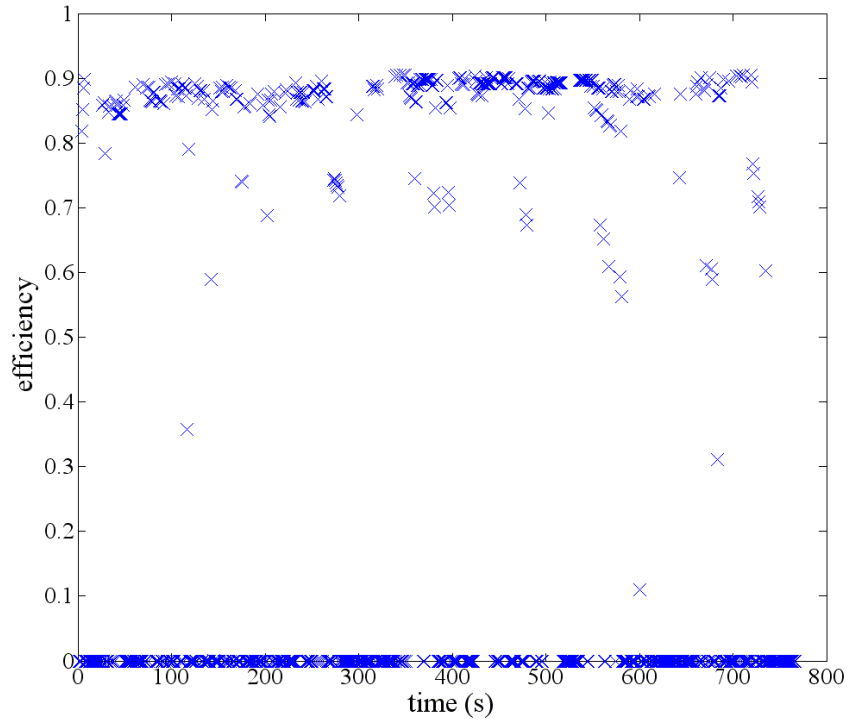

Figure A.43 – M/G efficiency over the UDDS. Motoring average efficiency is 85.1%.

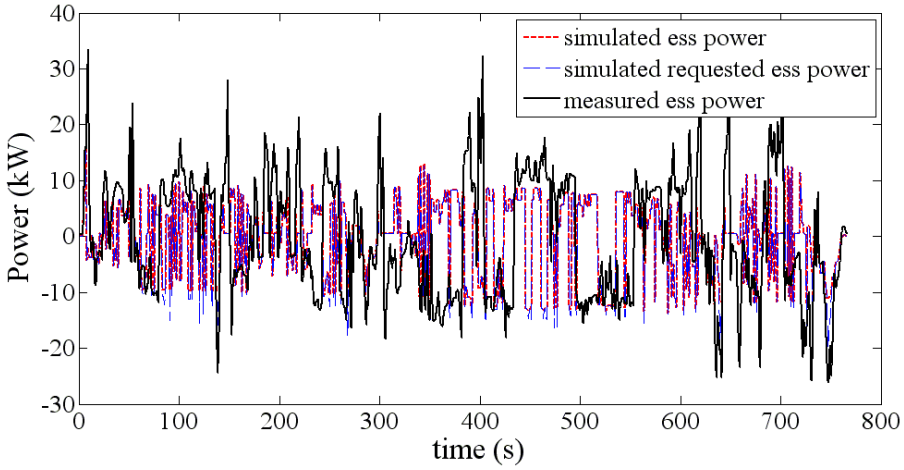

Figure A.44 - ESS power consumption over the HWFET.

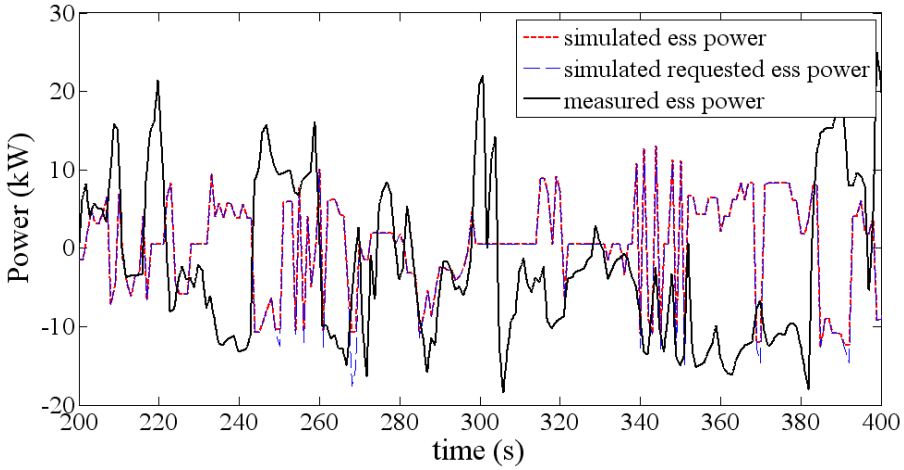

Figure A.45 - ESS power consumption over the HWFET for a smaller segment of time.

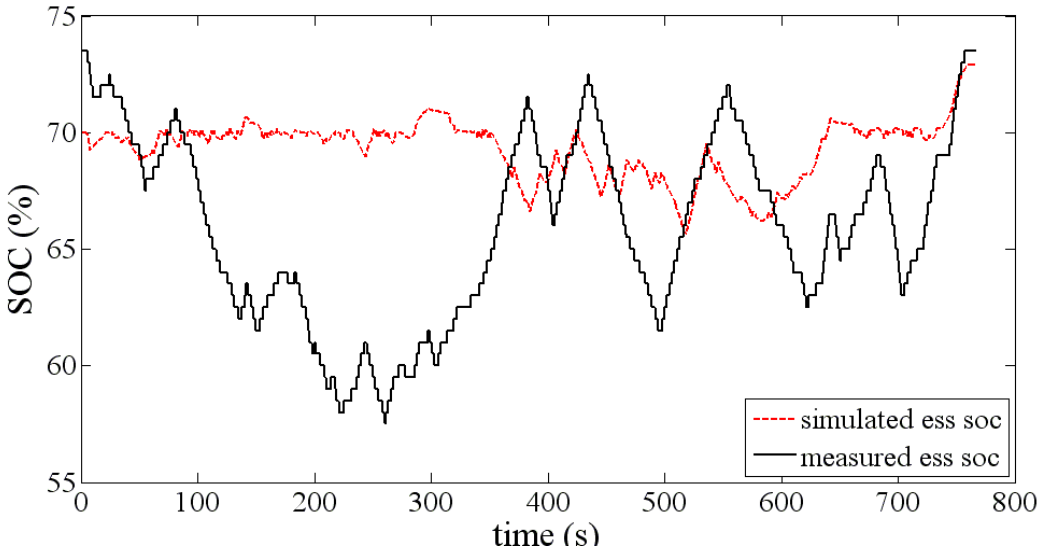

Figure A.46 - ESS SOC over the HWFET. The control strategy utilised in the simulation is different to the actual vehicle however the final SOC is the same.

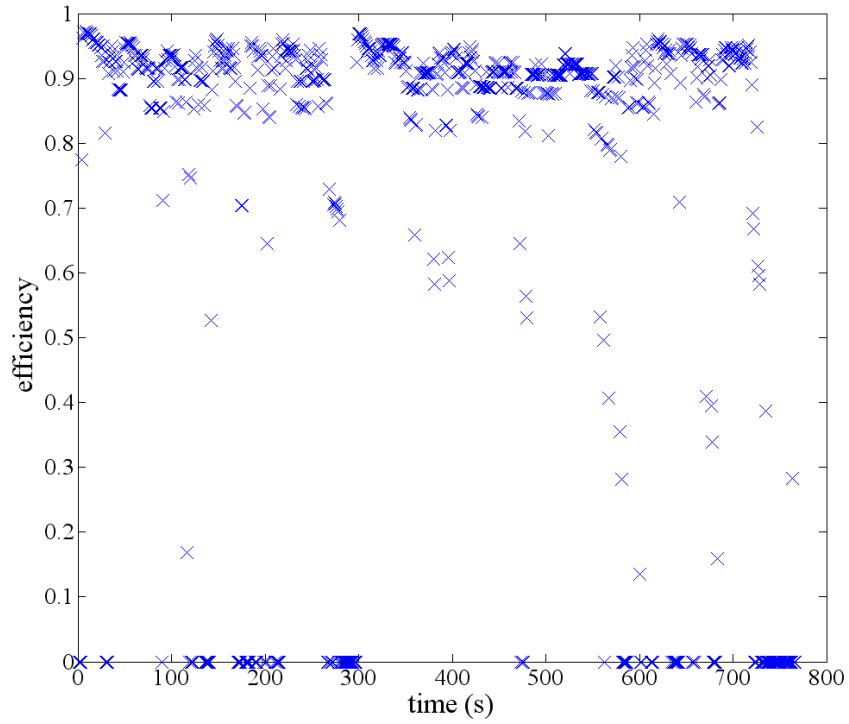

Figure A.47 - Drivetrain efficiency for the Hyundai Sonata Hybrid 2011 on the HWFET. Average drivetrain efficiency is 92.4%.

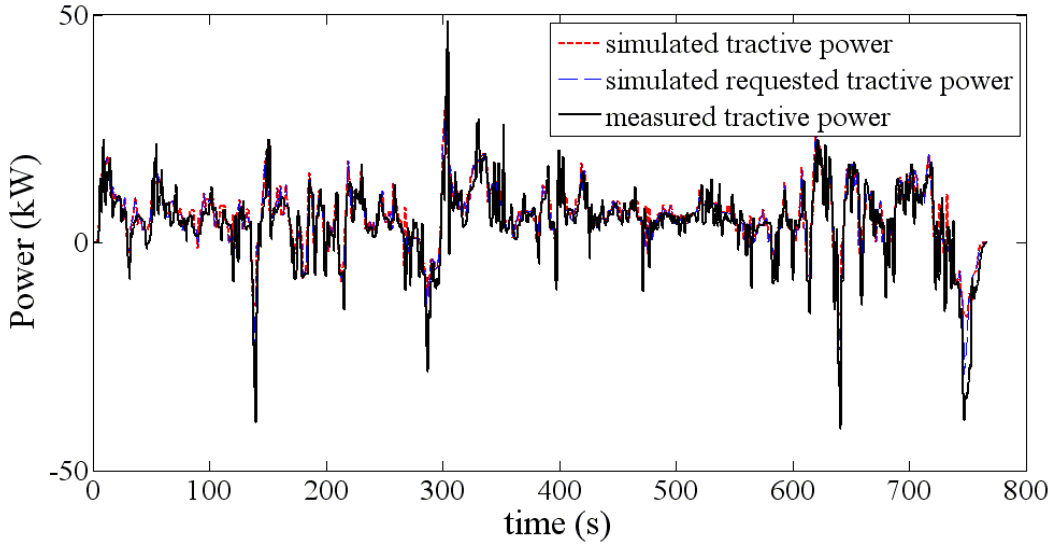

Figure A.48 - Tractive power consumption over the HWFET.

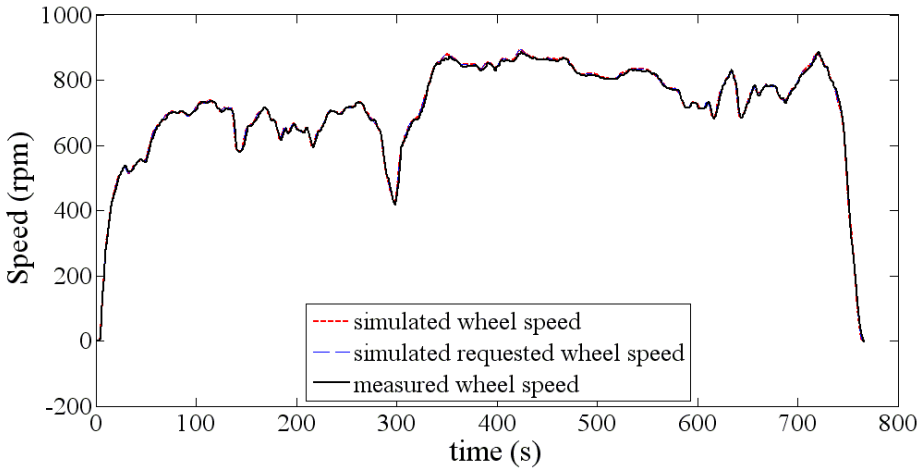

Figure A.49 - Wheel speed over the HWFET. Vehicle chassis dynamometer speed has been used to calculate wheel speed with a wheel radius of 0.287 m.

A.1.4 Honda CR-Z Operating on UDDS

Table A.3 – Honda CR-Z 2010 specifications as used in the ADVISOR software.

Description	Symbol	Value	Unit
Mass	M	1211	kg
Rolling Resistance Coefficient	f_r	0.00648	-
Air Density	ρ	1.2	kg/m^3
Coefficient of Aerodynamic Drag	C_D	0.25	-
Frontal Area of Vehicle	A_f	2.427	m^2
Gravitational Acceleration	g	9.81	m/s^2
Wheel Radius	r_d	0.275	m

The following demonstrates the signals and specifications utilised for the Honda CR-Z 2010 test vehicle on the UDDS drive cycle.

Appendices

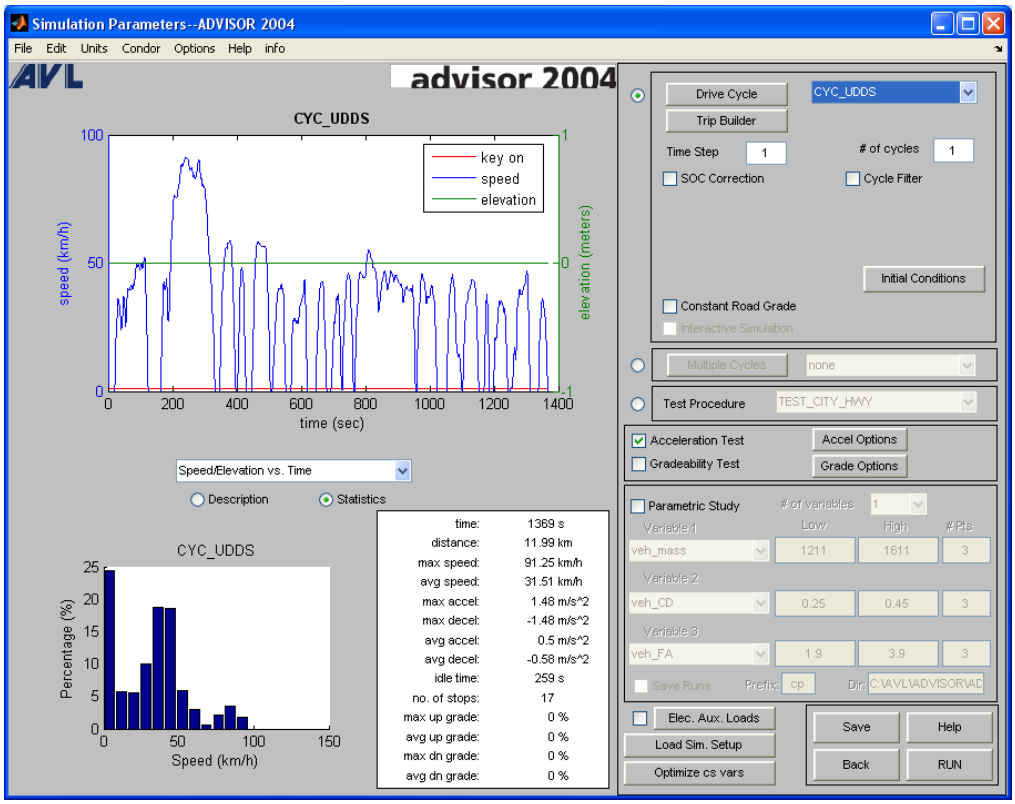

Figure A.50 - UDDS drive profile used for testing the developed model.

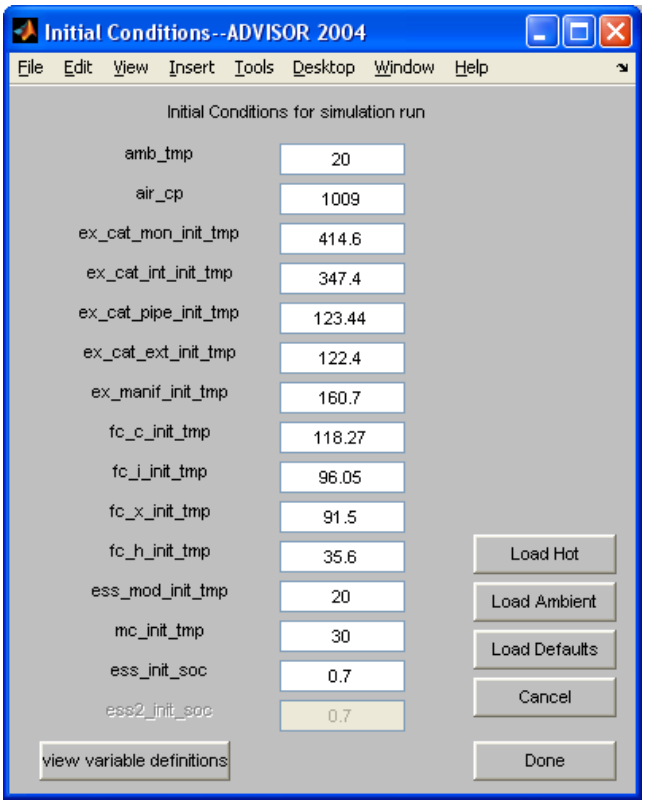

Figure A. 51 - Initial conditions specified for the simulations to ensure hot start testing.

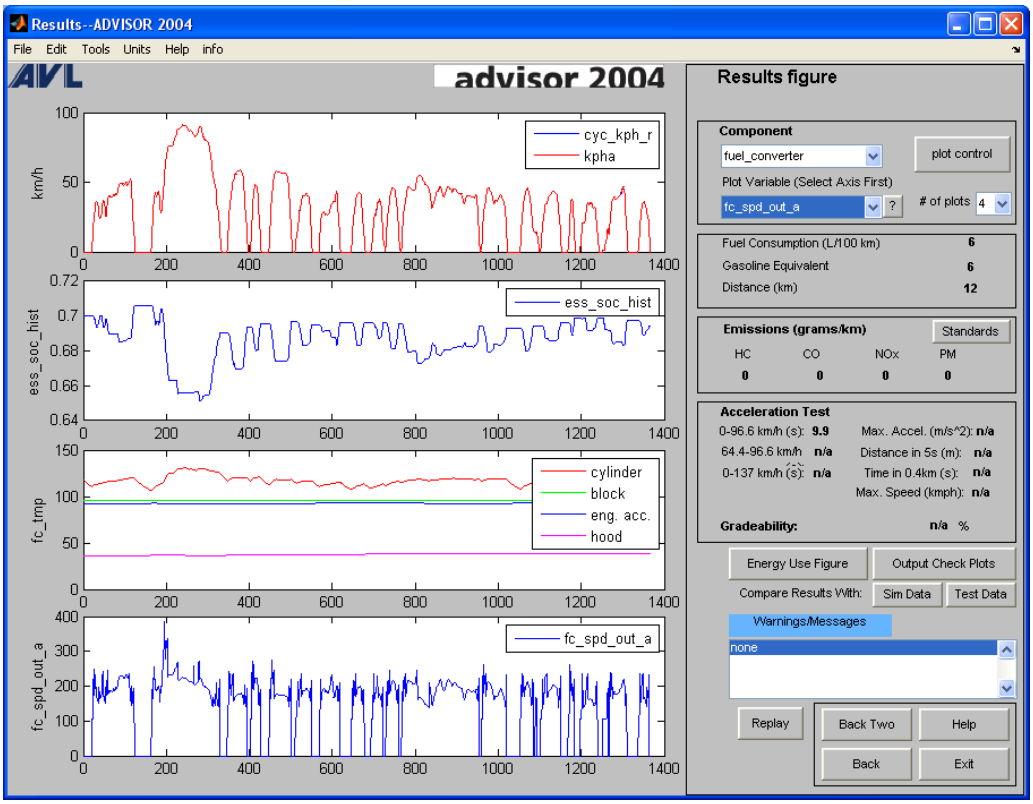

Figure A.52 - Results of the Honda CR-Z model for the UDDS. Measured data indicates that fuel consumption is 6.04 L/100km.

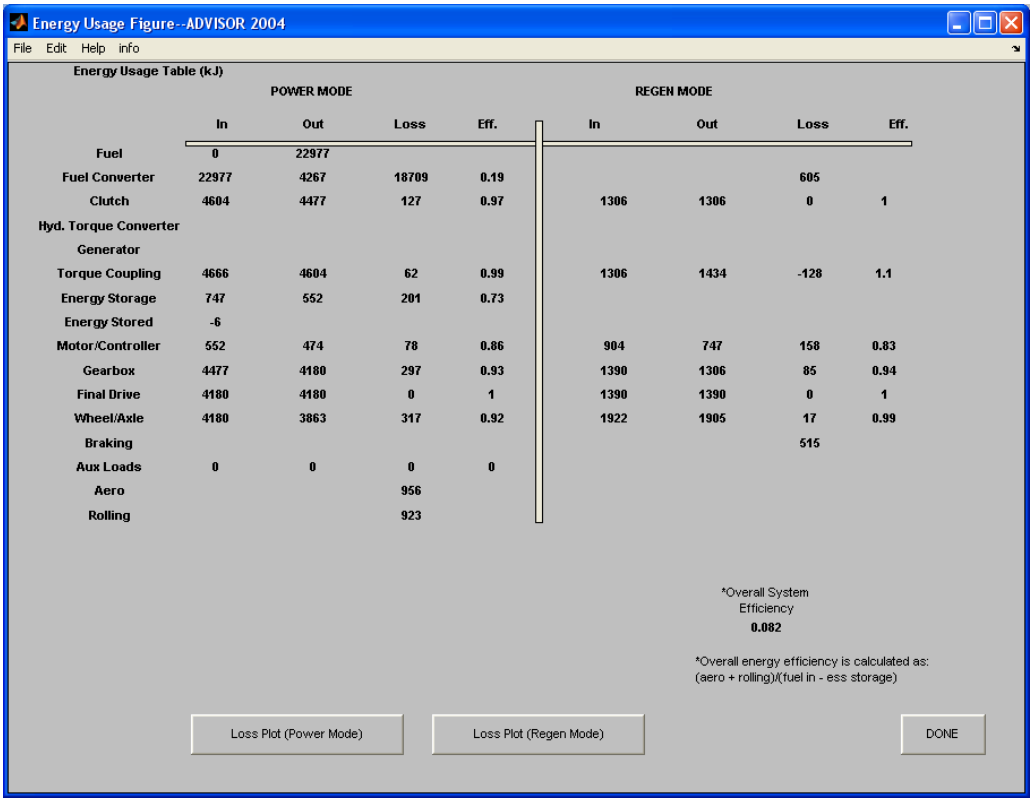

Figure A.53 - Energy usage figure identifying the efficiency of components in the powertrain and drivetrain for the Honda CR-Z.

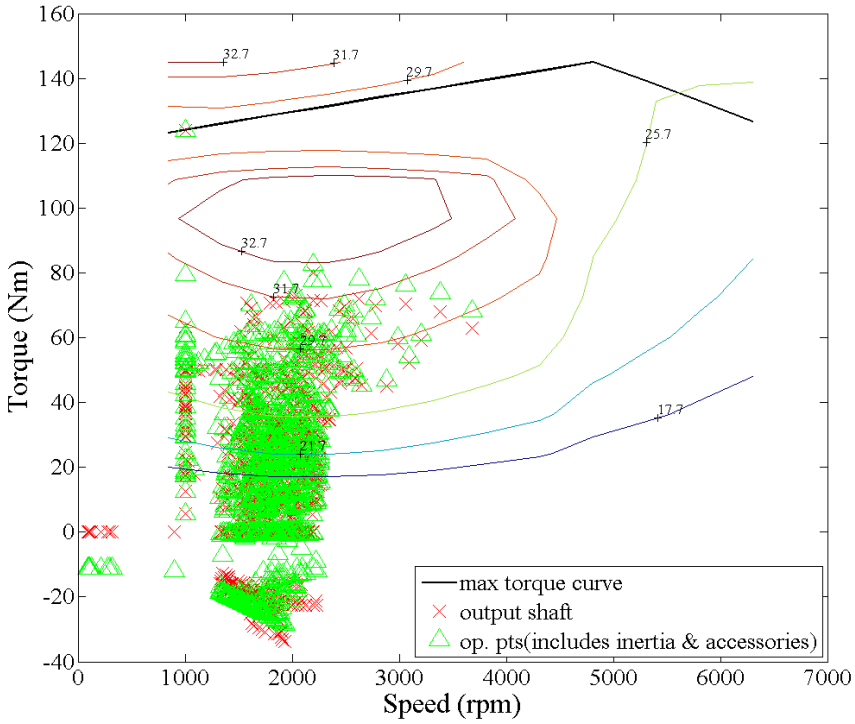

Figure A.54 - ICE operating points for the UDDS.

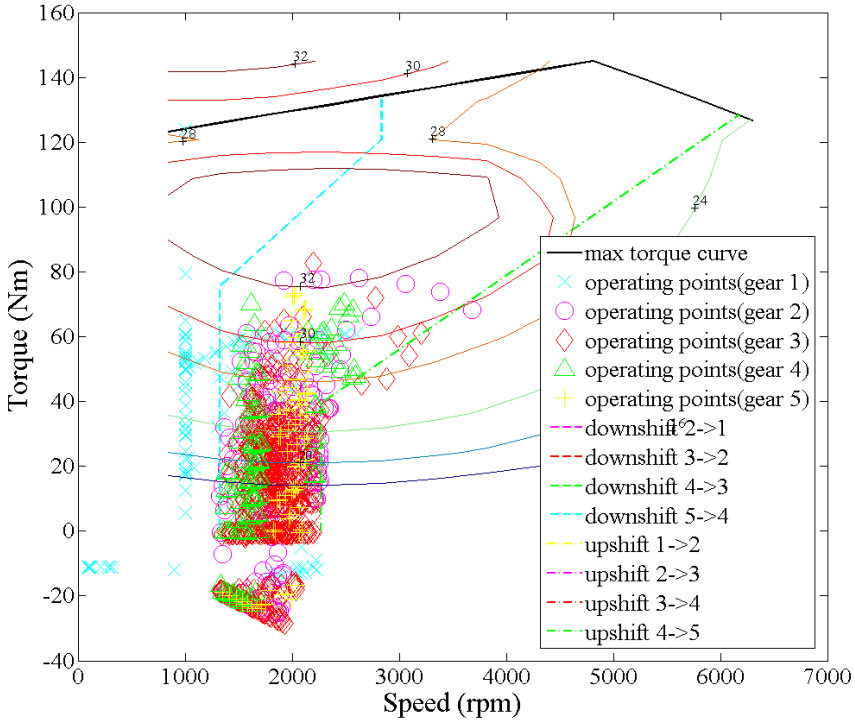

Figure A.55 - Operating points for ICE highlighting the gear speed limits for the original controller.

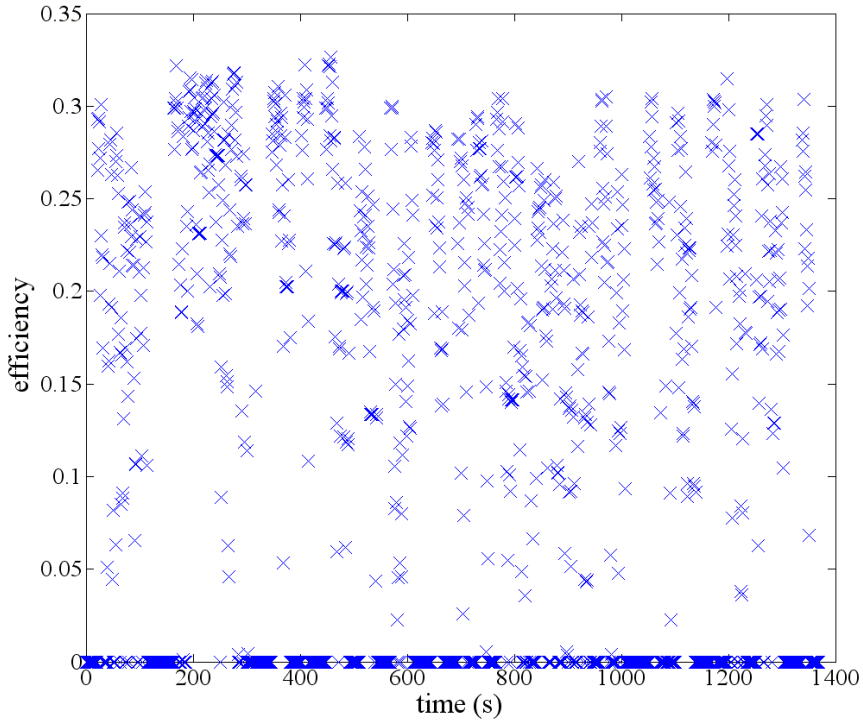

Figure A.56 - ICE efficiency over the UDDS. Average ICE efficiency is 16.5%.

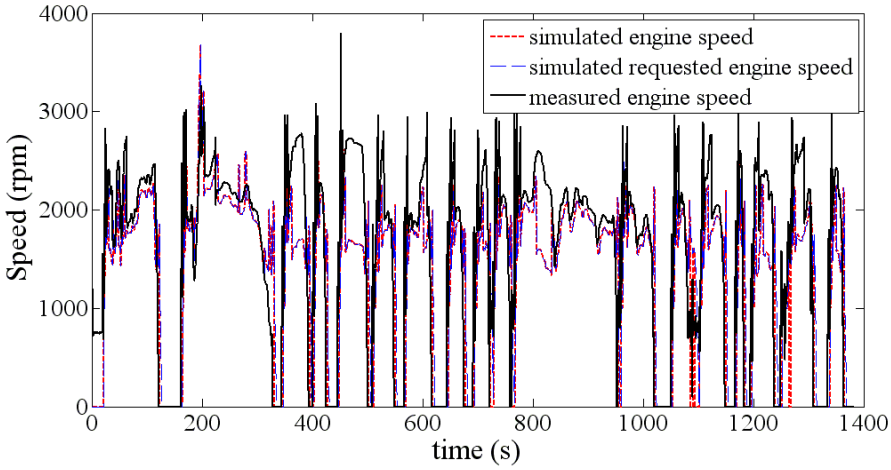

Figure A.57 - ICE speed for the UDDS drive profile. Variations in ICE speed are due to the gear ratios selected for the transmission as well as the wheel radius.

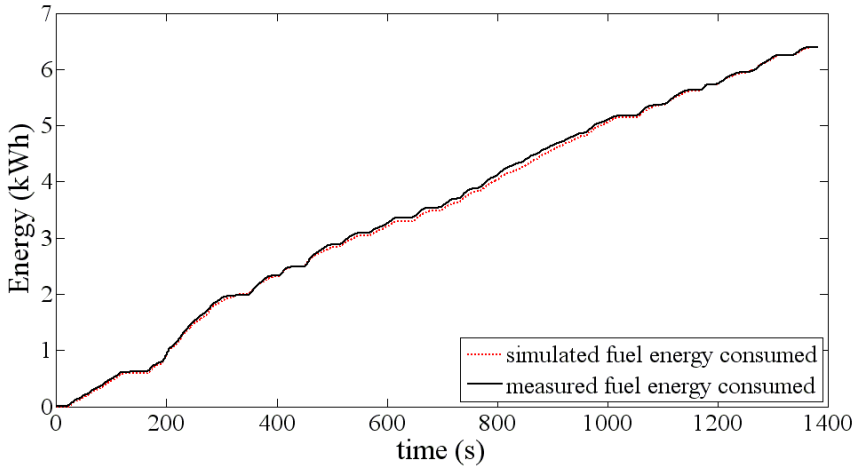

Figure A.58 - Total fuel consumption over the UDDS. Simulated ICE is operating very closely to the measured data.

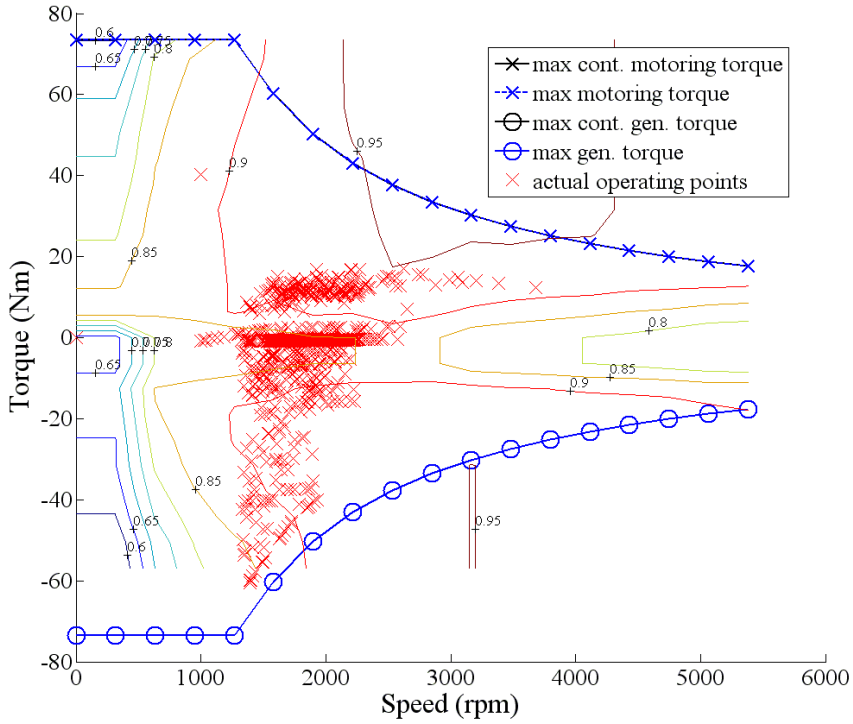

Figure A.59 – M/G operating points for the IMA coupled between the ICE and transmission.

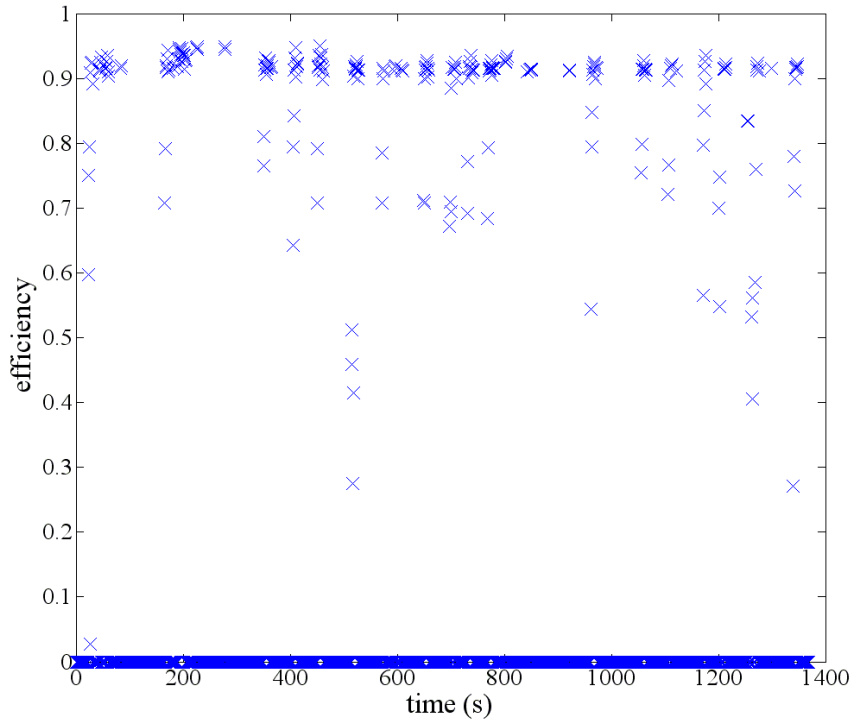

Figure A.60 – M/G efficiency over the UDDS. Motoring average efficiency is 85.9%.

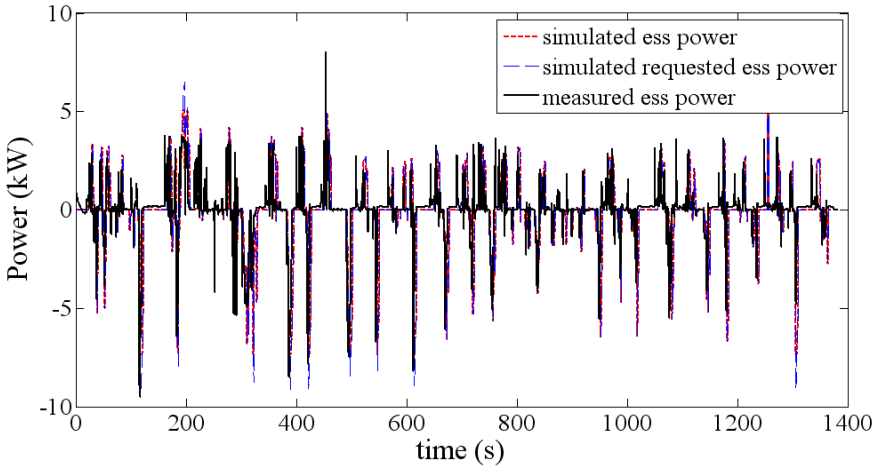

Figure A.61 - ESS power consumption during the UDDS. Requirement is reflected in the size of the traction motor at 10 kW.

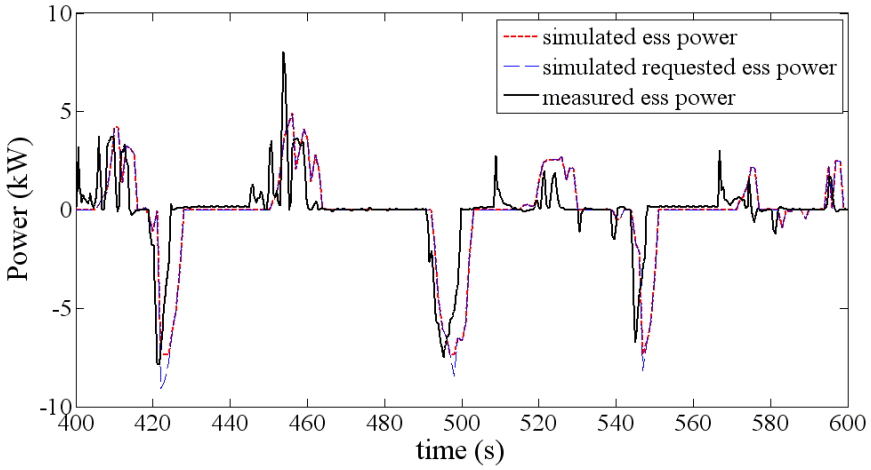

Figure A.62 - ESS power consumption for a smaller segment of time.

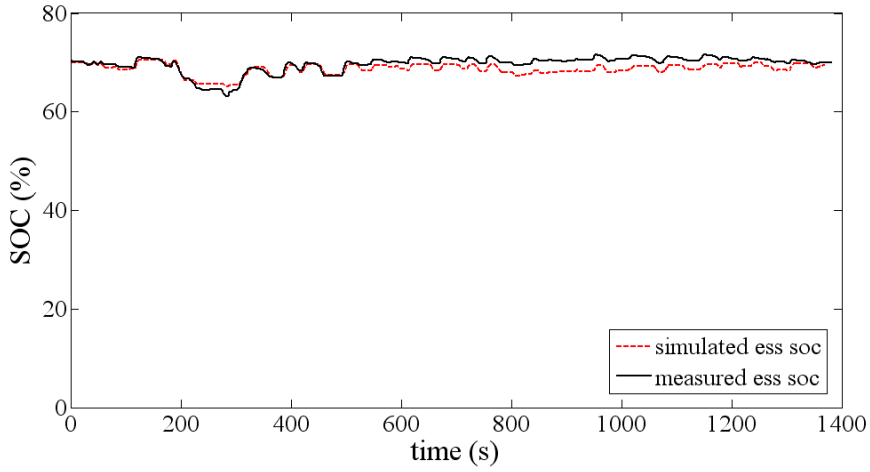

Figure A.63 - ESS SOC for the UDDS. Due to the simple topology it was quite easy to identify a similar charging/discharging profile.

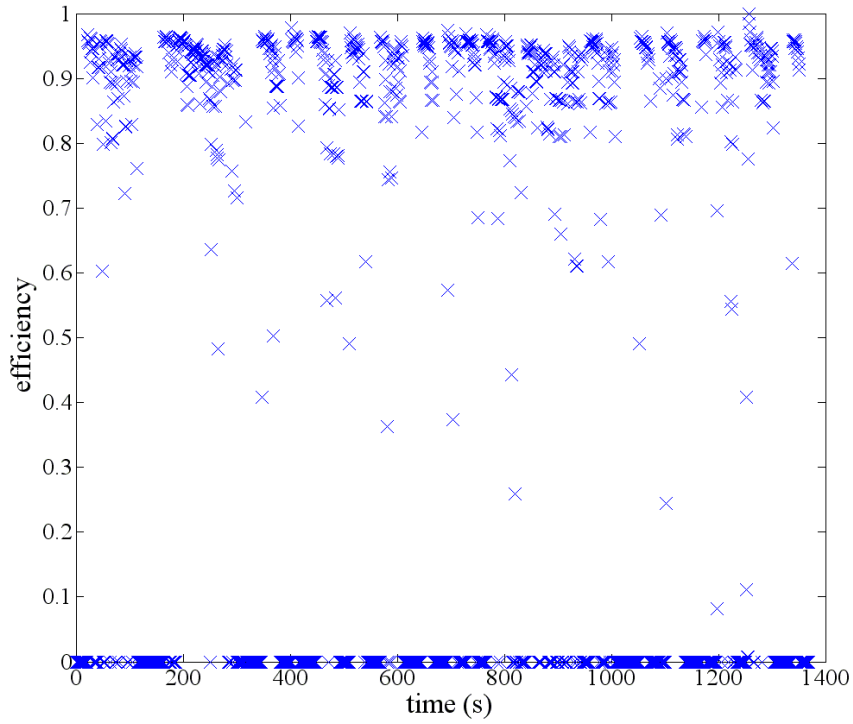

Figure A.64 - Drivetrain efficiency for the Honda CR-Z on the UDDS. Average drivetrain efficiency is 93.4%.

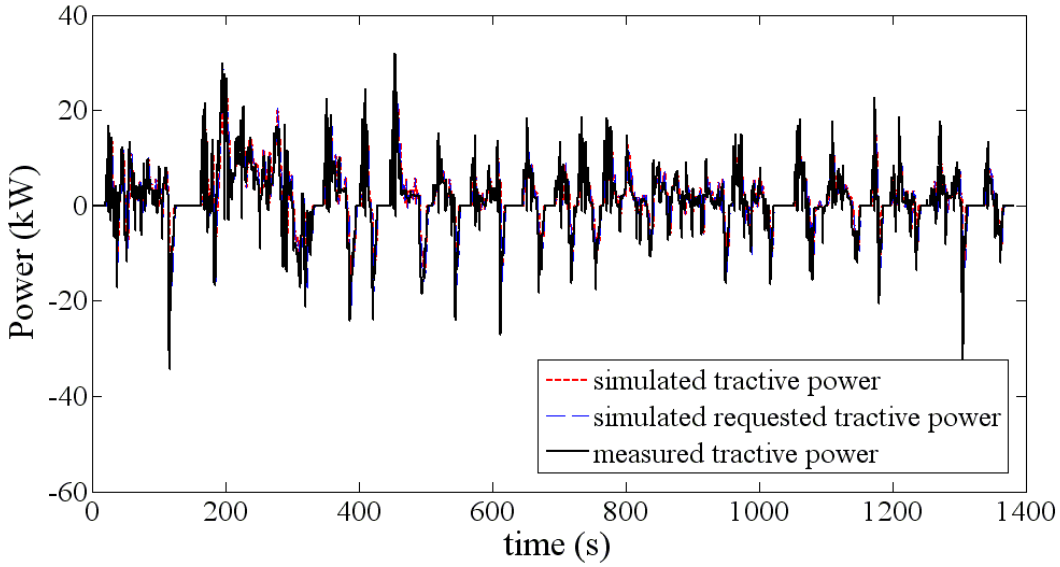

Figure A.65 - Tractive power required to propel the vehicle over the UDDS.

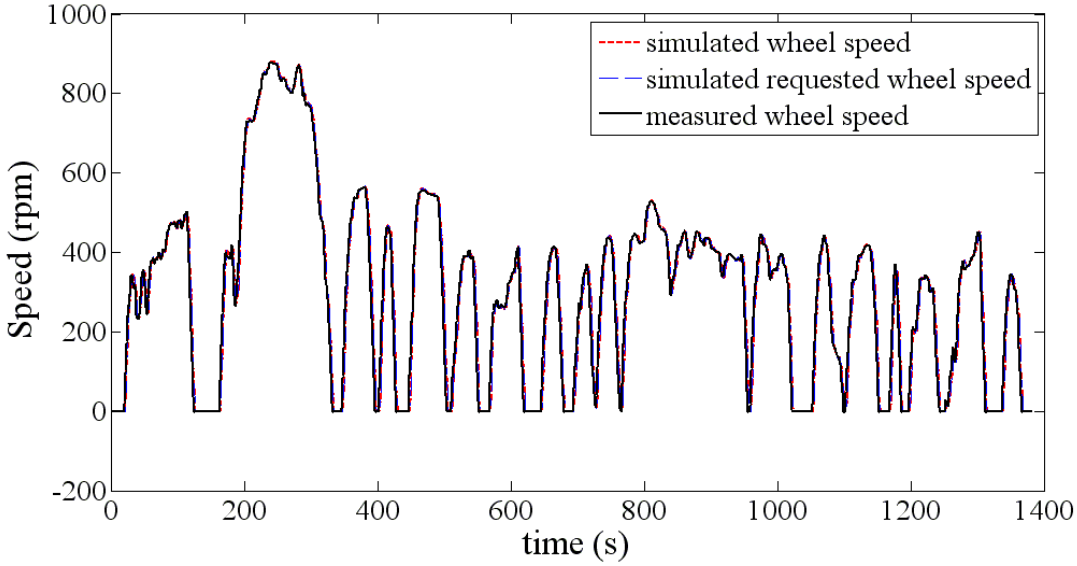

Figure A.66 - Wheel speed achieved by the vehicle with a wheel radius of 0.275 m. Wheel speed is calculated from chassis dynamometer speed using the same wheel radius as seen in simulation.

A.1.5 Honda CR-Z Operating on HWFET

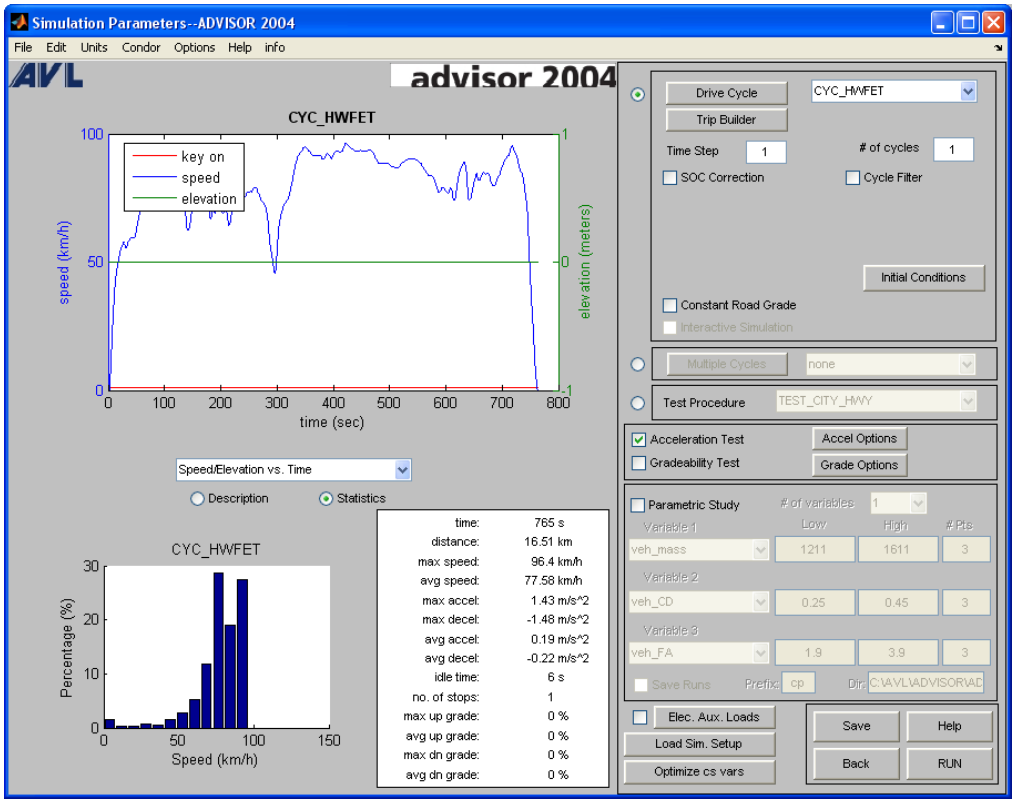

Figure A.67 - HWFET drive profile used for testing the developed model.

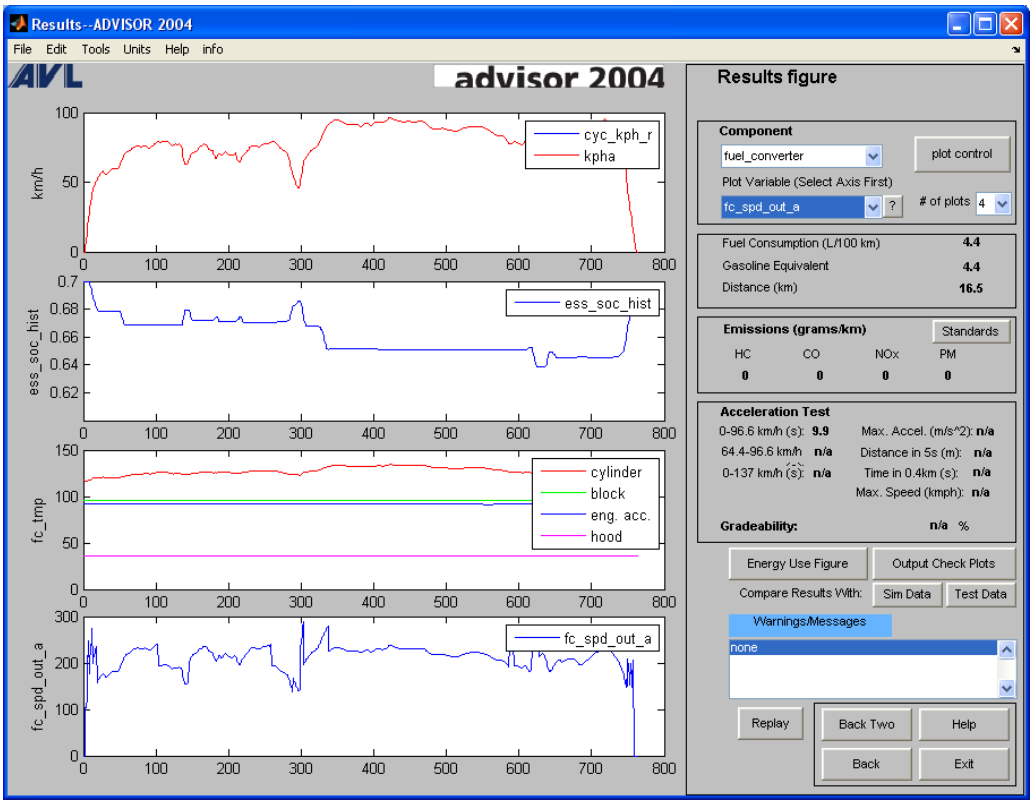

Figure A.68 - Results of the Honda CR-Z model for the HWFET. Measured data indicates that fuel consumption is 4.48 L/100km.

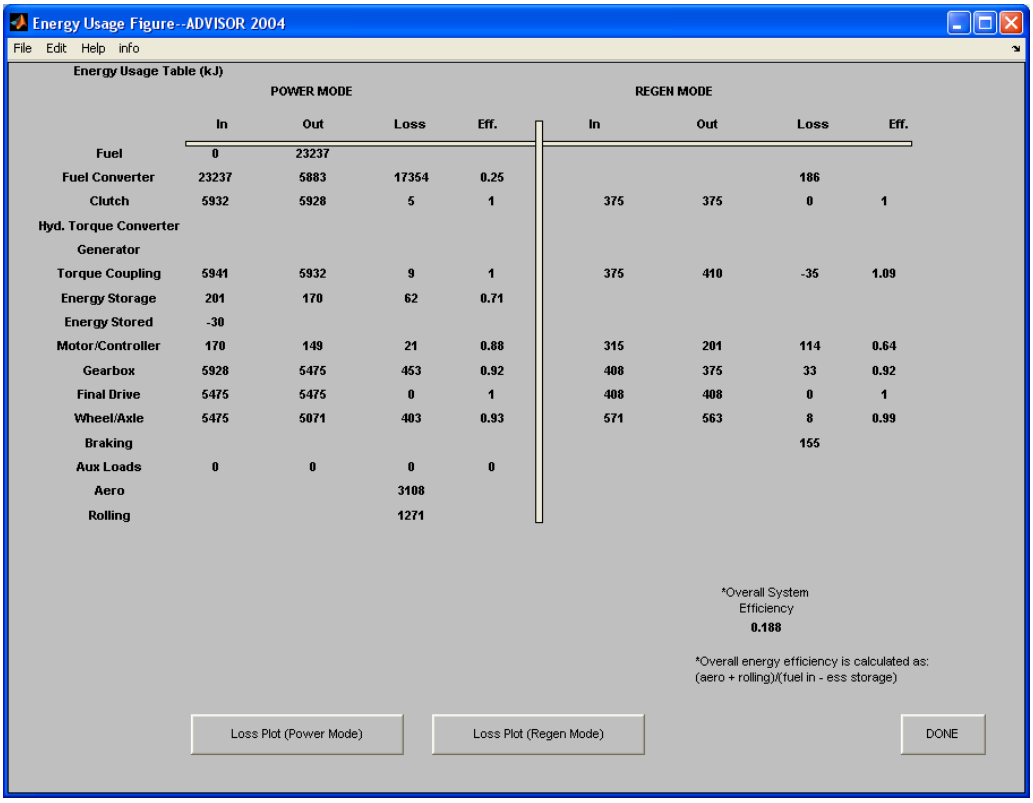

Figure A.69 - Energy usage figure identifying the efficiency of components in the powertrain and drivetrain for the Honda CR-Z.

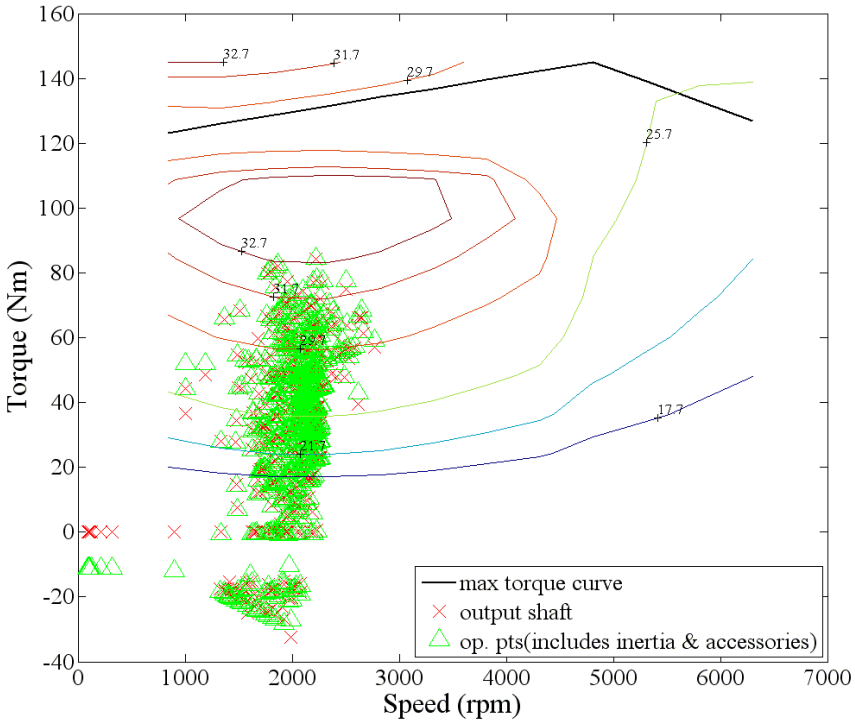

Figure A.70 - ICE operating points for the HWFET.

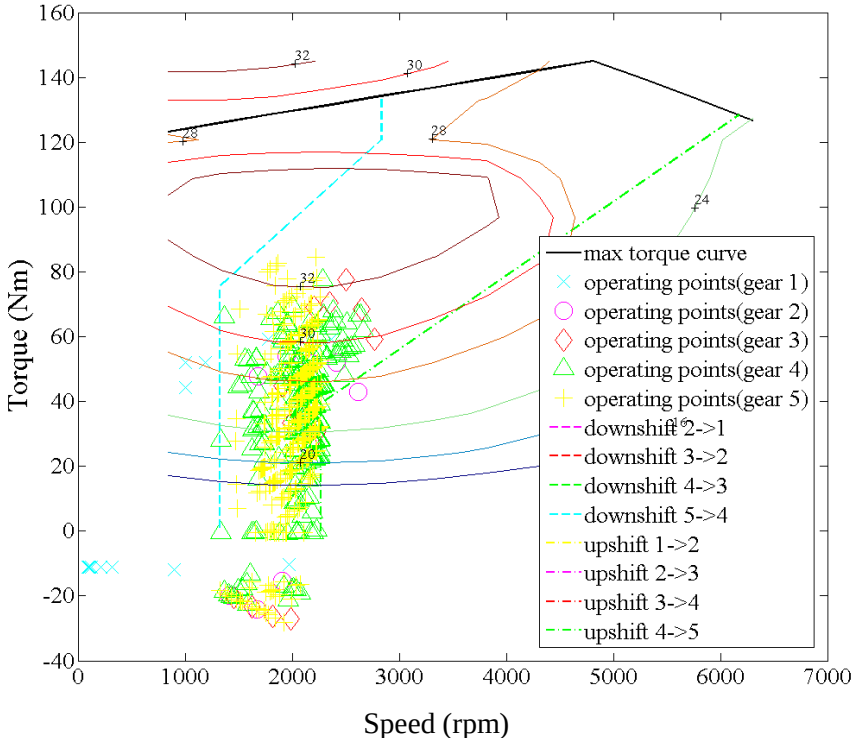

Figure A.71 - Operating points for ICE highlighting the gear speed limits for the original controller.

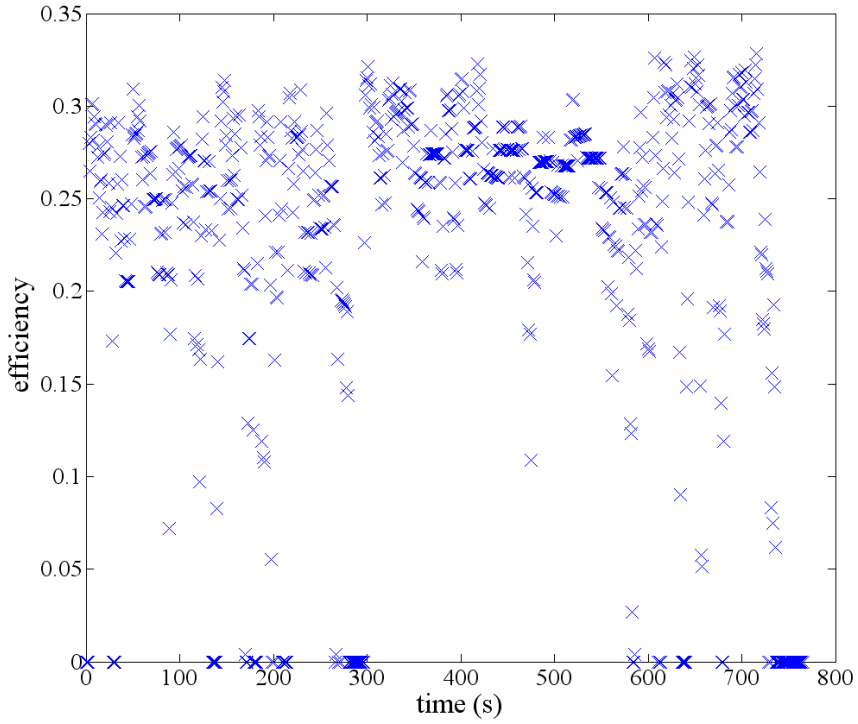

Figure A.72 - ICE efficiency over the HWFET. Average ICE efficiency is 24.6%.

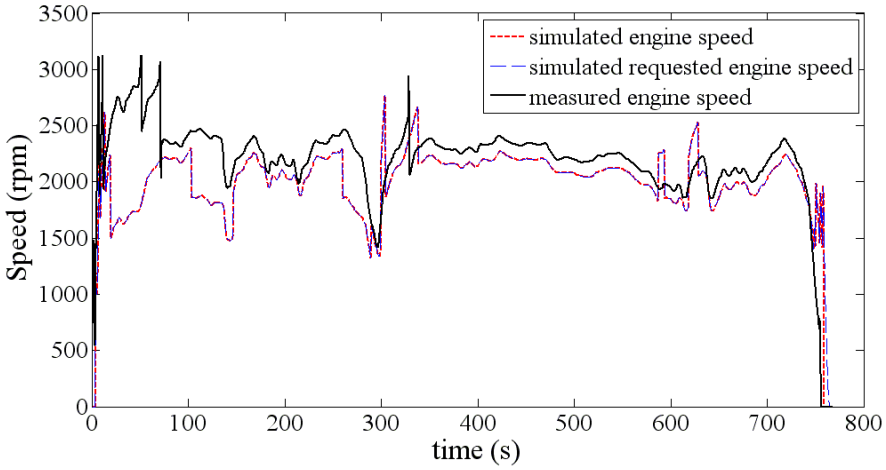

Figure A.73 – ICE speed for the HWFET drive profile. Variations in ICE speed are due to the gear ratios selected for the transmission as well as the wheel radius.

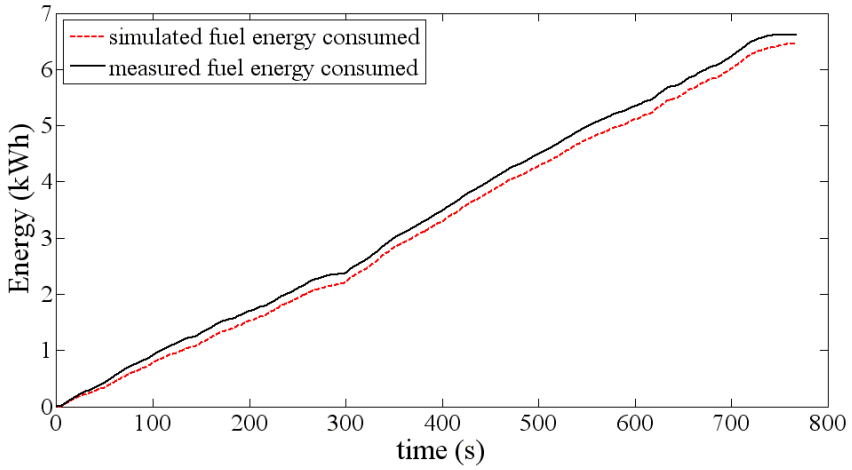

Figure A.74 - Total fuel consumption over the UDDS. Simulated ICE is operating very closely to the measured data.

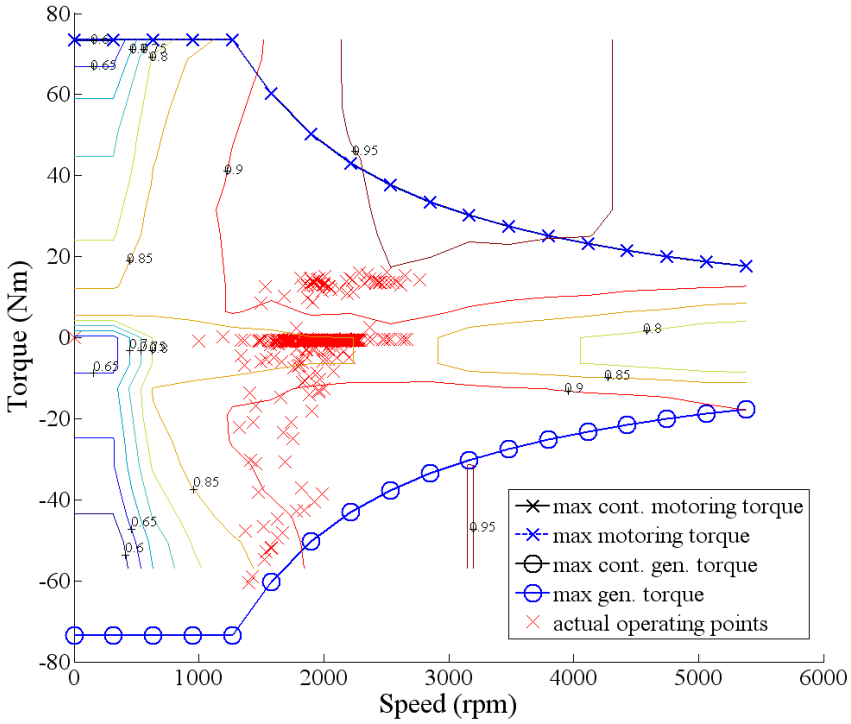

Figure A.75 – M/G operating points for the IMA coupled between the ICE and transmission.

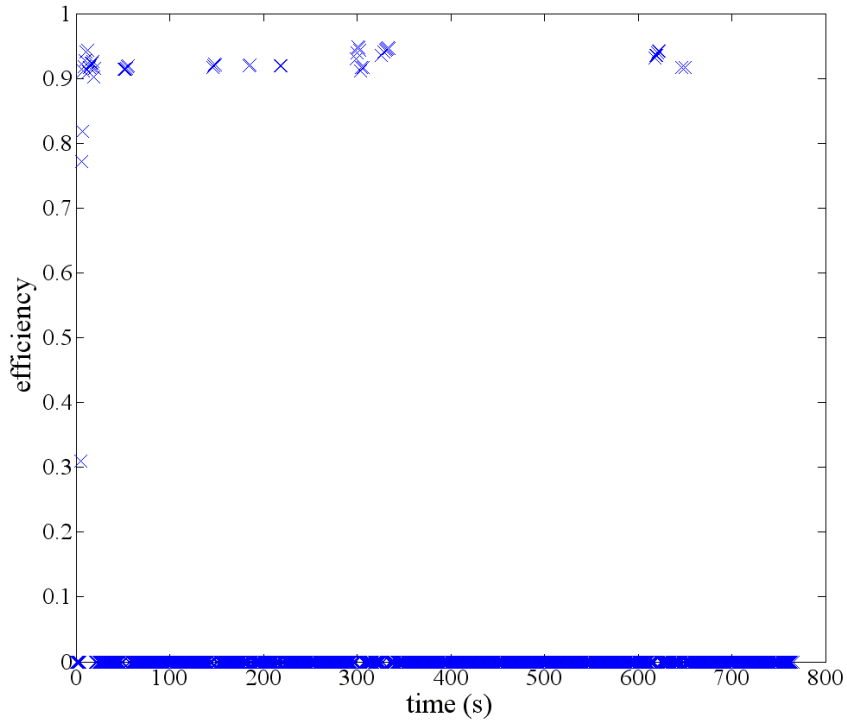

Figure A.76 – M/G efficiency over the UDDS. Motoring average efficiency is 87.7%.

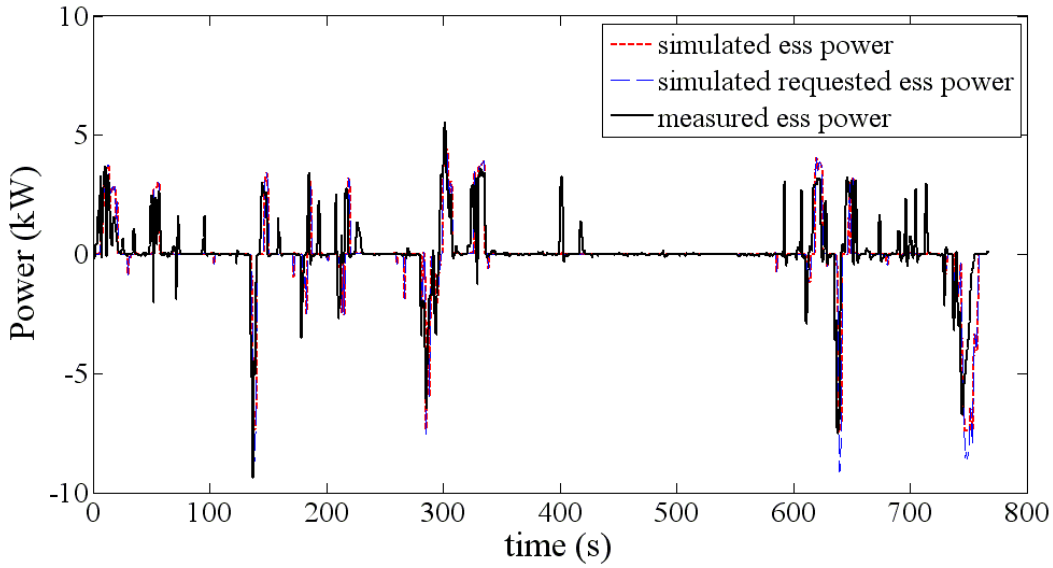

Figure A.77 - ESS power consumption during the HWFET. Requirement is reflected in the size of the traction motor at 10 kW.

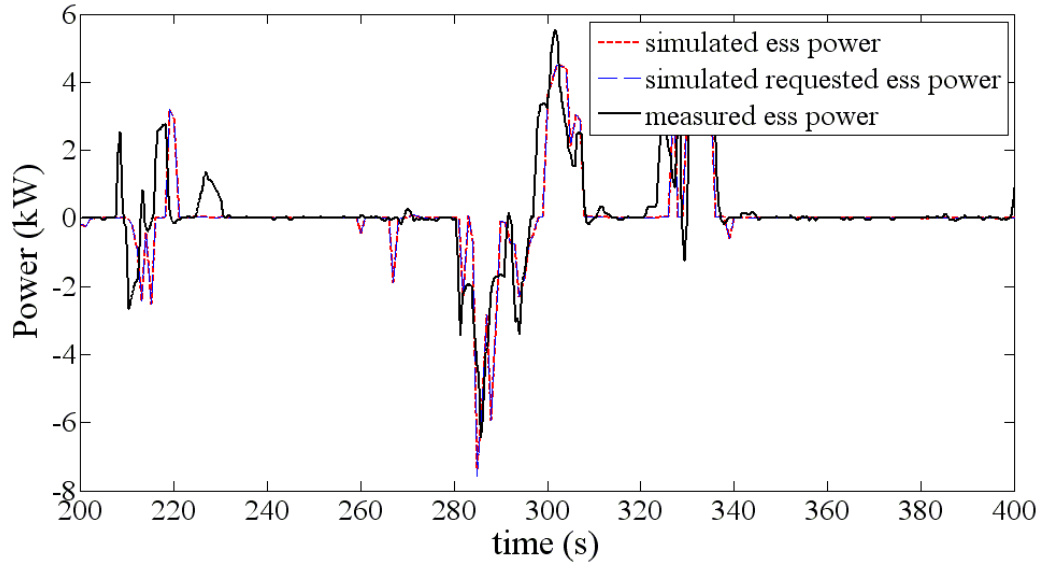

Figure A.78 - ESS power consumption for a smaller segment of time.

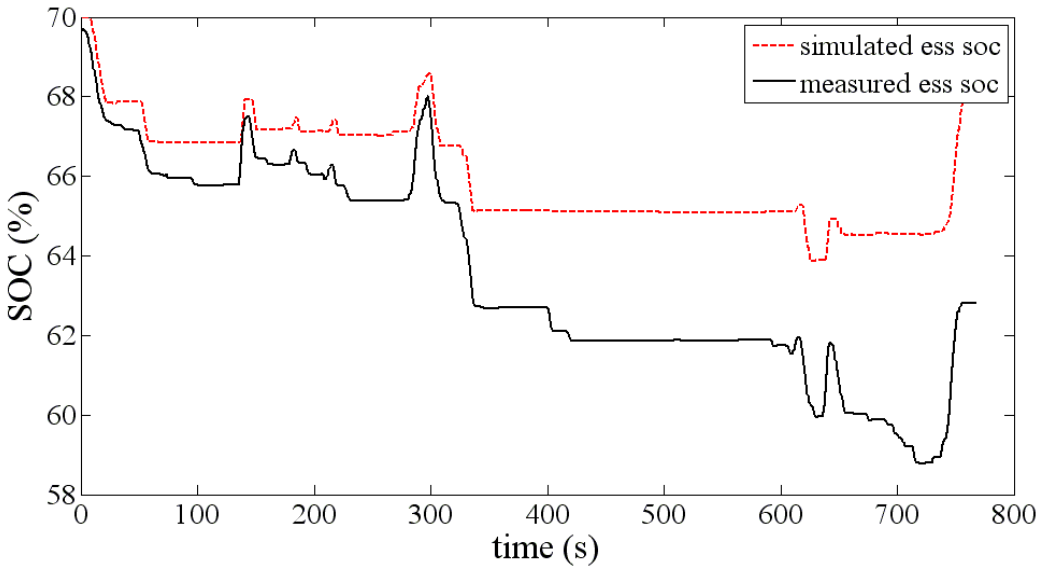

Figure A.79 - ESS SOC for the HWFET. Difference is due to efficiency maps of M/G and ESS.

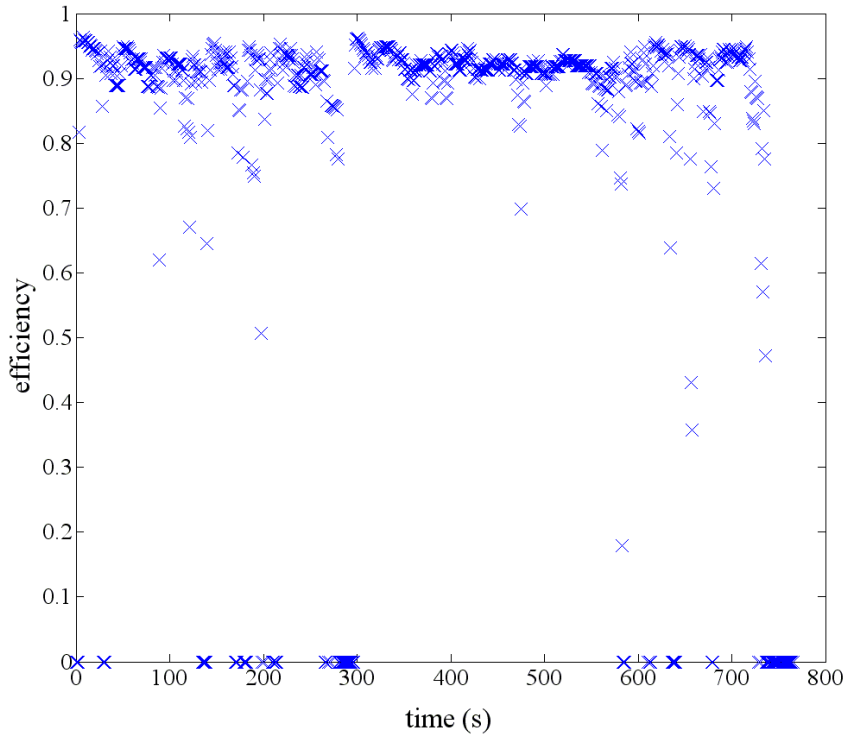

Figure A.80 - Drivetrain efficiency for the Honda CR-Z on the HWFET. Average drivetrain efficiency is 92.4%.

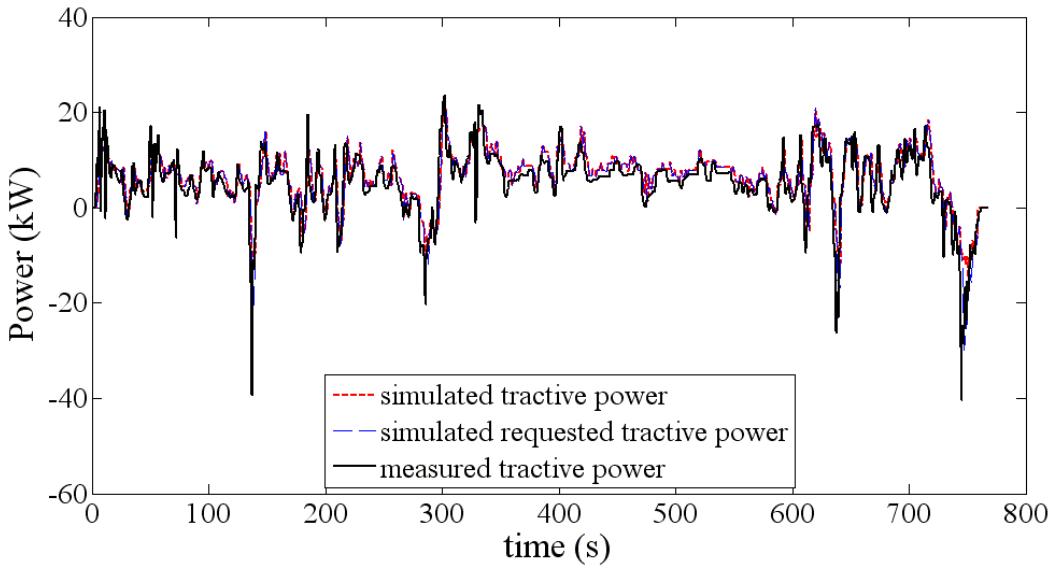

Figure A.81 - Tractive power required to propel the vehicle over the HWFET.

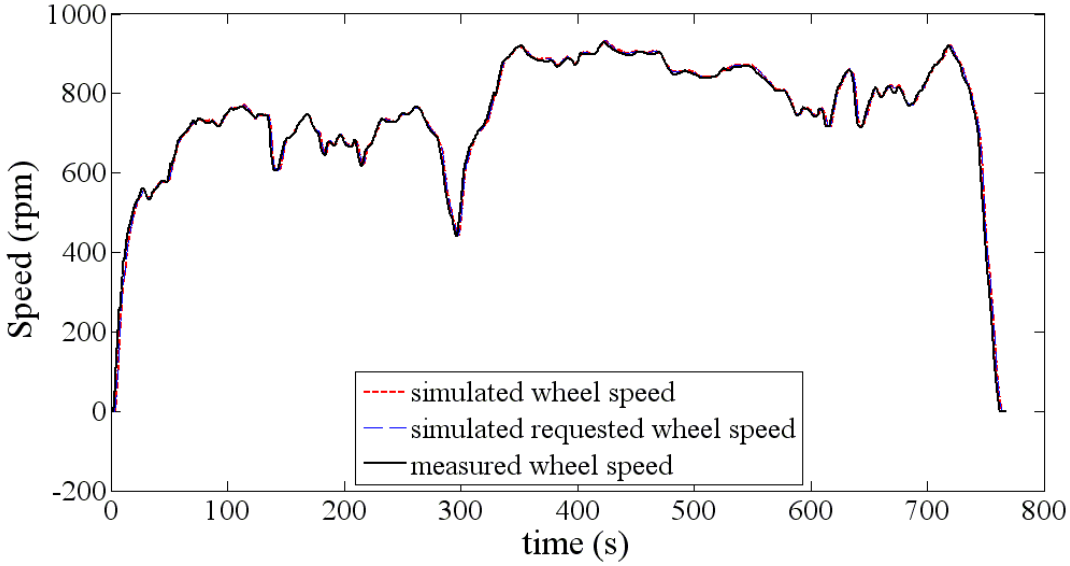

Figure A.82 - Wheel speed achieved by the vehicle with a wheel radius of 0.275 m. Wheel speed is calculated from chassis dynamometer speed using the same wheel radius as seen in simulation.

A.2 Experimental Setup

Table A.4 - Item list for the experimental setup of the power-split plug-in hybrid electric test vehicle.

Item	Specifications	Quantity	Cost	Link
Battery Bank	**Winston (Thunder Sky)** – 160 Ah, 3.2 V, 5.6 kg	8	~$1728 (from Web Page)	http://www.alibaba.com/product-free/121313505/Winston_Thunder_Sky_160_Ah_LiFePO4.html
Torque Sensor (rear axle)	**Rotary Torque Transducer** – 0-200 Nm, up to 6000 RPM – (^Depends on location in drivetrain) Signal requirements 4-20mA or 1-5V.	1	~$800-$1,600 (from Web Pages)	**Korean Supplier** http://www.aliexpress.com/item/rotary-torque-transducer-TCR-1-20kgf-cm/556458181.html **Chinese (Mainland)** http://www.alibaba.com/product-gs/563823723/Rotary_Torque_Transducer.html http://www.alibaba.com/product-gs/578447038/rotary_torque_transducer.html
ICE and ACVT	**ICE and Automatic Continuous Variable Transmission (ACVT) -** (At least 6kW) 150cc ACVT Engine (Does not have to be 150cc as long as ICE power rating is at least 6 kW, with ACVT)	1	~$690 (from Web Page) Australia Chinese ? $0-$100, min order 100	**Australian Supplier** http://www.xtrememotorbikes.com.au/d1646-41/150cc-auto-quad-engine-new/ **Chinese (Mainland)** http://www.alibaba.com/product-gs/200468595/engine.html
Please get items listed below if they are less than the indicated price and have the rated specs.				

Bi-directional DC-DC Converter (EM)	**Brushless DC motor Controller –** 48V, 360A	2	<$535.00	http://www.alibaba.com/product-gs/521059958/5kw_brushless_dc_motor_controller_72V.html
Bi-directional DC-DC Converter (GEN)	**Brushless DC motor Controller –** 48V, 600A	1	<$535.00	http://www.alibaba.com/product-gs/521177742/High_Power_BLDC_Controller_for_10KW.html
Electric Motor	**Brushless DC motor –** 3kW, 48 V (As long as controller voltage matches motor voltage.)	2	<$470.00	http://www.alibaba.com/product-gs/482291968/BLDC_motor.html
Generator	**Brushless DC motor –** 6kW, 48 V (As long as controller voltage matches motor voltage.)	1	<$470.00	http://www.alibaba.com/product-gs/482291968/BLDC_motor.html
DC Contactor	**Double Contactor/Reversing Contactor -** 48V, 300A	3	<$165.00	http://www.alibaba.com/product-gs/424718204/DC_Contactor_for_electric_forklift.html

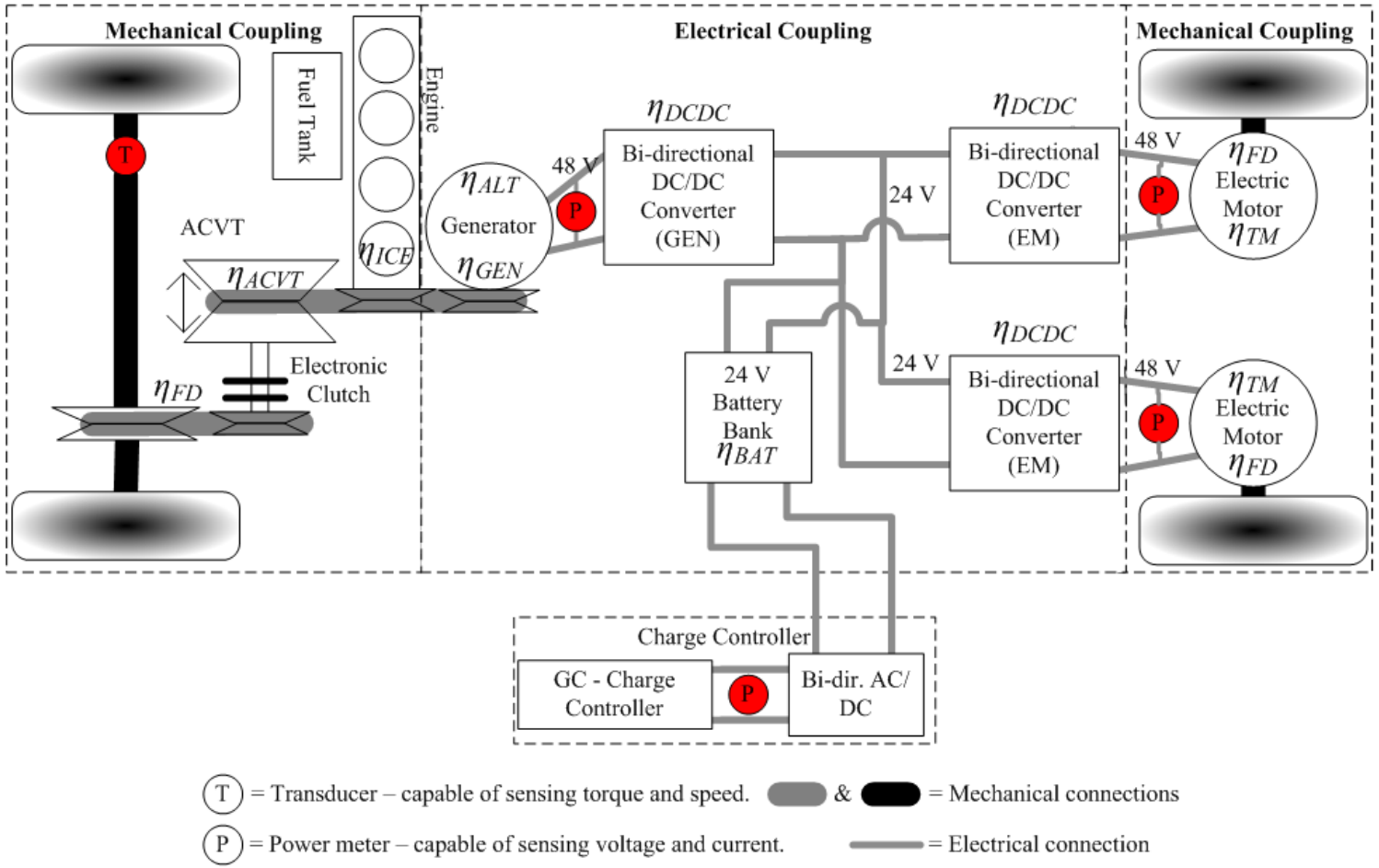

Figure A.83 - Block diagram of the power-train for a power-split plug-in hybrid electric test vehicle

A.3 Drive Cycles utilised in Predictive Analysis

A.3.1 UDDS

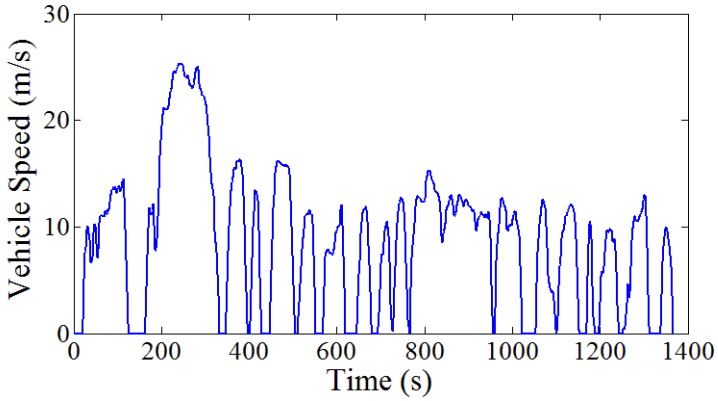

Figure A.84 - Urban dynamo driving schedule.

A.3.2 HWFET

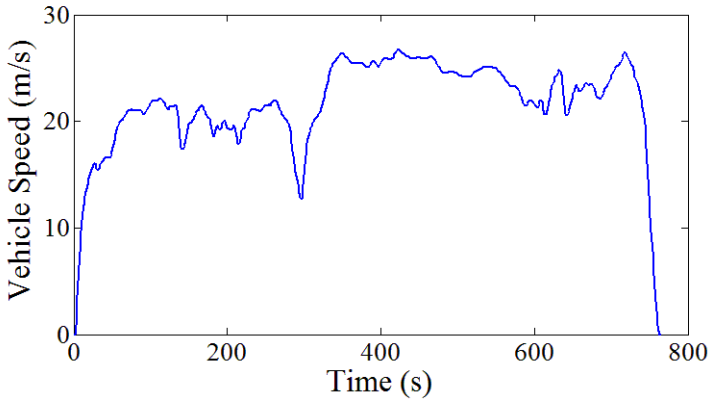

Figure A. 85 - Highway fuel economy test.

A.3.3 US06

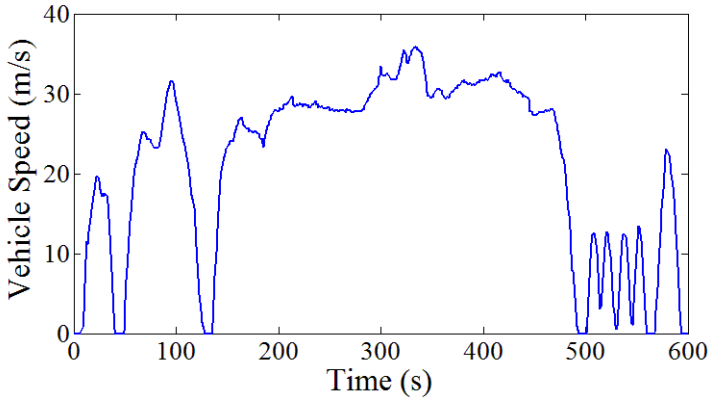

Figure A.86 - US Environmental Protection Agency's supplemental FTP.

A.3.4 NEDC

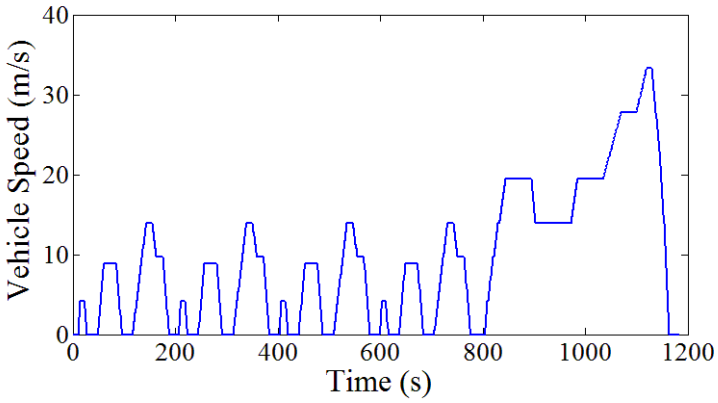

Figure A.87 – New European drive cycle.

A.3.5 LA92

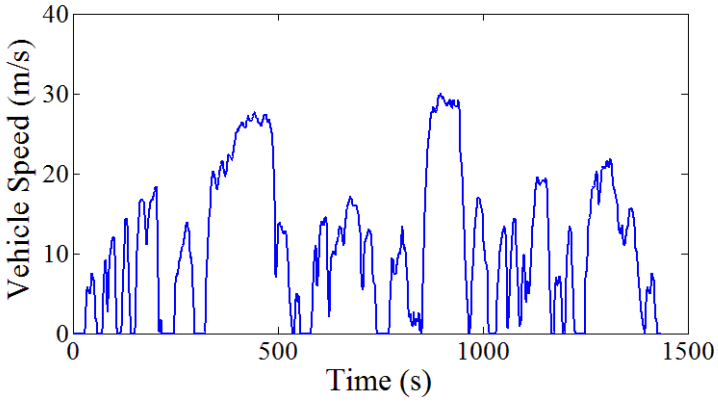

Figure A.88 - Unified driving schedule – emissions test.

A.3.6 NurembergR36

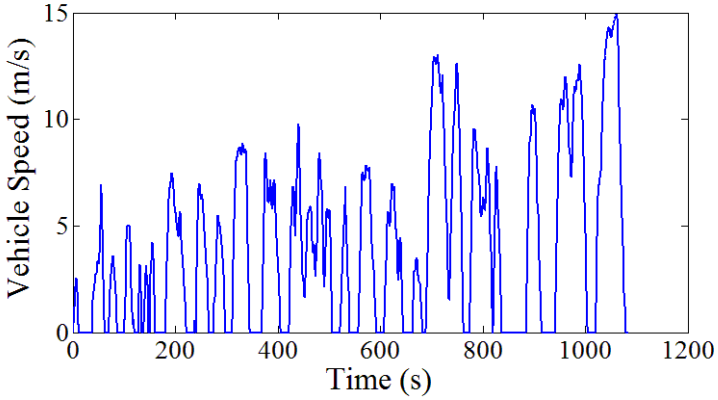

Figure A.89 - Drive cycle for bus route 36 in Nuremberg, Germany.

A.3.7 **HL07**

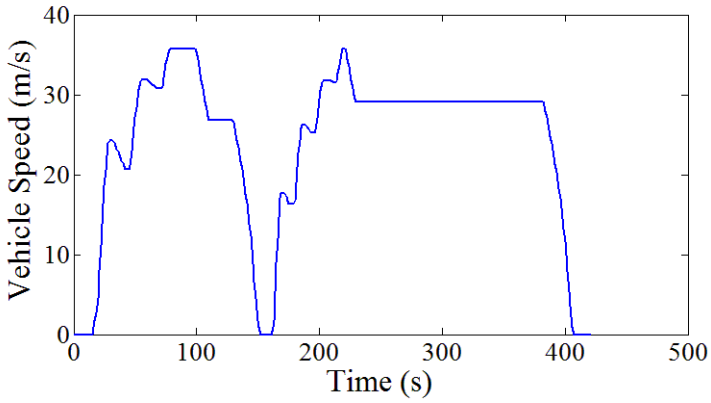

Figure A.90 - An aggressive driving schedule determined in combination with the federal test procedure.

A.3.8 **WVUCITY**

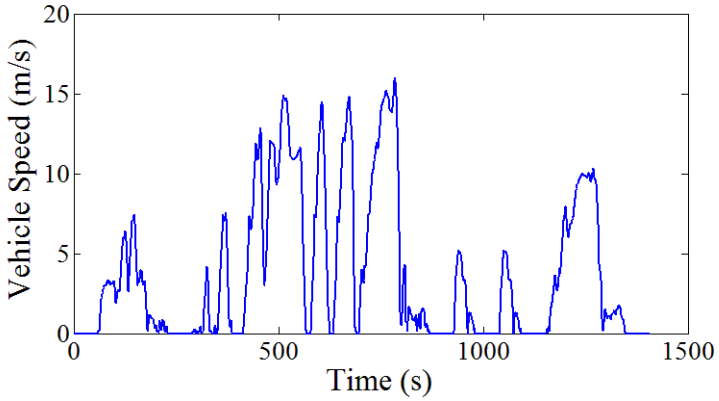

Figure A.91 - West Virginia city driving schedule.

A.4 SOC Swing Controller

This controller is defined in Sections 5.2 to 5.6 of this thesis. Operation of this controller is demonstrated on the Toyota Prius 2010 model over the UDDS of Figure A.84. The following simulation results demonstrate the limitations of the designed EMS controller on the Toyota Prius 2010 vehicle configuration. Firstly, Figure A.92 demonstrates the clear ICE on/off periods with respect to the SOC of the ESS. Note that as the vehicle approaches the destination the energy sent to recharge the ESS is reduced, due to the monitoring of E^*_{total} and t^*_{trip}. Following SOC of the ESS, the ICE efficiency of operation is demonstrated for the defined t_{on} in Figure A.93. During ICE shutdown, operating efficiency is recorded at zero since no output power is developed by the ICE.

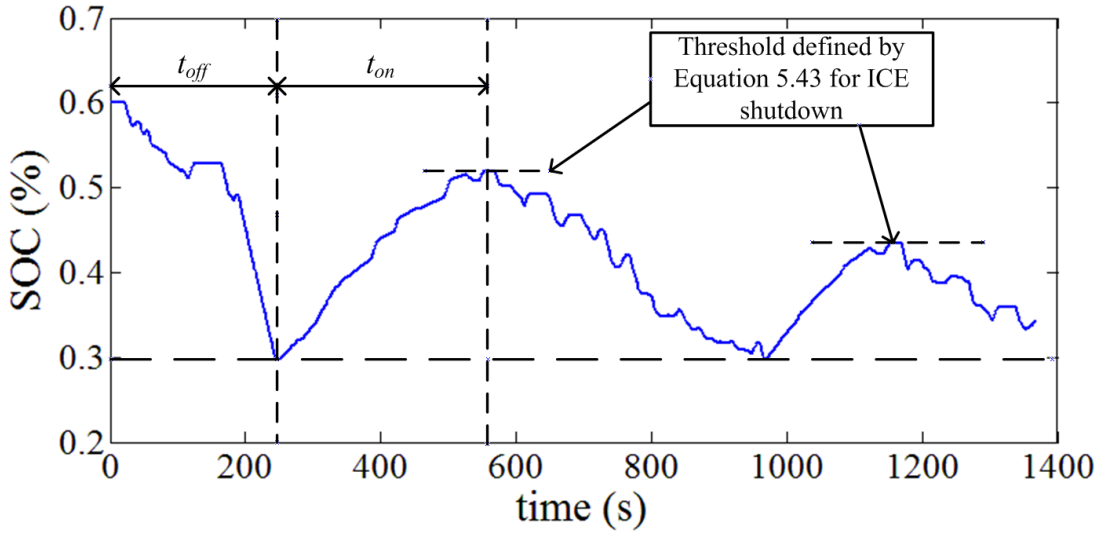

Figure A.92 – Operation of the Toyota Prius 2010 model for the SOC swing defined in Sections 5.2 to 5.6 of this thesis.

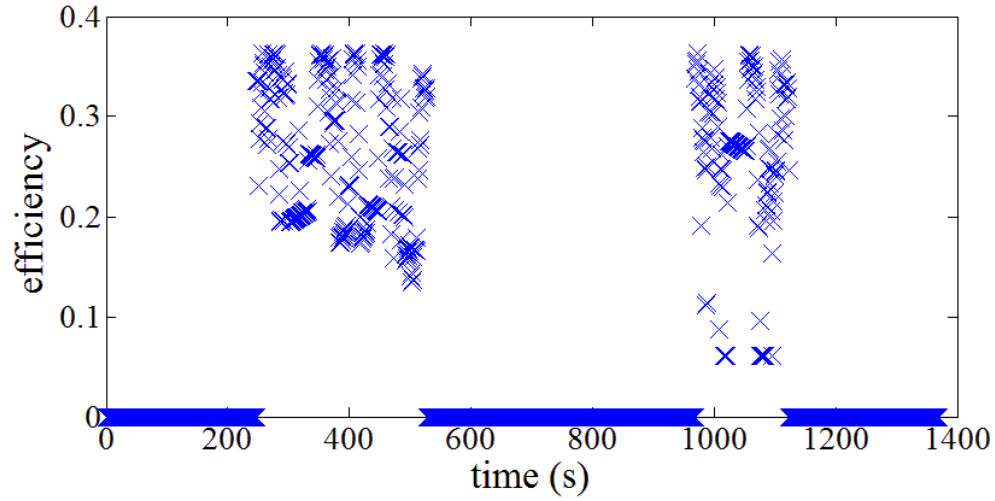

Figure A.93 – Toyota Prius 2010 ICE operating efficiency over the UDDS for the periods of t_{on}.

Observing the vehicle speed trace from simulation it is noted that during periods of ICE shutdown, the ESS and M/G combination cannot satisfy the drivetrain demand. Figure A.95 identifies that the vehicle speed trace is missed by up to 20km/h during one of the periods of ICE shutdown (at the 200 second mark). For this reason the SOC swing controller is not suitable for implementation using the Toyota Prius 2010 test bench and an alternative controller must be sourced. This is the reason for designing the proposed predictive controller of Chapter 5.

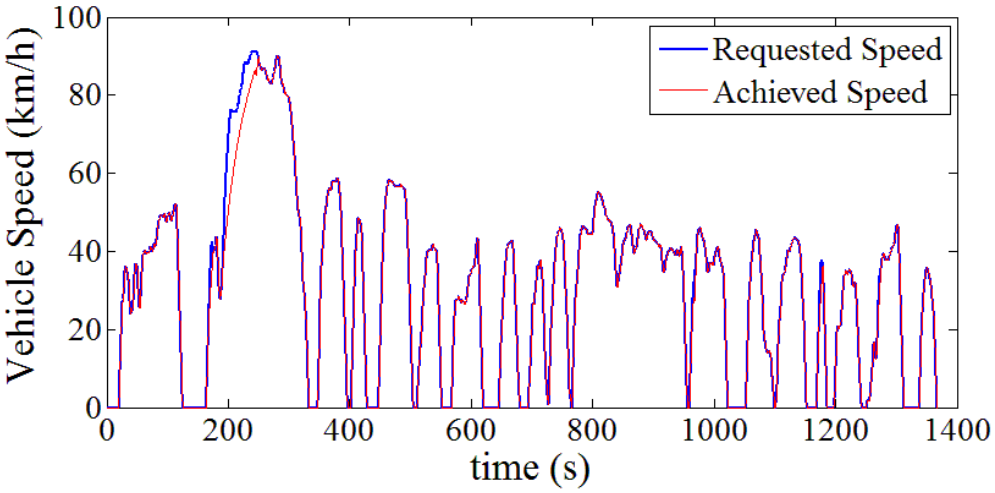

Figure A.94 - Vehicle speed trace comparison of requested and achieved vehicle speeds.

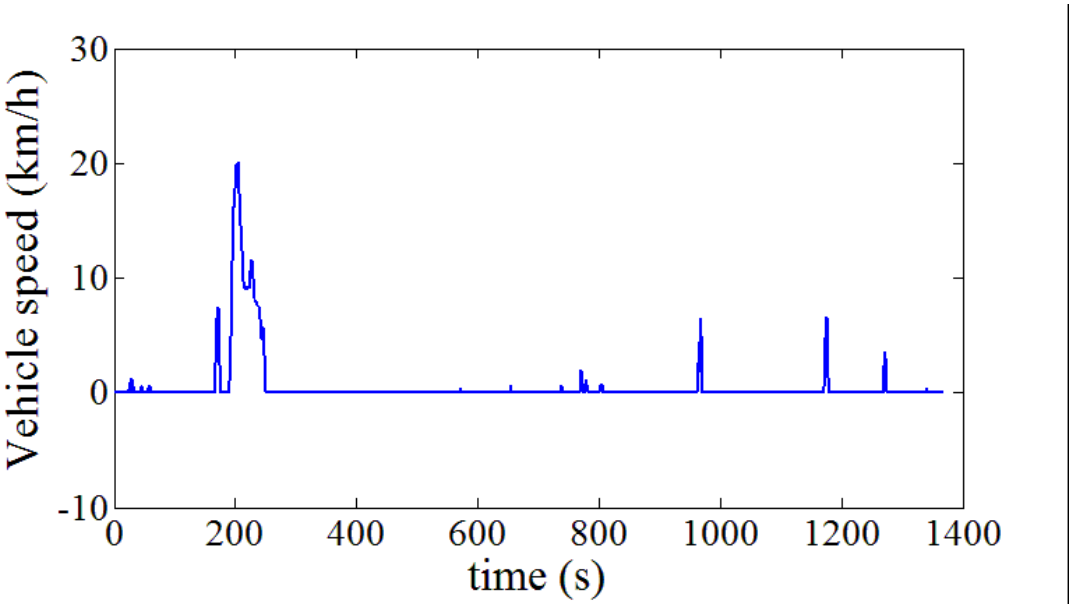

Figure A.95 - Vehicle speed trace miss for Toyota Prius 2010 operating with the SOC swing controller.